Design, Synthesis and Characterization of Novel
Exogenous Smart/Bioresponsive Contrast Agents
for Magnetic Resonance and Optical Imaging

Design, Synthese und Charakterisierung neuartiger
exogener intelligenter/bioreaktiver Kontrastmittel
für die Magnetresonanz und optische Bildgebung

DISSERTATION

der Fakultät für Chemie und Pharmazie

der Eberhard-Karls-Universität Tübingen

zur Erlangung des Grades eines Doktors

der Naturwissenschaften

2008

vorgelegt von

Anurag Mishra

This PhD thesis was prepared at the Max-Planck Institute for Biological Cybernetics (chemistry laboratory of the Department Physiology of Cognitive Processes, Prof. Dr. Nikos K. Logothetis) in collaboration with the Institute for Organic Chemistry, Eberhard-Karls-University, Tübingen under the guidance of Prof. Dr. Klaus Albert during the period from December 2003 to December 2007.

Hereby I declare the fact that I am writing this work and no different than the indicated aids have been used.

Tübingen, December, 2007

Abbreviations

Boc	*tert*. Butoxy carbonyl
^{t}Bu	*tert* butyl
c	Concentration
δ	Chemical shift in ppm (NMR)
CBz	Chlorobenzoformate
CCl_4	Carbon tetrachloride
$CDCl_3$	Chloroform-deuterated
CH_2Cl_2	Dichloromethane
CLIO	Cross-linked iron oxid
DCC	Dicyclohexylcarbodiimide
DMAP	4-Dimethylaminopyridine
DMF	N,N-Dimethylformamide
DO3AMP	DO3A-methyl phosphonic acid
D_2O	Deuteriumoxid
EDC	1-Ethyl-3-(3'-dimethylaminopropyl) carbodiimide
EDTA	Ethylenediaminetetraacetic acid
EGTA	Ethylene glycol bis(2-aminoethylether)-N,N,N',N'-tetraacetic acid
Equ	Equation
ESI-MS	Electron Spray Ionization-Mass Spectrometry
Et	Ethyl
Et_2O	Diethyl ether
EtOAc	Ethyl acetate
$EuCl_3.6H_2O$	Europium trichloride hexahydrate
Fig.	Figure
FITC	Fluorescein isothiocyanate
g	gram (s)
GABA	gamma-amino butyric acid
$GdCl_3.6H_2O$	Gadolinium trichloride hexahydrate
h	hour (s)
H_2	Hydrogen

Abbreviations

HBr	Hydrobromic acid
HCl	Hydrochloric acid
HOBt	Hydroxybenzotriazole
HPLC	high performance liquid chromatography
HSA	human serum albumin
ESI-HRMS	Electron spray ionization-high resolution mass spectrometry
Hz	hertz
i-Pr	isopropyl
J	coupling constant (NMR)
K_2CO_3	Potassium carbonate
λ	lambda
LiOH	Lithium hydroxide
Ln	lanthanide
Me	Methyl
MeCN	acetonitrile
MeOH	Methanol
MeOD	Methanol-deuterated
mg	milligram
m/z	Mass to charge ratio (MS)
mL	milliliter (s)
mmol	millimole
mM	millimolar
MoAb	Monoclonal antibody
Na_2CO_3	Sodium carbonate
$NaHCO_3$	Sodium bicarbonate
NaOH	Sodium hydroxide
Na_2SO_4	Sodium sulphate
NMM	N-Methylmorpholine
NH_3/MeOH	methanolic ammonia
p	para
Pd-C	Palladium carbon
PPH_3	triphenylphosphine
Ph	Phenyl

Abbreviations

P_5P	Pyridoxyl-5-phosphate
PyBroP	Bromo-tris-pyrrolidino-phosphonium hexafluorophosphate
Ra-Ni	Raney nickle
R_f	Retention factor (TLC)
RT	Retention time (HPLC)
RP-HPLC	Reverse phase- high performance liquid chromatography
SPIO	superparamagnetic iron oxide
TEA	triethylamine
TFA	Trifluroacetic acid
THF	Tetrahydrofuran
UV	Ultraviolet

Acknowledgements

Knowledge in itself is a continuous process. At this moment of my substantial enhancement, I have found this rare opportunity to evince a word of thanks to all those who have played a key role in the successful completion of my PhD thesis.

My heartfelt thanks to Prof. Dr. Klaus Albert, Institute for Organic Chemistry, Tübingen University, for providing his unconditional support, guidance and optimal resources allocation that helped me in the successful completion of my doctoral projects.

I wish to express my deepest reverence to Prof. Dr. Nikos K. Logothetis, Director, Department Physiology of Cognitive Processes, Max Planck Institute for Biological Cybernetics, for his unrestricted support, suggestions, valuable guidance and providing me the facilities during the course of the investigation.

I owe a sincere thanks to my esteemed advisors Dr. Josef Pfeuffer, Head of MR Imaging and Spectroscopy, Max Planck Institute for Biological Cybernetics (currently Siemens AG, Medical Solutions, Boston, USA) and Dr. Anil Mishra, INMAS, Delhi, India for their sincere guidance, co-operation, constant encouragement, patience and belief in me.

I would like to thank Prof. Dr. Martin E. Maier, Institute for Organic Chemistry, Tübingen University, for his helpful reviewing the doctoral thesis and giving valuable comments and suggestions.

I am very thankful to Prof. Dr. Almut Schuez and Dr. Santiago Canals for their help in performing and designing *in vivo* histological experiments of neuroanatomical tracers and their advices in writing of the some biological part of thesis.

I express my special thanks to our biology group, MPI for Biological Cybernetics, Dept. Ugurbil: Dr. Joern Engelmann, my lovely wife Ritu Mishra and Hildegard Schulz for performing cell studies and tremendous guidance. The work in this thesis would not have been possible without their collaboration.

I express my cordial gratitude to Dipl.-Ing. Michael Beyerlein and Dr. Rolf Pohmann for performing the MR experiments at 1.5T, 3T and 7T.

Acknowledgements

Table of Contents

Table of Contents

Table of Contents

Table of Contents

CHAPTER 1

Literature Review

1.1. Introduction.

Magnetic Resonance Imaging (MRI) is a valuable and versatile technique for visualizing internal structures first described in 1978[1]. It is an extension of Nuclear Magnetic Resonance (NMR) spectroscopy used in chemistry. Molecular imaging using magnetic resonance techniques is a rapidly growing field in diagnostic medicine and basic neuroscience. The high spatial resolution and the undisputed capacity of differentiating soft tissues have highly contributed to the widespread use of this imaging modality. MRI offers the potential of realistic three dimensional imaging of biological structures, where the signal is based upon the resonance of water protons. With the advent of improved variety of technologies both in terms of hardware/software and the versatile techniques, it is possible to obtain detailed anatomical, physiological and metabolic/functional information with carefully designed experiments, which could address various intriguing questions concerning neural mechanisms of cognitive functions in the primate, which is the thrust area of our research.

1.1.1. Advantages and Disadvantages of MR Techniques over non MR Techniques.

The prime advantage of MR techniques is their non-invasiveness and flexibility. Both biochemical spectroscopy and spatial information (imaging) can be easily performed without destroying the sample, which is a great asset for biomedical and physiological research. An additional advantage of MR methods versus other comparable techniques is the lack of exposure to potentially damaging ionizing radiation. The majority of non-NMR-based techniques used for imaging or for *in vivo* studies of metabolism involve ionizing radiation in one form or another. For example, computer assisted tomography (CT) uses X-rays, and nuclear medicine based techniques like gamma scintigraphy and positron emission tomography (PET) involves the administration of radioactive tracers. Even traditional studies of metabolic processes in intact cells and organs use compounds labeled with radioactive isotopes of hydrogen and/or carbon. The ability of MR to obtain a wide range of information in a single experiment is not normally possible with any other modality. For example, PET can be effectively used to measure metabolism non-invasively;

2

however, the spatial resolution of the images (~3 mm) is relatively poor, so that correlation of the results with anatomy is difficult without the use of other supplementary techniques like CT etc. PET imaging can also detect activity-induced increases in blood flow. Even though nuclear medicine techniques have the advantage of high penetration and sensitivity and the ability to pick up micromolar tissue concentration, they usually lack chemical specificity. Similarly, while CT can provide rapid, relatively high-resolution cross-sectional images, it cannot provide soft-tissue details and metabolic or physiological information. On the other hand MR techniques can achieve high spatial resolution (pixel dimensions of 100 mm or better) but the spectral resolution concentrations are in millimolar range.

The contrast resolution (visualization of low-density objects with similar soft tissue characteristics) of MR is ~10 times better than conventional radiography thereby making it a modality-of-choice with high diagnostic potentials. MR Imaging differs from other imaging modalities because signal and contrast are multiparametric in both the intrinsic MR properties of the tissue and the method of measurement (the sequence & scan parameters chosen). MR contrast depends on differences in proton-spin density (local tissue water concentration), magnetic susceptibility (oxygenation state and presence of other magnetic 'impurities'), molecular diffusion (directionally sensitive to diffusivity of water), perfusion (sensitive to capillary flow), and relaxation times. Bulk flow and magnetization transfer that provides indirect information about proton nuclei that are not in water, are other interesting determinants.

As outlined above, the greatest disadvantage of MR techniques compared with other modalities is its intrinsic insensitivity. The signal that can be generated in the NMR experiment is small, and for practical purposes, most strongly coupled with the ubiquitous presence of tissue water (almost ~70%) resulting in a relatively large signal due to the ^{1}H nucleus in water that is effectively at a concentration in the tens of molar range. It is possible to measure signals from cubes (voxels) of tissue as small as ~0.3 mm from the human brain, generating the high-quality images used in clinical MRI. Other nuclei of metabolites found *in vivo* are typically at much lower concentrations.

For example, the ^{31}P nucleus in ATP in tissues is at a typical tissue concentration of 1-10 mM (~10^4 to 10^5 orders of magnitude less than that of water),

which, when combined with lower sensitivity of the ^{31}P nucleus (0.066 relative to ^{1}H), results in a total decrease in sensitivity of $\sim 10^6$. The cubic volume needed to obtain the same signal will thus be approximately 100 times larger on each side (i.e., $\sim 3cm$) as a broad approximation as other factors also contribute to differences in sensitivity between different nuclei. For example, the use of higher field strengths and small surface coils placed closer to the tissue of interest, it is often the case in animal studies, will make it possible to sample much smaller volumes of tissue. Nevertheless, regardless of the field strength and size of the coil, the NMR signals from water will always be detectable at resolutions approximately two orders of magnitude greater than those of other NMR-sensitive nuclei. Thus, compounds present in submillimolar or micromolar concentrations cannot practically be detected directly in tissues. This problem has been addressed to some extent by developing stronger 'magnets' for MR.

The stronger the magnetic field (B_0), the more nuclei on average will align with this magnetic field. Thus, as B_0 becomes stronger, a larger signal can be generated. This effect is the main reason for the current drive in NMR to build stronger magnets, in as much as more signals generally means that higher spatial resolution images and better spectra can be obtained. Recent advances in the development of high field magnets and low-noise probes optimized for microimaging have made possible MR imaging of small biological samples with resolutions of less than 10 μm. The development of miniaturized imaging equipment and reporter probes has improved the ability to perform MR studies in animal models of diseases, such as transgenic and knockout mice. The ability of MR technologies to encompass studies of cells, animals, and humans should therefore, greatly enhance the translation of knowledge obtained in basic biomedical research to humans[2-7].

1.1.2. Associated issues when working in a High-Magnetic-Field Environment.

As seen above, an inevitable consequence of carrying out biomedical MR investigations is the need to work in a high-magnetic-field environment. Although no known intrinsic risks are known to be associated with high magnetic fields; however, the presence of the magnetic field can affect equipment/accessories routinely used in animal research. One of the very few dangers associated with NMR is the potential for ferromagnetic objects that are not held in place to be attracted to the magnet.

Fortunately, an increasing amount of monitoring equipment is now available that is designed to function in relatively close proximity to NMR magnets[8-11].

1.2. Background and Significance

The spatial resolution of MR is high and it also offers physiological sensitivity, production of detailed images that provides an insight into how physiological functions occur *in situ* is a somewhat tricky affair. By the selection of appropriate pulse sequences the image contrast in MRI could be enhanced. It can also be made sensitive to diffusion, perfusion and macroscopic blood flow. The potential of MRI procedures can be further exploited when applied in concurrence with magnetopharmaceuticals [Contrast Agents (CAs)] in both clinical and experimental settings that can improve the ability to resolve different anatomical structures or pathologies on the MR image. The contrast media enhance the image quality by magnetically tickling the surrounding water protons, thereby altering the tissue response during MR measurements. This allows the organs and other tissue administered with the contrast agent to stand out from the surrounding organs or other nearby tissue. Using advanced categories of these agents it is now possible to obtain fairly detailed information on cellular events in addition to the anatomical data normally revealed by MRI[12-16].

1.2.1. Relaxation Parameters.

Relaxation can be considered in two parts: recovery toward equilibrium (longitudinal) alignment and transverse decay. Both of these processes can be described mathematically by exponential terms, governed by time constants, T_1 (for longitudinal recovery) and T_2 (for transverse decay). It is these parameters, T_1 and T_2 which are properties of the water microenvironment and thus of different tissue types, that lend MRI its inherent power to distinguish between different tissues (even of similar density). T_1 and T_2 differ between tissues because the physicochemical microenvironments of tissues differ (especially water mobility and the presence of microstructures, macromolecules and membranes).

It is useful to consider the parameters that determine the relaxation rate ($R=1/T$) of a contrast agent in order to appreciate how modulation of these in response

to a biological event can produce the desired change in relaxivity of the activated system.

$$R_{1p} = R_{1p}{}^{IS} + R_{1p}{}^{OS} \qquad \text{(Equ. 1)}$$

$$R_{1p}{}^{IS} = Cq/55.6 * 1/T_{1M} + \tau_m \qquad \text{(Equ. 2)}$$

The total paramagnetic relaxation rate enhancement of the free water protons (R_{1p}) is made up of contributions (Equation 1) from the inner sphere ($R_{1p}{}^{IS}$) and outer sphere ($R_{1p}{}^{OS}$) relaxation mechanisms. The inner sphere mechanism consists of interactions between Gd^{3+} and directly bound water molecules, whereas the outer sphere mechanism consists of interactions with second sphere and closely diffusing water molecules. The greatest control can be exerted over the large inner sphere contribution (Equation 2), where C = molar concentration of paramagnetic compound, q = number of bound water molecules, T_{1M} = longitudinal relaxation time of the bound water protons and τ_m = mean residence lifetime in coordination sites (Fig. 1). At the magnetic field strengths typically used in MR imaging, the longitudinal relaxation time of the bound water protons T_{1M} is dominated by the molecular rotation (rotational correlation) time τ_R. The slower the Gd^{3+} complexe tumbles, the faster the relaxation rate.
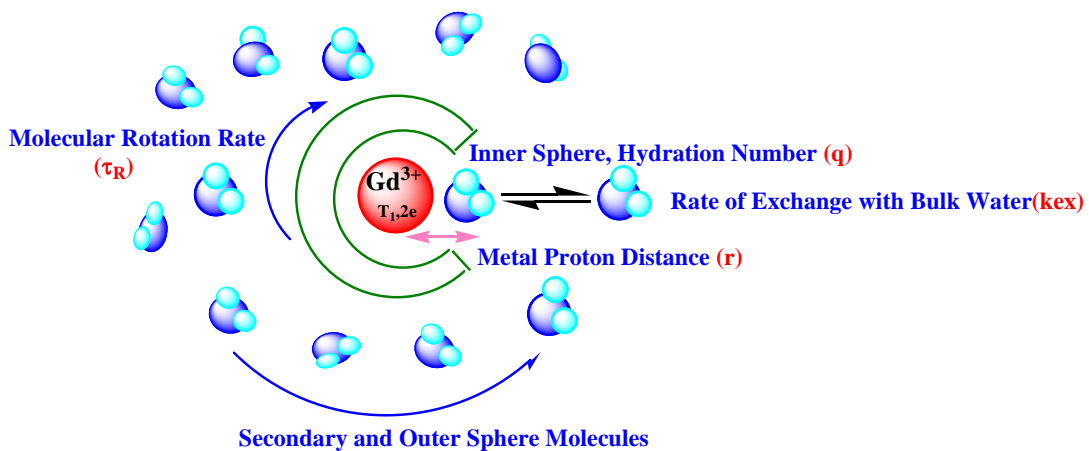
Figure 1: Schematic representation of a Gd^{3+} chelate with one inner-sphere water molecule, surrounded by bulk water, kex refers to the water/proton exchange rate and $1/T_{1,2e}$ to the relaxation rate of the Gd^{3+} electron spin.

Thus, the parameters q, τ_m and τ_R are those that are the most amenable to modulation in response to a biological event to generate specific contrast agents[15,17-19].

1.2.2. Endogenous and Exogenous Contrast Agents.

A particularly powerful paradigm for functional MRI of microvascular hemodynamic incorporates paramagnetic materials that create significant image contrast. These include exogenous (lanthanide/transition metal chelates) and endogenous (deoxygenated hemoglobin) agents for mapping cerebral blood volume/flow and neuronal activity. Accurate interpretation of these maps requires an understanding of the biophysics of susceptibility-based image contrast and its relationship with microscopic tissue parameters and NMR imaging parameters[8-10,20-23].

1.2.3. Lanthanide Metal Chelates.

The transition metal and paramagnetic lanthanide ions suitable as MR contrast agents are all potentially toxic at or near doses required for NMR relaxation changes. A major difficulty in the development of any of the paramagnetic metals as CAs has been to diminish this toxicity to administration. This toxicity can only be reduced by coordinating the metal to ligands that are too obstinate to be displaced by water, while leaving one coordination site open for a water molecule, to allow inner sphere spin transitions, or transitions between the nuclei metal and a ligand to which they are directly bound. With chelation of these ions, acute toxicity is reduced and elimination rate is increased thereby reducing the chance of long-term toxicity. CAs are primarily Gadolinium-based compounds, which are chelated (complexed with suitable ligands) to reduce toxicity. Choice of a proper ligand is very important to ensure that Gd^{3+} does not dissociate from the complex in the body in presence of phosphate, citrate, transferrin and other endogenous chelating substances. Gd^{3+} ion exhibits the strongest effect of all elements on longitudinal relaxation time. Commonly used CA are polyaminocarboxylate complexes of the highly paramagnetic Gd^{3+}.

Lanthanide metal chelates can enhance MR image quality by influencing the precession of surrounding water protons, thereby altering the tissue response during MR measurements. CAs are being used clinically to detect or characterize lesions, to delineate pathological structures or to indicate the status of organ function or blood

flow, thereby ultimately improving the accuracy of prognoses. The potentials of MR techniques have extended from routine clinical applications to exciting uses in developmental biology as a tool for the study of embryonic cell differentiation[17,24-26].

1.2.4. Evolution of Contrast Agents.

The ligands of Gd-chelates belong to two different type of structures- Acyclic (open-chain compounds) and macrocyclic ligands. Owing to entropy considerations, chelating ligands are usually several orders of magnitude more strongly coordinating than their monodentate analogues. Most widely used chelators for the complexation of Gd^{3+} are diethylenetriaminepentaacetate (DTPA) and 1,4,7,10-tetraazacyclododecane-1,4,7,10-tetraacetate (DOTA) (Fig. 2). DTPA is a readily available octadentate ligand. Non-specific acyclic probes like GdDTPA that accumulates nonspecifically and are excreted rapidly ($t\frac{1}{2}$=90 min), constitute the first generation of CAs. DTPA chelates are easily derivatized. Various complexes have been designed and evaluated using thermodynamic stability, rates of excretion, toxicity, lipophilicity, and biodistribution, percent change in MR signal intensity as criteria keeping GdDTPA as the gold standard. The complexes are anionic, and therefore, quite water-soluble (usually to about 0.5–1.0 M). They are marked by unselective biodistribution over the extracellular fluid and the resultant contrast is dependent on their tissue permeability versus the clearance rate. Stability of the majority of macrocyclic gadolinium chelates is higher than that of acyclic complexes.

Macrocyclic ligands useful in MRI are derivatives of tetramine, cyclen (1,4,7,10-tetraazacyclododecane). 1,4,7,10-tetraazacyclododecane-1,4,7-tricarboxylic acid (DO3A) is itself not an ideal chelating agent for Gd^{3+} contrast agents because it is only heptacoordinate, but it serves as a starting point for the synthesis of numerous derivatives since a 12-atom ring appears to be ideal for MRI contrast agents. DO3A derivatives have been developed as neutral macrocyclic Gd chelates.

GdDOTA was the first marketed product in this series. GdDOTA is as safe as GdDTPA and has similar diagnostic efficacy. It targets no specific anatomical site or physiological function. Owing to a lower entropy loss in chelation, it releases less free Gd^{3+} into their physiological surroundings than do their linear acyclic counterparts. The major distinct advantage of GdDOTA over GdDTPA lies in its lower relative viscosities that it diffuse faster and pass through the injection needle more quickly for

a given applied pressure, thereby minimizing patient discomfort because a burning sensation due to osmolality is felt otherwise.
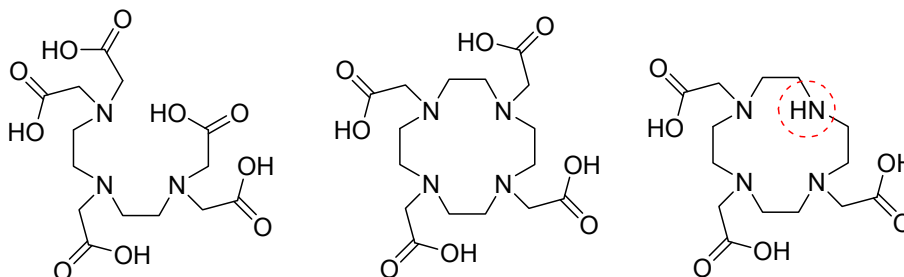
Figure 2. Structures of DTPA, DOTA, DO3A

New types of contrast agents are continually being developed to keep up with the request for more organ specific contrast media to be used in routine MR imaging as well as interventional MR to improve image quality. These constitute the 2nd generation of CAs which is also called as the affinity-targeted agents. They are directed to targets of interest more efficaciously, thereby achieving higher local concentrations at lower dosages. Increasing specificity (for organs, diseased tissue) by tagging to tissue-specific molecules by functionalization, altering lipophilicity, altering clearance properties by inducing reversible binding to circulating proteins, binding with macromolecular agents to affect the overall rotational correlation time and increasing the number of Gd^{3+} per unit molecule; use of MoAb and/or their associated fragmented; avidin as targeting vector; foliated Gd^{3+} are some glaring examples of this class. This concept has potential applications in imaging of important cellular and molecular moieties non-invasively in nano- and picomolar concentrations.

Imaging of cellular activities or physiological function using bioresponsive CAs resulted in development of the third generation of CAs. They are 'turned on' only in the presence of a threshold concentration of a specific molecule. The concept is to utilize injectable compounds of high tissue specificity with the ability to provide information of the physicochemical environment, when activated in response to a change in some biochemical event. The choice of the biochemical target, the chelates

9

and the physiological/pathological situation are critical deterministic parameters in the designing, development and applications of such agents in imaging the biological functions. The numbers of molecules in the first coordination sphere, the water exchange rate and the rotational correlation time have a strong effect on their relaxivity. As their relaxivity can be dictated by these specific changes in critical parameters of the cellular/tissue microenvironment, they generate a signal dependent on vital variables in their immediate microenvironment due to the modulation of relaxivity, thereby resulting in conditional enhancement of contrast. Thus, these smart/bioactivated contrast agents can act as a reporter of their biochemical microenvironment where they are distributed through various parameters as outlined below. In the context of smart CAs, the percentage change in relaxivity rather than absolute relaxivity is more important[27-32].

From medicinal chemist's point of view, many metallopharmaceuticals may be said to have been prepared on empirical ground taking mostly the analogy from designing of radiopharmaceutical for nuclear medicine, but research in certain instances in the designing of Smart Contrast Agents (SCAs) has been the result of sound reasoning based on theoretical concepts of drug design and molecular imaging. It is in order to look at depth on their development in particular.

Evolution of Contrast Agents
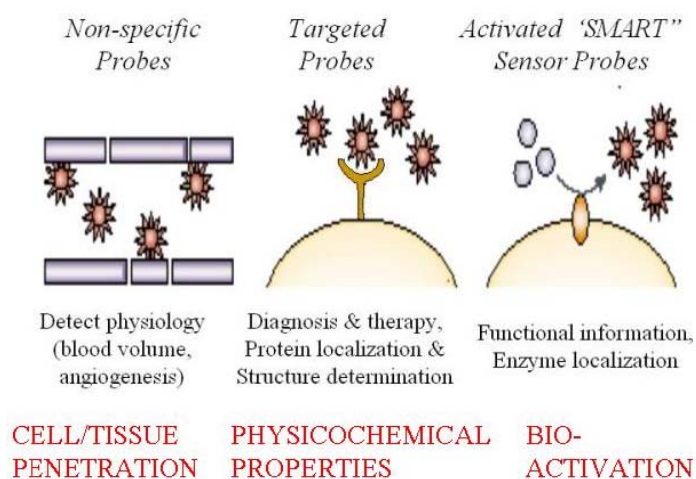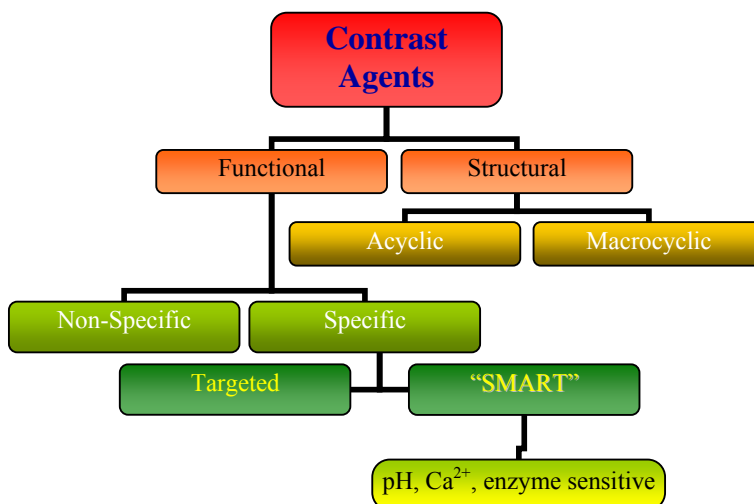
Schematic diagram of different generations of MR contrast agents

1.2.5. Smart/Bioactivated Contrast Agents as Functional Biochemical Markers.

The chemical structure of smart CAs could be tailored to respond to the changes in internal *milieu* by sensing the changes in biochemical environment upon specific activation. SCAs have been initially developed for applications in developmental biology to follow cell movements and lineages in developing frog embryos when injected at early stages of their development permitting the tracking of the labeled progeny cells in 3D MR images acquired from the embryo over several

days. CAs were subsequently used to track DNA delivery to specific cells, detect gene expression, and follow changes in the activity of enzymes beyond their value in basic research; all of these procedures have potential applications in clinical work in the area of gene therapy, etc. In principle, the relaxivity of these designer switchable magnetopharmaceuticals can be modified to be conditionally dependent on certain variables like enzymatic activities, signaling messenger, calcium ion concentration, ion channel functions, receptors systems, degree of glycation of proteins, temperature, pH, pO_2, gene expression and molecular recognition involved[33-40].

1.2.5.1. pH-activated contrast agents. pH is one of the most important factors for designing SCAs. We all know that the external medium is slightly basic but the opposite situation is observed in tumor tissues. The intracellular pH, on the other hand is almost the same for both kind of cells due to homeostatic mechanism. Therefore triggering MRI contrast agents by pH variation seems like a promising method for highlighting tumors. Increased glycolytic activity may cause a significant pH decrease in the extracellular region of certain tumors relative to surrounding healthy tissue. Overall pH is an important physiological indicator; many research groups have designed pH-sensitive contrast agents[41].

Aime *et al* have developed a pH-sensitive contrast agent with 30 Gd^{3+} chelates and 114 ornithine residues (Fig. 3a)[42].The chelates are conjugated to the amino acid chain via squaric esters, which readily react with amines. This agent is sensitive in the physiological range from pH 4.5 to 8.5. Hovland *et al* have developed a pH-sensitive CA which is a DO3A derivative with a tertiary amine containing side arm (Fig. 3b)[43]. The side arm amine contains two long alkyl chains. The Gd^{3+} complex of a DOTA-tetramide derivative has been prepared by Sherry *et al* who observed an interesting behavior of the agent with change of pH[35]. The relaxivity of the pH-sensitive contrast agent increases when pH increases from 4 to 6, but decreases between pH 6 to 8.5 and is constant between 8.5 to 10.5 (Fig. 3c). Aime *et al* have introduced hydrogencarbonate as pH sensitive contrast agent (Fig. 3d)[44]. It has been a ternary complex between a Gd^{3+} chelate and carbonate ions. Lowe *et al* employed a toluenesulphonamide as a pH labile ligation group in a Gd(DO3A) chelates; as the pH of a solution is reduced, the sulphonamide becomes protonated and dissociates from

the metal center (Fig. 3e)[45]. Later Woods *et al* observed a similar pH-sensitive dissociation in complexes with one *p*-nitrophenolic ligating group (Fig. 3f)[46].
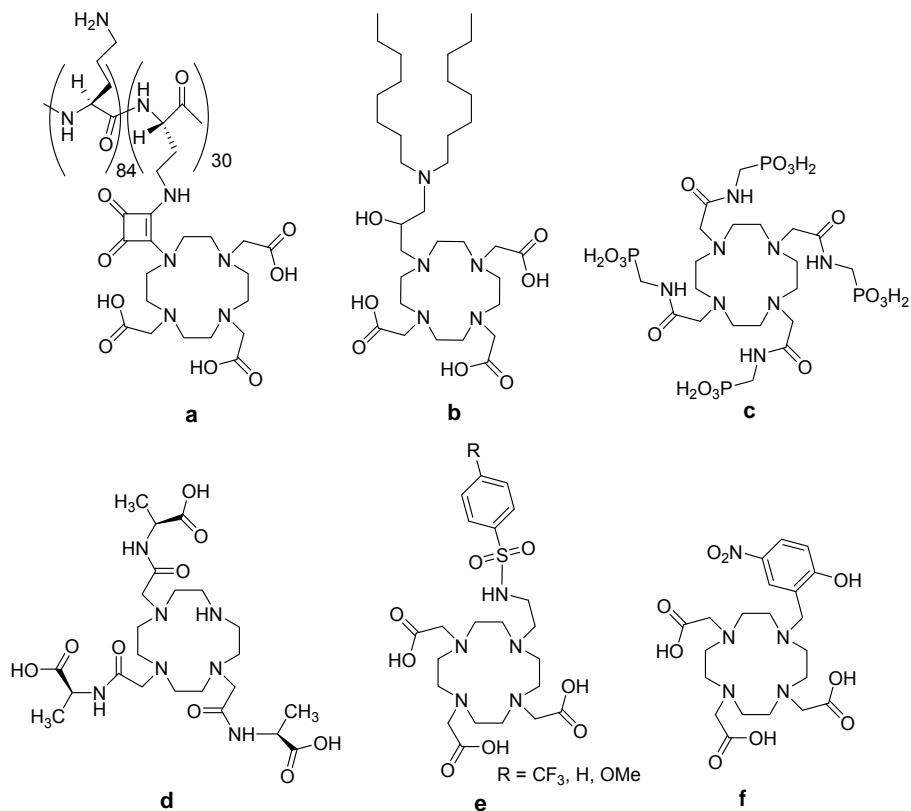
Figure 3. Reported ligands as pH sensitive CAs.

1.2.5.2. Metal ion concentration activated contrast agents. Abundant metals ions are essential or beneficial to life, such as calcium, magnesium, iron, copper etc. Its deficiency and excess may cause several deceases. *In vivo* determination of metal ion distribution is thus highly desirable and progresses have been towards the design of MRI SCAs sensitive to the concentration of metal ions[47].

The use of MRI to detect fluctuations in the concentration of vital metal ions has recently received much attention. The pioneering work in this area was conferred by Meade and co-workers who focused on the important role played by intracellular calcium(II) in signal transduction (Fig. 4a)[39,40]. Zinc(II) is another significant metal ion that regulates synaptic transmission and cell death. Selectively sensing Zn^{2+} ions

with contrast agents had been previously discussed by Hanaoka *et al* and Trokowski *et al* (Fig. 4b and 4c)[48,49]. Desreux *et al* embarked on an innovative approach based on self-assembly towards the development of iron-activated GdDO3A-based CA (Fig. 4d)[50]. Recently, Que *et al* introduced copper(II) sensitive SCA (Fig. 4e)[51].
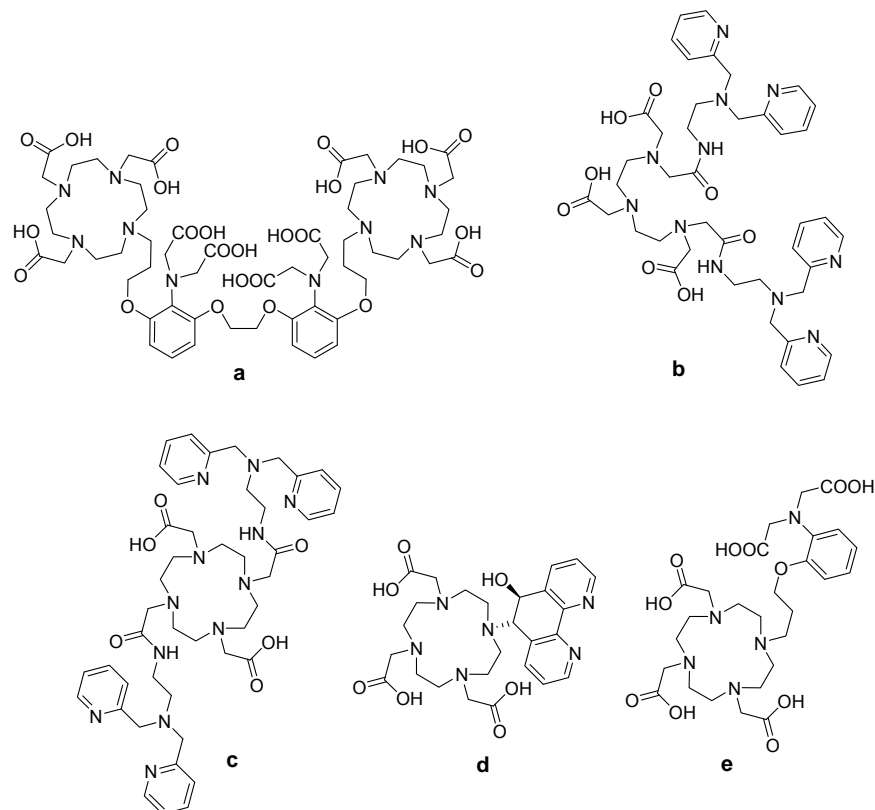
Figure 4. Reported ligands as metal sensitive CAs.

1.2.5.3. Enzyme-activated contrast agents. The elaboration of enzyme responsive MRI contrast agents could provide a means of measuring enzyme activity and enzyme localization. The sensitivity of MRI contrast agents to specific enzymes depends on the mechanism of their interaction. Provided the interactions between a contrast agent and an enzyme are sufficiently strong, a large increase in relaxivity will be observed due to the increased rotational correlation time of the adduct[52].

The first enzyme activated macrocyclic MR contrast agents was reported by Li *et al*, and was developed in response to the need to correlate developmental biological

events with gene expression during an imaging experiment[37,38]. The mechanism of the inner sphere T_1 relaxation phenomena (q) suggested a means to create a contrast agent with two distinct relaxation states, weak and strong (Fig. 5a). Anelli *et al* have synthesized a DTPA derivative which can detect carbonic anhydrase (Fig. 5b)[53]. The gadolinium complex contains a sulfonamide group in place of one of the carboxylic acid arms of the DTPA, helping it to selectively target the enzyme carbonic anhydrase. Perez *et al* have utilized the difference in relaxivity between solitary CLIO particles and that in close proximity to other CLIO particles to detect DNA cleaving agents (Fig. 5c)[54].
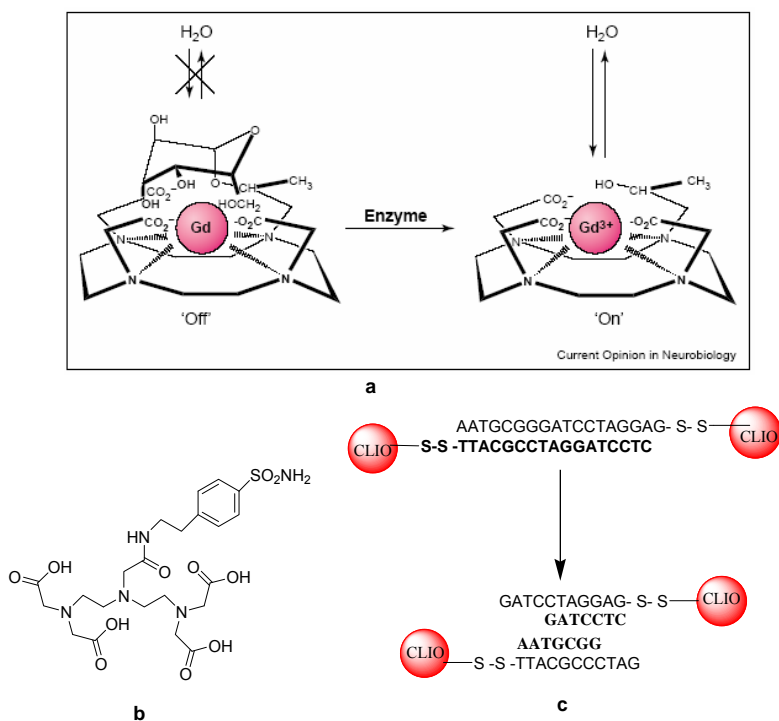
Figure 5. Reported compounds as enzyme sensitive CAs.

1.3. Project Conceptulations

The core project of the thesis deals with developing a MRI approach for detecting neuronal activity and to translate activity into changes in MR image contrast. A modulation of water relaxivity by contrast agents can be achieved by specific physiological or biochemical triggers that can be changes in pH, calcium ion, neurotransmitter concentration, or enzymatic activity. The purpose of this project was to design and synthesize a new class of gadolinium (Gd)-based calcium ion, pH, and enzyme sensitive "smart" contrast agents that are capable of reporting on the brain activity status by contrast change in MR images. The thesis also involves in development of Gd-based neuroanatomical tracers and some precursors towards targeted contrast agents which can be useful in MRI as well as optical imaging.

1.3.1. Objective

The broad objective of development and evaluation of the new exogenous smart contrast agents encompasses the following steps;

- Designing and development of innovative novel & clever exogenous smart/bioresponsive contrast agents those are responsive to the change in microenvironment surroundings.

- Fully characterization of those by NMR, mass spectrometry, elemental analysis, crystallography and HPLC.

- *In vitro* MR relaxation measurements simulating different physiological conditions like different pH, calcium ion concentration and enzymatic activity, dependent on the type of contrast agents.

- *In vivo* MR measurements in the rat and monkey to evaluate the exogenous contrast agents and its change upon functional activation.

1.3.2. Specific Aim

The specific aim in the proposed projects, we want to develop *novel exogenous smart/bioresponsive contrast agents*, which reflect-like hemoglobin in blood–*changes of neuronal activity*, but which are located in the extra-cellular space, independent of the hemodynamic and may reflect more directly changes in neuronal activity.

CHAPTER 2

New Class of Gd-based Targeted Contrast Agents for MR and Optical Imaging Derived from DO3A-ethylamine

2.1. Introduction

Targeted CAs localize to specific molecular targets with high affinity and specificity, thus enhancing the diversity of MR applications. They are able to recognize specific target molecules inducing an enhancement of water proton relaxation rate on binding with the target molecule[17,55,56]. A diverse variety of targeting ligands have been chemically coupled with CAs depending on the nature of final and specific application of the CA. Asialoglycoproteins have been used for liver-specific application due to their high affinity for ASG receptors located uniquely on hepatocytes[57,58]. Tumor selective accumulation of porphyrin based CA is attributed to high affinity of these compounds to necrotic tissue[59]. DTPA-bisamide based ligands have been used for diagnosis of several types of malignancy on the basis of molecular recognition of sialic acid residues[60]. Monoclonal antibodies (MoAbs) and antibody fragments provide highly specific target recognition and binding for CAs. Breast cancer cells expressing Her-2/neu receptors were imaged *in vivo* with a two step labeling protocol using biotinylated Herceptin MoAb and avidin-GdDTPA conjugates[61].

Based on previous reports on the synthesis and applications of targeted CAs, we have developed straightforward synthetic routes for the preparation of targeted CAs derived from DO3A-ethylamine (DO3A-EA, **7**), with potential for further conjugation with other molecules containing appropriate reactive groups (Fig. 6).

In an effort to obtain a precursor that can enable noninvasive imaging of imperative processes *in vivo* using MRI, Gd loaded DO3A-ethylamido-biotin (**Gd-9**) has been synthesized by conjugating DO3A-EA with biotin. Similar systems based on DOTA after loading with metallic radionuclide's like yttrium or indium are also being explored at *in vivo* level for application in radioimmunotherapy[62-66]. This technology has found useful application in the medical field to *in vivo* localize and image cancer cells and to pretarget drugs to tumors[67] where MoAb-avidin/biotin act as targeting macromolecule/effecter molecule pairs[68]. Pretargeting approach takes advantage of the fact that biotin binds strongly to the proteins avidin and streptavidin resulting in signal amplification.

The second conjugate GdDO3A-ethylthiourea-FITC (**Gd-12**) possesses fluorophore fluorescein on one arm and is intended to obtain a precursor for bimodal imaging where the macrocyclic part serves for MR visualization and FITC part for optical imaging. CAs anticipated for cell labeling can be designed from this precursor for tracking cells *in vivo* by MR and/or fluorescence imaging. Cell therapies, in last few years, have reached new heights with some studies also entering into clinical trials. But the pace of development of an effective cell based therapy has been slowed down by the paucity of technology for tracking cells' fate *in vivo*. Recently de Vries *et al* have reported the use of MRI for tracking transplanted cells and obtained detailed view of cells biodynamic *in vivo*[69-71]. Agents based on the use of bimodal imaging have been applied to disease detection by attaching a target-specific site[72] or to observe cellular localization and migration[73-75]. This gives rise to the need for developing intracellular CAs that will help in obtaining improved contrast and our precursor can serve as a template for obtaining them.
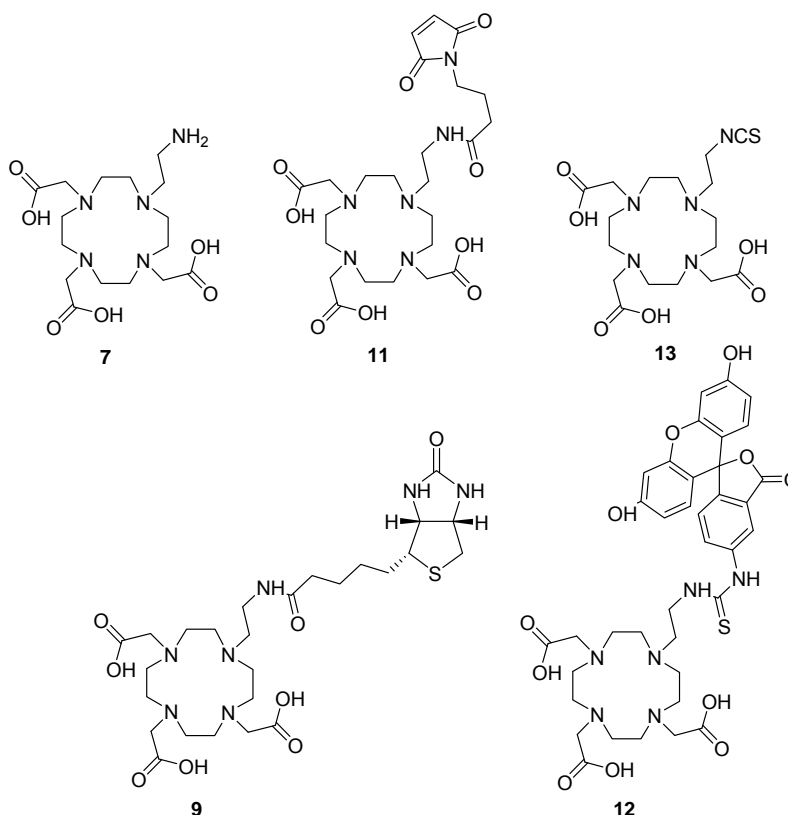
Figure 6. Studied ligands

Additionally, in order to encompass the complete range of chemical reactivity, the nucleophilic "arm" of DO3A-EA was exchanged with electrophile groups, and two new precursors were designed and synthesized. The amino group of DO3A-EA is transformed to isothiocyanate, resulting in the formation of DO3A-ethyl-isothiocyanate (**13**). This molecule possesses selective reactivity towards amines, thus providing the possibility of using it as a precursor for conjugation with biomolecules like proteins, peptides and MoAbs[76-79]. The other precursor, DO3A-ethylamidopropyl-maleimide (**11**), obtained by coupling of amine with 4-maleimidobutyric acid, further enhances the diversity of application by exploiting its reactivity towards sulphydryl groups and therefore, prospects for combining with thiol containing peptides, dendrimers, oligonucleotides[72,80-82]. These precursors can serve as important building blocks in the designing of targeted CAs with desirable traits.

2.2. Experimental Section

2.2.1. *In vitro* Cell Studies of Gd-12

Cell experiments were done in 96 well microplates by inoculation of NIH-3T3 mouse fibroblasts (1 x 10^4 cells/well) cultured in Dulbecco's Modified Eagle's Medium supplemented with 10% foetal bovine serum, 4 mM L-glutamine, 100 μg/mL streptomycin and 100 U/mL penicillin (all purchased from Biochrom AG, Germany). After 24 hours cells were incubated with various concentrations (up to 150 μM) of **Gd-12** for additional 18 hours. After repeated cell washing with Hanks' buffered saline (Biochrom AG, Germany), cell related FITC fluorescence (Ex 485 nm/Em 530 nm) was evaluated in a multiplate reader (BMG Labtech, Germany). Subsequently, fluorescence microscopy was performed with the same cells on a Zeiss Axiovert 40 CFL (Germany) to observe the cellular localization of **Gd-12**.

Evaluation of cytotoxicity was done by addition of propidium iodide and a detergent with subsequent fluorescent reading (Ex 530 nm/Em 645 nm). In addition, by combination of the two fluorescence readings correlation is established between the FITC fluorescence and the total cell number per well. Experiments were run three times each with six replicates. Statistical analysis was performed by ANOVA with Dunnett's post test. P values < 0.05 were considered significant.

2.2.2. Sample Preparation for Relaxivity Measurements

Different concentrations (0.8 mM, 0.6 mM, 0.4 mM, 0.1 mM) of **Gd-9** and (1 mM, 0.7 mM, 0.4 mM, 0.1 mM) of **Gd-12** were prepared in phosphate buffer in 1.5 mL Eppendorf tubes at physiological pH to measure relaxivity.

The measurement of the relaxation rates R_1 and R_2 (longitudinal and transverse relaxation) of Gd-complexes were performed at 300 MHz (7T) on a vertical 7T/60 cm MRI Biospec system (Bruker Biospin, Germany)[83]. Up to 16 tubes could be measured simultaneously. The relaxation rate measurements of the samples were performed at room temperature (~21˚C).

2.2.3. MR Study of Avidin-Gd-9 Interaction

To measure the enhancement of R_1 and R_2, MRI experiments were performed with increasing concentrations of avidin (Fluka, Germany) proportional to constant concentration of **Gd-9** (0.4 mM) incubated for 3 h at 37°C. The longitudinal relaxivity (r_1) and transverse relaxivity (r_2) was determined from concentration dependent measurements of relaxation rates (R_1 and R_2) of **Gd-9**.

2.2.4. *In vitro* MR Studies of Gd-12 with Cells

For MR imaging of cells, exponentially growing 3T3 cells were labeled with 80 and 150 μM **Gd-12** in 175 cm^2 tissue culture flasks for 18h. After repeated washing with Hanks' buffered saline, cells were trypsinized, centrifuged and re-suspended in 1.5 mL Eppendorf tubes at the rate of 1 x 10^7 cells in 500 μL complete DMEM. Cells were allowed to settle before making MR measurement. As control served tubes with only medium, cells without **Gd-12**, and cells re-suspended in medium containing the extracellular contrast agent Magnevist® (Schering, Germany) at 50 μM.

MRI of the cell pellets was also performed at 300 MHz (7T) using T_1- and T_2-weighted spin-echo sequences at room temperature (~21˚C), see above description.

The axial slice of interest was positioned through the cell pellet. Experimental parameters for T_1 were: field of view 17 x 6.9 cm^2, matrix 512 x 256, slice thickness 1.5 mm, SW 70 kHz, TE 14.6 ms, TR 40-6000 ms, 2 averages (logarithmic time steps, 80 images). For T_2, similar parameters were used, but TR = 8 s and TE = 15-675 ms (linear time steps, 45 echoes).

Sagittal images were obtained with field of view 11.3 x 6.9 cm^2, matrix 256 x 256, slice thickness 2 mm, SW 70 kHz, TE 10.9 ms, TR 1600 ms, 4 averages for T_1 weighted images, and field of view 12.5 x 6.8 cm^2, matrix 256 x 256, slice thickness 2 mm, SW 70 kHz, TE 90 ms, TR 8000 ms, 2 averages for T_2 weighted images.

2.3. Results and Discussions

2.3.1. Synthesis of Ligands

DO3A-EA (**7**) is a bifunctional ligand bearing amine group that is readily reactive towards most electrophiles such as aldehydes, carboxylic acids and isothiocyanates to form various molecules for the development of targeted CAs. Though DO3A-EA has already been part of several synthetic schemes[84-86], we report here the application of DO3A-EA in a new context, as precursor for the synthesis of CAs to design relaxometric MRI as well as optical probes. We have developed dual synthetic routes to obtain **7** depending on the choice of protection and deprotection method (Scheme 1).

In the first route **7** was obtained from cyclen in 39% yield over 3 steps, by the reaction with *tert*-butylbromoacetate to get the tri-substituted product **3**[87]. Alkylation with **1**[88] gave **4** and the corresponding carboxylate derivative **7** was obtained by cleaving the *tert*-butyl groups by the treatment of neat TFA at room temperature. Attempts for the selective deprotection of Boc group in compound **4** led to deprotection of *tert*-butyl ester groups and the formation of a multi-product mixture. Thus, an alternative 3-step route was designed also starting from cyclen to form the methyl ester **6**. After monoalkylation of cyclen[86] with **1**, **2** was isolated in 63% yield. By alkylation with methylbromoacetate, ligand **5** was obtained and the acid labile Boc protecting group of amine was cleaved with TFA to get methyl protected ligand **6** and subsequent treatment with LiOH gives **7**.

After the successful synthesis of precursors, the bioconjugate ligand **9** was synthesized in a two step reaction (Scheme 2). Biotin conjugated DO3A-EA compound **8** was obtained by the coupling of biotin with ligand **6** using EDC/HOBt/NMM in DMF. The choice of such mild conditions for the conjugation of biotin with DO3A-EA and amide bond formation was mandatory due to the sensitivity of biotin towards harsh conditions (temperature etc). In the following step,

22

ligand **9** was obtained in 77% yield by deprotection of methyl groups with LiOH in THF:MeOH:H$_2$O (3:2:2).
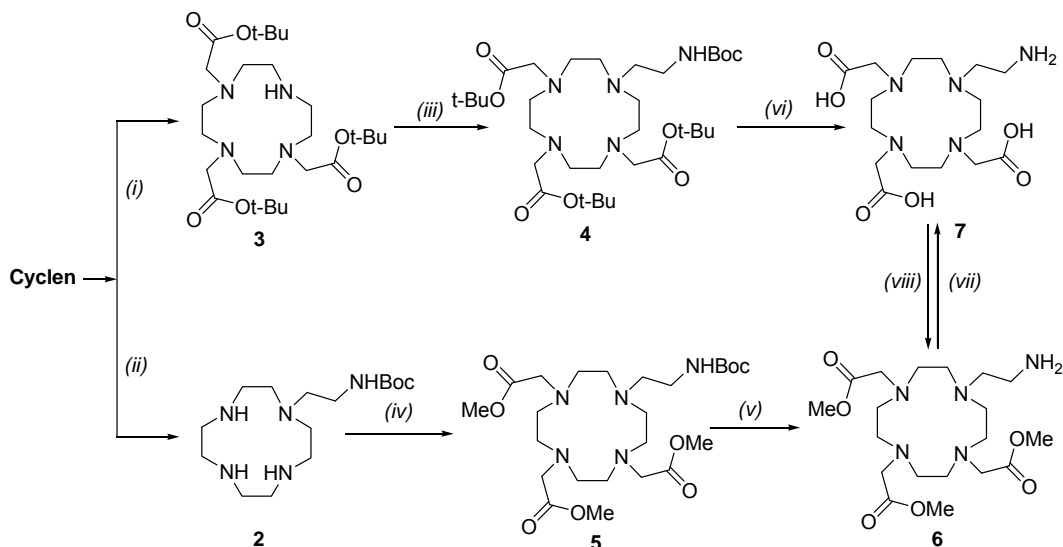
Scheme 1. Reagents and conditions: *(i)* *tert*-butylbromoacetate, NaHCO$_3$, MeCN, 71%; *(ii)* *N*-Boc-bromoethylamine (**1**), toluene, 68%; *(iii)* **1**, K$_2$CO$_3$, DMF, 72%; *(iv)* methylbromoacetate, Na$_2$CO$_3$, MeCN, 82%; *(v)* MeOH, TFA, 80%; *(vi)* TFA, 64%; *(vii)* LiOH;THF;MeOH (3:2:2), water, 64%; *(viii)* MeOH.HCl, 95%.

In a similar manner, a novel precursor **11** bearing maleimide arm was synthesized when starting from **6** as described for biotin conjugates. It is well known that the maleimide group reacts selectively with sulphydryl groups to form macromolecules[76-79]. Two maleimide conjugates were synthesized, compound **10**, obtained from compound **6** by using 4-maleimidobutyric acid and EDC/HOBt/NMM in DMF at room temperature, and ligand **11**, obtained by deprotection of methyl groups in the presence of LiOH (Scheme 2).

Two molecules were synthesized in single step reactions when starting from **7** (Scheme 3). The first ligand **12** possessing two moieties, fluorescence unit, and the macrocycle which can complex with paramagnetic metals was synthesized by coupling of FITC with **7** at pH 8. During the reaction, pH was not allowed to exceed

8.5 since at pH > 9, a lactone cleavage on FITC part occurs, leading to the formation of a side product. The second molecule (**13**) was synthesized in one step by transforming the amino group into NCS with thiophosgene. The yield of the reaction was moderate (58%), although a molecule obtained this way provides possibility for further couplings with amine containing organic and bioorganic molecules to form the desirable product[72,80-82].
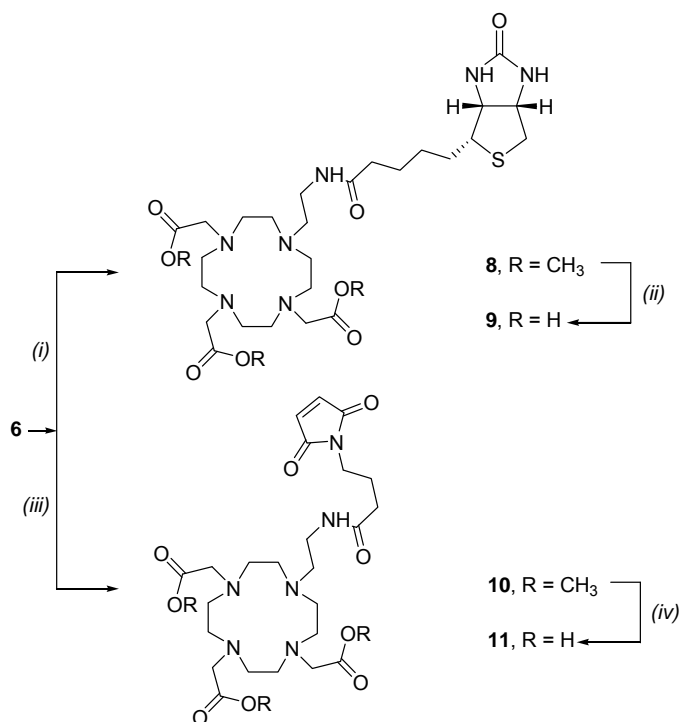
Scheme 2. Reagents and conditions: *(i)* biotin, NMM, HOBt, EDC, DMF, 55%; *(ii)* LiOH, THF, MeOH, water, 77%; *(iii)* 4-maleimidobutyric acid, NMM, HOBt, EDC, DMF, 66%; *(iv)* LiOH, THF, MeOH (3:2:2), water, 86%.

Finally, Gd^{3+} complexes were synthesized for ligands **9** and **12** (Fig. 7). During loading $GdCl_3.6H_2O$ in biotin containing ligand **9** reaction temperature was kept under 60°C because of possible degradation of biotin moiety. For loading Gd^{3+} in FITC containing compound **12,** pH of the solution was maintained in the range 7-8, as at lower pH the precipitation of the ligand was observed.

As a summary of the synthetic schemes described above, we would like to point that the presented straightforward and facile synthesis, although not quite novel,

is very suitable for the easy preparation of precursors in the design and preparation of targeted CAs. With the same methodology, it was possible to synthesize various targeted model probes, quite different in their behavior and potential application, which should actually be the major advantage of such approach.
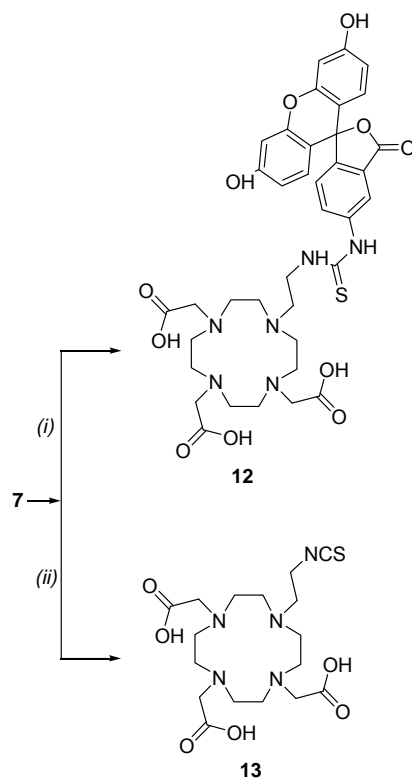
Scheme 3. Reagents and conditions: *(i)* FITC, water, Na_2CO_3, 55%; *(ii)* $CSCl_2$, water, CCl_4, 59%.
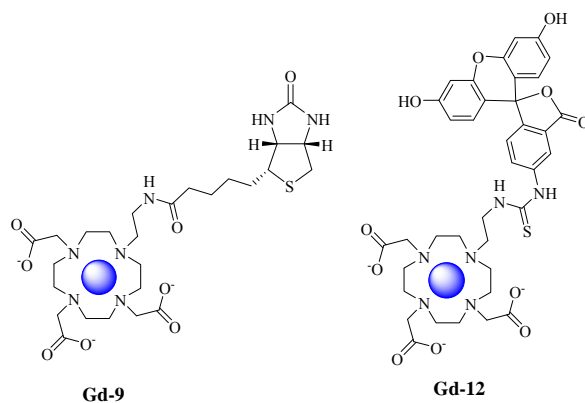
Figure 7. Structures of Gd^{3+}-complexes of **9** and **12**.

2.3.2. Biochemical Applications

2.3.2.1. In Vitro Relaxometry of Gd-9. The biotin-avidin association has found widespread applications in biomolecule detection, medical diagnostics, immunoassays, cytochemistry and nano-science[89-93]. This is primarily due to the strength of the interaction between the ligand and the tetrameric protein ($K_d \approx 1.3$ x 10^{-15} M) which in turn allows for the cross-linking of different biotinylated molecules[93].

To scrutinize the effect of binding on the longitudinal and transverse relaxivities, we performed MRI experiments with increasing concentrations of avidin proportional to constant concentration of **Gd-9** (0.4 mM). A linear enhancement in relaxivity was observed demonstrating strong binding of **Gd-9** in the biotin binding pocket of tetramer avidin (Fig. 8). This gain in relaxivity suggests a decrease in molecular rotational correlation time τ_R.
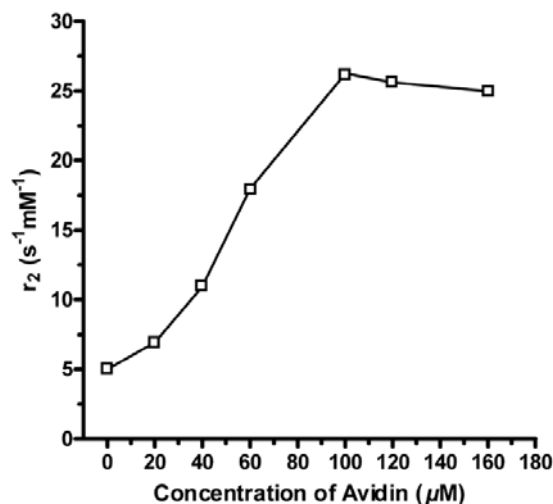
Figure 8. *In vitro* MR measurement of transverse relaxivity, r_2 **Gd-9** with varying concentrations of avidin. MR experiment was performed at 300 MHz (7T) and 21°C with constant concentration of **Gd-9** (400 μM) and increasing amount of avidin in different tubes. A linear relaxation enhancement was observed up to 100 μM (0.25 equivalents). At higher ratios relaxivity r_2 remained constant. [Error for all r_2 values was less then ($\pm$ 0.6) s^{-1}mM^{-1} and is not displayed].

Similar to literature reports, proposing that one avidin molecule strongly binds four equivalents of biotin[94], we obtained saturation in relaxivity at ratios higher than 4:1 between **Gd-9** and avidin. MR longitudinal relaxivity, $r_1 = (3.32 \pm 0.03)$ s^{-1}mM^{-1} and transverse relaxivity, $r_2 = (5.02 \pm 0.14$ s^{-1}mM^{-1}) of **Gd-9** (0.4 mM) was observed at pH 7.4. The mixture of **Gd-9** and avidin showed maximum relaxivity enhancement of 45% in $r_1 = (4.82 \pm 0.09)$ s^{-1}mM^{-1} and 423% in $r_2 = (26.24 \pm 0.58)$ s^{-1}mM^{-1} relative to the unbound biotinylated Gd^{3+} complex.

In future applications, the MRI contrast sensitivity can be therefore improved by designing CAs using the above precursor, as the biotin-avidin association is expected to enhance the signal by means of *in situ* accumulation of the agent. Avidin has been already utilized for drug delivery through the blood brain barrier[93]. It is important for future non-invasive, e.g. human research applications, which do not afford intracranial injections. Additionally, there is possibility to utilize this precursor for diagnosis and imaging using MR, based on pretargeting approach in combination with avidin coupled MoAbs. Pretargeted delivery of radionuclides has shown promising results in treatment of lymphoma and solid tumors but remains as a sophisticated approach needing optimization of dose and administration schedules[63-65]. Although our model precursor exhibits probability for use in MR imaging but translation to a system for *in vivo* application is hampered by certain drawbacks. Hydrolysis of DTPA-biotin and DOTA-biotin by endogenous biotinidase has been reported[95]. This problem has been successfully overcome by chemically modifying the structure in order to effectively block biotinidase[66,96]. In addition, endogenous biotin levels (10^{-8}-10^{-7} mol/L), immunogenicity of avidin and high and prolonged renal uptake markedly affect efficacy of avidin and streptavidin based pretargeting strategies[63,67,97]. Efforts are being made to develop an appropriate delivery method to prevail over these predicaments[98,99].

2.3.2.2. In Vitro Cell Studies of Gd-12. MR relaxivity of **Gd-12** at pH 7.4 was $r_1 = (5.36 \pm 0.05)$ s^{-1}mM^{-1} and $r_2 = (7.52 \pm 0.16)$ s^{-1}mM^{-1}. *In vitro* studies of this Gd^{3+} loaded complex were done with NIH-3T3 mouse fibroblast cell cultures to demonstrate its potential for developing multifunctional CAs. **Gd-12** up to 150 μM did not show significant cytotoxicity after 18 hours of incubation (propidium iodide

assay), although a decrease in number of cells was observed at concentrations above 100 μM (Fig. 9).
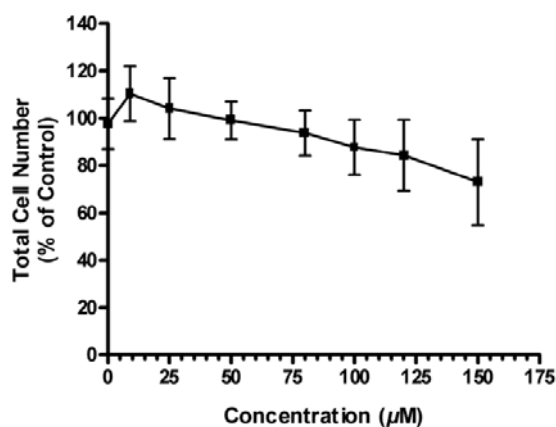
Figure 9. Cytotoxicity of **Gd-12** at different concentrations. Calculated from same plates after addition of PI and a detergent followed by measurement of Pi fluorescence. At concentrations of **Gd-12** higher than 100 μM, a decrease in cell number was observed which was not statically significant compared to control. Values are means ± SD (n = 3).
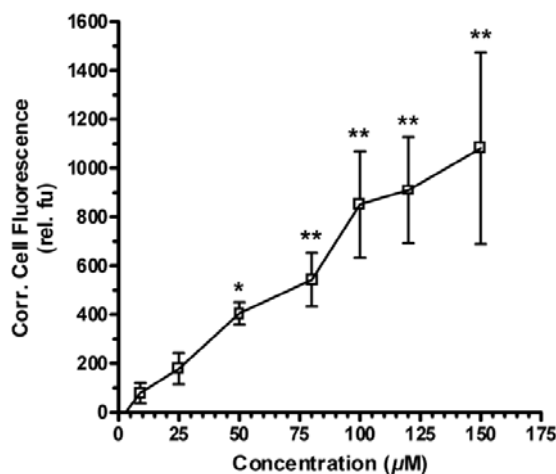
Figure 10. Increase in fluorescence intensity of cells labeled with varying concentrations of **Gd-12**. Cells were incubated with various concentrations of **Gd-12** for 18 h, given several washes followed by fluorescein fluorescence measurement. After the addition of propidium iodide (PI) and detergent, PI

fluorescence was measured to correlate the cell bound fluorescein fluorescence with cell number resulting in corrected cell fluorescence. Values are relative fluorescence units (rel. fu) displaying mean ± SD (n = 3); *p < 0.05; **p < 0.01, statistically significant differences compared to control.

However, a concentration dependent increase in cell related FITC fluorescence was observed indicating cell binding/internalization of the compound (Fig. 10). At concentrations higher than 50 μM this increase was statistically significant. Fluorescence microscopy of living cells displayed a faint but detectable uptake of the compound into cells at concentrations higher than 50 μM. Figure 11 shows examples of cellular localization of **Gd-12** after incubation with 80 and 150 μM for 18 h and subsequent washing. Beside a faint diffused fluorescence (asterisks), vesicles showing brighter fluorescence (arrows), were located around the nuclear area of the cells indicating to an endosomal uptake mechanism.

Figure 12 shows results of the MR study on 3T3 cells. The presence of Magnevist$^\circledR$ in medium enhanced the contrast in T_1-weighted images by increasing brightness of supernatant, whereas there is almost no difference in T_2. Cells themselves induce only a minor change in T_1-weighted images in comparison to medium only. In T_1-weighted images, the cell pellet is distinguished by the darker image intensity at the bottom of the container which can be viewed also in the absence of any CA. **Gd-12** labeled cells show a sufficient uptake of the compound to enhance contrast in T_1- and, especially, T_2-weighted images at concentrations above 80 μM. The corresponding relaxation rate R_1 in the cell layer was significantly increased in comparison to control to 121% and 131% of control for 80 μM and 150 μM, respectively. A more pronounced enhancement in R_2 was observed; R_2 increased to 144% and 152 % of control, respectively.

Interestingly, contrast enhancement in T_2-weighted images was found to be larger in comparison to T_1. The pronounced T_2 shortening may be caused by the accumulation of the compound in intracellular vesicles inducing local magnetic field in homogeneities due to compartmentalization. Such a behavior is generally observed in the presence of supraparamagnetic particles with large magnetic moment, which also show strong compartmentalization[100].
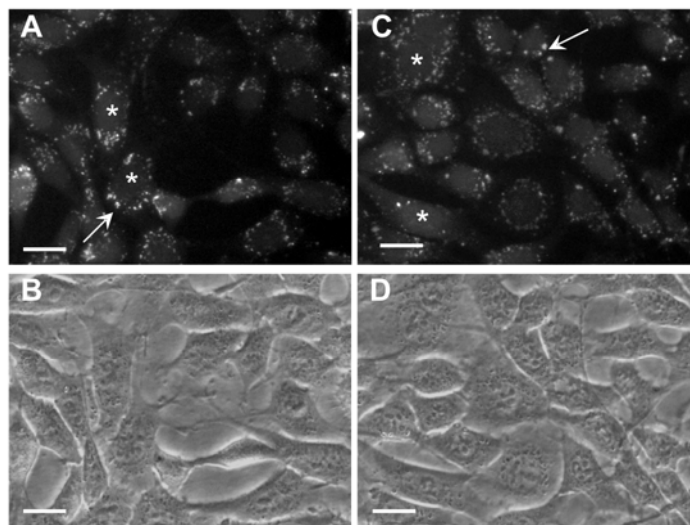
Figure 11. Optical evidence for intracellular localization of **Gd-12** in unfixed NIH 3T3 cells. Cells were incubated with 80 (A, B) and 150 μM (C, D) of **Gd-12** for 18 h as described in materials and methods. A and C show fluorescein fluorescence and B and D corresponding phase contrast pictures. The scale bars represent 20 μm. Arrows exemplarily point towards vesicles while asterisks indicate diffused fluorescence.
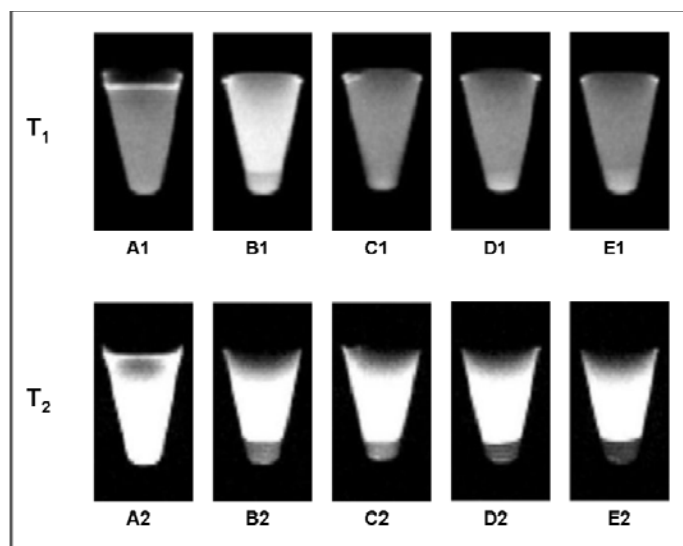
Figure 12. T_1- and T_2-weighted images of control and NIH 3T3 cell pellets labeled with **Gd-12** for 18 h. (A1-E1): T_1-weighted images. (A1) Medium only. (B1) Pelleted cells in medium with 50 μM Magnevist®. (C1) Pelleted cells in

medium. (D1) Pelleted cells labeled with 80 μM **Gd-12** in medium. (E1) Pelleted cells labeled with 150 μM **Gd-12** in medium. (A2-E2): Respective T_2-weighted images.

Our results indicate that this model agent is detectable inside cells by both MR and fluorescence methods. Thus, it can serve as a precursor to develop substances that can be used for bimodal (MR and fluorescence) imaging, as well as for development of intracellular contrast agents optimized for cellular internalization. In addition, this molecule can be further modulated for disease detection and diagnosis, gene/drug delivery, elucidating signaling pathways or to study biological and biochemical mechanisms[100,101]. For early disease detection, a bimodal contrast agent Gd^{3+}-DTPA coupled with Oregon Green 488 containing an angiogenesis-specific site cNGR has been recently reported[72]. A similar dual mode approach was used by Modo *et al.* to investigate how neural stem cells migrated and integrated into various brain regions in the same individual over time[73,74]. Aime *et al.* used Gd-chelate of HP-DO3A as a T_1-agent for MRI visualization, with the corresponding Eu-chelate as a reporter in fluorescence microscopy to detect localization and migration of stem cells[75].

2.3.3. Conclusions

In conclusion, we report the potential of the ligand DO3A-EA as a multipurpose precursor, from which various targeted CAs can be synthesized after single step conjugation with organic molecules/biomolecules. With such methodology two new targeted CAs and two new precursors were synthesized and characterized. MR experiments verified that the strong and specific interaction between biotin and avidin can be proved with the relaxivity of biotin functionalized DO3A-EA (**Gd-9**). Cell studies and relaxivity measurement indicate that FITC conjugated DO3A-EA (**Gd-12**) can serve as a model to develop agents that can be used for imaging both by MR and fluorescence methods. Maleimide functionalized DO3A-EA (**11**) and DO3A-ethyl-isothiocyanate (**13**) precursors were synthesized having a potential for the specific binding with biomolecules via sulphydryl and amino groups, respectively. Additionally, the presented precursors **7**, **11** and **13** cover the entire range of reactivity for the coupling to electrophilic and nucleophilic groups. They possess a great potential for coupling with biological molecules, proteins, vitamins and antibodies for the ease and facile synthesis of various kinds of targeted contrast agents.

31

CHAPTER 3

Synthesis and Characterization of Lanthanide Complexes of DO3A-Alkylphosphonates: pH sensitive Smart Contrast Agents

3.1. Introduction

The development of new DO3A based lanthanide(III) complexes with the potential application as contrast agents in MR imaging is currently a great challenge for many scientists, in particular for their use in the high field magnets. The special requirements for these contrast agents have to combine a fast water exchange rate with effective coupling of the gadolinium–water vector and the tumbling of the complex as outlined in the literature[102-104]. In addition, a greater contribution from the water molecules in the second coordination sphere is desirable[103,105]. Introduction of different functional groups such as alkylphosphonates at the fourth nitrogen of the DO3A molecule is shown to result in improved relaxivity properties of the complexes[25,106]. Gd^{3+} complexes of phosphonate-containing chelates, generally, have the advantage of a relatively fast water exchange rate due to a greater steric demand of the phosphonic acid moiety and the presence of a second-sphere water shell, which also contributes to the overall relaxivity[107]. It is also known that the phosphonic/phosphinic acid derivatives and their complexes differ in some properties (size and shape of the coordinating group, overall hydrophilicity or acidity/basicity of the ligands) when compared with their acetate analogs[108,109].

A number of phoshonate containing lanthanide complexes and comparisons with carboxylate analogues have been reported in previous years[110-113]. It has been shown that the presence of two phosphonate moieties decreases the number of water molecules in the inner sphere, but increases the second hydration sphere, thus enhancing the relaxivity properties of the complexes[112]. It has also been suggested that the relaxivity of the phosphonate containing derivatives increases at low pH, due to protonation of the phosphonate groups. This process was used by Sherry and co-workers to prepare a molecule containing amidophosphonate groups exhibiting pH-sensitivity close to the physiological range (pH 6-7)[35]. Recently, the possibility for *in vivo* application was demonstrated by the determination of the pH of tumour tissue. pH maps with improved spatial resolution were obtained compared to the MR spectroscopic methods used before[114].

A series of publications describes methylphosphonate derivatives of DO3A[115-117]. The compounds exhibit a similar structure to those of DOTA lanthanide(III)

complexes and exist as a mixture of two isomers containing one water molecule in the inner sphere. The alteration of the distance between the phosphonate group and the DO3A core by appending aliphatic chains of various lengths could lead to different interactions between the lanthanide ions and the phosphonate side chain. This allows a controlled variation of the coordination environment of the lanthanide(III) centre leading to new properties of the complexes.

Therefore, phosphonate complexes seem to be promising systems for the design and application of ligands and CAs, particulary for high-field MRI. Herein, we report the facile synthesis of two new DO3A based ligands (**16** and **17**, Fig. 13) and the physicochemical investigations of their Gd^{3+} and Eu^{3+} complexes. The studied compounds differ by the polarity/charge of the phosphonate groups, thereby defining the coordination properties of the compounds towards water and hence influencing relaxivity.

Ln-16   **Ln-17**
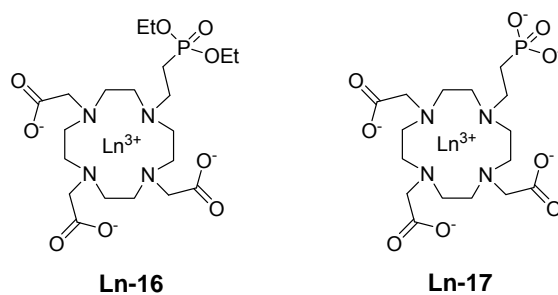
Figure 13. Studied phosphonate containing Complexes

3.2. Experimental Section

3.2.1. Luminescence studies

Inductively coupled optical emission spectrometry for $[Eu^{3+}]$ analyses was performed using a Jobin-Yvon Ultima 2 spectrometer. Lifetime or emission spectral measurements were measured with a Perkin-Elmer LS 55B or a Fluorolog-3 (Jobin-Yvon/Instruments s.a.) following direct excitation of the Eu ion at 397 nm followed by monitoring the integrated intensity of light (620 nm for europium) emitted during a fixed gate time, t_g, a delay time, t_d, later. At least 20 delay times were used covering 3 or more lifetimes. A gate time of 0.1 ms was used, and excitation and emission slits

were set to 10 and 2.5 nm band-pass respectively. The obtained decay curves were fitted to the equation below using Microsoft Excel:

$$I = A_0 + A_1 \exp(-kt) \qquad \text{(Equ. 3)}$$

Where I = intensity at time t after the flash, A_0 = intensity after the decay has finished, A_1 = pre-exponential factor and k = rate constant for decay of the excited state.

3.2.2. Sample Preparation for Relaxivity Measurements

The measurement of the longitudinal and transverse relaxation rates (R_1 and R_2) of the complexes **Gd-16** and **Gd-17** were performed at 300 MHz (7T) on a vertical 7T/60 cm MRI Biospec system (Bruker Biospin, Germany), using a protocol described previously[83]. Up to 16 tubes could be measured simultaneously. The relaxation rate measurements of the samples were performed at room temperature (21 $^{\circ}$C). Different concentrations of **Gd-16** and **Gd-17** (1 mM, 0.7 mM, 0.4 mM, 0.1 mM) were prepared in 1.5 ml Eppendorf tubes. The pH of the solutions was adjusted by addition of small quantities of solid lithium hydroxide or paratoluenesulfonic acid.

To study the interaction of the complexes with the proteins, the MRI experiments were performed with increasing concentrations of human serum albumin (HSA) (Aldrich, Germany) proportional to constant concentration of **Gd-16** (0.5 mM) incubated for 2 h at 37 °C.

3.3. Results and Discussions

3.3.1. Synthesis of Ligands

Ligand design was based on cyclen-type ligands. The macrocycle contains three carboxylate groups; along with the nitrogen atoms of the cyclen ring these form stable complexes with Ln^{3+} ions. One nitrogen atom was appended with a phosphonic acid linked via an ethyl chain which acts as a potentially responsive group by participating in the Ln^{3+} ion coordination with a differing affinity to the carboxylate. During the synthesis, compound **16** with the ethyl protected phosphonates was obtained and their Gd^{3+} and Eu^{3+} complexes were investigated as charge neutral systems.
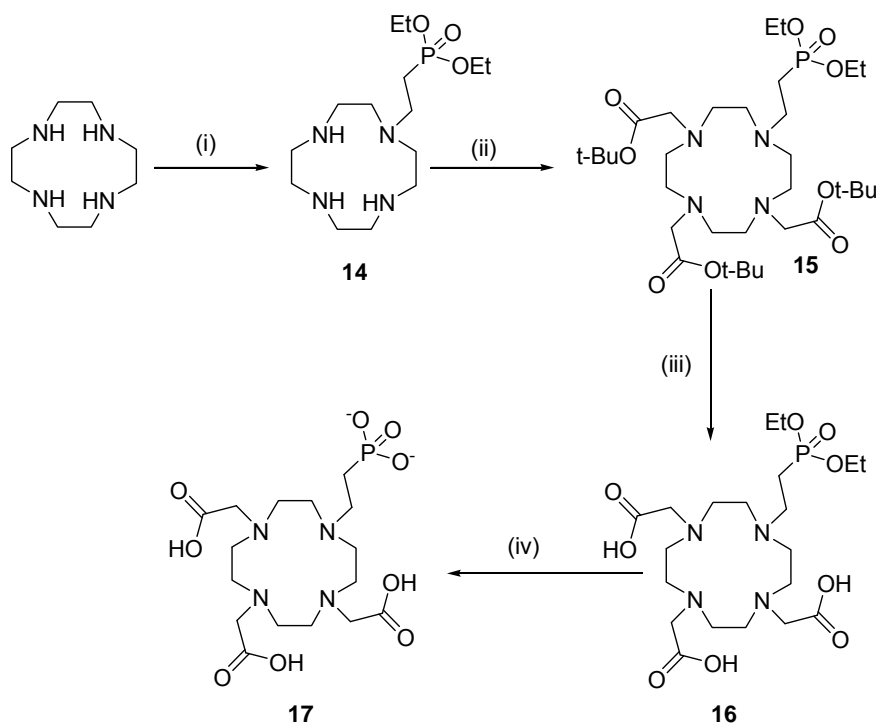
Scheme 4. *Reagents and conditions:* i) diethyl-2-bromoethylphosphonate, LiOH, EtOH:H$_2$O (9:1), 43%; ii) *tert*-butylbromoacetate, Na$_2$CO$_3$, MeCN, 76%; iii) TFA, 72%; iv) HBr (33% in CH$_3$COOH), 69%.

Ligand **17** was obtained starting from cyclen in a four-step procedure (Scheme 4). For **17,** the more convenient and logical route (alkylation of **3** with diethyl 2-bromoethylphosphonate) was tried in the presence of several bases (Na$_2$CO$_3$, K$_2$CO$_3$, NaOH, NaH), solvents (CH$_3$CN, DMF) and temperatures (r.t.→70 ^{o}C) in order to obtain **15**. Even using harsher conditions and long reaction times, most of the reactant **3** was still present in the reaction mixture, along with a maximum of 15% of the product **15**. The reason for this was found to be an elimination of diethyl 2-bromoethylphosphonate under basic conditions, which led to a small yield of the desired product. Instead, the first step in the synthesis of **17** was a monoalkylation of cyclen with diethyl 2-bromoethylphosphonate to get **14**, leading to the double-protected ligand **15** by further alkylation with *tert*-butyl bromoacetate and producing an overall yield of 33% when starting from cyclen. In the third step the corresponding carboxylate derivative **16** was obtained after cleavage of the *tert*-butyl groups by treatment of **15** with neat TFA at room temperature. The final synthetic step was

deprotection of the ethyl groups in a 33% HBr/acetic acid solution at 70 °C to give the ligand **17**.

All ligands were recrystallized from ethanol, purified by RP-HPLC and characterized with different physicochemical methods. The number of resonances and their corresponding multiplicities in the ^{1}H and ^{13}C{^{1}H} NMR spectra are consistent with the structures displayed in Scheme 4.

Complexes were prepared by mixing the ligands with the corresponding lanthanide chloride salts in aqueous solution which was kept at neutral pH during the complexation. All Ln^{3+} complexes were characterized by mass spectrometry and the appropriate isotope pattern distribution characteristic for Gd^{3+} and Eu^{3+} complexes was recorded. In addition to MS, each Eu^{3+} complexes was also characterized by ^{31}P{^{1}H} NMR spectrometry.

3.3.2. ^{31}P{^{1}H} NMR studies of Eu^{3+} loaded complexes of ligands 16 and 17

The ^{31}P{^{1}H} NMR spectra of the **Eu-17** complex were recorded in D_2O at a pD range from 3 to 7 (Fig. 14). The phosphorus chemical shifts remained constant at pD 7 to 5 (29.7 - 29.8 ppm for **Eu-17**). A high field shift of about 5 ppm in **Eu-17** was detected when the pD decreased from 5 to 3. This corresponds to the protonation of the $-PO_3^{2-}$ group. In each case, a broad line was observed which might be due either to the paramagnetic influence of the Eu^{3+} ion and/or to dynamic exchange processes. At pD below 3, complex decomposed.

In the case of the ester protected phosphonates, the **Eu-16** complex generates three sharp resonances in the ^{31}P{^{1}H} NMR spectrum consistent with the presence of stereoisomers[107]. It gave rise to broad resonances when the ^{31}P{^{1}H} NMR spectra were recorded at pD = 7 and it remain same until pD = 4. Consequently, because of the short ethyl chain forces the phosphonate group closer to the paramagnetic Eu^{3+} ion.
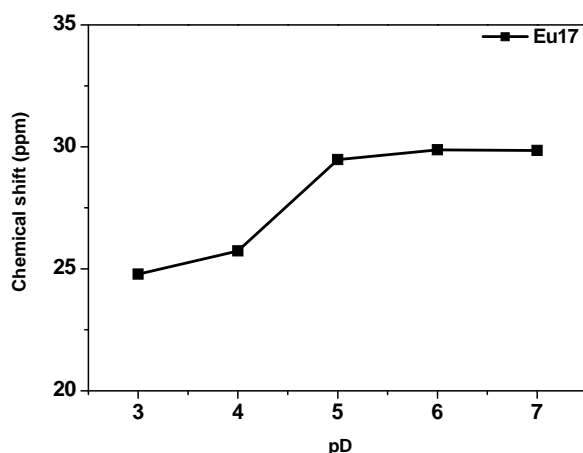
Figure 14. Dependence of δ_P of **Eu-17** on the pD.

3.3.3. *In Vitro* Relaxometric Experiments

3.3.3.1. Longitudinal relaxivity of Gd-16 and Gd-17 at different pH. The paramagnetic properties of the complexes **Gd-16** and **Gd-17** were studied by relaxometry at 300 MHz (7T) and 21°C. The relaxivities of the compounds were calculated as the slope of the function shown in equation 4, where $T_{1,obs}$ is the measured T_1, T_1,d is the diamagnetic contribution of the solvent (calculated to be 0.28 s^{-1}) and [Gd-L] is the concentration in mmol of the appropriate Gd^{3+} complex. Changes in the relaxivity of **Gd-17** was observed to occur in the pH range 4 to 7 (Fig. 15b). The relaxivity values for the complex **Gd-17** increased by 50 %, when the pH was adjusted to 4. This result is comparable with the data obtained from ^{31}P{^{1}H} NMR spectroscopy of the analogous Eu^{3+} complex, suggesting that the change of the relaxivity is a result of the protonation/deprotonation processes of the phosphonate groups at different pH.

$$1/T_{1,obs} = 1/T_{1,d} + r_{1*}[GdL^n] \qquad \text{(Equ. 4)}$$

Unlikely **Gd-17**, complex **Gd-16** exhibit no relaxivity change in slightly acidic to neutral conditions, and the value was constant at about 4.3 mM^{-1}s^{-1} for **Gd-16**. This relaxivity value is comparable to **Gd-17,** which indicates that complex have one inner-sphere water molecule. Nevertheless, a large decrease of the relaxivity was noticed at pH > 7 (Fig. 15a). This is probably a result of the

38

adduct formation with anions such as bicarbonate which can displace inner sphere water molecules. This phenomenon has already been observed on other DO3A type complexes and has been extensively studied in previous reports[44,118,119].
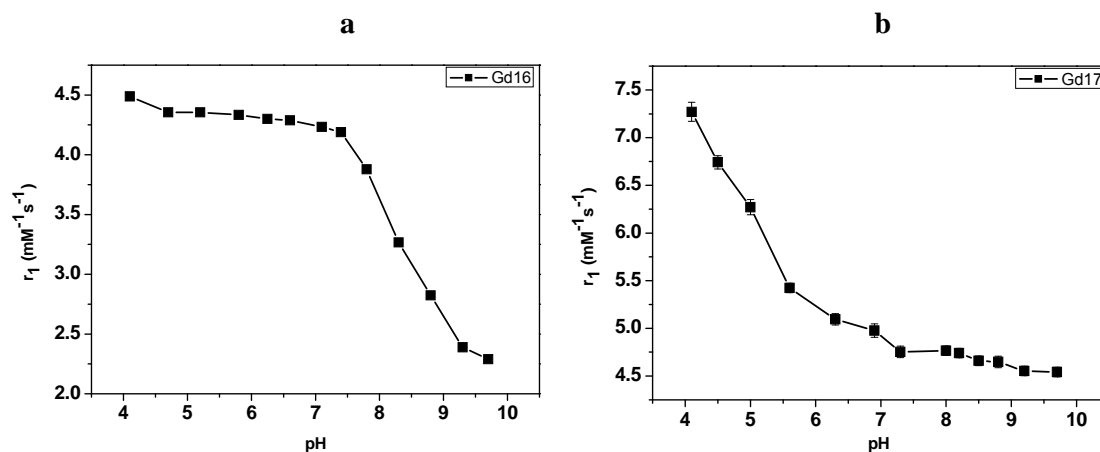
Figure 15. pH dependence of the longitudinal relaxivity (r_1) of Gd-complexes.

3.3.3.2. Binding of Gd-16 to HSA. Binding of neutral Gd^{3+} complexes to HSA has been shown markedly to promote the enhancement of relaxivity, mainly due to the change of molecular rotational correlation time (τ_R) in the studied complexes[120-123]. To investigate the interaction of the ester protected, neutral complex **16** with HSA on R_1 and R_2, relaxometric experiment with increasing concentration of HSA proportional to constant concentration of **Gd-16** (0.5 mM) was performed. As expected, longitudinal relaxation rate R_1 did not increase upon binding of the complex to HSA, but remained constant. This is in accordance to the Solomon–Bloembergen–Morgan theory predicting that at high magnetic field (>4.7 T), the relaxivity changes with the inverse of τ_R suggesting that no relaxivity increase should be expected upon binding of the CA to a large molecule[124]. On the other hand, an enhancement in transverse relaxation rates, R_2 of complex was observed consistent with non-covalent association of **Gd-16** to HSA. Thus, at physiological pH and ambient temperature, the increase in R_2 of the ternary adduct of **Gd-16** with HSA showed a maximum enhancement of 118 % relative to the unbound **Gd-16** complex (Table 1). This effect has already been observed with HSA-bound complexes[123] and on different systems such as in the association of avidin with

biotinylated Gd^{3+} complexes, consistent with ternary complex formation; thus the decrease of τ_R leads to a stronger R_2 enhancement at high magnetic field[125,126].

Table 1. R_1 and R_2 of the Gd^{3+} complex **Gd-16** (0.5 mM) in the presence and absence of HSA

Complex	HSA (mM)	R_1 (s^{-1})	R_2 (s^{-1})
Gd-16	0	2.3	3.3
	1	2.2	7.2

3.3.4. Luminescence studies

Luminescence lifetime measurements for the Eu^{3+} complexes of ligands **16** and **17** were recorded at pH 4, pH 7 and pH 10 in H_2O and D_2O. The data obtained revealed some useful information concerning the europium coordination environment and the apparent number of coordinated water molecules, q (Table 2)[127]. For the ester complex of **16**, dominant mono-aqua species seem to form at both pH 7 and pH 4. When parallel experiments were undertaken at pH 10, the q value in both cases tended towards a value of less than 0.3, consistent with the dissociation of the phosphonate ester arm for **16** and the replacement with hydrogencarbonate. Such behaviour has been observed earlier for certain DO3A complexes of Tb^{3+} and Eu^{3+},[44,127] and is consistent with the pH/relaxivity profiles obtained with the Gd^{3+} complexes. In contrast, the Eu^{3+} complexes of the phosphonate ligand **17** did not show any evidence for competitive bicarbonate binding, under the same conditions.

Addition of HSA (0.6mM) at pH 7.4 to the Eu^{3+} complex in water at pH 7.4 lowered the apparent q value to unity for each complex examined (Fig. 16), except in the case of **Eu-17**, where the results were compromised by evidence of precipitation. The displacement of at least one water molecule by Asp and Glu side-chains of the protein has earlier been suggested to account for the lowering of relaxivity/q values in related lanthanide-DO3A complexes[120].

.

Table 2. Emission lifetimes and estimated q values of Eu^{3+} complexes at neutral and acidic pH/pD.

pH/pD 7

Complex	τ (ms) D$_2$O	τ (ms) H$_2$O	q
Eu-16	1.35	0.46	1.42
Eu-17	1.70	0.47	1.55

pH/pD 4

Complex	τ (ms) D$_2$O	τ (ms) H$_2$O	q
Eu-16	1.36	0.46	1.42
Eu-17	0.59	0.29	1.80

The analysis of the spectral form and relative band intensities of Eu^{3+} emission spectra in aqueous media allows a good deal of information to be gleaned concerning the local Eu^{3+} coordination environment[35,127-129]. For the Eu^{3+} complex of **17**, the form of the emission spectrum (Δ_{exc} 397 nm) changed as the pH was reduced from 7 to 4 (Fig. 17a). The most significant change was the 100% decrease of the overall emission intensity and the lowering of the ratio of the $\Delta J = 2$ / $\Delta J = 1$ at band intensities from 2.3:1 to 1.2:1. This parameter has been established to probe the nature and polarisability of the axial donor in such systems. Such behaviour is consistent with the onset of complex dissociation and the formation of a less emissive and more highly hydrated species.

The emission spectra of the phosphonate ester complex at pH 7 was also clearly different (Fig. 17b). In this case, there is a marked change in the ratio of the $\Delta J = 2$ / $\Delta J = 1$ at band intensities. This difference in emission spectral behaviour is consistent with the q value found for this charge neutral complexes, **16** is predominantly a mono-aqua system.
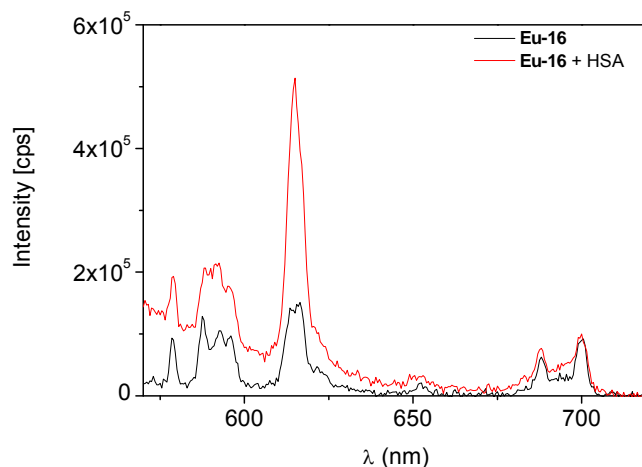
Figure 16. Luminescence emission spectra of **Eu-16** before and after addition of HSA (0.6 mM), pH 7 (λ_{ex}=397 nm)
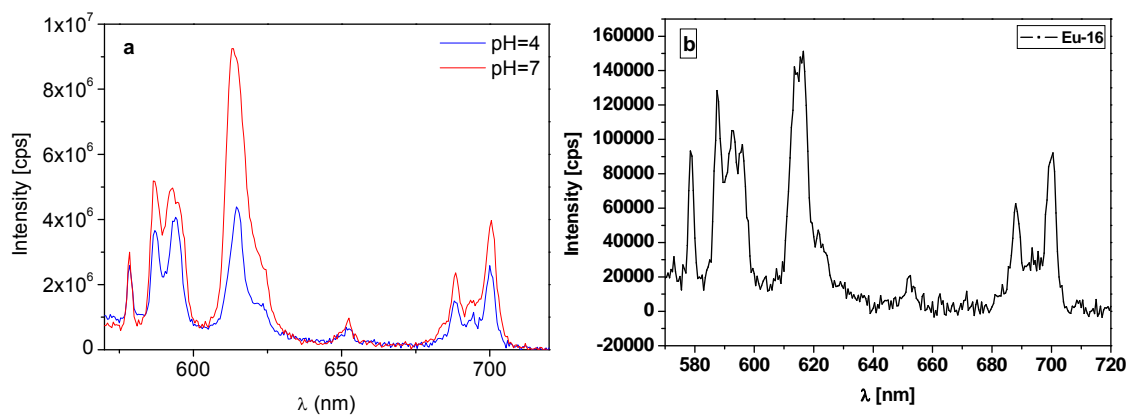
Figure 17. a) Luminescence emission spectra of **Eu-17** at pD 4 and pD 7 (λex=397 nm); **b)** Luminescence emission spectra of **Eu-16** at pH 7 (λex=397 nm).

3.3.5. Conclusions

The results obtained from the studies described above reveal several interesting and specific properties of the complexes under investigation.

The diester Gd^{3+} complexes display constant relaxivites in acidic and neutral media, which decrease after basification and an apparent increase of the

hydroxide/ bicarbonate concentration. In addition, ester complex forms ternary complex with HSA, indicated by the change of the form of the luminescence emission spectra of their Eu^{3+} complex, as well as by the decrease of the apparent number of water molecule coordinated to the lanthanide ion. This did not dramatically affect the longitudinal relaxation rates of the Gd^{3+} complex, but as the relaxometric studies were performed in a high magnetic field their transverse relaxation rate did increase. Among the ester complex, a different number of coordinated inner-sphere water molecule was observed. Obviously the shorter ethyl chain in **Gd-16/Eu-16** brings the hydrophobic ethyl groups closer to the Ln^{3+} ion and reduces the extent of complex hydration around the lanthanide ion.

The complex bearing acid exhibit different behaviour. Increase in the concentration of hydroxide/bicarbonates did not affect relaxivity, as the affinity toward the anions by the double negatively charged complexes is certainly minimised. Nevertheless, the monoprotonation of the phosphonate groups at slightly acidic media could be detected by all performed spectroscopic experiments. The slight low frequency shift observed in the $^{31}P\{^1H\}$ NMR spectra of Eu^{3+} complex is consistent with a pKa value between pD 4 and 5. To this end, the most pronounced r_1 change in Gd^{3+} complex was observed in the same region (pH/pD 4-5) indicating that the process of (de)protonation of the phosphonate group is directly determining the local hydration environment of the Gd^{3+} complex. Luminescence studies on the Eu^{3+} complexes allowed hydration chnage to be assessed. The decomplexation of the ternary phosphonate anion from the lanthanide metal complex resulted in addition of a coordinated water molecule and thus an increase in the relaxivity by the Gd^{3+} complex.

The corresponding DO3A-methylphosphonate complex does not exhibit any pH sensitivity at all. The phosphonate group is strongly bound to the gadolinium ion and is not protonated in the pH range 3 to 8. Thus, by introducing one or two more carbon atoms into the alkyl chain leads to a reduced metal phosphonate interaction which becomes pH sensitive. This can now be exploited to prepare pH sensitive contrast agents.

CHAPTER 4

Synthesis and Relaxation Properties of Novel Bis-polyazamacrocyclic Gd^{3+} Complexes: An Attempt towards Calcium Sensitive MRI Contrast Agents

4.1. Introduction

Revealing the role of calcium in neural signalling is a hot field in neuroscience research. The extracellular concentrations of Ca^{2+} and Mg^{2+} play important roles in both physiological and pathological processes in the nervous system. Significant fluctuations in their concentrations occur in association with normal brain activity, as well as with a variety of pathological phenomena including ischemia, hypoglycaemia, and seizures[130,131]. Intracellular Ca^{2+} has an important role in muscular contraction, neural transduction, and hormonal secretion[132]. Changes in the cytosolic concentration of Ca^{2+} trigger changes in cellular metabolism and are responsible for cell signalling and regulation[133]. The development of selective fluorescent reporter molecules has helped in the understanding of multiple roles of calcium[134].

For the detection of neuronal activity by MRI, the central challenge lies in translating the activity into changes in MR image contrast. In an effort towards this objective, we designed Gd^{3+} based systems whose relaxivity is potentially influenced by the variations of Ca^{2+} concentration in the physiological range, in particular in the extracellular space. We report here the facile synthesis and physicochemical characterization of novel bismacrocyclic Gd^{3+} complexes, derived from DO3A-ethylamine (DO3A-EA), DO3A-propylamine (DO3A-PA) and *p*-aminobenzyl-DO3A (*p*ABn-DO3A). The fundamental in the design of **25-27, 31** and **36** is to keep most of the coordination properties of DO3A-type ligands for Ln^{3+}. The macrocycle contains three carboxylate groups and four nitrogens from the cyclen ring to form a stable complex with Ln^{3+}. The fourth nitrogen is appended with a potentially reactive group (aryl/alkyl amine) where anhydrates of DTPA/EDTA are reacted to form bismacrocyclic CAs through amide bonds. The two macrocyclic units hold a lanthanide ion each, while the EDTA-bisamide/DTPA-bisamide constitutes the calcium sensitive core (Fig. 18). We specifically aim at sensing the variation of Ca^{2+} concentration in the extracellular space, which is in the millimolar range. The common fluorescent Ca^{2+} indicators used in biological applications and based on $BAPTA^{4-}$ are adapted to assess the cytosolic free Ca^{2+} concentration in the micromolar range (H_4BAPTA = 1,2-bis(o-aminophenoxy)ethane-N,N,N',N'-tetraacetic acid). The relaxivity response of a probe with a Ca^{2+} affinity of K ~ 10^6 M such as that of $BAPTA^{4-}$ would be already leveled off at the millimolar level.

Therefore, the Ca^{2+} binding moiety in the central part of our ligands was designed to have a reduced affinity towards Ca^{2+} in order to shift the range to higher Ca^{2+} concentrations where the probe is expected to have a relaxivity response.

The proton relaxivities of the new Gd^{3+} complexes were studied by relaxometric titrations at variable Ca^{2+} concentrations. In the objective of relating the Ca^{2+} dependent relaxivity response to the microscopic parameters of the Gd^{3+} chelate, we carried out a detailed mechanistic study. We used UV-Vis absorbance and luminescence lifetime measurements on the corresponding Eu^{3+} complexes to assess the number of inner-sphere water molecules and their variation on Ca^{2+} addition. The Gd^{3+} complexes of **25-27** have been characterized by variable temperature ^{17}O NMR spectroscopy and variable field relaxivity measurements (Nuclear Magnetic Relaxation Dispersion) which allowed us to calculate the parameters describing water exchange and rotational dynamics of the chelates.
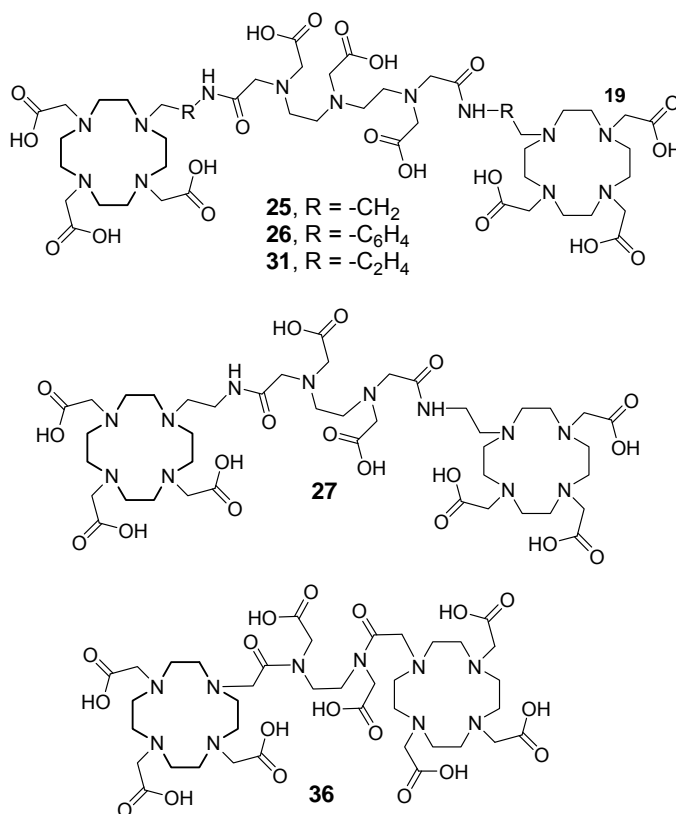
Figure 18. Structures of the ligands studied.

46

4.2. Experimental Section

4.2.1. Relaxometeric Titrations

^{1}H relaxometric titrations were performed on a Bruker Avance 500 spectrometer (11.75 T, 500 MHz) and at 300 MHz (7T) on a vertical 7T/60 cm MRI Biospec system (Bruker Biospin, Germany), at 25°C. The pH was maintained by 0.1 M KMOPS buffer and solutions of $CaCl_2$ and $MgCl_2$ were used for the titrations.

4.2.2. UV-Vis Measurements

UV-Vis spectra of the europium(III) complexes of **25**, **26** and **27** were obtained on a Perkin-Elmer Lambda 19 spectrometer, in thermostatizable cells with a 10 cm optical length (λ = 577.0 – 581.5 nm) with data steps of 0.05 nm. The sample concentrations were about 0.01 M and the temperature dependence was measured for a large temperature range (typically between 280 and 360 K). The technique has been described in details in a previous publication[135].

4.2.3. Luminescence Measurements

The luminescence measurements were performed on a Varian eclipse spectrofluorimeter, equipped with a 450 W xenon arc lamp, a microsecond flash lamp and a red-sensitive photomultiplier (300–850 nm). The luminescence spectra were obtained after excitation at $^5L_6\leftarrow{}^7F_0$ band (394 nm). All measurements were carried out in solutions containing 5 mM of Eu^{3+} complexes of **25**, **26** and **27** in 30 mM KMOPS buffer (pH 7.20) at 25°C. The luminescence decay was recorded in the short phosphorescence lifetime mode and experiments were repeated at least 5 times under each condition. The luminescence lifetime was calculated from the monoexponential fitting of the average decay data.

4.2.4. NMRD Measurements

The ^{1}H NMRD profiles were recorded on a Stelar Spinmaster FFC fast-field-cycling relaxometer covering magnetic fields from 2.35×10^{-4} T to 0.47 T, which corresponds to a proton Larmor frequency range of 0.01-20 MHz. The temperature was controlled by a VTC90 temperature control unit and fixed by a gas flow. The relaxivity at higher fields was recorded using Bruker Minispecs mq30 (30 MHz), mq40 (40 MHz) and mq60 (60 MHz), and on a Bruker 4.7 T (200 MHz) cryomagnet

with a Bruker Avance-200 console and on a Bruker Avance 500 spectrometer (500 MHz). The temperature was measured by a substitution technique[136] or by a preliminary calibration using methanol and ethylene glycol standards[137].

4.2.5. ^{17}O Relaxation Measurements

The transverse ^{17}O relaxation rates $(1/T_2)$ were measured in the temperature range 277–344 K, on a Bruker Avance 500 (11.75 T, 67.8 MHz) spectrometer. The temperature was calculated according to previous calibration with ethylene glycol and methanol[137]. The samples were contained in 5 mm NMR tubes and enriched with *tert*-butanol to allow for the BMS correction[138]. The $1/T_2$-data were measured by the Carr–Purcell–Meiboom–Gill spin-echo technique. Acidified water (HClO$_4$, pH 3.8) was used as external reference. Analysis of the ^{17}O NMR and ^{1}H NMRD experimental data was performed with the Visualiseur/Optimiseur programs running on a Matlab platform version 6.5[139,140].

4.3. Results and Discussions

4.3.1. Synthesis of Ligands

Based on metal ions with different physical properties like paramagnetic or fluorescent for non-invasive imaging, DO3A is an eminent building block for the synthesis of macrocyclic Ln^{3+} complexes for MR or optical imaging. These types of chelating agents contain more than six coordinating sites on the macrocycle, which are essential to form a stable complex with Ln^{3+} under physiological conditions. One of the nitrogen of macrocycle was appended with a reactive group like ethylamine, propylamine/*p*-aminobenzyl to form known bifuctional precursors DO3A-EA, DO3A-PA and *p*ABn-DO3A. All ligands bearing an amine group that is readily reactive towards most electrophiles such as anhydrides, aldehydes, carboxylic acids and isothiocyanates[84,86,125].

The tri-substituted product **3** was synthesized by the reaction of *tert*-butylbromoacetate on cyclen[87]. Alkylation on **3** with bromoacetonitrile gave cyano containing ligand **18** and the corresponding amine derivative **19** was obtained by the reduction of the cyano group in the presence of Ra-Ni, H$_2$, and 7N NH$_3$/MeOH by using Parr-apparatus at room temperature[141,142]. After the successful synthesis of

precursor **19**, the bismacrocyclic ligands **22** and **23** were synthesized by conjugation of 2.5 equivalents of **19** with 1 equivalent of DTPA-bisanhydride/EDTA-bisanhydride respectively in dry DMF and purified by preparative RP-HPLC. Finally, ligands **25** and **27** were obtained in 55-70% yield by deprotection of *tert*-butyl groups with neat TFA and were purified by RP-HPLC. (Scheme 5).
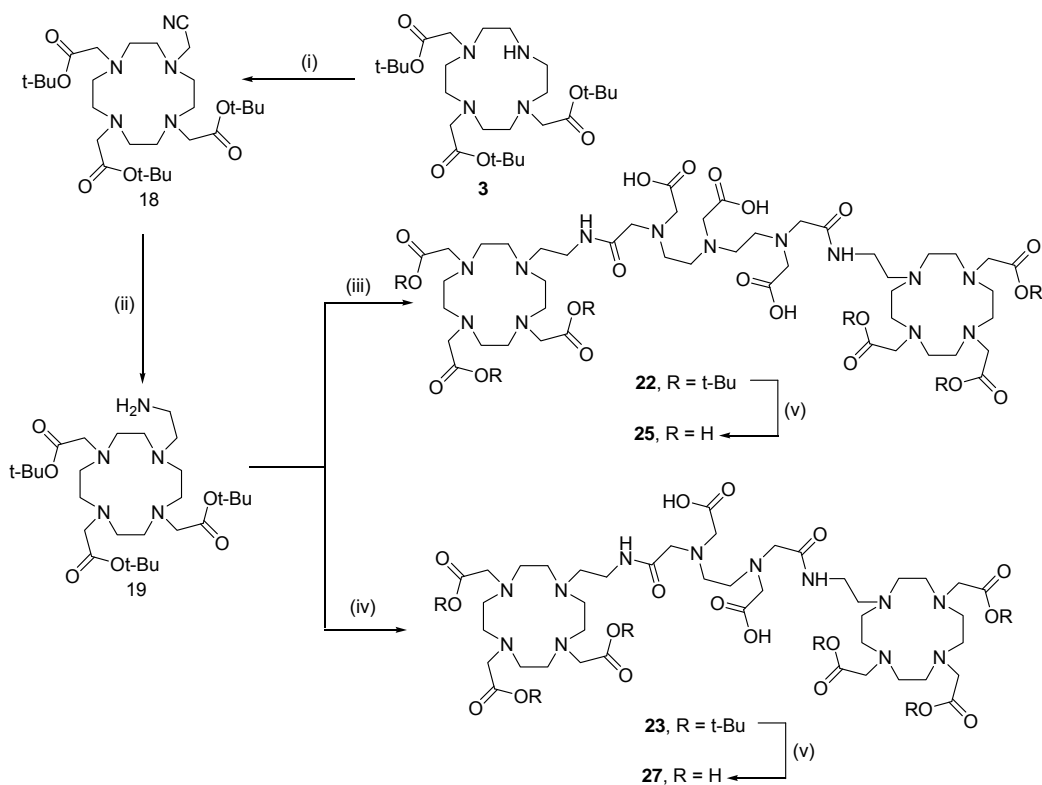
Scheme 5. Synthesis of ligands **25** and **27**. Reagents and conditions: *(i)* bromoacetonitrile, MeCN, 78%; *(ii)* Ra-Ni, H_2, NH_3/MeOH (7N), 72%; *(iii)* DTPA-bisanhydride, DMF, 39%; *(iv)* EDTA-bisanhydride, DMF, 52%; *(v)* TFA, 55-70%.

In a similar manner, ligand **26** was synthesized in a 4-step synthesis starting from **3**. Alkylation on **3** with *p*-nitrobenzylbromide gave *p*-nitrobenzyl containing ligand **20** and the corresponding *p*-aminobenzyl derivative **21** was obtained by the reduction of the nitro group in the presence of, H_2, Pd/C (10%) and MeOH as a solvent in the Parr-apparatus at room temperature[143]. The bismacrocyclic ligand **24** was synthesized by conjugation of 2.5 equivalents of **21** with 1 equivalent of DTPA-bisanhydride in dry DMF and purified by preparative RP-HPLC. Finally, ligand **26**

was obtained in 60-65% yield by deprotection of *tert*-butyl groups with TFA at room temperature and further on purified by preparative RP-HPLC (Scheme 6).
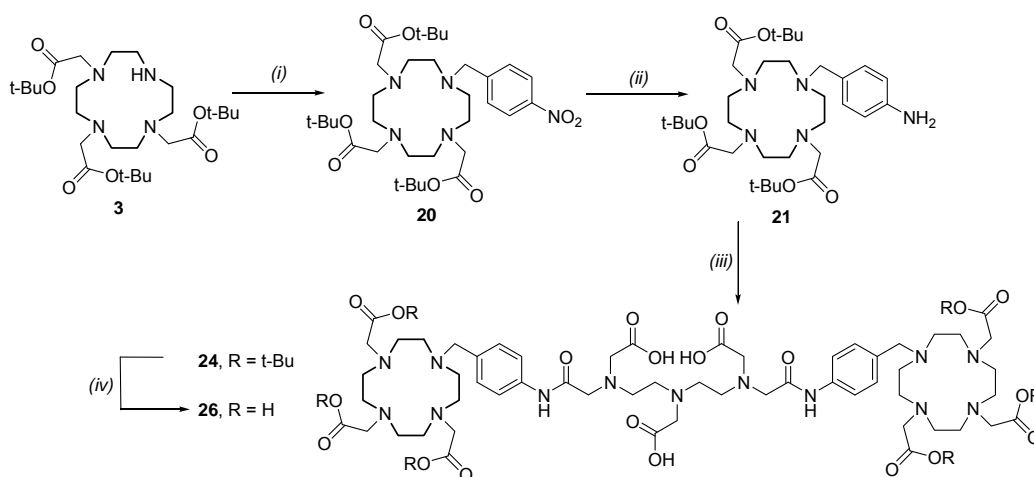
Scheme 6. Synthesis of ligand **26**. Reagents and conditions: *(i)* 4-nitrobenzylbromide, MeCN, 82%; *(ii)* Pd/C (10%), H$_2$, MeOH, 90%; *(iii)* DTPA-bisanhydride, DMF, 42%; *(iv)* TFA, 55-60%.

Ligand **31** was also synthesized in a 4-step synthesis starting from **3**. Michael addition on **3** with acrylonitrile gave cyano containing ligand **28** and the corresponding amine derivative **29** was obtained by the reduction of the cyano group in the presence of Ra-Ni, H$_2$, and 7N NH$_3$/MeOH by using Parr-apparatus at room temperature. After the successful synthesis of precursor **29**, the bismacrocyclic ligand **30** was synthesized by conjugation of 2.5 equivalents of **29** with 1 equivalent of DTPA-bisanhydride in dry DMF and purified by preparative RP-HPLC. Finally, ligand **31** was obtained in 55-60% yield by deprotection of *tert*-butyl groups with neat TFA and purified by RP-HPLC. (Scheme 7).

Fifth bismacrocyclic ligand **36** was synthesized in a 5-step synthesis starting from N,N'-dibenzyldiaminoethane. Alkylation on N,N'-dibenzyldiaminoethane with *tert*-butylbromoacetate gave dibenzyl containing ligand **32** and the corresponding secondary diamine derivative **33** was obtained by the cleavage of the dibenzyl group in the presence of Pd/C (10%), and 7N NH$_3$/MeOH by using Parr-apparatus at room temperature. Further alkylation of ligand **33** with bromoacetylbromide gave dibromo containing precursor **34**. After the successful synthesis of precursor **34**, the

bismacrocyclic ligand **35** was synthesized by alkylation of 2.5 equivalents of **3** with 1 equivalent of **34** in dry DMF and purified by classical flash chromatography. Finally, ligand **36** was obtained in 65-70% yield by deprotection of *tert*-butyl groups with neat TFA and finally purified by RP-HPLC (Scheme 8).
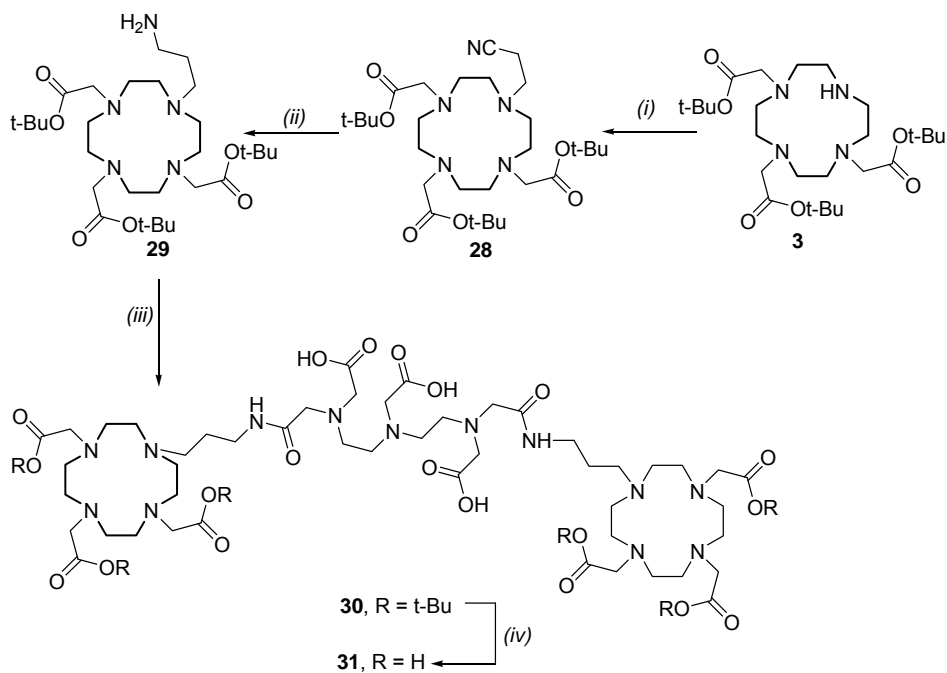
Scheme 7. Synthesis of ligand **31**. Reagents and conditions: *(i)* acrylonitrile, MeOH, TEA, 62%; *(ii)* Ra-Ni, H$_2$, NH$_3$/MeOH (7N), 78%; *(iii)* DTPA-bisanhydride, DMF, 35%; *(iv)* TFA, 55-60%.

Scheme 8. Synthesis of ligand **36**. Reagents and conditions: *(i) tert*-butylbromoacetate, MeCN, 88%; *(ii)* Pd/C (10%), H$_2$, MeOH, 90%; *(iii)* bromoacetylbromide, NaOH, H$_2$O/CH$_2$Cl$_2$, 72%; *(iv)* **3**, MeCN, 65%; *(v)* TFA, 65-70%.

4.3.2. Ca^{2+} relaxometric titrations of the Gd^{3+} complexes

To investigate the sensitivity of the Gd^{3+} complexes towards Ca^{2+}, we measured the longitudinal relaxation times, T_1, of water protons as a function of the Ca^{2+} concentration. The relaxivity, r_1, was calculated for each Ca^{2+} concentration from Equation 5.

$$\frac{1}{T_{1,obs}} = \frac{1}{T_{1,d}} + r_1[\text{Gd}] \quad (\text{Equ. 5})$$

Where $T_{1,obs}$ is the observed longitudinal relaxation time, $T_{1,d}$ is the diamagnetic relaxation time in the absence of the paramagnetic substance and [Gd] is the concentration of Gd^{3+}.

The titration curves were drawn by plotting the relaxivity as a function of the Ca^{2+}/Gd$_2$L molar ratio (Fig. 19). The effect of Ca^{2+} on the relaxivity is different for all the complexes. For **Gd$_2$-25** and **Gd$_2$-27**, the relaxivity is increasing by 15 and 32 %,

respectively, upon addition of Ca^{2+}. On the other hand, **Gd$_2$-26** is practically insensitive towards Ca^{2+} (~6% relaxivity change). In this molecule, the Ca^{2+} binding site is separated by a rigid and sterically demanding benzene ring from the Gd^{3+} chelating unit which renders the Gd^{3+} containing moiety insensitive to Ca^{2+} coordination. For **Gd$_2$-25** and **Gd$_2$-27**, the effects of Mg^{2+} have also been tested. The relaxivity increases with increasing Mg^{2+} concentration, to reach a plateau at a slightly higher Mg^{2+}/**Gd$_2$-25** molar ratio than that observed with Ca^{2+}, however, the maximum relaxivity is identical in the two cases. By adding additional 1.2 equivalents of Ca^{2+} to this sample, no relaxivity change is observed. The relaxivity remain same while adding excess of Mg^{2+} concentration in **Gd$_2$-27**. The titration curves for **Gd$_2$-25** and **Gd$_2$-27** have been analysed to obtain the association constants, K_A, for the Gd^{3+} complex – Ca^{2+} (or Mg^{2+}) interaction:

$$Gd_2L + Ca \rightleftharpoons CaGd_2L \quad \text{where} \quad K_A = \frac{[CaGd_2L]}{[Gd_2L][Ca]} \quad\quad \text{(Equ. 6)}$$
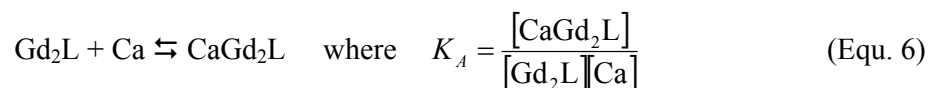
The curves were fitted according to Equation 7, where r_1^{obs} is the experimentally observed relaxivity, K_A is the association constant between the Gd^{3+} complex and Ca^{2+} or Mg^{2+}, c_{Gd2L} and c_{Ca} are the total concentrations of the Gd^{3+} complex and the Ca^{2+}/Mg^{2+} ion, respectively, and r_1^0 and r_1^f are the initial and final relaxivities in the titration. In this fitting procedure, the association constant K_A and the initial and final relaxivities r_1^0 and r_1^f were the adjustable parameters. Similarly to previously investigated bismacrocyclic complexes[39,40,144], 1:1 binding stoichiometry was assumed.

$$r_1^{obs} = \frac{\left(K_A c_{Gd_2L} + K_A c_{Ca} + 1\right) - \sqrt{\left(K_A c_{Gd_2L} + K_A c_{Ca} + 1\right)^2 - 4K_A^2 c_{Gd_2L} c_{Ca}}}{2K_A} - \left(r_1^f - r_1^0 + r_1^0 c_{Gd_2L}\right) \times 1000 \quad \text{(Equ. 7)}$$

The apparent association constants obtained from the fit are $\log K_A = 3.6 \pm 0.1$, 3.4 ± 0.1 and 2.7 ± 0.1 for the **Gd$_2$-25**-Ca, **Gd$_2$-27**-Ca and **Gd$_2$-25**-Mg systems, respectively. Ca^{2+} forms a less stable complex with **Gd$_2$-25** than with $DTPA^{5-}$ (the conditional stability constant of $CaDTPA^{3-}$ at pH 7.0 is $\log K = 6.65$). Such a decrease in stability can be expected, since in the central part of **Gd$_2$-25** have only the three nitrogens and three carboxylates which are coordinated to Ca^{2+}, in contrast to the three nitrogens and five carboxylates available in $DTPA^{5-}$. Indeed, the hydration

numbers determined from the luminescence lifetime measurements on the corresponding Eu^{3+} complexes in the absence and presence of Ca^{2+} (see below) indicate that the amide function remains coordinated to the lanthanide even after Ca^{2+} binding. The association constant obtained for the Mg^{2+} adduct formed with **Gd$_2$-25** is slightly lower than that with Ca^{2+}, in accordance with the general tendency of Mg^{2+} to form less stable complexes than Ca^{2+}.
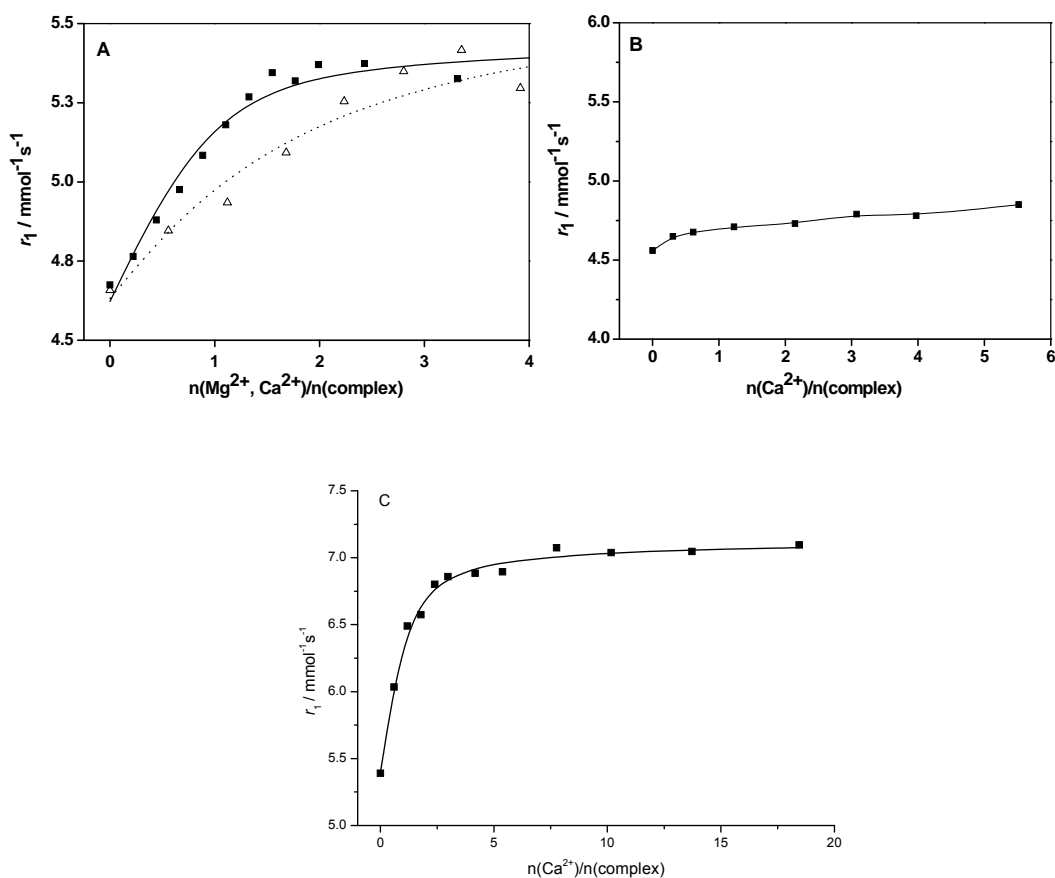
Figure 19: Relaxometric Ca^{2+} (full squares) and Mg^{2+} (empty triangles) titration curves of **Gd$_2$-25** (A), **Gd$_2$-26** (B) and **Gd$_2$-27** (C) performed at 25°C and 11.75 T. The lines correspond to the fit as explained in the text.

Nevertheless, the selectivity of the DTPA-bisamide unit towards Ca^{2+} vs. Mg^{2+} is much less important than that of $BAPTA^{4-}$ (selectivity over 10^5), a ligand which was specifically designed for Ca^{2+} complexation[134]. The value of the

association constant calculated for **Gd$_2$-27** is also considerably lower than the conditional stability constant of CaEDTA^{2-} at pH 7.0 (log K = 7.79)[145]. For **Gd$_2$-31** and **Gd$_2$-36**, relaxivity did not change in the presence of high amount of Ca^{2+}.

4.3.3. Luminescence and HR-UV-Vis absorption studies to assess the hydration state of Eu^{3+} complexes

In order to gain more insight into the factors that are responsible on the molecular level for the Ca^{2+} dependent relaxivity change of **Gd$_2$-25** and **Gd$_2$-27**, first of all we have assessed the hydration state of the corresponding Eu^{3+} complexes before and after Ca^{2+} addition. The number of water molecules directly coordinated to Gd^{3+} is one of the fundamental parameters influencing the relaxivity. One of the widely used methods for the determination of the hydration number is to measure the luminescence lifetime decays on the corresponding europium(III) complexes[146-148]. This technique is based on relating the difference in luminescence lifetimes measured in H$_2$O and D$_2$O solutions to the hydration number. Hydration numbers were determined for **Eu$_2$-25**, **Eu$_2$-26** and **Eu$_2$-27** complexes in the absence, and for **Eu$_2$-25** and **Eu$_2$-27** also in the presence of 2 and 5 equivalents of Ca^{2+}, respectively. These Ca^{2+}/Ln$_2$L complex ratios correspond to the saturation of the relaxometric titration curves obtained for the Gd^{3+} complexes. The hydration numbers were calculated according to the revised equation of Beeby et al.[148] (equation 8):

$$q = A'(\Delta k_{H_2O} - k_{D_2O})_{corr} \qquad \text{(Equ. 8)}$$

where A' is 1.2 ms and the correction factor for the contribution of the second and outer sphere water molecules is -0.25 ms^{-1}. The experimental luminescence lifetimes measured in H$_2$O and D$_2$O solutions and the corresponding hydration numbers q are listed in Table 3.

Table 3. Experimentally measured luminescence lifetimes and calculated hydration numbers of the Eu^{3+} complexes, and relaxivity values (25 °C, 500 MHz) of the Gd^{3+} analogues.

Complex	τ_{H2O} [ms]	τ_{D2O} [ms]	q	r_1 [mmol^{-1}s^{-1}]
Eu_2-25	0.60	1.59	0.9	4.7
Eu_2-25 with 2 equiv. Ca^{2+}	0.62	1.57	0.9	5.4
Eu_2-26	0.51	0.91	0.7	4.6
Eu_2-27	0.54	1.84	1.3	5.4
Eu_2-27 with 5 equiv. Ca^{2+}	0.47	1.62	1.5	7.1

The non-integer numbers of q often imply equilibrium between non-hydrated and monohydrated or between mono- and bishydrated species. Such hydration equilibrium can be investigated by high resolution UV-Vis measurements on the Eu^{3+} complexes. The Eu^{3+} ion has an absorption band in the visible spectrum (578 – 582 nm) whose wavelength is very sensitive to even small changes in the coordination environment. Although the intensity of this $^7F_0 \rightarrow {}^5D_0$ transition is low, the bands are relatively narrow which allows distinguishing different coordination states of the metal, except for the Eu^{3+} aqua ion, which is not observable due to its extremely low molar absorption. This transition has been previously used to determine the number of species present in solution, and, in particular, to characterize hydration equilibrium for Eu^{3+} complexes[135,149-152]. For Eu^{3+} complexes which have two differently hydrated forms in aqueous solution, one observes two absorption bands, separated by ~0.5 nm, belonging to the two species. The band at higher wavelength is attributed to the chelate with the higher hydration number and the band at lower wavelength to that with lower hydration number. In general, the total coordination number observed for Eu^{3+} complexes can be either 8 or 9, consequently the hydration equilibrium is between 8- and 9-coordinated complexes.
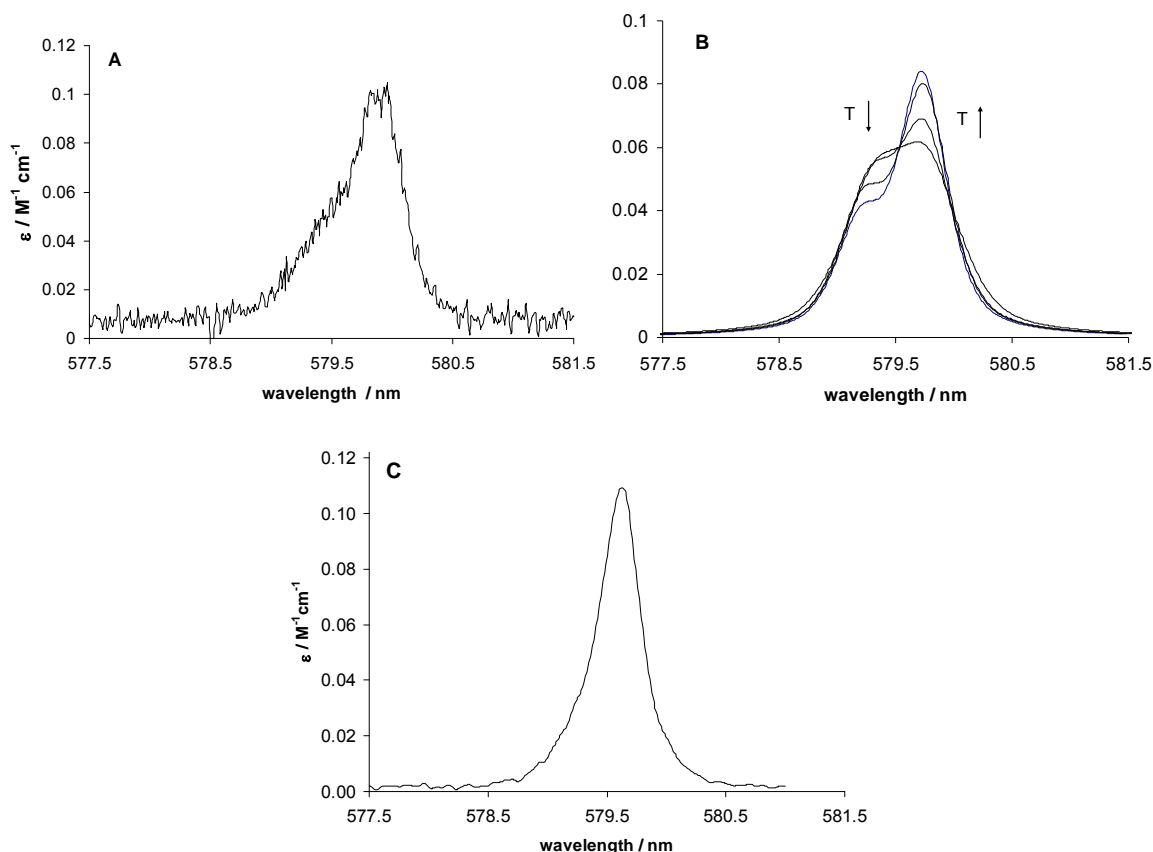
Figure 20: Representative UV-Vis spectra of **Eu$_2$-25** (A), **Eu$_2$-26** (B) and **Eu$_2$-27** (C) at 25°C (A, C) or as a function of temperature (B; T = 92 °C, 44 °C, 16 °C and 5 °C).

High resolution UV-Visible spectra were recorded in aqueous solutions of **Eu$_2$-25**, **Eu$_2$-26** and **Eu$_2$-27** complexes. In the region of the $^5D_0 \leftarrow {^7}F_0$ transition, the spectra of **Eu$_2$-25** and **Eu$_2$-27** show a temperature invariant absorption peak with a shoulder while that of **Eu$_2$-26** has two distinct, temperature dependent absorption bands (Fig. 20). The intensity ratio of these two bands changes with temperature: the band at shorter wavelengths is decreasing, while that at longer wavelengths is increasing with temperature. By analogy to previously studied systems[150-152], we relate this temperature dependency to the existence of hydration equilibrium. The band at lower energy (579.7 nm) is assigned to the non-hydrated, while that at ca. 579.2 nm is attributed to a monohydrated species (equation 9).

$$Eu_2L^2 + 2\ H_2O \leftrightarrows Eu_2(H_2O)_2\ L^2 \qquad \text{(Equ. 9)}$$
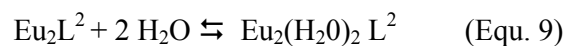
As the effective concentration of the solvent is constant, the equilibrium constant corresponding to Equation 10 may be written as:

$$K_{Eu} = \frac{\left[Eu_2(H_2O)_2 L^2\right]}{\left[Eu_2 L^2\right]} \qquad \text{(Equ. 10)}$$

The reaction enthalpy, ΔH^0, and the reaction entropy, ΔS^0, for the equilibrium may be obtained from the temperature dependence of K_{Eu}:

$$\ln K_{Eu} = \frac{\Delta S^0}{R} - \frac{\Delta H^0}{RT} \qquad \text{(Equ. 11)}$$

The ratio of the integrals of the two bands is related to the equilibrium constant, and its temperature dependence yields the reaction enthalpy and entropy (Fig. 21). The fit of the data in Fig. 21 to Equation 12 resulted in $\Delta H^0 = $ -(7.8 ± 1) kJ mol^{-1}, $\Delta S^0 = $ -(25 ± 5) J mol^{-1} K^{-1} and $K_{Eu}^{298} = (1.2 \pm 0.3)$.

$$\ln\left(\frac{Int_q}{Int_{q+1}}\right) = -\frac{\Delta H^0}{RT} + \frac{\Delta S^0}{R} + \ln\left(\frac{I_q}{I_{q+1}}\right) \qquad \text{(Equ. 12)}$$
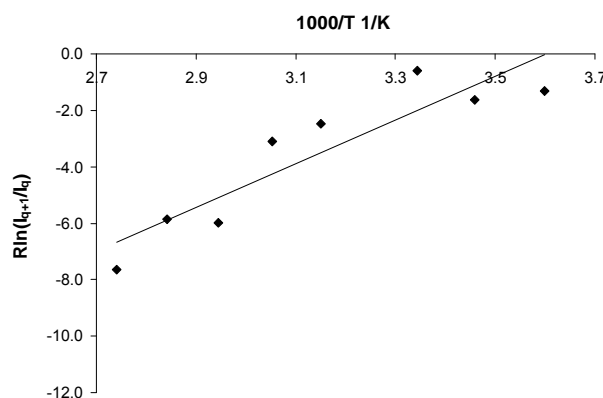

Figure 21: Ratio of the integrals of the two absorption bands attributed to $q = 0$ and $q=1$ species in the UV-Vis spectrum of **Eu$_2$-26** as a function of the inverse temperature. The straight line represents the linear least-squares fit to the data points as explained in the text.

The average hydration number derived from the equilibrium constant is 0.55 at 298 K, in acceptable accordance with $q = 0.7$ obtained from the luminescence decay measurements. If we assume that the overall coordination number of the lanthanide ion can be either 8 or 9, it implies that in both the non-hydrated (CN = 8) and monohydrated (CN = 9) species another donor atom from the central part of the ligand (an amide or a carboxylate oxygen) completes the coordination sphere. Given the important steric demand and rigidity that the benzyl group represents, this scenario seems rather unlikely. Moreover, the Ca^{2+} independency of the relaxivities for the **Gd$_2$-26** complex indicates that Ca^{2+} binding has no effect on the hydration state of the lanthanide ion. This would mean that if a donor group is bound to the lanthanide ion from the central part of the molecule, it will remain coordinated even after Ca^{2+} binding. The other, likely more probable coordination mode involves the binding of the macrocycle amines and carboxylates to the lanthanide, plus one water molecule in the monohydrated species. The bulky and highly hydrophobic benzyl group directly attached to the amine nitrogen prevents the coordination of another donor atom, thus in this case the coordination equilibrium observed in the UV-Vis spectrum would correspond to non-hydrated CN=7 and monohydrated CN=8 species. This hypothesis seems to be also supported by the high negative value of the activation entropy calculated for the water exchange on **Gd$_2$-26** (see below), indicative of the associative activation mode of the exchange process. This is indeed in contrast to the nine-coordinated Gd^{3+} poly(aminocarboxylate) complexes which have, in the great majority of the cases, a dissociatively activated water exchange[153].

The temperature invariance of the UV-Vis spectrum for **Eu$_2$-25** and **Eu$_2$-27** suggests that no hydration equilibrium exists in the sense as depicted for **Eu$_2$-26**. Nevertheless, the presence of a shoulder next to the main band in the $^7F_0 \rightarrow {}^5D_0$ transition range implies that there are at least two different coordination environments. By taking into account all available experimental information from luminescence, UV-Vis absorption and relaxivity data, we can hypothesise the existence of two species as depicted in Fig. 22. In all cases, the macrocyclic carboxylates and nitrogens are coordinated to the lanthanide(III) ion. The inner coordination sphere is then completed in different manners: in **Ln$_2$-25** we expect the coordination of the amide oxygen, while the ninth coordination site can be occupied either by a water molecule or one of the central carboxylates. This hypothesis is in

accordance with the hydration number of $q = 0.9$ determined by luminescence. It also explains the increase of the relaxivity of the Gd^{3+} complex on Ca^{2+} coordination in the central part of the ligand which will involve the carboxylate, coordinated to the lanthanide in the absence of Ca^{2+}. We expect that on Ca^{2+} binding this carboxylate is replaced by an inner sphere water molecule leading to the relaxivity increase observed for **Gd$_2$-25**. The luminescence lifetime measurements do not indicate a change in q on Ca^{2+} addition (Table 3), however, the uncertainty generally associated to the q values determined by this method is at least ±0.25 (certain authors estimate this uncertainty as high as ±0.5)[148]. By taking this into consideration, the luminescence measurements do not confute our hypothesis. An analogous scenario has been previously proposed for bismacrocyclic GdDO3A complexes with a BAPTA-bisamide central bridging unit[144].

For **Ln$_2$-27**, we suggest that, in addition to the macrocycle nitrogens and carboxylates, the first coordination sphere of the lanthanide ion is completed by two water molecules in one species and one water and one amide in another species. It is supported by the hydration number $q = 1.3$ obtained for **Eu$_2$-27** by luminescence. On the other hand, the increase of q and of the relaxivity observed on Ca^{2+} addition evidences the transfer of the donor group from Ln^{3+} to Ca^{2+}. The detachment of this amide from the Gd^{3+} then results in the entering of second inner sphere water. The higher hydration number determined for **Ln$_2$-27** as compared to **Ln$_2$-25** is also consistent with the respective structure of the two complexes: the shorter bridging unit in the EDTA-bisamide derivative bismacrocycle implies more steric constraint which then prevents the simultaneous coordination of the amide and a central carboxylate to the lanthanide ion, leading to a higher q. In contrast, such a coordination mode is more accessible in **Ln$_2$-25** possessing a longer, thus more flexible DTPA-bisamide bridging unit. For both **Ln$_2$-25** and **Ln$_2$-27**, the overall coordination number remains $CN = 9$ before and after Ca^{2+} addition.
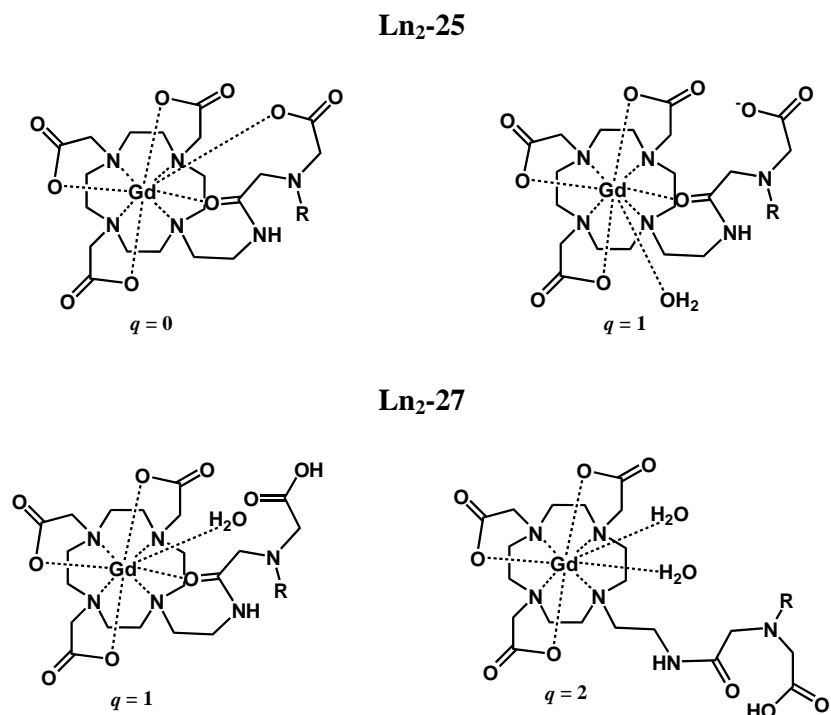
Ln$_2$-25

Ln$_2$-27

Figure 22. Proposed structures present in solutions of **Ln$_2$-25** and **Ln$_2$-27**. In both cases, Ca^{2+} binding in the central part of the bismacrocycle favours the presence of the more hydrated species. For better understanding only half of complexes are shown.

4.3.4. Evaluation of the parameters influencing relaxivity of the Gd^{3+} complexes

For all the three systems, variable temperature ^{17}O NMR and ^{1}H NMRD relaxometric data have been acquired and analysed simultaneously on the basis of the Solomon-Bloembergen-Morgan approach. The experimentally measured paramagnetic ^{17}O chemical shifts were considerably smaller than what would be expected for a Gd^{3+} complex with the given q value, therefore, they have not been included in the final fitting. A similar diminution of the chemical shifts has been previously reported in systems with a significant second sphere contribution to ^{17}O and ^{1}H relaxation[107,144,154]. An important second sphere effect has been proved to exist for bismacrocyclic Gd^{3+} complexes of analogous structure[40,144]. Therefore, the common Solomon-Bloembergen-Morgan model was extended with a second sphere contribution to proton relaxivity[155], as it has been done for other systems[115,156-159]. Certain of the large number of parameters were fixed in the fit[160]. Namely, the number

of inner-sphere water molecules (q) was fixed to the values found from luminescence lifetimes measurements (0.9 and 1.3 for **Gd$_2$-25** and **Gd$_2$-27**, respectively). For **Gd$_2$-26**, the actual q value was calculated for each temperature by using the reaction enthalpy and entropy of the hydration equilibrium as determined for the Eu^{3+} analogue from the variable temperature UV-Vis study. The distance of Gd^{3+} from the water proton (r_{GdH}) was fixed to 3.1 Å; the distance of the closest approach of the outer sphere water molecules to Gd^{3+} (a) was fixed to 3.6 Å. The hyperfine coupling constant ($A/\hbar$) was set to -3.8×10^6 rad·s^{-1}, a value found previously for GdDOTA[160]. The activation energy E_V had to be fixed to 1 kJ·mol^{-1}, otherwise the fit converged to negative values. Parameters related to the second hydration sphere were fixed to the following values:[107,154,161,162] the number of second-sphere water molecules (q^{2nd}) was set to 1, the Gd-2nd sphere proton distance (r_{GdH}^{2nd}) to 3.5 Å. The residence time of the second-sphere water (τ_m^{2nd}) was set to 50 ps and its enthalpy of activation to 35 kJ·mol^{-1}. The parameters leading to the best least-squares fits are listed in Table 4 and compared with the parent GdDOTA. The simultaneous fits are depicted in Fig. 23.

Table 4: Best-fit parameters obtained by the simultaneous analysis of transverse ^{17}O relaxation rates and proton relaxivities for **Gd$_2$-25**, **Gd$_2$-26** and **Gd$_2$-27** complexes in the absence of Ca^{2+}. Parameters obtained from the fit of NMRD data for Gd$_2$-25 in the presence of Ca^{2+} are also presented. Values in *italics* were fixed during the fit.

Parameter	Gd$_2$-25	Gd$_2$-26	Gd$_2$-27	GdDOTA[d]
r_1 [mmol^{-1}s^{-1}] 20 MHz / 37 °C	6.22	8.19	6.05	3.83
k_{ex}^{298} [10^6 s^{-1}]	0.52±0.06	0.8±0.1	80±20	4.1
$\Delta H^{\ddagger}$ [kJ mol^{-1}]	39.3±1.4	20.1±2.2	20±4	49.8
$\Delta S^{\ddagger}$ [J mol^{-1}K^{-1}]	-3.6±4.2	-64.5±6.6	-27±12	+49
τ_{RH}^{298} [ps]	390±8 450±10[c]	1060±210	200±25	77
E_R [kJ mol^{-1}]	30±6 30±5[c]	30±4	24±7	16.1
τ_V^{298} [ps]	20.6±1.1	25.0±0.9	20.5±3.1	11
Δ^2 [10^{20} s^{-2}]	0.43±0.03	0.26±0.02	0.6±0.1	0.16
D^{298}_{GdH} [10^{-10}m^{2}s^{-1}]	28±2	21±1	25±8	22
E_{DGdH} [kJ mol^{-1}]	19±2	18±3	25±9	20
q^a	*0.9* 1.1±0.1[c]	*0.5*[b]	*1.3*	1
q^{2nd}	*1*	*1*	*1*	-

[a] obtained from luminescence data on the Eu^{3+} complex
[b] at 298 K; in the fit, q was calculated for each temperature from the UV-Vis measurements on the Eu^{3+} complex
[c] from fitting the NMRD curves in the presence of Ca^{2+}. The parameters describing water exchange, electron spin relaxation, and second and outer sphere relaxation were fixed to the values obtained without Ca^{2+}.
[d] from [160]

With regard to the water exchange rate, the **Gd₂-25** and **Gd₂-26** complexes are considerably different from **Gd₂-27**. The water exchange is remarkably fast on **Gd₂-27** ($k_{ex}^{298} = 8\times10^7\,s^{-1}$), about 20 times faster than on GdDOTA. It is interesting to note that Congreve et al. reported a similarly fast water exchange ($k_{ex}^{298} = 11\times10^7\,s^{-1}$) for the Gd^{3+} complex of a DO3A ligand bearing an N-linked CH_2-CH_2NHCO-pyridyl moiety[163]. For the Eu^{3+} analogue of this chelate they found $q = 1.1$ by luminescence, a slightly lower value than $q = 1.3$ for **Eu₂-27**. They interpreted the unexpectedly fast water exchange in terms of a steric destabilization of the Ln-water binding interaction by the coordination of the sterically demanding N-linked amide. The same explanation can be evoked in the case of **Gd₂-27**. We should also note that the **Gd₂-27** complex is present in an aqueous solution as a mixture of two differently hydrated species. Consequently, the water exchange rate calculated here represents an effective value which we cannot decompose to the individual k_{ex} values corresponding to each of the two species.

In contrast to **Gd₂-27**, in **Gd₂-25** the participation of a central carboxylate in the Gd^{3+} coordination creates a different coordination environment with less than one inner sphere water in average and results in a low exchange rate ($k_{ex}^{298} = 0.5\times10^6\,s^{-1}$). A k_{ex}^{298} value in the same order of magnitude ($k_{ex}^{298} = 2.4\times10^6\,s^{-1}$) was found for the bismacrocyclic GdDO3A complex with a BAPTA-bisamide central unit[144].

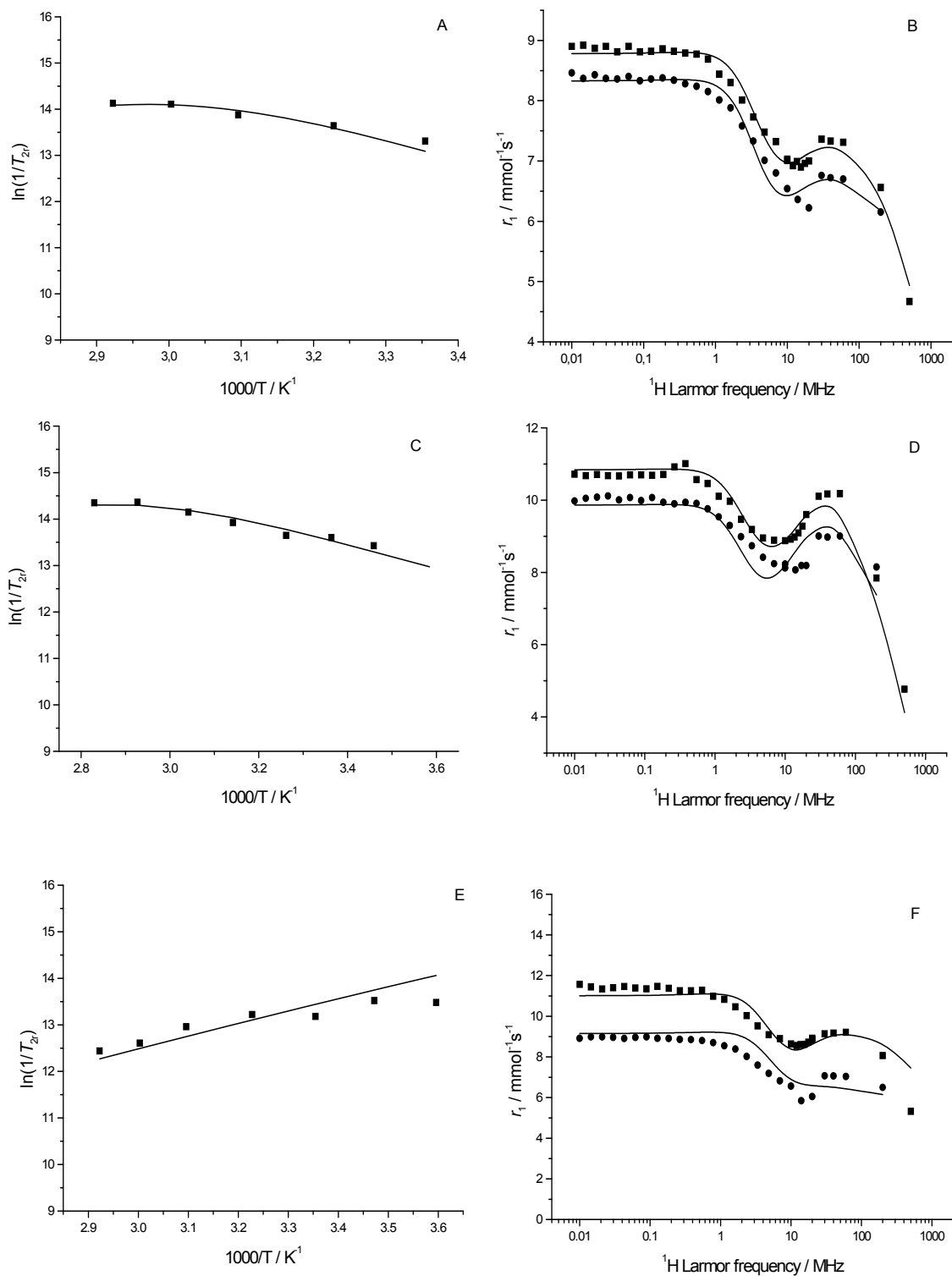**Figure 23.** Simultaneous fitting of ^{17}O NMR ($\ln(1/T_{2r})$ ■) and ^{1}H NMRD (25°C ■, 37°C ●) data of **Gd$_2$-25** (A, B), **Gd$_2$-26** (C, D) and **Gd$_2$-27** (E, F) in the absence of Ca^{2+}.

The rotational correlation time, τ_R, is influenced by the size and the rigidity of the complex. All three systems studied have higher molecular weight and therefore higher τ_R than GdDOTA, which is also reflected in the higher relaxivity values. We note the remarkably high relaxivity of **Gd$_2$-26** which is the most rigid among the three complexes due to the presence of the benzyl groups and, accordingly, has the highest τ_R. In spite of the size difference of the two other systems, **Gd$_2$-25** and **Gd$_2$-27**, their relaxivities are comparable since the smaller τ_R of **Gd$_2$-27** is compensated by a higher hydration number. In all cases, we also expect an influence of second sphere water on the overall relaxivity due to the number of negatively charged carboxylate groups in the central part of the molecules. For all three complexes studied, the relaxivities exceed that of GdDOTA.

The relaxivity of **Gd$_2$-26** is practically invariant upon Ca^{2+} addition (Fig. 19B). Concerning the Ca^{2+} dependent systems, transverse ^{17}O relaxation rates (for **Gd$_2$-25** and **Gd$_2$-27**) and ^{1}H NMRD profiles (for **Gd$_2$-27**) have been measured in the presence of 3 and 4 equivalents of Ca^{2+}, respectively. For both complexes, the ^{17}O $\ln(1/T_{2r})$ data were identical with those obtained in the absence of Ca^{2+}. It confirms that the water exchange rate, k_{ex}, is not affected by the presence of Ca^{2+}. The NMRD profiles of **Gd$_2$-25** in the presence of Ca^{2+} have been fitted to the Solomon-Bloembergen-Morgan theory by calculating the rotational correlation time and its activation energy and fixing the other parameters to the values found for the Ca^{2+}-free system (Fig. 24). By fixing the hydration number to the value determined by luminescence, no acceptable fit of the NMRD curves could be obtained. Therefore q was also adjusted in the final fit. The value calculated in this way, $q = 1.1$, is slightly higher than that determined by luminescence (0.9). The rotational correlation time is also increased when Ca^{2+} is bound in the central part of the molecule ($\tau_R^{298} = 390$ and 450 ps before and after Ca^{2+} binding, respectively). In overall, the relaxivity increase observed upon Ca^{2+} addition is mainly due to the increase of the hydration number of the Gd^{3+}. In addition, Ca^{2+} binding also leads to a slightly more rigidity of the entire molecule, resulting in a longer rotational correlation time, τ_R. **Gd$_2$-31** have one methylene group extra in between calcium chelating part and macrocycle as compare to **Gd$_2$-25**, and also relaxivity does not change by the addition of 5 equivalent of Ca^{2+}, this prove that there is no amide coordination with Ln^{3+} because of high distance

between macrocycles and amide coordinated DTPA. **Gd$_2$-36** does also not show any relaxivity change in the presence of Ca^{2+}, where we can conclude that with inverse amide we change coordination property of EDTA. EDTA normally has 6 coordination sites including 4 carboxylates and 2 amines, which is required for Ca^{2+} binding. In **Gd$_2$-36,** the central part of system is now rigid due to the inverse amide as well as we loose two coordination sites. Additionally because of inverse amide complex showed DOTA type bismacrocycle, that's why amide is tightly coordinated with Ln^{3+}.

Li *et al* reported a mechanistic study to assess the parameters that are responsible for the Ca^{2+} dependent relaxivity variation of GdDOPTA, a bismacrocyclic chelate of similar structure, possessing a Ca^{2+} binding BAPTA^{4-} unit as bridging part between the two macrocycles[40]. They considered that the rotational correlation time does not vary on Ca^{2+} binding. We think that the binding of the Ca^{2+} will render the molecule more rigid, as it is indeed reflected by the increase of the rotational correlation time calculated from the NMRD data. On the other hand, for GdDOPTA a more important variation of *q* was reported on Ca^{2+} coordination. By luminescence on the Tb^{3+} analogue, a hydration number of *q* = 0.47 and 1.05 was determined before and after Ca^{2+} binding; in contrast, for the Gd^{3+} complex, the fit of the NMRD profiles suggested *q* = 0.7 and 2.3 without and with Ca^{2+}, respectively. The relaxivity increase was also more significant (~80 % at 11.75T) for GdDOPTA, and was not sensitive to the presence of Mg^{2+}. We should note that due to the high association constant between the BAPTA^{4-} chelator and Ca^{2+} (K$_a$ ~ 10^6 M^{-1}), GdDOPTA might be adapted to report on the variation of Ca^{2+} concentration at the micromolar level (intracellular), but its relaxivity response will be levelled off at higher Ca^{2+} concentrations, such as those in the extracellular space (millimolar range). In order to probe variations at the millimolar level, the association constant should be decreased, as it is the case for our compounds. Unfortunately, the DTPA-bisamides do not have the great selectivity of BAPTA^{4-} for Ca^{2+} with respect to Mg^{2+}, which prevents practical application of this compound for Ca^{2+} sensing. But EDTA-bisamide is more selective towards Ca^{2+} with respect to Mg^{2+}, though molecule can be useful for further *in vitro* or *in vivo* selective Ca^{2+} sensing studies.
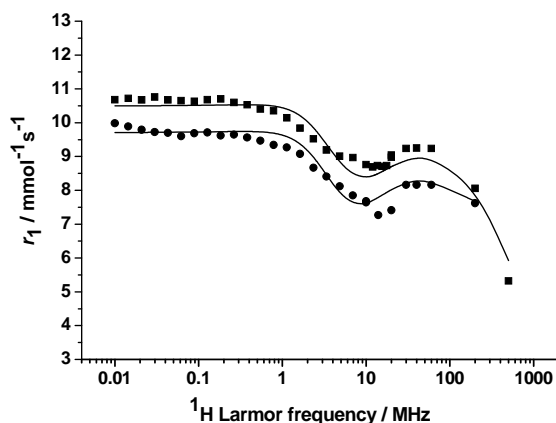
Figure 24. Fitting of ^{1}H NMRD (25°C ■, 37°C ●) data of **Gd$_2$-25** in the presence of 3 equivalents of Ca^{2+}.

4.3.5. *In vitro* relaxation study of Gd$_2$-27 in the extracellular matrix

In view of the fact that we know **Gd$_2$-27** showed best relaxivity changes in the presence of Ca^{2+} but no changes observed in the presence of Mg^{2+}, thus we conclude that this complex is good candidate for further *in vivo* studies. However before *in vivo* studies, complex should be measured with Ca^{2+} in *in vivo* matrix [extracellular matrix (ECM)]. This would tell us whether complex is showing same relaxivity changes in ECM as compare to normal buffer or not. We performed the relaxivity measurements at 37°C and 11.75 T in almost Ca^{2+} free ECM solution (0.3 mM Ca^{2+}), rest all other anions, cations and proteins are comparable with body system.

4.3.5.1. Sample Preparation of the extracellular matrix experiments. 36.1 mg of solid HEPES (1.5*10^{-4} mol) was dissolved in 1.5 ml of the ECM solution (the pink color changed into yellow). 400 μL of this buffered matrix solution, filtered via sterile 0.2 μm filter, was added to a 5 mm NMR tube (non-sterile) which already contained 8 μL of the stock complex solution. The resulting concentration of Gd^{3+} in the NMR tube was therefore 0.98 mM. In a sterile eppendorf, 1.47 mg of CaCl$_2$·2H$_2$O (1*10^{-5} mol) was dissolved in 1 ml of the buffered extracellular matrix solution. The resulting Ca^{2+} concentration of this solution was 10 mM. The 101 mM solution of EDTA was prepared by dissolution of 22.63 mg of Na$_2$H$_2$EDTA·2H$_2$O in 600 μL of the extracellular matrix containing 0.1 M HEPES buffer.

4.3.5.2. Relaxometric titrations with Ca²⁺ in ECM. The solution of Ca^{2+} was added by 10 µL until the overall Ca^{2+} concentration reached 2.4 mM. Then 11.8 µL of the EDTA solution was added, resulting in equivalent concentrations of EDTA and Ca^{2+}. After the addition of EDTA solution, we supposed that all Ca^{2+} complexes with EDTA and the system should behave as Ca-free (first point in Fig. 25). The relaxivity measurement of the final solution was repeated in three days and a slight relaxivity increase was observed (from 3.38 mmol⁻¹s⁻¹ to 4.22 mmol⁻¹s⁻¹). However, it has to be taken into account that the non-sterile solution was measured after three days; so many processes could have taken place. The experimental data together with the approximate time from the beginning of the titration are listed in Table 5. When we plot the relaxivity vs. the ratio of the concentration of Ca/complex, we can see a decreasing trend in the relaxivity with the increasing Ca^{2+} concentration (Fig. 25(A)).
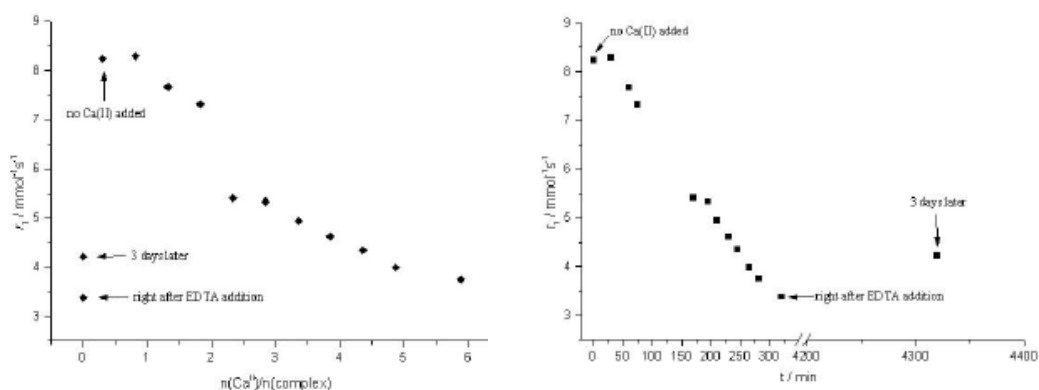

Figure 25: (A) Dependence of the relaxivity of **Gd₂-27** in ECM on the Ca^{2+} concentration; **(B)** Dependence of the relaxivity of **Gd₂-27** in ECM on the time (37°C, 11.75 T).

It is interesting to plot the relaxivity vs. the time from the beginning of the titration (Fig. 25(B)). We can see that the big step in relaxivity decrease (c(Ca)/n(complex) = 2.33) corresponds in fact to a longer pause between the measurements. It seems like if there was some mechanism initiated not only by the presence of Ca^{2+}, but also time dependent. Maybe the complex is attached to a protein, which degrades or aggregates in presence of Ca^{2+}, which changes its

conformation and terminates the protein-complex interaction or blocks the access of water to the first coordination sphere of the complex.

Table 5: Experimental data from the relaxometric titration of **Gd$_2$-27** with Ca^{2+} at 37°C and 11.75 T.

time / min	V_{total} / μL	r_1 / mmol^{-1}·s^{-1}	c(Ca^{II})/c(cmplx)
0	408	8.24	0.3
30	418	8.29	0.81
60	428	7.68	1.32
75	438	7.32	1.82
170	448	5.41	2.33
195	458	5.34	2.84
210	468	4.94	3.35
230	478	4.62	3.85
245	488	4.35	4.36
265	498	3.99	4.87
282	508	3.75	5.88
EDTA → 320	519.8	3.38	0
3 days	519.8	4.22	0

To investigate, if the decrease of the relaxivity was Ca^{2+} dependent, another titration was performed. The experimental set up was identical as in the previous case. At the beginning of the titration, the relaxivity of the sample with no Ca^{2+} added was measured four times during four hours. No relaxivity decrease was observed (Fig. 26). When Ca^{2+} was added, a relaxivity decrease occurred. We can conclude that the relaxivity decrease depends on the presence of Ca^{2+} and also on time (the relaxivity value is not the same at the same Ca^{2+} concentrations in the two titrations because the second titration was faster). This confirms that until Ca^{2+} is added, the complex has a high relaxivity (higher than in pure water, which indicates the possible interaction of the complex with a protein). Once Ca^{2+} is added, the relaxivity drops. The experimental data are listed in Table 6.

A third essay was done by adding all the amount of Ca^{2+} at one time (100 μL of 10 mM Ca^{2+} solution) to the complex solution in extracellular matrix and measuring the relaxivity immediately after that (it was done at 25°C in order to save the time needed to temperate the sample). The aim was to see if there is a relaxivity increase caused by the interaction of Ca^{2+} with the complex before the degradation of the solution takes place. The relaxivity of the complex in extracellular matrix solution

69

at 25°C and 11.75 T before the addition of Ca^{2+} was 9.16 $mmol^{-1}s^{-1}$. The increase in the relaxivity with decreasing temperature (comparing to the value measured at 37°C, 8.2 $mmol^{-1}s^{-1}$) is expected due to a longer rotational correlation time. Then, 100 µL of 10 mM Ca^{2+} solution in extracellular matrix / HEPES solution was added and the relaxivity was measured again. The time between the Ca^{2+} addition and the actual measurement was 6 minutes (experimental set up). The relaxivity dropped to a value 6.82 $mmol^{-1}s^{-1}$.
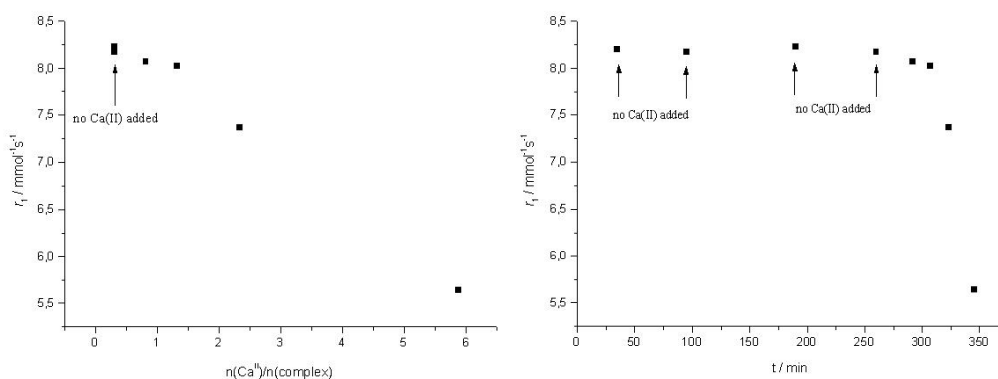

Figure 26: (A) Dependence of the relaxivity of **Gd₂-27** in ECM on the Ca^{2+} concentration; **(B)** Dependence of the relaxivity of **Gd₂-27** in ECM on the time (37°C, 11.75 T).

Table 6: Experimental data from the second relaxometric titration of **Gd₂-27** with Ca^{2+} at 37°C and 11.75 T in ECM. Time values correspond to the time passed from the preparation of the complex solution in the extracellular matrix. No EDTA was added in this titration.

time / min	V_{total} / µL	r_1 / $mmol^{-1} \cdot s^{-1}$	$c(Ca^{2+})/c(complex)$
35	408	8.20	0.3
65	408	8.17	0.3
190	408	8.23	0.3
260	408	8.17	0.3
292	418	8.07	0.81
307	428	8.03	1.32
323	448	7.37	2.33
345	508	5.64	5.88

4.3.6. Conclusion

In this work, we report the straightforward synthesis of five novel bismacrocyclic DO3A-type ligands **25-27**, **31** and **36**. They have a DTPA- or EDTA-bisamide moiety as the bridging part between the macrocycles representing a potential Ca^{2+} binding site. The relaxivities of the all Gd^{3+} complexes formed with **25-27**, **31** and **36** are considerably higher than that of currently used small-molecular-weight MRI contrast agents, in accordance with their larger size, increased rigidity or higher hydration number. The sensitivity of their relaxivity towards Ca^{2+} largely depends on the structure of the ligand. Upon Ca^{2+} addition, the relaxivities of **Gd$_2$-25** and **Gd$_2$-27** increase by 15% and 32%, respectively, while **Gd$_2$-26**, **Gd$_2$-31** and **Gd$_2$-36** are practically insensitive to Ca^{2+} binding. Hydration numbers were determined from luminescence lifetime measurements on the corresponding Eu^{3+} complexes in the absence and presence of Ca^{2+}. High resolution UV-Vis spectra of the Eu^{3+} complexes of **25**, **26** and **27** show a band with a shoulder, indicating at least two different coordination environments. This was related to differently hydrated species, in agreement with the non-integer q values obtained by luminescence. When Ca^{2+} is coordinated in the central part of the ligand, a donor group is removed from the coordination sphere of the lanthanide ion and is replaced by a water molecule which shifts the hydration equilibrium towards the more hydrated species.

Water exchange is relatively slow on **Gd$_2$-25** and **Gd$_2$-26**, while it is ~2 orders of magnitude faster on **Gd$_2$-27**; in all cases, it is insensitive to Ca^{2+} binding. Due to the benzene linker between the macrocycles and the central DTPA-bisamide unit, the **Gd$_2$-25** complex is particularly rigid, hence has a high relaxivity. A detailed analysis of the luminescence, ^{17}O NMR and NMRD data on the Eu^{3+} and Gd^{3+} complexes of **25** and **27** in the absence and presence of Ca^{2+} proved that the relaxivity increase observed upon Ca^{2+} addition can be ascribed to the increase in the hydration number, q, and to the slight rigidification of the complex induced by Ca^{2+} binding.

The complex **Gd$_2$-27** is then added to the extracellular matrix, it certainly interacts with some proteins because the resulting relaxivity is significantly higher than what was observed in only aqueous solutions. However, the addition of Ca^{2+} causes possibly a conformational change or an aggregation of the proteins, which terminate their interaction with the paramagnetic complex and the relaxivity

decreases. This relaxivity decrease is much more significant than the possible increase due to the interaction between the complex and Ca^{2+} and it happens at similar time schedule, so as a result, no relaxivity increase can be observed.

CHAPTER 5

Development of Biocytin-based Contrast Agents for Molecular Imaging: An Approach towards New *In Vivo* Neuroanatomical Tracers

5.1. Introduction

The advance of axonal tract-tracing and cell labeling methods has revolutionized neuroscience in the past three decades. The elementary purpose of neuronal tract-tracing is to chart anatomical connections within the nervous system providing useful information on afferent and efferent connectivity in the brain. Neuroanatomical tracers are used to ascertain the cells of origin that innervate a certain brain structure and/or the projection target of the axons of a given population of neurons (retrograde and anterograde tracers, respectively)[164,165]. Recent developments include the possibility to combine, for instance, different tracers allowing the comparison of multiple connections in the same animal, both quantitatively and qualitatively.

Numerous investigations using these classical neuroanatomical techniques have contributed valuable descriptions of connectivity in the mammalian brain[166-172]. These studies, however, require fixed processed tissue for data analysis and therefore cannot be applied to an animal participating in longitudinal investigations, where consecutive studies examining an entire circuit could be carried out in the same subjects. It is therefore important to seek alternatives that can be used in longitudinal *in vivo* experiments. Paramagnetic anterograde or retrograde tracers that can be visualized with magnetic resonance imaging (MRI) are of obvious importance. In contrast to the studies using conventional techniques, volume imaging with MRI-visible neuronal tracers provides indeed complete descriptions of large-scale three-dimensional (3-D) networks. Furthermore, such noninvasive technique could be repeatedly applied in the same experimental animal to visualize different neuronal pathways, and generate individualized connectivity maps that could guide, for instance, multiple and targeted electrophysiological recordings. Last but not least the technique is invaluable for longitudinal studies, such as those of plasticity and reorganization, or of neurodegenerative processes.

Manganese-enhanced MRI (MEMRI)[173,174] is a recently introduced technique that represents the first effort in the direction of studying neuronal connectivity *in vivo* by means of MRI[175]. It is based on the paramagnetic properties of the manganese ion and on the fact that, once taken up by neurons, manganese is transported anterogradely in the axon[175-183]. However, the technique presents several drawbacks

that can challenge its applicability, the most important being the potential toxicity of the ion in the tissue. It is well known that excessive accumulation of Mn^{2+} decreases energy metabolism, increases the production of free radicals, and induces cell death of both, neurons and glia, in experimental models[184,185]. Perturbations of the neuronal circuits under study, due to such toxicity would eliminate the value of Mn^{2+} as an *in vivo* neuronal tracer, particularly for functional studies, for quantitative 3-D analysis of connectivity, or for repetitive applications investigating the same pathway dynamically in time. Additional disadvantages of the manganese technique are its high diffusion at the injection site, which challenge the specificity of the resulting projections, and its incompatibility with other visualization systems[186-188]. For instance, at the end of an *in vivo* connectivity experiment using a paramagnetic tracer, it could be very informative to analyze the laminar and subcellular distribution of the neuronal connections. Such an experiment can not be performed by using current MEMRI methods.

Our aim was to develop non-toxic, efficient and multimodal neuronal tracers that allow both, *in vivo* brain connectivity studies by means of MRI and postmortem microscopic investigation in fixed tissue, in the same experimental animal. For this purpose we used biocytin[189] (Fig. 27) as a model neuroanatomical tracer, which is taken up by neurons and transported in both antero- and retrograde directions. Some characteristics make biocytin a good tracer model. It has been used in numerous tracing studies, both after intracellular or extracellular application, and much is known about its biophysical properties[190]. Due to its high affinity to avidin, it can be visualized by using a host of avidin conjugated markers at the light- and electron microscopic level. Extracellular application of biocytin results in very well localized injection sites with no uptake by fibers of passage or glial cells. These two last characteristics result in a high specificity of biocytin tracings. Finally, some authors have described transynaptic transfer of the molecule, allowing polysynaptic networks to be studied[191-193].

Structurally, biocytin has a combination of D-biotin and L-lysine, where carboxylate of D-biotin is connected with ϵ-amine of L-lysine via amide linkage (Fig. 27)[189]. It can be easily degraded in the presence of biotin-dependent carboxylase (biotinidase), a ubiquitous enzyme present in mammalian serum[194-196]. For this reason,

biocytin has relatively small half life *in vivo*, which forces short post injection survival times and increase the probability of partial reconstruction of neuronal projections. A number of strategies have been formulated to overcome this problem, including the use of sterically hindered amide bonds (either *tert*-amide or presence of α-kitone/carboxylate) to render the linkage stable to biotinadase[197,198]. We have first designed and synthesized a newly modified-biocytin, where propylamine is linked to amide of biocytin to make it *tert*-amide, which is more stable to biotinidase degradation, as compared to conventional biocytin. The presence of an additional amine group makes the modified biocytin a bifunctional neuroanatomical tracer, which can be attached to a fluorophore fluorescein to make it usable for optical imaging, or to a macrocycle to hold gadolinium and use it for MRI as potent noninvasive neuroanatomical tracers.

We have developed three novel and structurally different gadolinium containing biocytin-based neuroanatomical tract-tracers (**41**, **45** and **50**, Fig. 27). In the first tracer (**41**), GdDO3A-EA is connected with terminal end carboxylate of biocytin via amide bond. The second tracer (**45**), GdDOTA is connected with ϵ-amine of L-lysine via amide linkage. The third tracer (**50**) is derived from newly developed modified-biocytin where GdDOTA was coupled with propylamine via amide. **45** and **50** carry the unmodified L-lysine residue as it is thought to be important for cell uptake, and biotin is available in compounds (**41** and **50**) for avidin binding. The fourth tracer (**54**) has GdDOTA in **50** replaced with fluorophore fluorescein and can be useful for optical imaging.

The molecules we report in this study are a new class of biocytin-based and Gd-containing molecules that represent a new strategy for neuroanatomical tracing, combining the powerful spatial resolution of the conventional microscopic techniques with the whole brain tri-dimensional coverage and *in vivo* applicability of the MRI.
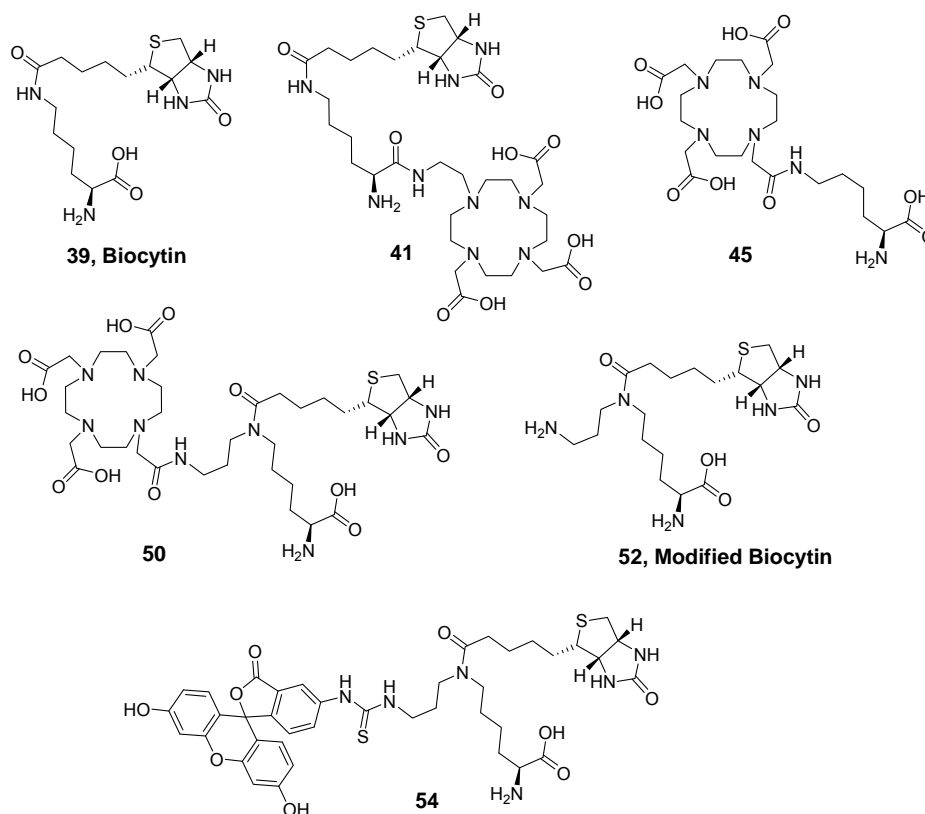
Figure 27. Structures of biocytin and other studied ligands.

5.2. Experimental Section

5.2.1. *In Vitro* MR Measurements

5.2.1.1 Sample Preparation for Relaxivity Measurements. Different concentrations (1 mM, 0.75 mM, 0.5 mM, 0.25 mM) of **Gd-41, Gd-45** and **Gd-50** were prepared in phosphate buffer in 1.5 mL Eppendorf tubes at physiological pH to measure relaxivity.

To examine the dependence of the relaxivity on the magnetic field, longitudinal and transverse relaxation rates (R_1 and R_2) of the **Gd-41, Gd-45** and **Gd-50** were performed at magnetic fields of 1.5T, 3T and 7T, corresponding to a proton frequency of 64 MHz, 123 MHz and 300 MHz, respectively. For 7T measurements, a vertical 7T/60 cm MRI Biospec system (Bruker Biospin, Germany); 3T measurements, a Trio System (Siemens Medical Solutions, Germany) was used; the 1.5T experiments were performed on a Siemens Avanto scanner.

5.2.1.2 MR Study of Avidin + Gd-41 and Gd-50 Interaction. To measure the enhancement of R_1 and R_2, MRI experiments were performed with increasing concentrations of avidin (Fluka, Germany) proportional to constant concentration of **Gd-41** and **Gd-50** (0.25 mM) incubated for 2 h at 37°C.

5.2.2. Rat Experiments

To test whether modified biocytin is more stable than conventional biocytin we performed iontophoretic injections of both compounds into the primary motor cortex of 4 albino rats (Sprague Dawley). Two rats (one with conventional and one with modified biocytin) were killed after a survival time of 24 hours and two rats (again one with conventional and one with modified biocytin) after a survival time of 96 h.

5.2.2.1. Injections. Rats were anaesthetized with 2% isoflurane. One injection per animal was made into the primary motor cortex at two or three different levels. In the animals with a survival time of 24 h, two injections were made, at a depth of 250 and 500 μm. In case of the animals with a survival time of 4 days, a third injection was made at a depth of 750 μm.

The tip diameter of the glass electrodes was 20 μm. Each injection was made over a period of 20 min, 7 sec on, 7 sec off, with 5 μA current in case of the animals with a survival time of 24 h, and 10 μA in case of the animals with a survival time of 4 days.

At the end of the procedure, the animals received an intra peritoneal injection of analgesics and antibiotics. The animals with a survival time of 96 h received another injection after 24 h.

5.2.2.2. Perfusion. After 24 h and 96 h respiration, the animals were anaesthetized with Isofluran and received then a lethal intraperitoneal injection of Narcoren. After cessation of all reflexes, the chest of the animal was opened and 0.4 ml of Liquemin was injected into the heart in order to prevent coagulation of the blood. Then a canule was inserted and the animals was perfused with PBS (phosphate buffer saline) for about 5 minutes and then with the fixative (4% paraformaldehyde in PBS).

After fixation in situ for 1 – 3 h, the brains were removed from the skull and kept in the fixative over night. During the next days, the brains were transferred

stepwise into 10%, 20% and then 30% sucrose, in each step until it has sunk. This took all together 96 h.

The brains were then cut with a freezing microtome into serial sections at a thickness of 70 μm.

5.2.2.3. Histological procedure.

- collect sections in PBS (using 0.1 M buffer; pH 7.3)
- 1% H_2O_2 in PBS (NaCl in 0.1m phosphate buffer) for 1 h to suppress endogen peroxidase activity
- Rinse in PBS
- 1 h treatment in Triton X-100 (0.5 % in 0.1 m PBS) (Triton makes it easier for the ABC-substances to enter the cell, since it cracks the membrane proteins).
- Incubation in avidin-conjugated peroxidase (Vector Laboratories, 1% in PBS, Note that the ABC-mixture must stand for 30 min before use.
- Rinse 1-3 x 10 min. in PBS
- 2-3 x 10 min. in Tris/HCl (0.15M, pH 7.9) (Tris can be made more basic than PB and this is better for the DAB-reaction)
- In DAB Fast Tablet Set-solution in water (contains diaminobenzidine 0.5% in Tris/HCl) and H_2O_2.
- Wash 3 x 10 min. in Tris/HCl
- Then mount sections on slices and air-dry overnight.

Dehydration on the next day in graded ethanols (70%, 80%, 2 x 99%, 2 x 100% ethanol, 2 x terpineole and 2 x xylene, cover in Eukitt or DePeX

5.2.3. *In vitro* Cell Study of 54

Cell experiments were done in single channel Ibidi slides by inoculation of N18 neuroblastoma cells (3 x 10^5 cells/ml) cultured in Dulbecco's Modified Eagle's Medium supplemented with 0.625% foetal bovine serum and 4 mM L-glutamine (all purchased from Biochrom AG, Germany). After 70-80% confluency, cells were incubated with 100 μM of **54** for 1 hour. Before washing cells were incubated with a nuclear stain Bisbenzimid 33342 (Hoechst 33342) for 5 mins. After repeated cell washings with Hanks' buffered saline (Biochrom AG, Germany), fluorescence microscopy was performed with cells on a Zeiss Axiovert 40 CFL (Germany) to

observe the cellular localization of **54**. The imaging conditions were kept constant for the observation of different samples. Cellular localization and distribution of **54** was observed by irradiating with blue light (470-/40 nm) and observing at 525/50 nm and nuclear labeling by Hoechst was observed at 460/50 nm. Also phase contrast images with DIC of the same area were made to observe if the cells maintain their normal morphology in the presence of compound.

5.3. Results and Discussions

5.3.1. Synthesis of Ligands

Conventional biocytin is naturally occurring conjugate of D-biotin and L-lysine and it has been acclaimed as an excellent classical neuroanatomical tracer. Previously biocytin has been synthesized efficiently by Wolf *et al.*[189] in five steps starting from ε-N-carbobenzoxy-L-lysine and although it has been described by other many researchers. We report here four step convenient synthetic route for the synthesis of ε-N-biotinyl-L-lysine, **39** starting from α-N-carbobenzyloxy-L-lysine methyl ester. Compound **37** was obtained by coupling of ε-amine of α-N-carbobenzyloxy-L-lysine methyl ester with carboxylate of D-biotin by using classical solution phase coupling reagents, NMM/EDC/HOBt in dry DMF at room temperature. Intermediate molecule **38** was obtained by deprotection of methyl group by LiOH and further α-N-carbobenzyloxy removal by Pd-C (10%), H_2 in Parr-apparatus at 50 psi yielded final ligand **39** (Scheme 9).

Previously described amine containing macrocyclic precursor tris-*tert*-butyl-DO3A-EA[84-86,125], **19** was synthesized in two steps, starting from alkylation of bromoacetonitrile on well known ligand tris-*tert*-butyl-DO3A **3**[87] to get cyano containing ligand **18**[141]. Cyano reduction of **18** in the presence Ra-Ni, H_2, 7N NH_3/MeOH in Parr-apparatus at 50 psi provided amine containing precursor tris-*tert*-butyl-DO3A-EA, **19**[142]. Protected biocytin conjugated tris-*tert*-butyl-DO3A-EA ligand **40** was synthesized by coupling of carboxylate of **38** with amine of **19**, in the presence of above described coupling reagents (NMM/EDC/HOBt). Corresponding carboxylate containing macrocyclic ligand **41** was obtained in two steps by deprotection of α-N-carbobenzyloxy in the presence of Pd-C (10%), H_2 in Parr-

apparatus at 50 psi and further acid labile *tert*-butyl groups were removed by neat TFA (Scheme 9).
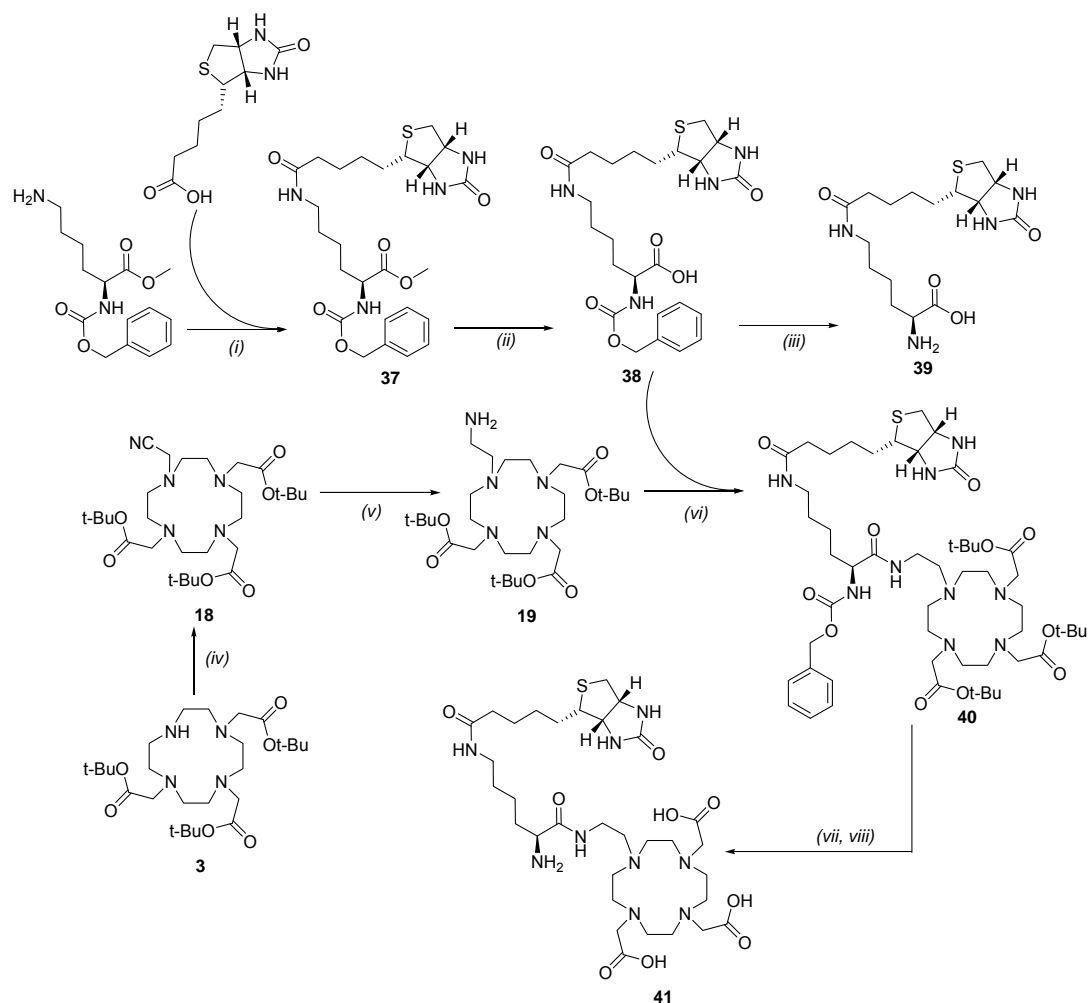
Scheme 9. Reagents and conditions: *(i)* D-biotin, α-N-carbobenzyloxy-L-lysine methyl ester, dry DMF, NMM, EDC, HOBt; *(ii)* LiOH [THF;MeOH;water (3:2:2)]; *(iii)* Pd-C (10%), H_2, MeOH; *(iv)* bromoacetonitrile, K_2CO_3, MeCN; *(v)* Ra-Ni, H_2, NH_3/MeOH (7N); *(vi)* dry DMF, NMM, EDC, HOBt; *(vii)* Pd-C (10%), H_2, MeOH; *(viii)* TFA.

In the scheme 10, free carboxylate holding macrocyclic precursor tris-*tert*-butyl-DOTA, **43** was obtained from cyclen in 52% yield over three steps, by the reaction with *tert*-butylbromoacetate to get the tri-substituted product **3** as reported previously[87]. Alkylation with benzylbromoacetate on fourth nitrogen gave **42** and the

corresponding carboxylate derivative **43** was obtained by deprotection of the benzyl group by the treatment of Pd-C (10%), H_2 in Parr-apparatus at 50 psi at room temperature. This precursor is useful to design variety of stable targeted contrast agents. By using **43**, we designed and synthesized lysine containing macrocyclic compound in 3 steps. ϵ-amine of α-N-carbobenzyloxy-L-lysine methyl ester coupled with carboxylate of **43** in the presence of NMM/EDC/HOBt in dry DMF at RT to give protected ligand **44**. Further three steps deprotection of α-N-carbobenzyloxy with Pd-C (10%), H_2 in Parr-apparatus at 50 psi and methyl group removal with LiOH in THF:MeOH:H_2O (3:2:2) and *tert*-butyl groups with neat TFA gives final lysine containing macrocyclic ligand **45** in good yield.
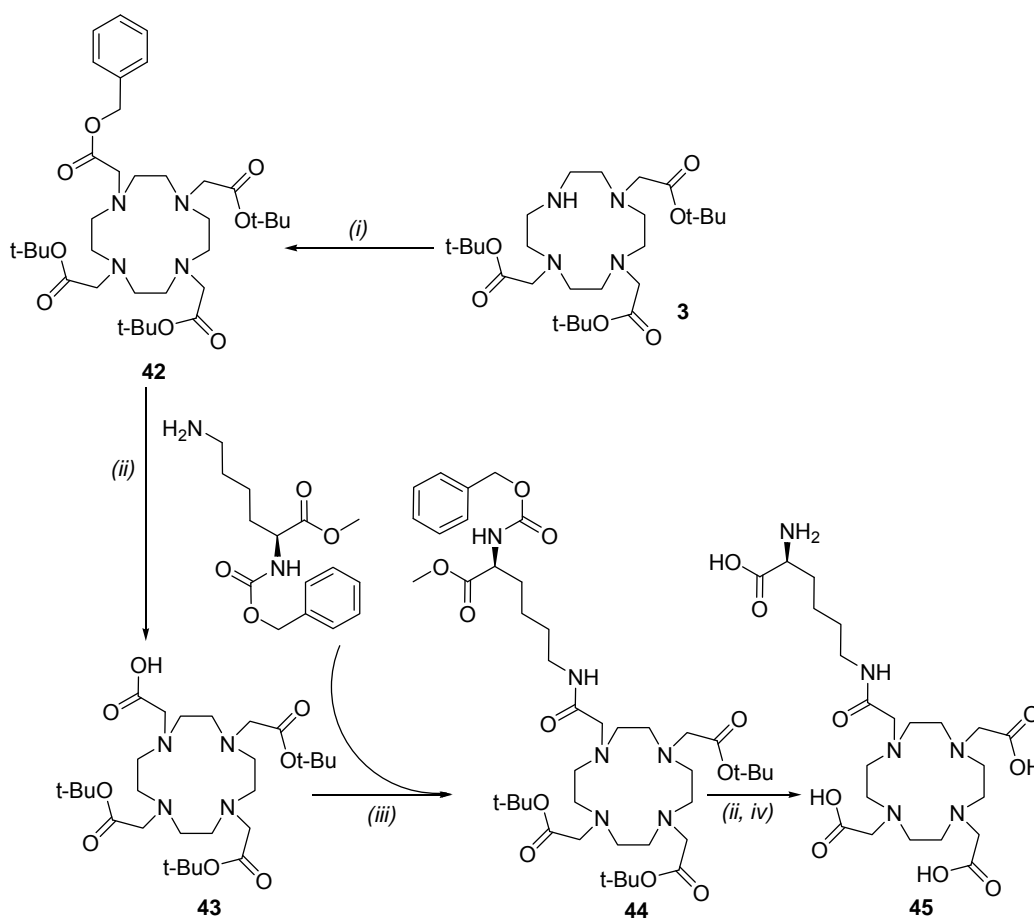
Scheme 10. Reagents and conditions: *(i)* benzylbromoacetate, K_2CO_3, MeCN; *(ii)* Pd-C (10%), H_2, MeOH; *(iii)* **3**, dry DMF, NMM, EDC, HOBt; *(iv)* LiOH [THF;MeOH;water (3:2:2)], TFA.
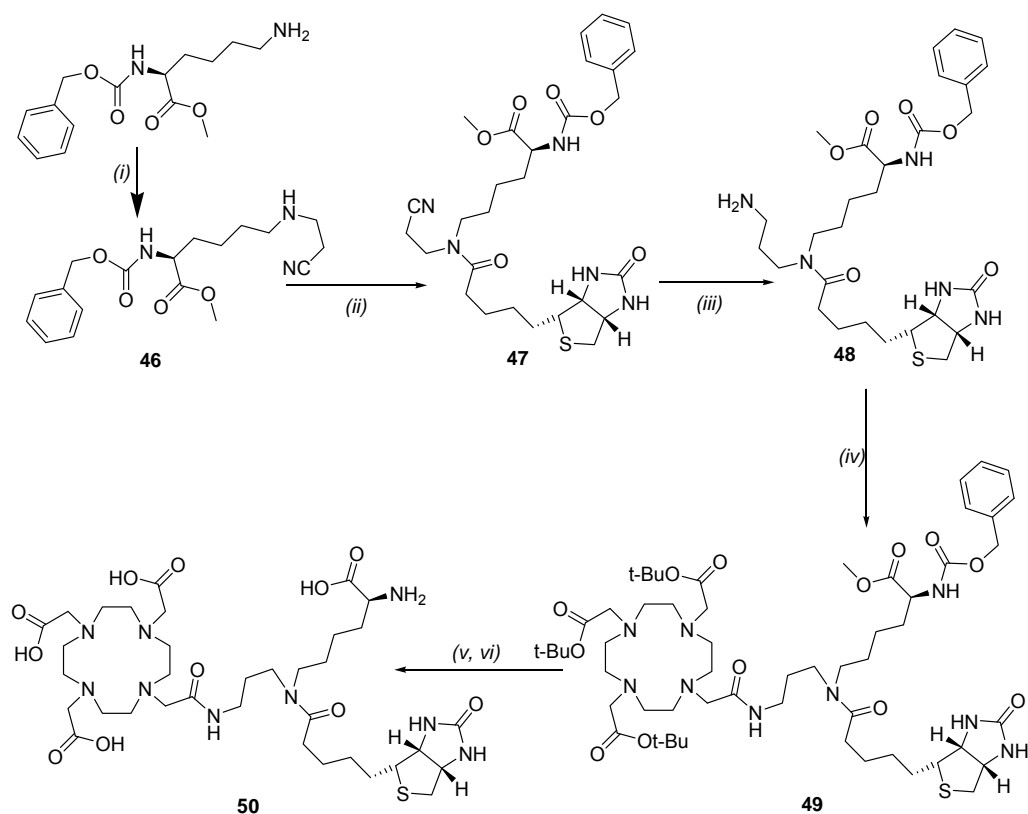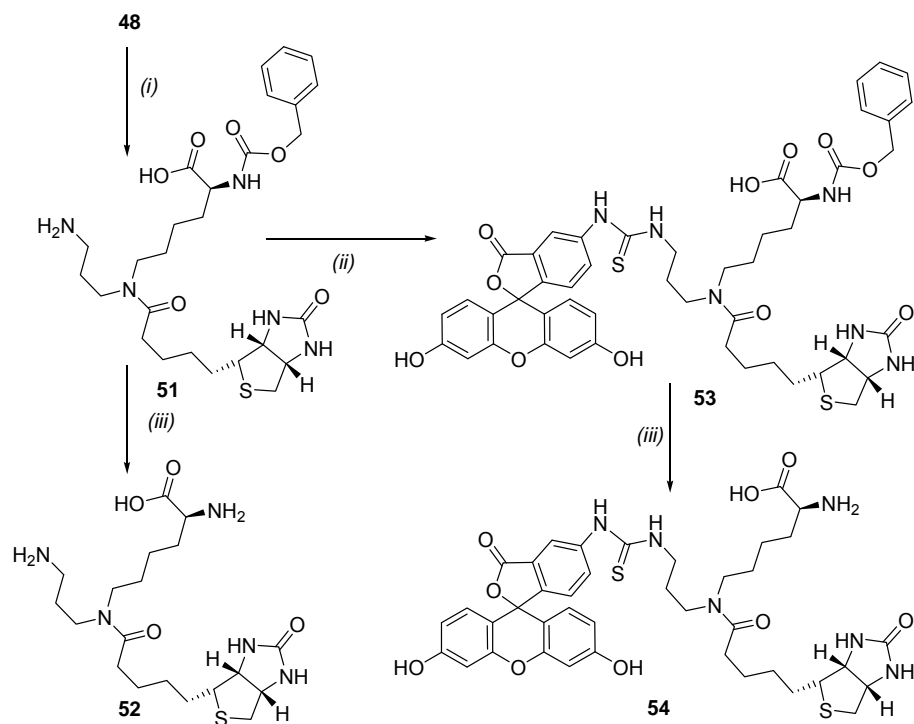
Scheme 11. Reagents and conditions: *(i)* acrylonitrile, TEA, MeOH; *(ii) D*-Biotin, PyBroP, DIEA, dry CH_2Cl_2; *(iii)* Ra-Ni, H_2, 7N NH_3/MeOH; *(iv)* **43**, NMM, EDC, HOBt, dry DMF; *(v)* Pd-C (10%), H_2, MeOH; *(vi)* LiOH [THF;MeOH;water (3:2:2)], TFA.

After the successful synthesis of macrocyclic precursor **43**, the bioconjugate ligand **50** was synthesized in seven step reaction (Scheme 11). Starting with Micheal addition by using acrylonitrile on α-N-carbobenzyloxy-L-lysine methyl ester gives cyano containing compound **46**. Cyano containing modified biocytin compound **47** was obtained after coupling with carboxylate of biotin with secondary amine of **46** by using PyBroP as coupling reagent in dry dichloromethane solvent by the addition of diisopropylamine as base. Concurrently by the selective reduction of cyano group in the presence of Ra-Ni, H_2, 7N NH_3/MeOH yielded amine containing protected modified biocytin compound **48**. Modified biotcytin conjugated tris-*tert*-butyl-DOTA compound **49** was obtained by the coupling of amine of **48** with ligand **43** using

NMM/EDC/HOBt in dry DMF at Room Temperature (rt). In the following step, final ligand **50** was obtained in 77% yield by three steps deprotection of methyl group with LiOH in THF:MeOH:H$_2$O (3:2:2), removal of α-N-carbobenzyloxy with Pd-C (10%), H$_2$ in Parr-apparatus at 50 psi and *tert*-butyl groups with neat TFA.

A novel amine bearing modified biocytin **52** was synthesized, starting from **48** in two steps by deprotection of methyl group with LiOH in THF:MeOH:H$_2$O (3:2:2) give compound **51** and removal of α-N-carbobenzyloxy with Pd-C (10%), H$_2$ in Parr-apparatus at 50 psi compound **52** was isolated. It is potential bifunctional neuroanatomical tracer, where either can be connected macrocyclic unit to make it a contrast agent for MRI as we described in previous scheme or by the coupling with fluorophore fluorescein can give tracer for optical imaging (Scheme 12).

The fluorophore fluorescein containing modified biocytin compound **54** was attempt to synthesize as shown in scheme 12. The most logical route to synthesize compound **54** in two steps starting from compound **51**, by coupling of FITC with **51** at pH 8-8.5 yeilded compound **53**. During the reaction we observed pH was not allowed to exceed 8.5 since at pH > 9, a lactone cleavage on FITC part occurs, leading to the formation of a side product. After getting protected FITC containing modified biocytin, we tried to cleave α-N-carbobenzyloxy with Pd-C (10%), H$_2$ in Parr-apparatus and some other reported mild cleavable reagents. But some degradation was observed in all these conditions.

Scheme 12. Reagents and conditions: *(i)* LiOH, THF;MeOH;water (3:2:2); *(ii)* FITC, water, pH 8-8.5; *(iii)* Pd-C (10%), H$_2$, MeOH.

After unsuccessful attempt for the synthesis of FITC conjugated modified biocytin, **54**, we designed second pathway to synthesize it in 5 steps starting from compound **47** (Scheme 13). By deprotection of α-N-carbobenzyloxy from **47** with Pd-C (10%), H$_2$ in Parr-apparatus give compound **55**. Further protection with acid labile Boc group provided compound **56**. After reduction of cyano group of **56** in the presence of Ra-Ni, H$_2$, 7N NH$_3$/MeOH in Parr-apparatus at 50 psi we obtained amine containing compound **57**. Compound **58** was isolated in a same way as described in the previous scheme, where FITC coupled with amine of compound **57** via thiourea linkage in water at pH 8-8.5. Finally removal of Boc group in the presence of formic acid yielded FITC conjugated modified biocytin, which is useful for optical imaging. Modified biocytin, **52** was also obtained after removal of Boc group from **57** in neat formic acid.
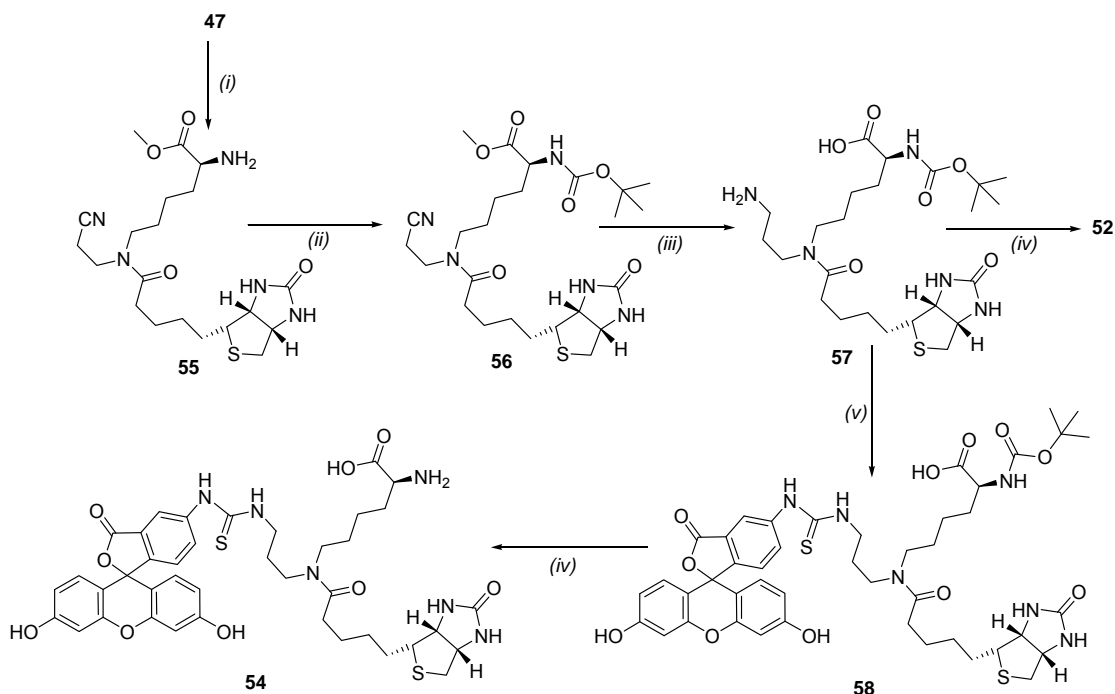
Scheme 13. Reagents and conditions: *(i)* Pd-C (10%), H$_2$, MeOH.; *(ii)* Bocanhydride, DCM, TEA; *(iii)* LiOH, THF;MeOH;water (3:2:2); Ra-Ni, H$_2$, 7N NH$_3$/MeOH; *(iv)* TFA; *(v)* FITC, water, pH 8-8.5.

All intermediate compounds (**38**-**40**, **48**, **49**, **51**-**54**, **57** and **58**) were purified by RP-HPLC as described methods in experimental section by using 0.1% TFA in acetonitrile and 0.1% TFA in water as mobile phases. Final compounds (**41**, **45** and **50**) were also purified RP-HPLC by using MeOH and water as mobile phase as described in experimental section.

Finally, Gd^{3+} complexes were synthesized for ligands **41, 45** and **50** (Fig. 28). During loading Gd^{3+} in biotin containing ligands reaction temperature was kept under 60°C because of possible degradation of bioconjugate moiety.
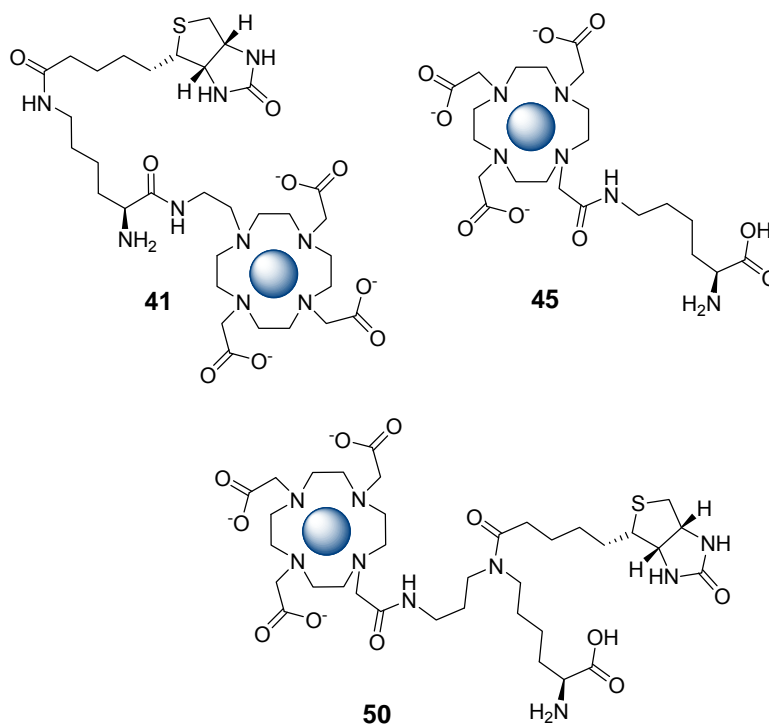
Figure 28. Structures of Gd^{3+}-complexes of **41, 45** and **50**.

5.3.2. *In Vivo* Histological Applications

In order to test the stability and feasibility as neuronal tracer of the newly synthesized modified biocytin, **52**, and compare it with the traditional biocytin, we perform a series of neuronal tract-tracing experiments in rats. We inject by means of iontophoresis a comparable amount of both tracers in the primary motor cortex of the rat. We divided the experimental animals in two groups with different survival times, 24 h and 96 h, respectively. After that time we perfused the animals and analyzed both, the intensity of the staining, reflecting the number of nondegraded tracer molecules in the tissue at that particular time, and the presence of anterogradely stained fibers and retrogradely labeled cells, to demonstrate the feasibility of the new tracer. As can be seen in Fig. 29, the amount of intact molecule (or molecule with intact avidin binding capacity) remaining in the tissue after 24 h, is clearly higher for the new modified biocityn compare to the conventional. As would be expected, this effect is even more dramatic when the survival time and thus, the time of exposure to endogenous biotinidase activity, is increased from 24 h to one day (Fig. 30). Interestingly, positively labeled fibers and cell bodies were found as far as 3.5 mm

from the injection site (Fig. 31), unequivocally demonstrating that the new modified biocytin molecule retains extraordinary tracer capacities after the modification.

The combination of the following characteristics, tracer capability and greatly improved stability, makes the new modified biocytin and excellent alternative for conventional histological studies, as well as a promising molecule for *in vivo* imaging of neuronal networks. A common problem in conventional histological techniques is the partial reconstruction of connections at the network level, or the incomplete reconstruction of dendritic and axonic arbors at the cellular level. Such problems that are caused by the endogenous degradation of the tracer molecule before the sacrifice of the animal will be greatly reduced with the reported molecule. On the other hand, the possibility to stably accumulate a greater amount of tracer molecules in a target tissue will increase the signal to noise ratio and thus, the probability of detection in MRI, a technique with less spatial resolution and sensitivity than any other light, confocal or electronic microscopy approach. All in all, we believe that the modified biocytin molecule that we report here represents a new tool with a broad range of applications in the neuroscience field.
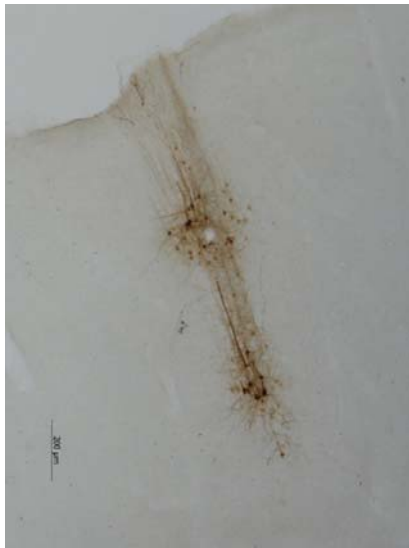
39   **52**

Figure 29. Histological studies of conventional biocytin (**39**) and modified biocytin (**52**) with the survival time 24h.
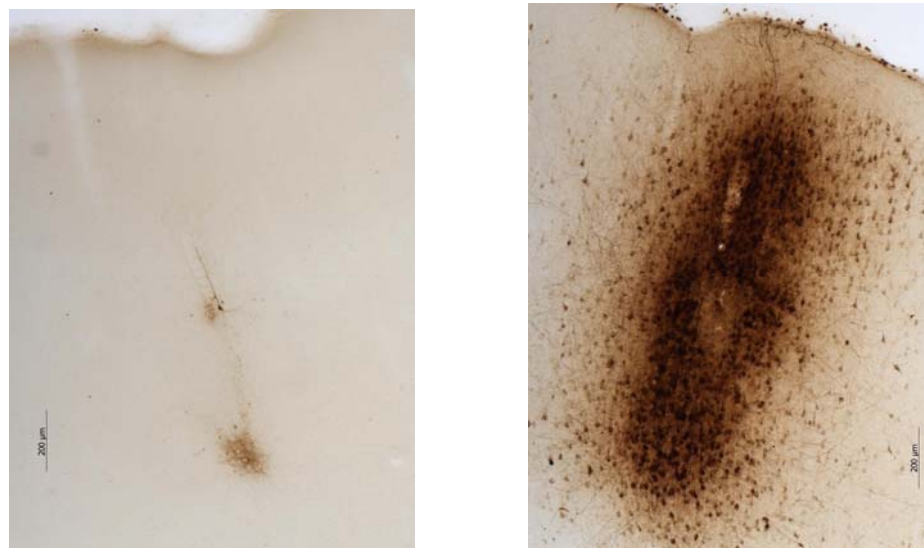
Figure 30. Histological studies of conventional biocytin (**39**) and modified biocytin (**52**) with the survival time 96h.
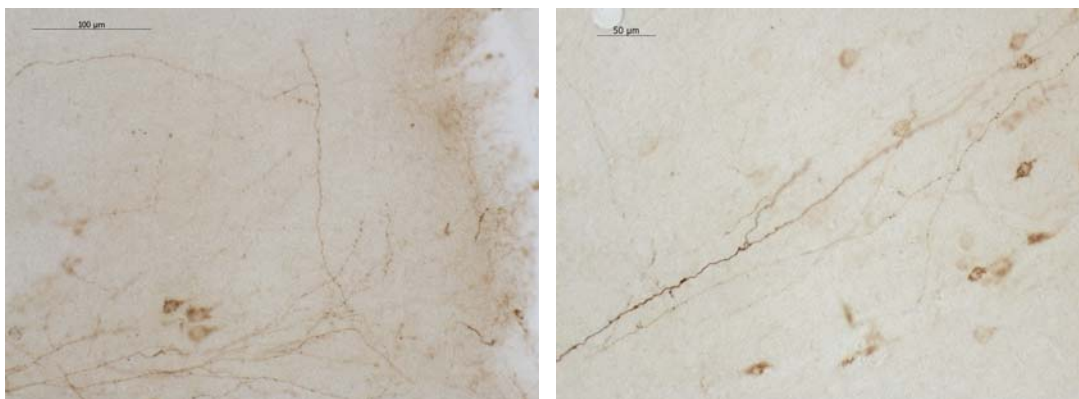

Figure 31. Histological studies of modified biocytin (**52**) with the survival time 96h; shows some retrograde tracing 3.5 mm away from injection site.

5.3.3. *In Vitro* **Biochemical Applications**

5.3.3.1. In Vitro **Relaxometry** *of Gd-41, Gd-45 and Gd-50.* To examine the effect of binding on the longitudinal and transverse relaxation rates, we performed MRI experiments at different field strengths (7T, 3T and 1.5T) with increasing concentrations of avidin proportional to constant concentrations of **Gd-41** (0.25 mM)**, Gd-45** (0.25 mM) and **Gd-50** (0.25 mM). **Gd-45** has no biotin, which has been used as control in these experiments. **Gd-45** has no interaction with avidin that's why

longitudinal and transverse relaxation rates were constant after adding excess of avidin protein. In contrast of **Gd-45**, **Gd-41** and **Gd-50** show a linear enhancement in relaxation rates which demonstrated strong binding of **Gd-41** and **Gd-50** in the biotin binding pocket of tetramer avidin (Fig. 32 and 33). This gain in relaxation rates suggest a decrease in molecular rotational correlation time τ_R. Similar to literature reports, proposing that one avidin molecule strongly binds four equivalents of biotin[94], we obtained saturation in relaxation rates at ratios higher than 4:1 between **Gd-41**; **Gd-50** and avidin.

As expected, MR longitudinal relaxation rate, R_1 of **Gd-41** slightly decreases, 12% upon binding of the complex to avidin at 7T, but at 3T it start increasing up to 31% and reaches 115% at 1.5T (Fig. 32, left side). This is in accordance to the Solomon–Bloembergen–Morgan theory predicting that at high magnetic field (>4.7 T), the relaxivity changes with the inverse of τ_R suggesting that relaxivity decrease should be expected upon binding of the CAs to a large molecule[124]. On the other hand, an enhancement in transverse relaxation rates, R_2 of complex was observed consistent with non-covalnet association of **Gd-41** to avidin. Thus, at physiological pH and ambient temperature, the increase in R_2 of the ternary adduct of **Gd-41** with avidin showed a maximum enhancement of 296% at 7T, 332% at 3T and 338% at 1.5T relative to the unbound **Gd-41** complex (Fig. 32, right side). This effect has already been discussed in first chapter with avidin-bound complex (**Gd-9**) consistent with ternary complex formation; thus the decrease of τ_R leads to a stronger R_2 enhancement at high magnetic field[125,126].

MR longitudinal relaxation rate, R_1 of **Gd-50** is also slightly decreases, 8% upon binding of the complex to avidin at 7T, but at 3T it start increasing slightly up to 8% and reaches 29% at 1.5T (Fig. 33, left side). On the other hand, an enhancement in transverse relaxation rates, R_2 of complex was observed consistent with non-covalnet association of **Gd-50** to avidin. Thus, at physiological pH and ambient temperature, the increase in R_2 of the ternary adduct of **Gd-50** with avidin showed a maximum enhancement of 103% at 7T, 97% at 3T and 93% at 1.5T relative to the unbound **Gd-50** complex (Fig. 33, right side).
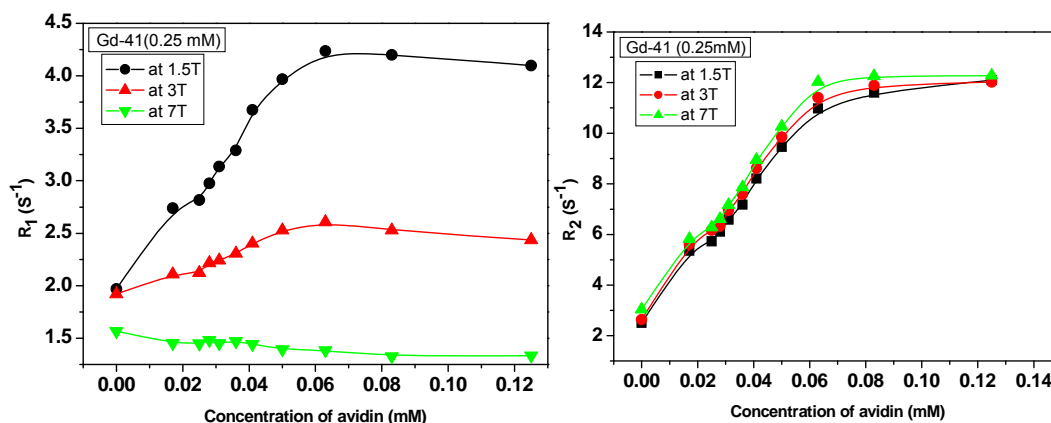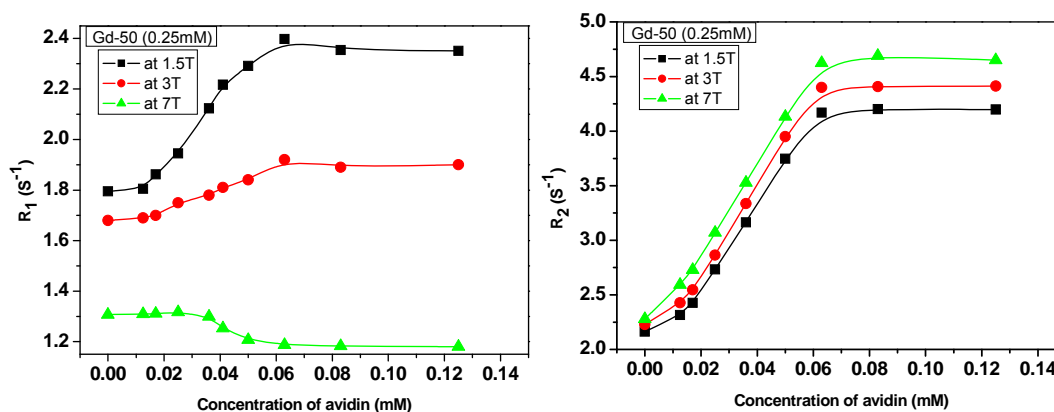
Figure 32. *In vitro* MR measurement of longitudinal (R_1) and transverse relaxation rate (R_2), **Gd-41** with varying concentrations of avidin. MR experiment was performed at different field strength 7T, 3T and 1.5T ($\approx 21°C$) with constant concentration of **Gd-41** (0.25 mM) and increasing amount of avidin in different tubes. A linear relaxation enhancement was observed up to 0.63 mM (0.25 equivalents). At higher ratios relaxation rates R_1 and R_2 remained constant. [Error for all R_1 and R_2 values was less then (± 0.5) s^{-1} and is not displayed].

Figure 33. *In vitro* MR measurement of longitudinal (R_1) and transverse relaxation rate (R_2), **Gd-50** with varying concentrations of avidin. MR experiment was performed at 7T, 3T and 1.5T ($\approx 21°C$) with constant concentration of **Gd-50** (0.25 mM) and increasing amount of avidin in different tubes. A linear relaxation enhancement was observed up to 0.63 mM (0.25

equivalents). At higher ratios relaxation rates R_1 and R_2 remained constant. [Error for all R_1 and R_2 values was less then (± 0.6) s^{-1} and is not displayed].

In future applications, the MRI contrast sensitivity can be therefore improved by designing CAs using the above approach, as the biotin-avidin association is expected to enhance the signal by means of *in situ* accumulation of the agent. Avidin has been already utilized for drug delivery through the blood brain barrier[93]. It is important for future non-invasive, e.g. human research applications, which do not afford intracranial injections. There are several studies and reports regarding biotin-avidin interaction *in vitro* and *in vivo*. Gruber *et al* presented few examples of biotin-fluoresceine conjugates with an ethylene diamine spacer was found to be the first fluorescent biotin derivative which truly mimicked D-biotin in terms of high affinity, fast association, and non-cooperative binding to avidin and streptavidin tetramers. In these varieties of biotin-fluoresceine conjugates, they observed that steric hindered spacer conjugates showed less fluorescence quenching effect in contrast to small and flexible conjugates. Our *in vitro* MR results also showed different relaxivity enhancement with different molecules, which prove above descriptions. **Gd-41** is more flexible as compared to **Gd-50,** and this was justified by 300% R_2 enhancement in **Gd-41** while **Gd-50** showed only 100% enhancement. Although **Gd-41** exhibits probability for use in MR imaging but translation to a system for *in vivo* application is hampered by certain drawbacks. Hydrolysis of DTPA-biotin and DOTA-biotin by endogenous biotinidase has been reported[95]. This problem has been successfully overcome by chemically modifying the structure in order to effectively block biotinidase[66,96]. In addition, endogenous biotin levels (10^{-8}-10^{-7} mol/L), immunogenicity of avidin and high and prolonged renal uptake markedly affect efficacy of avidin and streptavidin based pretargeting strategies[63,67,97]. Our DOTA-modified biocytin conjugate can be used for *in vivo* application because it has *tert*-amide which is unaffected by biotinidase enzyme. Stability of **Gd-50** has been compared by *in vivo* histological application of **52**.

5.3.3.2. In vitro cell study of 54. Fluorescence microscopy of living cells displayed a detectable uptake of the compound into N18 neuroblastoma cells. Figure 33 shows example of cellular localization of **54** after incubation with 100 μM for 1 h and subsequent washings. **54** was internalized very quickly up to the nucleus of the cells

with vesicular distribution in the cytoplasmic projections. Also very prominent binding to the cellular membrane was (Fig. 33).
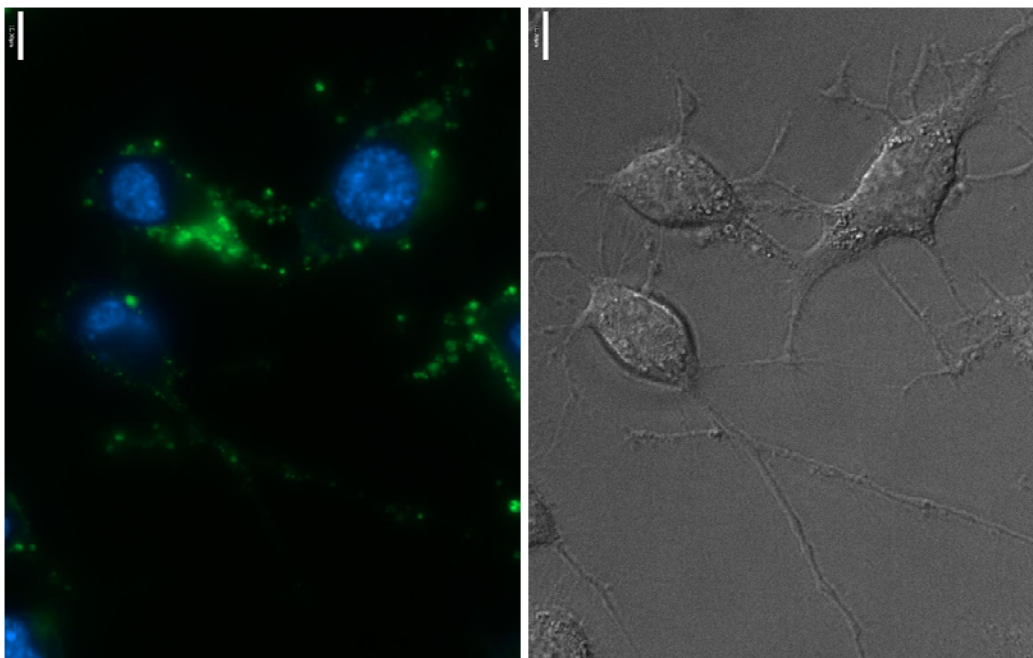

Figure 34. Optical evidence for intracellular localization of **54** in N18 neuroblastoma cells. Cells were incubated with 100 μM of **54** for 1 h in HEPES buffer as described in materials and methods.

5.3.4. Conclusions

In this chapter, we described synthesis and *in vitro* and *in vivo* applications of a stable modified biocytin (**52**), three structurally different macrocycle-biocytin derivatives (**Gd-41, Gd-45, Gd-50**) and one modified biocytin-fluoresceine conjugate (**54**).

Modified biocytin is designed and synthesized to be used as a stable classical anatomical neuroanatomical tracer in contrast to conventional biocytin. Stability and functionality of this molecule has been proved by *in vivo* histological studies, where a number of nondegraded tracer molecules were present in the tissue at that particular time, and the presence of anterogradely stained fibers and retrogradely labeled cells demonstrated feasibility of the new tracer.

Other macrocycle containing biocytin derivatives were designed to have neuroanatomical tracers to be used in MR imaging. As we proved in histological studies that our modified biocytin is more stable as compared to conventional biocytin, so compound **Gd-50** is a more appropriate tracer compared to **Gd-41**. Significant relaxivity enhancements in the presence of avidin show the potential of these CAs to be used not only as neuroanatomical tracers but also as diagnostic agents for cancer MR imaging. These CAs have been designed as neuroanatomical tracers, but they all have higher molecular weight as compared to modified biocytin. So before doing *in vivo* studies we have to prove that compounds are up taken by neuronal cells or not. It is tricky to know by MR that compounds are up taken by neuroblastoma cells; so we designed and synthesized a modified biocytin-fluoresceine conjugate, which has almost similar molecular weight and charge as **Gd-50** and it is easy to check by optical imaging. New biocytin-fluoresceine conjugate has been tested in neuroblast cell line and it shows efficient uptake after 1 h incubation in N18 neuroblastoma cells.

The above studies and results reveal several interesting and specific properties of these different conjugates. Presented molecules in this study are a new class of biocytin-based and Gd-containing molecules that represent a new strategy for neuroanatomical tracing, combining the powerful spatial resolution of the conventional microscopic techniques with the whole brain tri-dimensional coverage and *in vivo* applicability of the MRI.

CHAPTER 6

Synthesis of Novel Macrocyclic Bifunctional Ligand for Development of "*Smart*" and "*targeted*" Contrast Agents:

[4,7-Bis-carboxymethyl-10-(2-amino-2-carboxyethyl)-1,4,7,10-tetraaza-cyclododec-1-yl]-acetic acid

6.1. Introduction

'*Smart*' MRI CAs exhibit dynamic and reversible modulation of their relaxivity by specific physiological or biochemical trigger events such as changes in pH[41-46], calcium ion concentration[47-51], enzymatic activity[52-54], or the binding of an intracellular messenger. '*Targeted*' CAs are able to recognize specific target molecules inducing an enhancement of water proton relaxation rate on binding with the target molecule[17,55]. Mostly '*smart*' or '*targeted*' CAs can possess bifunctionality: '*Bifunctional*' chelating agents have the ability to incorporate lanthanide ions to make strong and stable chelates and contain in addition a chemically highly reactive group[199].

In previous research, acyclic and macrocyclic polyaminocarboxylate chelating agents have gained considerable attention[200-204]. The most promising agents studied so far are the acyclic chelating agent diethylenetetraaminepentaacetic acid (DTPA) and macrocyclic chelating agent [4,7,10-tris-carboxymethyl-1,4,7,10-tetraaza-cyclododec-1-yl]-acetic acid (DOTA). Since our interest is to develop new macrocyclic contrast agents, the *in vivo* stability of the derivatives is of prime importance. It has been shown that, compared to acyclic CAs-macrocyclic derivatives form extraordinarily stable complexes with a variety of paramagnetic metal ions under physiological conditions[201,203,205,206].

Derivatives of DOTA [for example DOTA-tris (*tert*-butyl) ester] emerged as a useful synthon for the synthesis of various '*targeted*' CAs after conjugation with a variety of biomolecules like peptides, bile acid, and proteins[35,79,207-211]. [4,7-Bis-carboxymethyl-1,4,7,10-tetraaza-cyclododec-1-yl]-acetic acid (DO3A) is a part of DOTA and which is more stable as compared to acyclic chelates but less stable as DOTA. Several DO3A derivatives were extensively investigated in the recent years[35,39,43-45]. DOTA is most stable chelates for paramagnetic metal ions but due to compact structure it has less water exchange rate. [4,7,10-tris-carboxymethyl-1,4,7,10-tetraaza-cyclododec-1-yl]-propionic acid (DO3A-N-PA) is alternate of DOTA, which has similar stability constant but 5 times fast water exchange rate as compare to DOTA. DO3A-N-PA has three arms as an acetic acid which can bind tightly with lanthanide ions but propionic acid as fourth arm which is weakly

associated with paramagnetic metal ions. It is a useful precursor to develop variety of "*targeted*" CAs. A major limitation of these ligands is that the carboxylate group allows the possibility only for amide or ester bond formation. That's why they restrict to develop "*smart*" CAs. In contrast to above molecules amine containing synthon [4,7-bis-carboxymethyl-10-(2-aminoethyl)-1,4,7,10-tetraaza-cyclododec-1-yl]-acetic acid (DO3A-EA) is a bifunctional ligand, bearing amine group that is readily reactive towards most electrophiles such as aldehydes, carboxylic acids and isothiocyanates to form various molecules for the development of *'smart'* and *'targeted'* CAs. This synthon have similar kinetics like DTPA/DO3A derivatives.
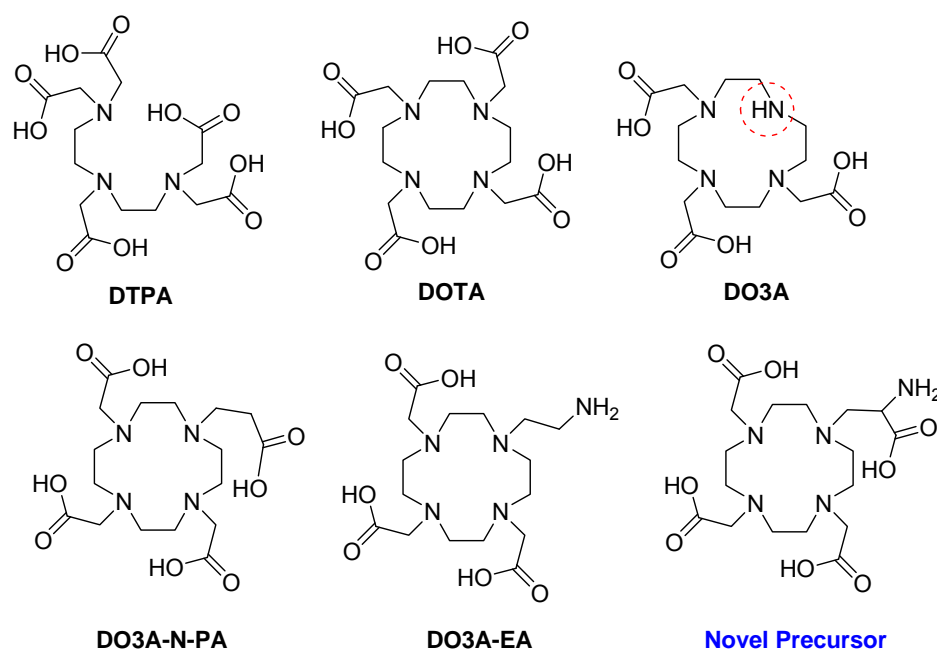
Figure 35. Novel precursor with all other discussed ligands

In an effort to develop new *'specific'* MRI contrast agents, we designed and developed a novel multipurpose bifunctional chelating agent [4,7-Bis-carboxymethyl-10-(2-amino-2-carboxyethyl)-1,4,7,10-tetraaza-cyclododec-1-yl]-acetic acid; [DO3A-α-aminopropionic acid (DO3A-αAPA)], which is based on DO3A, where the secondary nitrogen at position 10 in the macrocycle is alkylated by brominated serine molecule. This precursor is combination of DO3A-EA and DO3A-N-PA, where it has carboxylate free to hold lanthanide ions with extraordinary stability under physiological condition and highly reactive amine to reacts with any electrophiles.

This molecule serve as useful precursors for developing *'smart'* or *'targeted'* contrast agents based on lanthanide chelates in the design of relaxometric MRI probes as shown in Fig. 35. We also present in this chapter a variety of possible applications of this macrocyclic ligand after conjugation with diverse organic molecules. This demonstrates the significance and potential of these precursors in the design of *'smart'* as well as bifunctional *'targeted'* CA.

6.2. Results and Discussions

6.2.1 Synthesis of Ligand

We present here the synthesis of novel precursor DO3A-αAPA in a new context, as precursor for the synthesis of CAs to design relaxometric MRI as well as optical probes. We have design and developed a synthetic route to obtain **64** depending on the choice of protection and deprotection method (Scheme 14).

In this route final ligand **64** was obtained from cyclen in over 5 steps, by bromination on hydroxyl group of N-carbobenzyloxy-L-serine methyl ester gives compound **59**. During reaction of compound **59**, we have been observed that reaction should not heat more then 60ºC, after few hour compound should be extracted by diethyl ether and purified by flash chromatography by using hexane and ethyl acetate. The most logical route to synthesize ligand **61** in one step by alkylation of **59** on tri-substituted product **3**, but due to elimination of bromine group in high basic condition gives starting compound as well as lots of side products. Keeping all things in mind we design another approach to get desired product, in this way **59** was monoalkylated on cyclen by using toluene as solvent and without any additional base to give compound **60**. Alkylation on **60** by *tert*-butylbromoacetate gives ligand **61** with good yield. This is a precursor where you can selectively deprotect methyl, Cbz groups and use them to develop variety of smart' or *'targeted'* CAs. Free acid containing protected ligand **62** was obtained by mild hydrolysis of methyl group in the presence of LiOH. Reactive amine containing protected precursor **63** was obtained by deprotection of Cbz group in the presence of (10%) Pd-C using methanol as solvent in Parr-apparatus at50 psi. By the treatment of cocktail TFA and 1N NaOH, final compound **64** was isolated after RP-HPLC purification in very good yield.
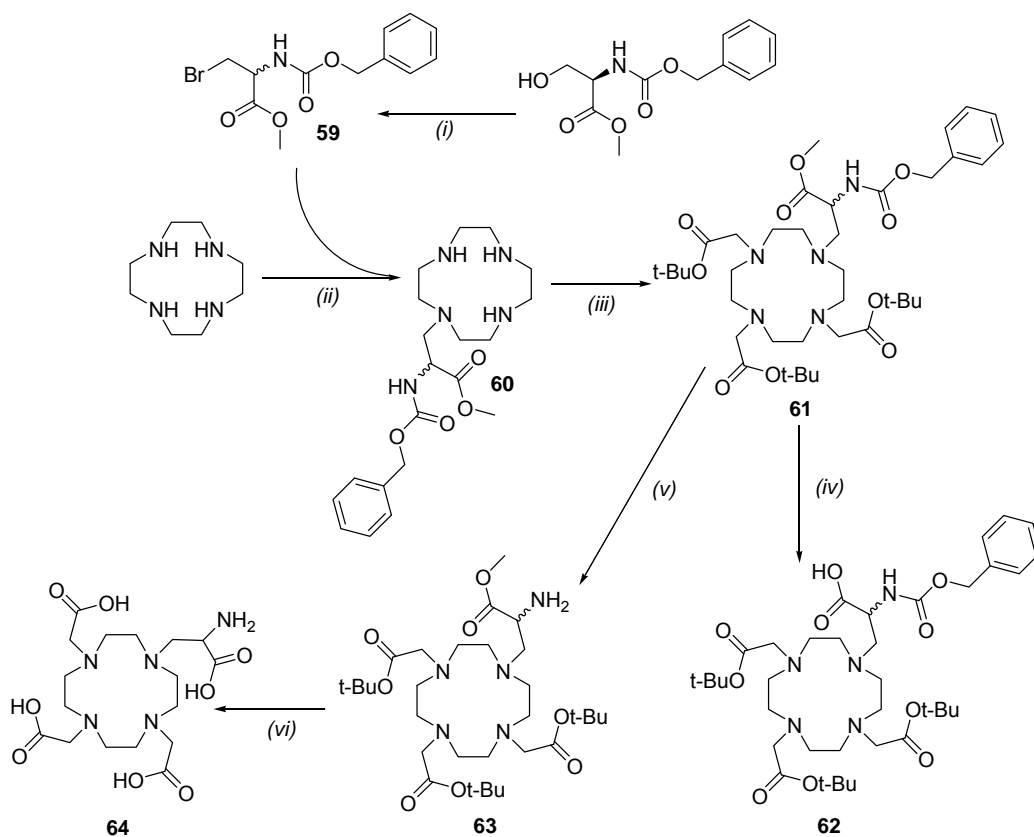
Scheme 14. Reagents and conditions: *(i)* NBS, PPh$_3$, DMF; *(ii)* dry toluene; *(iii)* *tert*-butylbromoacetate, NaHCO$_3$, CH$_3$CN; *(iv)* LiOH [THF;MeOH;water (3:2:2)]; *(v)* Pd-C (10%), H$_2$, MeOH; *(vi)* TFA, 1N NaOH.

Ligands **62**, **63** and **64** have all kind of possibility to react selectively with electrophiles and neucleophiles. Compound **62** has potential to react proteins/ peptides/oligoneuclides to develop targeted contrast agents. Compound **63** has possibility to react easily with Pyridoxy-5-phosphate to develop enzyme sensitive contrast agents and also easily modified with EGTA, EDTA, BAPTA etc to develop calcium sensitive contrast agents. By coupling with biomolecules it can easily convert in as CAs for pretargeted diagnosis and therapy.
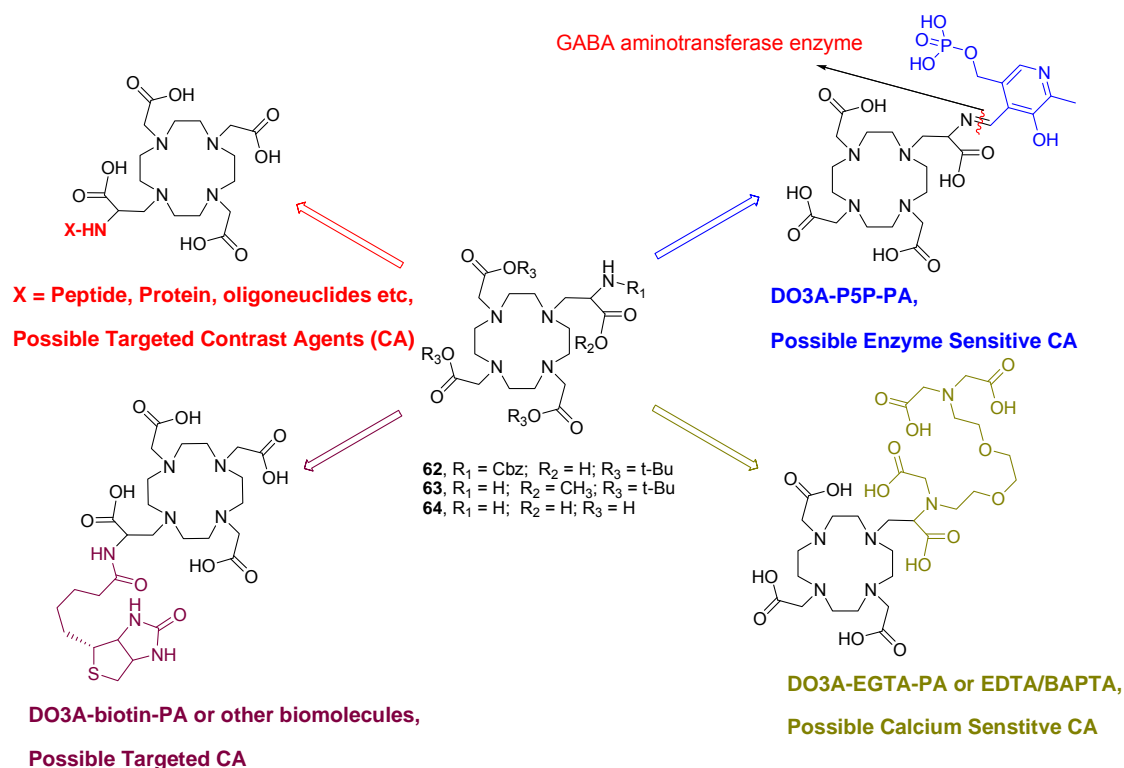
Scheme 15: Possible applications of novel precursors

6.2.3. Conclusion

In conclusion, we report the potential of the ligand DO3A-αAPA as a multipurpose precursor, from which various targeted CAs can be synthesized after single step conjugation with organic molecules/biomolecules. Additionally, the presented precursors cover the entire range of reactivity for the coupling to electrophilic and nucleophilic groups. They possess a great potential for coupling with biological molecules, proteins, vitamins and antibodies for the ease and facile synthesis of various kinds of targeted contrast agents.

7. SUMMARY, CONCLUSIONS AND OUTLOOK

The first part of thesis contained synthetic bifunctional probes based on DO3A-EA preloaded with gadolinium which were prepared for applications in targeted MRI and optical imaging. A convenient route of synthesis is reported, which allowed conjugation of this probe with biomolecules for the preparation of model MR contrast agents for targeted imaging.


7, DO3A-EA   **11**   **13**

9   **12**
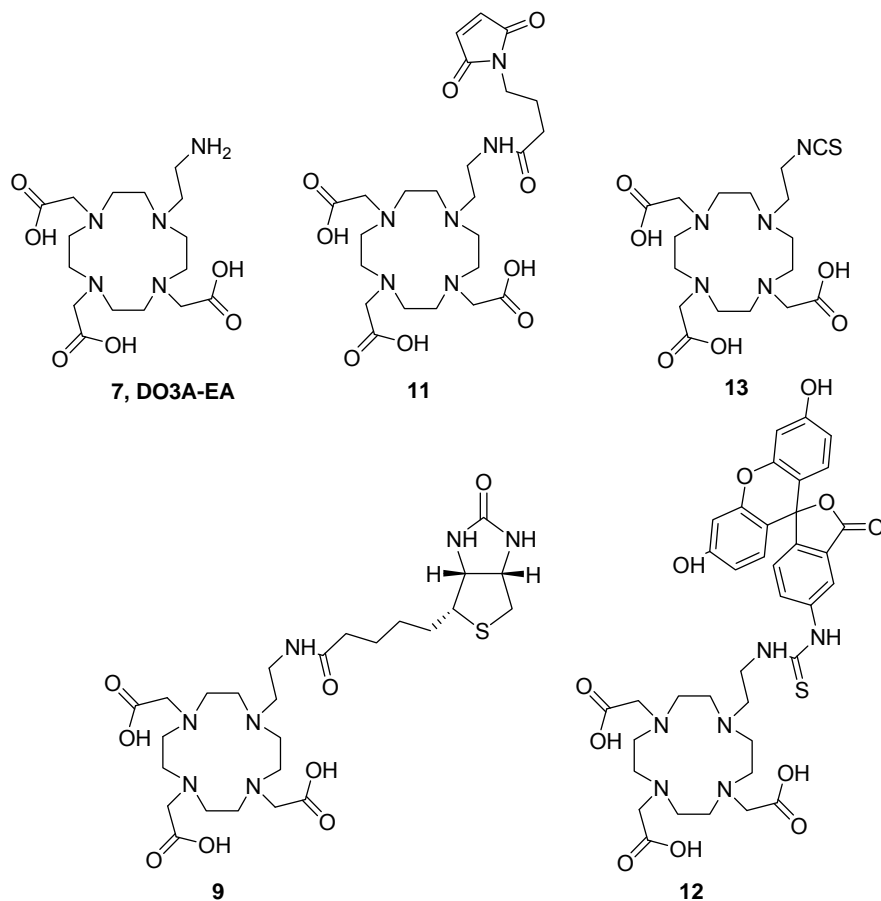
The conjugated probes have the following interesting properties: 1) **Gd-9** can be used for targeted imaging using an avidin-biotin system. 2) The fluorescent probe **Gd-12** is a bimodal compound, which can be used for both MR and optical imaging. The precursors, **11** and **13** contain a highly reactive moiety, which can interact with free SH-terminal and N-terminals of biological molecules, respectively. *In vitro* MR relaxivity studies were performed at a 300 MHz using different concentrations and chemical environments. MR relaxivity for ligand **Gd-9** at pH 7.4, r_1 was (3.32 ± 0.03)

$s^{-1}mM^{-1}$ and r_2 was (5.02 ± 0.14) $s^{-1}mM^{-1}$. For the mixture of **Gd-9** with avidin, at pH 7.4, relaxivity increased linearly with the avidin concentration. A relaxivity enhancement of 45% for r_1 and more than 400% for r_2 with respect to the unbound biotinylated Gd^{3+} complex was found at a ratio of 4:1. Fluorescence microscopy and spectroscopy of **Gd-12**-labeled 3T3 mouse fibroblasts showed a concentration-dependent intracellular uptake, which however was concomitant to a slight increase in toxicity up to 150 μM. MR studies on labeled cells indicated a contrast enhancement in both T_1- and T_2-weighted images by the internalized compound, with the effect being more pronounced in T_2-weighted images. Our results indicate that DO3A-ethylamine is a multipurpose precursor, from which various targeted contrast agents can be synthesized after a single-step conjugation with organic/bioorganic molecules.

In the second phase of work contained four DO3A-based lanthanide(III) complexes bearing ester protected and unprotected phosphonate groups which have been synthesized and analyzed. The ligands were made by four-step synthetic procedures and purified with preparative RP-HPLC, after which they were used to prepare gadolinium(III) and europium(III) complexes. Relaxometric experiments were performed on Gd^{3+} complexes at 300 MHz (7T), varying the pH of the solutions or the concentration of human serum albumin (HSA). It was found that when the pH of the medium was changed from neutral to pH 4 the longitudinal relaxivity of **Gd-17** complex increased by 50%. Diethyl ester of this complex **Gd-16** did not change longitudinal relaxivity in the same pH range but their transverse relaxivity increased upon binding to HSA. ^{31}P NMR experiments on Eu^{3+} complexes showed the change in the chemical shift of acid and diester complexes in the same region where the highest relaxivity changes were observed and proved the stability of the complexes in the investigated pH range. Luminescence studies on europium(III) complexes additionally supported observations obtained by NMR methods. The change in the form of the luminescence emission spectra, and the reduction in q value upon addition HSA proved the ternary adduct formation between the charge neutral diester complex and HSA. Similarly, the change in the emission spectra showing a phosphonate bound structure at pH 7 to a species where the phosphonate oxygen is not coordinated at pH 4 in parallel to the increase of q value supporting the hypothesis that the deprotonation of phosphonates is the main reason for the distinct relaxivity change from slightly acidic to the neutral solution media.

16   **17**
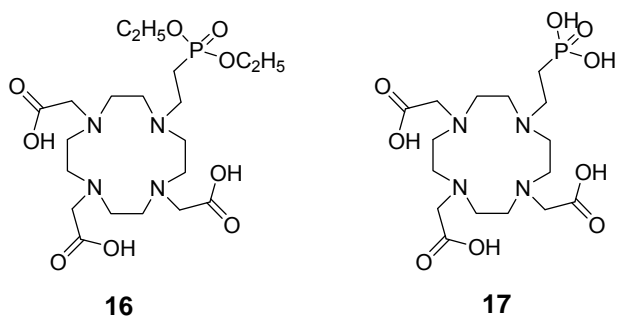
The third part of this thesis described some novel GdDO3A-type bismacrocyclic complexes; conjugated to Ca^{2+} chelating moieties like EDTA- and DTPA-bisamides, were synthesized as potential 'smart' MRI contrast agents. Their sensitivity towards Ca^{2+} was studied by relaxometric titrations. A maximum relaxivity increase of 15, 6 and 32 % was observed upon Ca^{2+} binding for **Gd$_2$-25**, **Gd$_2$-26** and **Gd$_2$-27**, respectively.


25, R = -CH$_2$
26, R = -C$_6$H$_4$

27
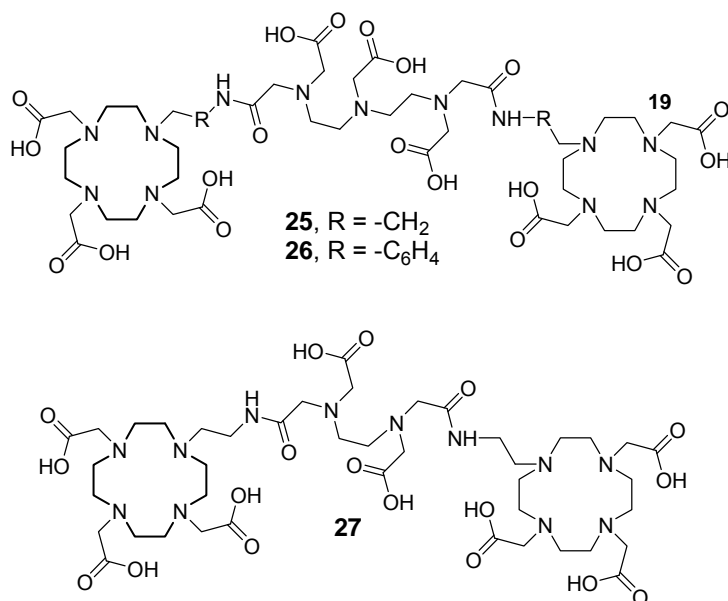
The apparent association constants are $logK_A = 3.6\pm0.1$ for **Gd$_2$-25** and $logK_A = 3.4\pm0.1$ for **Gd$_2$-27**. For the interaction between Mg^{2+} and **Gd$_2$-25**, $logK_A = 2.7\pm0.1$ has been determined, while no relaxivity change was detected with **Gd$_2$-27**. Luminescence lifetime measurements on the Eu^{3+} complexes in the absence of Ca^{2+} gave hydration numbers of q = 0.9 (**Eu$_2$-25**), 0.7 (**Eu$_2$-26**) and 1.3 (**Eu$_2$-27**). The parameters influencing proton relaxivity of the Gd^{3+} complexes were assessed by a combined NMRD and ^{17}O NMR study. Water exchange is relatively slow on **Gd$_2$-25** and **Gd$_2$-26** (k_{ex}^{298} = 0.5 and 0.8 x 10^6 s^{-1}), while it is faster on **Gd$_2$-27** (k_{ex}^{298} = 80 x

10^6 s^{-1}); in any case, it is not sensitive to the presence of Ca^{2+}. The rotational correlation time, $\tau_R{}^{298}$, differs for the three complexes and reflects their rigidity. Due to the benzene linker, the **Gd$_2$-26** complex is remarkably rigid, with a correspondingly high relaxivity despite the low hydration number (r_1 = 10.2 mM^{-1}s^{-1} at 60 MHz, 298 K). Based on all available experimental data from luminescence, 17O NMR and NMRD studies on the Eu^{3+} and Gd^{3+} complexes of **25** and **27** in the absence and presence of Ca^{2+}, we conclude that the relaxivity increase observed upon Ca^{2+} addition can be mainly ascribed to the increase in the hydration number, and, to a smaller extent, to the Ca^{2+} induced rigidification of the complex.

In the fourth phase, our aim was to synthesize multimodal neuronal tracer molecules that can be visualized not only by microscopic techniques in postmortem fixed tissue, but also by MRI in living animals, allowing *in vivo* brain connectivity studies to be performed. In order to achieve our goal, we designed and synthesized three novel and structurally different gadolinium containing biocytin-based neuroanatomical tract-tracers (**41**, **45**, and **50**).

104
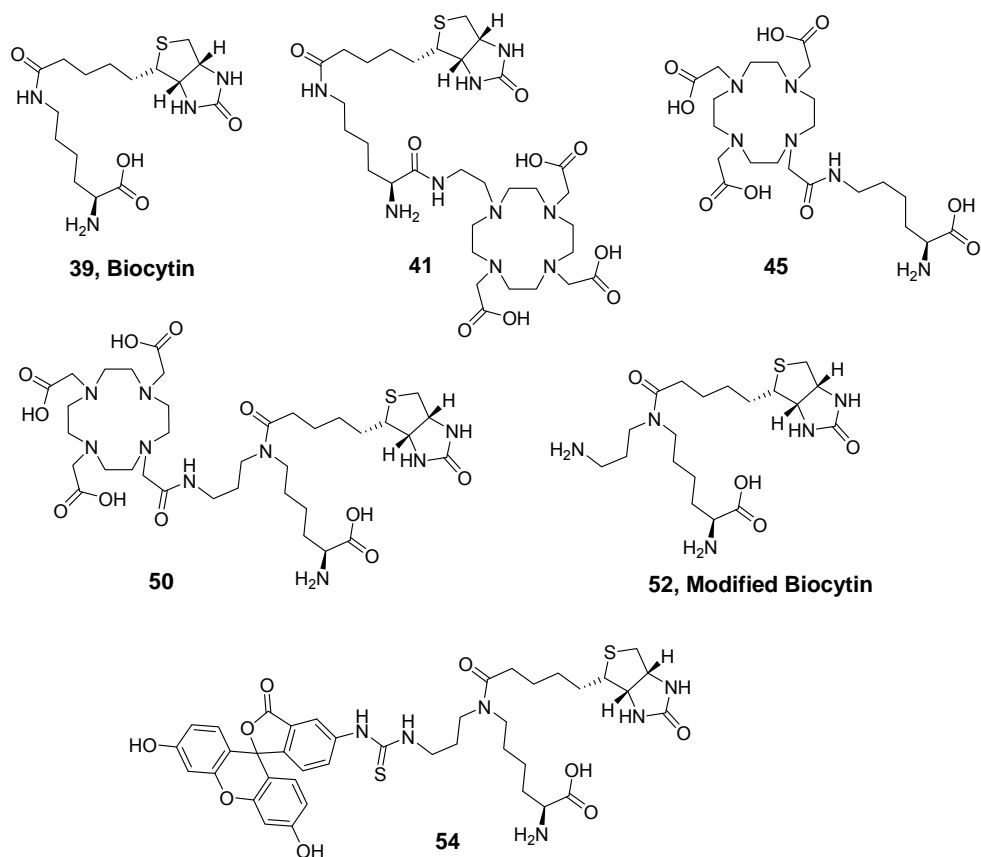
In the first tracer (**41**), Gd-DO3A-EA is connected with biocytin via amide linkage. The second tracer (**45**) is based on Gd-DOTA precursor coupled to L-lysine via amide. The third tracer (**50**) is derived from newly developed modified-biocytin where propylamine is linked to amide of biocytin giving the possibility to couple Gd-DOTA as MRI marker. *In vitro* MR experiments with increasing concentrations of avidin were performed at 7T. A linear enhancement in transverse relaxivity (r_2) for Gd loaded **41**, **45**, and **50** (439-168% respectively) were observed demonstrating strong binding of **41** and **50** tracers in the pocket of tetrameric avidin. By replacing Gd-DOTA with FITC in **50**, the efficiency of cell internalization was demonstrated microscopically with fluorescence methods with compound **54**. Comparative histological results of **39** and **52** clearly showed that modified biocytin (**54**) is functionally same but more stable as compare to conventional biocytin. Our preliminary results suggest that the class of biolytic-based and Gd-containing molecules here described, represents a new strategy for neuroanatomical tracing that combines the powerful spatial resolution of the conventional microscopic techniques with the whole brain tri-dimensional coverage and *in vivo* applicability of the MRI.

7.1. Comparative Relaxivity Data of Studied Complexes.

Relaxivity measurements were acquired by taking the slope of a plot of the (R_1 and R_2) relaxation rate versus concentration, where relaxivity (r_1 and r_2) is a measure of the ability of a contrast agent to shorten T_1 or T_2 (Table 7).

Contrast Agents	r_1 (mM^{-1}S^{-1})	r_2 (mM^{-1}S^{-1})
Gd-9	3.32 ± 0.03	5.02 ± 0.14
Gd-12	5.36 ± 0.05	8.57 ± 0.11
Gd-16	4.30 ± 0.05	6.45 ± 0.10
Gd-17	4.03 ± 0.05	6.10 ± 0.12
Gd$_2$-25	4.67 ± 0.03	7.01 ± 0.15
Gd$_2$-26	4.56 ± 0.04	6.84 ± 0.10
Gd$_2$-27	5.32 ± 0.03	8.51 ± 0.11
Gd$_2$-31	4.81 ± 0.05	7.69 ± 0.13
Gd$_2$-36	3.94 ± 0.02	5.91 ± 0.15
Gd-41	4.69 ± 0.06	7.86 ± 0.02
Gd-45	4.39 ± 0.09	6.84 ± 0.06
Gd-50	4.05 ± 0.06	6.85 ± 0.02

Table 7. MR measurements of the contrast agents in aqueous solution were performed at 7T at room temperature.

8. MATERIALS AND METHODS

8.1. Chemicals and Working Techniques

The chemicals were purchased from the firms Acros, Aldrich, Fluka, Merck, Strem and VWR. All reagents were obtained from commercial suppliers, and were used without further purification unless otherwise stated. All solvents were distilled and/or dried prior to use by slandered methodology except for those, which were reagent grades. Anhydrous solvents were obtained as follows: dichloromethane and chloroform by distillation from calcium hydride; THF, diethyl ether and toluene by distillation from sodium and benzophenone. Absolute triethylamine and diisopropylamine were distilled over calcium hydride prior to use. Unless and otherwise mentioned, all the reactions were carried out under a nitrogen atmosphere and the reaction flasks were pre-dried by heat gun under vacuum. All the chemicals, which were air or water sensitive, were stored under inert atmosphere. Pure water (18 MΩ cm^{-1}) was used throughout. All glass lab ware was washed with a mixed acid solution and thoroughly rinsed with deionized, distilled water[212]. Compound that are not described in the experimental part were synthesized according to the literature.

8.2. Reversed Phase High-Performance Liquid Chromatography (RP-HPLC)

HPLC was performed at room temperature on a Varian PrepStar Instrument, Australia, equipped with PrepStar SD-1 pump heads. UV absorbance was measured using a ProStar 335 photodiode array detector at 214 nm and 254 nm. This detector is equipped with a dual-path length flow cell which enables measurement of absorption of analytical and preparative samples without changing the flow cell. Reversed-phase analytical HPLC was performed in a stainless steel Chromsep (length 250 mm, internal diameter 4.6 mm, outside diameter 3/8 inch and particle size 8 μm) C$_{18}$ column and preparative HPLC was performed in a stainless steel Chromsep (length 250 mm, internal diameter 41.4 mm, outside diameter 2 inch and particle size 8 μm) C$_{18}$ column (Varian, Advanced Chromatographic Solutions). The compounds were purified using one of the three methods.

Method A: the gradient was used with the mobile phase starting from 95% solvent A (water) and 5% of solvent B (MeOH) to 70% B in 10 min, 100% B in 18min, 100% B isocratic till 24 min and decreased to 5% B in 28 min.

Method B: isocratic mode was maintained with mobile phase starting from 97% solvent A (water) and 3% of solvent B (MeOH) for 8 min.

Method C: the gradient was used with the mobile phase starting from 90% solvent A (0.1% TFA in water) and 10% of solvent B (0.1% TFA in MeCN) to 70% B in 20 min, 100% B in 28min, 100% B isocratic till 34 min and decreased to 10% B in 38 min.

The flow rate generally used for analytical HPLC was 1 mL/min and for preparative HPLC was 41 mL/min. All the solvents for HPLC were filtered through a nylon-66 Millipore filter (0.45μm) prior to use.

8.3. NMR-Spectroscopy

Analytical ^{1}H, ^{13}C and ^{31}P NMR spectra were recorded on a Bruker 250 MHz and 400 MHz spectrometer (^{1}H; internal reference CDCl$_3$ at 7.27 ppm, MeOH at 50 ppm or D$_2$O at 4.75 ppm); 62.9 MHz and 100 MHz spectrometer (^{13}C; internal reference CDCl$_3$ at 77.0 ppm, MeOH at 50 ppm or TMS at 0.0 ppm); 62.9 MHz and 100 MHz spectrometer (^{31}P; external reference 85% H$_3$PO$_4$ 0.0 ppm). All experiments were performed at 25°C. Data are reported as follows: chemical shift (multipilicity: s = singlet, d = doublet, t = triplet, dd = doublet of doublet, m = multiplet, br = broadened, J = coupling constant (Hz), integration, peak assignment in italic form.

8.4. Mass Spectrometry

ESI low resolution mass spectra (ESI-MS) were recorded on SL 1100 system (Agilent, Germany) with ion-trap detection in positive and negative ion mode. HR-FT-ICR mass spectra were measured on an APEX 2 spectrometer from Bruker Daltonic with electrospray ionization method (ESI). High resolution mass (HRMS) are reported as follows: (ESI): calcd mass for the related compound by found mass.

8.5. Melting points

Melting points were determined with a Büchi Melting point B-540 apparatus and were not corrected.

8.6. Chromatographic methods

Flash column chromatography was performed using flash silica gel 60 (70-230 mesh) from Merck. Analytical thin layer chromatography (TLC) was performed on aluminum sheet silica gel plates with 0.2 mm thick silica gel 60 F_{254} (E. Merck, Germany) using different mobile phase. The compounds were visualized by UV_{254} light and TLC plates were developed in Iodine chamber.

8.7. Relaxometric Measurement Parameters

8.7.1. Relaxaometric Measurement Parameters at 7T.

The measurement of the relaxation rates R_1 and R_2 (longitudinal and transverse relaxation) of the **Gd-41** and **Gd-50** were performed at 300 MHz (7T) on a vertical 7T/60 cm MRI Biospec system (Bruker Biospin, Germany), which was described recently[83,125]. Up to 16 tubes could be measured simultaneously. The relaxation rate measurements of the samples were performed at room temperature (~21°C).

For R_1, a spin echo saturation recovery sequence was used varying repetition time TR and keeping the echo time TE minimal and constant. Typical parameters were: field of view 17 x 6.9 cm^2, matrix 512 x 256, slice thickness 4 mm, SW 70 kHz, TE 15 ms, TR 40-8000 ms (logarithmic time steps, 80 images). For R_2, a multi-spin-echo sequence was used with a long TR between excitations. Similar parameters were used, but TR = 8 s and TE = 17-850 ms (linear echo time steps, 50 echoes).

Fitting of $T_{1,2}$ values was done voxel wise on selected ROIs using the MATLAB program. The longitudinal relaxivity (r_1) and transverse relaxivity (r_2) was calculated from the slope of $R_{1,2}$ versus the CA concentration by an error-weighted linear regression. The errors for all r_1 values were less then 2% and are not displayed on graphs. The Gd(III) concentrations were determined by ICP-OES.

8.7.2. Relaxaometric Measurement Parameters at 3T and 1.5T.

For R_1 measurements at field strengths 3T and 1.5T, an inversion recovery sequence was used to obtain images from a 2 mm thick slice through the samples. The inversion time was varied from 23 ms to 3000 ms in about 12 steps. The images were read out with a turbo spin echo technique, acquiring 5 echoes per scan. The repetition time TR was 10 s to ensure complete relaxation between the scans. A resolution of 256 × 256 voxels over a Field-of-view of 110 × 110 mm^2 was reached. Six averages

were acquired within less than 25 min. For the R_2 measurements at low fields, a simple spin-echo sequence with varying echo time was used. With the same slice thickness, spatial resolution and Field-of-view as in the R_1 measurements, about 10 images with different T_E, varying from 12 ms to 1 s, were acquired with a repetition time of 8s within 34 min each.

8.7.3. Data analysis[125].

The *fitting* to relaxivity curves was performed with self-written routines under MATLAB 6.5 R13 (The Mathworks Inc.). The series of T_1 and T_2 relaxation data were fitted to the following equations: a) T_1 series with varying $t = TR$: $S = S0\,(1 - \alpha \cdot \exp(-t\,/\,T_1))$. b) T_2 series with varying $t = TE$: $S = S0 \exp(-t\,/\,T_2) + \beta$. Nonlinear least-squares fitting of three parameters S_0, T_1/T_2, and α/β was done for each voxel with the Gauss-Newton method (MATLAB function `nlinfit`). For each fitted parameter, the 95% confidence intervals were calculated (MATLAB functions `nlparci`, `nlpredci`) and used as an error estimate of the fitted relaxation times T_1/T_2 and S_0 (initial signal at $t = 0$). The fit procedure resulted in parameter maps of T_1, T_2, S_0 and corresponding error maps σ_{T1}, σ_{T2}, σ_{S0}.

Image-regions around the tubes were defined as Regions Of Interest (ROIs), and the means and distribution width of the relaxation times of voxels in these regions were calculated: An *iterative* Gaussian fit was used to determine mean and standard deviation (SD) of a distribution with outliers. For this purpose, a distribution histogram was first fitted to a Gaussian to estimate mean and SD. The tails of the distribution were then discarded by using a threshold of three SDs. A repeated fit proved to be robust and converged to the 'true' Gaussian mean and width of the distribution barring the outliers, observed as a result of the non-linear fit of noisy voxels.

The processing of the relaxation data thus resulted in specific $R_{1,2} = 1/T_{1,2}$ values for each tube sample including the standard deviation in the selected ROI ensemble. The ensemble error matched closely the errors of a single-voxel fit, which showed that no further systematic errors were introduced by the image encoding. Finally, the relaxivity $r_{1,2}$ was calculated from the slope of $R_{1,2}(c)$ versus the concentration c of the contrast agent by an error-weighted linear regression.

8.8. Experimental Procedures

All the experimental procedures are arranged in the ascending order of number of the compound.

[4,7-Bis-butoxycarbonylmethyl-10-(N-Boc-2-aminoethyl)-1,4,7,10-tetraaza-cyclododec-1-yl]-acetic acid *tert*-butyl ester (4).
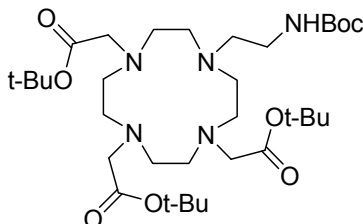
A solution of **3** (0.8 g, 1.5 mmol) and K_2CO_3 (0.43 g, 3.1 mmol) in 5 mL DMF was stirred at room temperature for 1 h. **1** (0.418 g, 1.9 mmol) was added in one aliquot to the above solution and the reaction mixture was heated at 70-80°C for 7-8 h. The reaction was monitored by TLC and developed in an iodine chamber. After completion, the reaction mixture was poured into 150 mL water and extracted with CH_2Cl_2 (3x50 ml). The organic layer was evaporated under reduced pressure and purified by column chromatography (silica gel, 5% MeOH in CH_2Cl_2; R_f = 0.55) to give 1.49 g (72%) of **4** as off white solid**.**

^{1}H NMR (CDCl$_3$, 250 MHz), δ (ppm): 1.45 (s, 36H); 2.71-4.6 (m, 26H); 5.35 (s, 1H). **^{13}C NMR** (CDCl$_3$, 62.9 MHz), δ (ppm): 27.5; 47.7; 48.6; 49.2; 50.4; 51.4; 53.1; 54.3; 78.8; 81.7; 84.0; 164.7; 169.7.

ESI-HRMS (+): calcd $C_{33}H_{63}N_5O$: m/z 658.47494 $(M+H)^+$ and found 658.47418 $(M+H)^+$.

[4,7-Bis-methoxycarbonylmethyl-10-(N-Boc-2-aminoethyl)-1,4,7,10-tetraaza-cyclododec-1-yl]-acetic acid methyl ester (5).

A solution of **2** (0.8 g, 2.5 mmol), Na_2CO_3 (2.08 g, 20.0 mmol) and methylbromoacetate (0.84 mL, 8.7 mmol) in MeCN (100 mL) was stirred at 60-70°C for 7-8 h. The reaction was monitored by TLC and developed in an iodine chamber.

After completion, the reaction mixture was filtered and washed with CH_2Cl_2 (2x20 ml). The filtrate was evaporated under reduced pressure and purified by column chromatography (silica gel, 5% MeOH in CH_2Cl_2; R_f = 0.55) to give 1.08 g (82%) of **5** as off white solid**.**
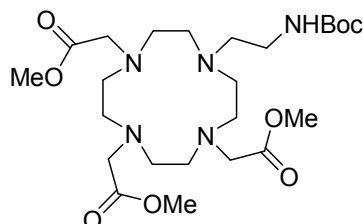
^{1}H NMR (CDCl$_3$, 250 MHz), δ (ppm): 1.24 (s, 9H); 2.23-2.71 (m, 18H); 3.06 (s, 2H); 3.09 (s, 2H); 3.17 (s, 4H); 3.56 (s, 3H); 3.63 (s, 6H); 5.43 (s, 1H). **^{13}C NMR** (CDCl$_3$, 62.9 MHz), δ (ppm): 27.7; 36.9; 49.7; 51.0; 51.7; 51.98; 54.1; 54.6; 55.1; 78.3; 156.3; 173.2; 173.5.

ESI-HRMS (+): calcd $C_{24}H_{45}N_5O_8$: m/z 532.33409 (M+H)$^+$ and found 532.33416 (M+H)$^+$.

[4,7-Bis-methoxycarbonylmethyl-10-(2-aminoethyl)-1,4,7,10-tetraaza-cyclododec-1-yl]-acetic acid methyl ester (6).
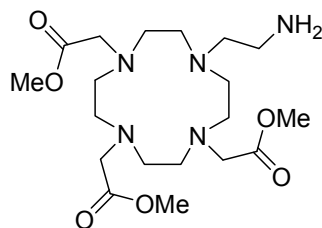
Reaction 1: A solution of **5** (1.0 g, 1.9 mmol) in TFA (2 mL) and CH_2Cl_2 (8 mL) was stirred at room temperature for 1-2 h. The solvent was evaporated under reduced pressure and the residue was dissolved in a minimum volume of MeOH (1 mL), followed by addition of diethyl ether dropwise at 0-5˚C and stirr for 1 h at room temperature. The TFA salt of the compound was precipitated and filtered through a G-4 sintered funnel under nitrogen. The precipitate was dissolved in water, neutralized

by addition of 1M Na_2CO_3 and evaporated under reduced pressure at 50°C for 2 h to give 0.65 g (80%) of **6** as off white solid.

Reaction 2: A solution of **7** (0.4 g, 1.0 mmol) in MeOH (10 mL) and HCl gas was passed in reaction mixture for 3-4 h. Finally, the round bottom flask was tightly closed with a stopper and stirred overnight. The solvent was evaporated under reduced pressure and dissolved in a minimum volume of MeOH (1 mL), followed by addition of diethyl ether dropwise at 0-5°C and stir for 1 h at room temperature. The compound was precipitated and filtered through a G-4 sintered funnel under nitrogen. The precipitate was dissolved in water, neutralized by adding 1 M Na_2CO_3 and evaporated under reduced pressure at 50°C for 2 h to give 0.31g (95%) of **6** as white solid.

^{1}H NMR (MeOD, 250 MHz), δ (ppm): 2.46-2.80 (m, 20H); 3.32 (br. s, 6H); 3.65 (s, 3H); 3.70 (s, 6H). **^{13}C NMR** (MeOD, 62.9 MHz), δ (ppm): 38.3; 46.7; 50.9; 52.0; 52.2; 52.7; 52.9; 56.4; 57.5; 173.4; 174.5.

ESI-HRMS (+): calcd $C_{19}H_{37}N_5O_6$: m/z 432.28166 $(M+H)^+$ and found 432.28157 $(M+H)^+$.

[4,7-Bis-carboxymethyl-10-(2-aminoethyl)-1,4,7,10-tetraaza-cyclododec-1-yl]-acetic acid (7, DO3A-EA).
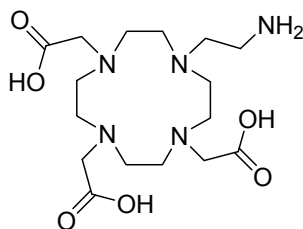
Reaction 1: A solution of **4** (2.0 g, 3.0 mmol) in TFA (10 mL) was stirred at room temperature for 18-20 h. The reaction was monitored by ESI-MS. The solvent was evaporated under reduced pressure and dissolved in a minimum volume of MeOH (1 mL) followed by addition of diethyl ether dropwise at 0-5°C and stir for 1 h at room temperature. The compound was precipitated and filtered through a G-4

sintered funnel under nitrogen. The precipitate was dissolved in water and neutralized by adding 1 M Na_2CO_3.

Reaction 2: A solution of **6** (0.5 g, 1.16 mmol) in 14 mL of THF:MeOH:water (3:2:2) was stirred at 0-5°C for 15 min and then LiOH (0.06 g, 0.25 mmol) was added. The reaction mixture was stirred for 2-3 h at room temperature. The progress of the reaction was checked by ESI-MS. After completion, the reaction mixture was concentrated under reduced pressure. The compound was purified by preparative HPLC (condition B, λ = 214 nm, RT = 2.4 min). After lyophilization, 0.76 g (64%) of **7** as white powder was obtained.

^{1}H NMR (D$_2$O, 250 MHz), δ (ppm): 2.70 -3.20 (m, 12H); 3.30-3.7 (m, 10H); 3.89 (br. s, 4H). **^{13}C NMR** (D$_2$O, 62.9 MHz), δ (ppm): 36.5; 48.4; 48.6; 50.8; 52.5; 53.7; 57.6; 170.7; 176.6.

ESI-MS (+): calcd $C_{16}H_{31}N_5O_6$: m/z 390.2 (M+H)$^+$; found 390.2 (M+H)$^+$.

[4,7-Bis-methoxycarbonylmethyl-10-{2-[5-(2-oxo-hexahydro-thieno[3,4-d]imidazol-4-yl)-pentanoylamino]-ethyl}-1,4,7,10-tetraaza-cyclododec-1-yl]-methylacetate (8,).
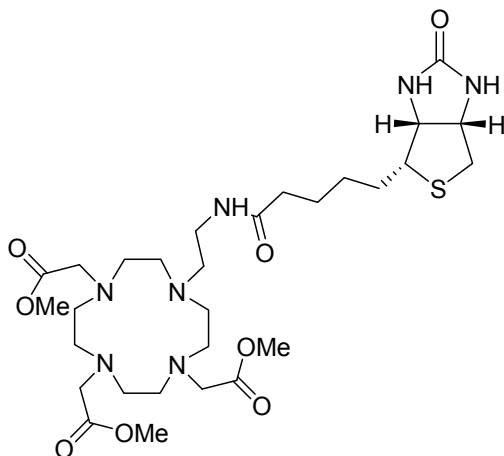
A solution of methyl protected DO3A-EA (**6**) (0.38 g, 0.88 mmol), biotin (0.2 g, 0.82 mmol), NMM (0.18 mL, 1.7 mmol) and HOBt (0.13 g, 0.96 mmol) in DMF (5 mL) was stirred at 0-5°C for 15 min and then EDC (0.19 g, 0.99 mmol) was added. The reaction mixture was stirred overnight at room temperature. The reaction was monitored by TLC and developed in an iodine chamber. After completion, the

reaction mixture was poured in water, extracted with CH_2Cl_2 (3x100 mL), organic layer was dried over Na_2SO_4, filtered, filtrate was evaporated under reduced pressure and purified by column chromatography (silica gel, 10% MeOH in CH_2Cl_2; R_f=0.25) to give 0.32 g (55%) of **8** as dark yellow viscous oil.

^{1}H NMR (D$_2$O, 250 MHz), δ (ppm): 1.35-1.67 (m, 6H); 2.25 (t, J=6.87 Hz, 2H); 2.70-3.29 (m, 12H); 3.45-3.61 (m, 17H); 3.71 (s, 6H); 3.81 (s, 3H); 4.35-4.40 (m, 1H); 4.54-4.59 (m, 1H). **^{13}C NMR** (D$_2$O, 62.9 MHz), δ (ppm): 22.6; 25.5; 25.8; 31.7; 33.1; 37.5; 46.6; 48.1; 49.8; 50.7; 51.4; 52.2; 53.2; 58.1; 59.9; 165.6; 171.1; 174.9.

ESI-HRMS (+): calcd $C_{29}H_{51}N_7O_8S$: m/z 658.35926 $(M+H)^+$; found 658.35913 $(M+H)^+$.

[4,7-Bis-carboxymethyl-10-{2-[5-(2-oxo-hexahydro-thieno[3,4-d]imidazol-4-yl)-pentanoylamino]-ethyl}-1,4,7,10-tetraaza-cyclododec-1-yl]-acetic acid (9, DO3A-ethylamido-biotin).
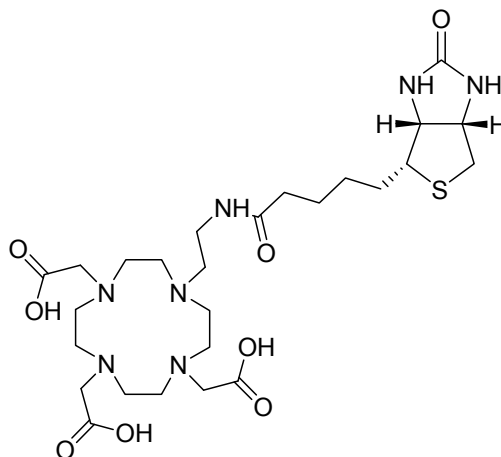
A solution of **8** (0.1 g, 0.15 mmol) in 10 mL of THF:MeOH:water (3:2:2) was stirred at 0-5˚C for 15 min and then LiOH (12 mg, 0.5 mmol) was added. The reaction mixture was stirred for 3 h at room temperature. The progress of the reaction was monitored by ESI-MS. After completion, the solvent was evaporated under reduced pressure and the residue was purified by preparative HPLC [method A, λ = 214 nm, retention time (RT) = 9.4 min]. After lyophilization, 72 mg (77%) of **9** as white solid compound was obtained.

¹H NMR (D₂O, 250 MHz), δ (ppm): 1.37-1.45 (m, 2H); 1.61-1.68 (m, 4H); 2.27 (t, *J*=6.87 Hz, 2H); 2.74-3.23 (m, 14H); 3.32-3.38 (m, 9H); 3.48 (s, 3H); 3.75 (s, 3H); 4.39-4.44 (m, 1H); 4.58-4.62 (m, 1H) . **¹³C NMR** (D₂O, 62.9 MHz), δ (ppm): 22.7; 25.4; 25.7; 28.0; 33.0; 33.2; 37.5; 46.1; 46.8; 48.3; 49.1; 52.7; 53.1; 54.4; 58.0; 59.8; 163.0; 169.3; 174.7.

ESI-HRMS (+): calcd $C_{26}H_{45}N_7O_8S$: m/z 616.31231 (M+H)⁺, found 616.31194 (M+H)⁺.

[4,7-Bis-methoxycarbonylmethyl-10-{2-[4-(2,5-dioxo-2H-pyrrol-1(5H)-yl)-butanamido]-ethyl}-1,4,7,10-tetraaza-cyclododec-1-yl]-methylacetate (10). A solution of **6** (0.2 g, 0.46 mmol), 4-maleimidobutyric acid (0.127 g, 0.69 mmol), NMM (0.15 mL, 1.38 mmol) and HOBt (0.103 g, 0.76 mmol) in DMF (5 mL) was stirred at 0-5˚C for 15 min and then EDC (0.147 g, 0.76 mmol) was added. The reaction mixture was stirred overnight at room temperature. The progress of reaction was monitored by TLC using CH_2Cl_2:MeOH, 9:1 and R_f of **(10)** was 0.2. After completion, the reaction mixture was poured in excess of water and extracted with CH_2Cl_2 (3x100 mL). Combined organic layers were dried over Na_2SO_4, filtered, filtrate was evaporated under reduced pressure and the residue was purified by column chromatography (silica gel, 10% MeOH in CH_2Cl_2) to give 0.14 g (66%) of **10** as dark yellow viscous compound.
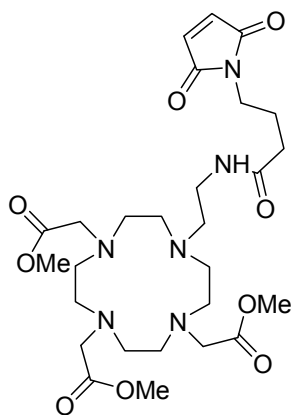

¹H NMR (D₂O, 250 MHz), δ (ppm): 1.86-1.92 (m, 2H); 2.36 (t, *J*=7.32 Hz, 2H); 2.42-2.80 (m, 18H); 3.25-3.38 (m, 6H); 3.51-3.57 (m, 4H); 3.73 (s, 3H); 3.80 (s, 6H); 6.69 (s, 2H); 8.37 (br s, 1H). **¹³C NMR** (CDCl₃, 62.9 MHz), δ (ppm): 24.5; 32.9; 36.2; 37.4; 50.2; 50.8; 51.7; 52.5; 54.9; 55.1; 55.4; 133.9; 170.5; 171.2; 173.4; 173.7.

ESI-HRMS (+): calcd $C_{27}H_{44}N_6O_9$: m/z 597.32425 (M+H)$^+$, found 597.32421 (M+H)$^+$.

[4,7-Bis-carboxymethyl-10-{2-[4-(2,5-dioxo-2H-pyrrol-1(5H)-yl)-butanamido]-ethyl}-1,4,7,10-tetraaza-cyclododec-1-yl]-acetic acid (11, DO3A-ethylamidopropyl-maleimide).

A solution of **10** (0.1 g, 0.17 mmol) in 14 mL of THF:MeOH:water (3:2:2) was stirred at 0-5°C for 15 min and then LiOH (20 mg, 0.83 mmol) was added. The reaction mixture was stirred for 3 h at room temperature. The progress of the reaction was monitored by ESI-MS. After completion, the solvent was evaporated under reduced pressure and the residue was purified by preparative HPLC (method A, λ = 214 nm, RT = 5.8 min). After lyophilization, 72 mg (86%) of **11** as off-white solid compound was obtained.
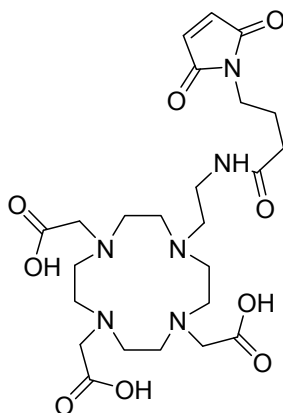
^{1}H NMR (D$_2$O, 250 MHz), δ (ppm): 1.80-1.94 (m, 2H); 2.37 (t, *J*=7.48 Hz, 2H); 3.03 (t, *J*=6.10 Hz, 2H); 3.20-3.31 (m, 10H); 3.40-3.51 (m, 15H); 3.83 (s, 4H). **^{13}C NMR** (D$_2$O, 62.9 MHz), δ (ppm): 25.5; 35.4; 38.0; 41.0; 51.1; 51.6; 53.1; 53.7; 53.9; 54.9; 56.8; 58.9; 137.1; 173.8; 175.8; 178.3.

ESI-HRMS (+): calcd $C_{24}H_{38}N_6O_9$: m/z 555.27730 (M+H)$^+$, found 555.27740 (M+H)$^+$.

[4,7-Bis-carboxymethyl-10-(2-fluoresceinthioureaethyl)-1,4,7,10-tetraaza-cyclododec-1-yl]-acetic acid (12, DO3A-ethylthiourea-FITC).
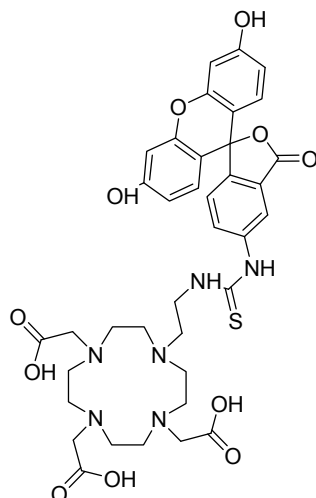

A solution of DO3A-EA (**7**) (0.1 g, 0.26 mmol) in 10 mL of water was stirred at room temperature and FITC (0.11 g, 0.28 mmol) was added at pH 8.5. During stirring, pH was maintained at 8.0-8.5 by addition of 1M Na_2CO_3. The reaction mixture was stirred for 18-20 h at room temperature in dark. The reaction was monitored by ESI-MS. The reaction mixture was evaporated under reduced pressure and the residue was purified by preparative HPLC (method A, $\lambda = 254$ nm, RT = 6.8 min). After lyophilization, 0.11 g (55%) of **12** as dark orange solid compound was obtained.

^{1}H NMR (D$_2$O, 250 MHz), δ (ppm): 2.86-2.99 (m, 18H); 3.38-3.42 (overlapped s, 6H); 3.75 (bs, 2H); 6.52 (s, 1H); 6.53 (s, 1H); 6.55 (s, 1H); 6.59 (s, 1H); 7.16 (t, $J = 4$ Hz, 2H); 7.20 (s, 1H); 7.49 (d, $J = 6.4$ Hz, 1H); 7.66 (s,1H). **^{13}C NMR** (D$_2$O, 62.9 MHz), δ (ppm): 43.5; 52.5; 53.2; 53.7; 53.9; 55.0; 59.9; 106.3; 115.1; 125.7; 127.7; 128.9; 132.1; 133.7; 134.2; 143.5; 161.4; 161.4; 176.8; 179.5; 179.8 183.3.

ESI-HRMS (+): calcd $C_{37}H_{42}N_6O_{11}S$: m/z 779.27050 (M+H)$^+$, found 779.27051 (M+H)$^+$.

Materials and Methods

[4,7-Bis-carboxymethyl-10-(2-isothiocyanatoethyl)-1,4,7,10-tetraaza-cyclododec-1-yl]-acetic acid (13, DO3A-ethyl-isothiocyanate).
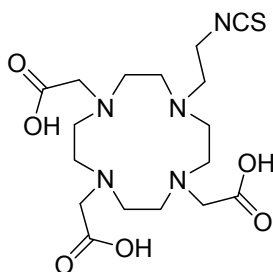
A solution of **7** (0.2 g, 0.5 mmol) in water (10 mL) was stirred at room temperature and thiophosgene (0.18 g, 1.5 mmol) in 5 mL CCl$_4$ was added dropwise. The pH of the mixture maintained 7.5-8 using 1M Na$_2$CO$_3$. The reaction was monitored by ESI-MS. The reaction mixture was evaporated and the residue was purified by preparative HPLC (method B, λ = 214 nm, RT = 2.7 min). After lyophilization, 0.13 g (59%) of **13** as light yellow solid was obtained.

^{1}H NMR (D$_2$O, 250 MHz), δ (ppm): 3.23-3.79 (m, 20H); 4.20 (br. s, 6H). **^{13}C NMR** (D$_2$O, 62.9 MHz), δ (ppm): 42.8; 48.5; 51.4; 51.9; 52.8; 55.9; 57.9; 129.3; 178.1; 179.0.

ESI-HRMS (+): calcd C$_{17}$H$_{29}$N$_5$O$_6$S: m/z 449.21768 (M+NH$_4$)$^+$, found 449.21790 (M+NH$_4$)$^+$.

Preparation of Gd^{3+} Complexes of Ligands 9, 11-13. The Gd complexes of ligands 9, 11-13 were prepared from respective solution of the ligand (1 eq) and solution of GdCl$_3$.6H$_2$O (1.1 eq). The reaction mixture was stirred at 50-60° C for 12-16 h. The pH was periodically checked and adjusted to 7.0-8.0 using a solution of Na$_2$CO$_3$ (1 M) and HCl (1 N) as needed. After 12-16 h, the reaction mixture was passed through chelex-20 to trap free Gd^{3+} ions, and the Gd-loaded complex was eluted. The fractions were lyophilized and white solids were obtained. The absence of free Gd^{3+} was checked with xylenol orange indicator.
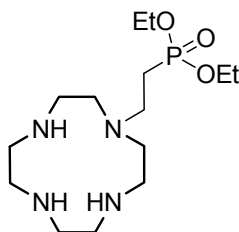
Gd-9. **ESI-MS** (-): calcd C$_{26}$H$_{42}$GdN$_7$O$_8$S: m/z 770.2; found 769.1 (M-H)$^-$.
Gd-11. **ESI-MS** (-): calcd C$_{24}$H$_{35}$GdN$_6$O$_9$: m/z 709.2; found 708.1 (M-H)$^-$.
Gd-12. **ESI-MS** (-): calcd C$_{37}$H$_{39}$GdN$_6$O$_{11}$S: m/z 932.2; found 931.3 (M-H)$^-$.

Materials and Methods

Gd-13. **ESI-MS** (-): calcd $C_{17}H_{26}GdN_5O_6S$: m/z 586.1; found 584.9 (M-H)$^-$.

**diethyl 2-(1, 4, 7, 10-tetraazacyclododecane-1-yl)ethylphosphonate (14)**.

A solution of LiOH (0.14 g, 5.8 mmol) and cyclen (4.00 g, 23.4 mmol) were dissolved in ethanol:water (20:2 ml) at room temperature and diethyl-2-bromoethylphosphonate (0.85 ml, 4.7 mmol) was added dropwise. The reaction mixture was refluxed for 8 h. The product was concentrated under reduced pressure and extracted from the reaction mixture using CH_2Cl_2 (4x100 ml). The dichloromethane layers were combined, dried over sodium sulfate and then concentrated in vacuo to yield 0.68 g (2.0 mmol, 43%) of **14** as colorless oil.

^{1}**H NMR** (CDCl$_3$, 250 MHz), δ (ppm): 1.25 (t, J=7.0 Hz, 3H); 1.26 (t, J=7.0 Hz, 3H) 2.03-1.80 (m, 2H); 2.89-2.59 (m, 21H); 4.12-3.94 (m, 4H). ^{13}**C{^{1}H} NMR** (CDCl$_3$, 62.9 MHz), δ (ppm): 16.3 ($^1J_{PC}$ = 5.7 Hz); 23.3 ($^1J_{PC}$ = 137.3 Hz); 45.1 ($^1J_{PC}$ = 8.6 Hz); 45.9; 48.0; 49.0; 50.5; 61.6 ($^1J_{PC}$ = 6.7 Hz). ^{31}**P{^{1}H} NMR** (D$_2$O, 62.9 MHz), δ (ppm): 32.6 (s).

ESI-HRMS: for $C_{14}H_{33}N_4O_3P$: calcd. 337.2363 (M+H)$^+$, found 337.2363 (M+H)$^+$.

[4,7-Bis-butoxycarbonylmethyl-10-(2-(diethoxyphosphoryl)ethyl)-1,4,7,10-tetraaza-cyclododec-1-yl]-acetic acid *tert*-butyl ester (15).
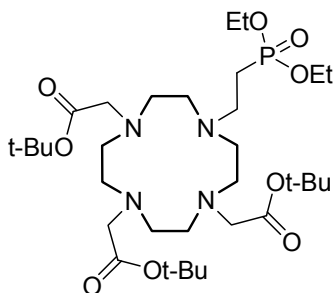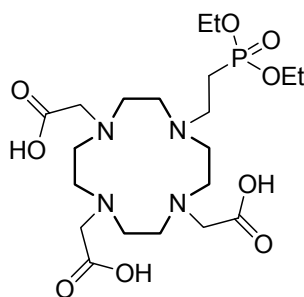
Materials and Methods

A solution of **14** (0.60 g, 1.8 mmol), sodium carbonate (1.89 g, 17.8 mmol) and *tert*–butylbromoacetate (0.91 ml, 6.2 mmol) in acetonitrile (50 ml) was stirred at 70°C for 6-7 h. The reaction was monitored by TLC. After completion, the reaction mixture was filtered and washed with CH_2Cl_2 (3x50 ml). The organic solvent was evaporated under reduced pressure and the residue was purified by column chromatography (silica gel, 5% MeOH in CH_2Cl_2) to give 0.93 g (76%) of **15** as a yellow gum.

^{1}H NMR (CDCl$_3$, 250 MHz), δ (ppm): 1.26-1.11 (t, *J*=7.0 Hz, 6H); 1.41 (s, 18H), 1.37 (s, 9H); 1.92-1.78 (m, 2H); 2.44-2.18 (m, 8H); 2.93-2.56 (m, 10H); 3.02 (br.s, 2H); 3.10 (br.s, 4H); 4.06-3.95 (m, 4H). **^{13}C{^{1}H} NMR** (CDCl$_3$, 62.9 MHz), δ (ppm): 16.1 (^{1}J$_{PC}$ = 5.9 Hz); 21.8 (^{1}J$_{PC}$ = 138.5 Hz); 27.4; 27.6; 48.0; 49.9; 50.2; 50.7; 53.2; 55.5; 56.3; 61.3 (^{1}J$_{PC}$ = 6.3 Hz); 82.0; 82.2; 172.4; 172.8. **^{31}P{^{1}H} NMR** (CDCl$_3$, 100 MHz), δ (ppm): 30.1 (s).

ESI-HRMS for C$_{32}$H$_{63}$N$_4$O$_9$P: calcd. 679.4405(M+H)$^+$, found 679.4418 (M+H)$^+$.

[4,7-Bis-carboxymethyl-10-(2-(diethoxyphosphoryl)ethyl)-1,4,7,10-tetraaza-cyclododec-1-yl]-acetic acid (16).

Compound **15** (0.90 g, 1.3 mmol) was dissolved in neat TFA (10 ml) with stirring at room temperature for 18 h. The reaction was monitored by ESI-LRMS. After completion, the pH was adjusted to 6 using 1N NaOH and the crude product was purified by preparative HPLC. After lyophilization, 0.49 g (74%) of **16** as yellow highly hygroscopic solid was obtained.


^{1}H NMR (D$_2$O, 250 MHz), δ (ppm): 1.29 (t, *J*=7.2 Hz, 6H); 2.22-2.11 (m, 2H); 2.99 (broad, 6H); 3.16 (broad, 4H); 3.36 (broad, 8H); 3.40 (s, 2H); 3.75 (s, 4H); 4.10 (q, *J*=7.2 Hz, 2H); 4.13 (q, *J*=7.2 Hz, 2H). **^{13}C{^{1}H} NMR** (D$_2$O, 62.9 MHz), δ (ppm):

13.4 ($^1J_{PC}$ = 5.7 Hz); 17.3 ($^1J_{PC}$ = 135.4 Hz); 43.6; 45.1; 46.3; 48.5; 49.4; 53.2; 54.5; 61.4 ($^1J_{PC}$ = 6.7 Hz); 168.4; 174.2. **^{31}P{^{1}H} NMR** (D$_2$O, 100 MHz), δ (ppm): 24.4 (s).

ESI-HRMS for C$_{20}$H$_{39}$N$_4$O$_9$P: calcd. 511.2527 (M+H)$^+$, found 511.2532 (M+H)$^+$.

[4,7-Bis-carboxymethyl-10-(2-phosphonoethyl)-1,4,7,10-tetraaza-cyclododec-1-yl]-acetic acid (17).
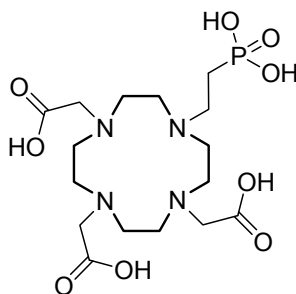
A solution of **16** (300 mg, 0.59 mmol) in 10 ml of 33% HBr in acetic acid was stirred at 60°C for 18 h. The progress of the reaction was monitored by ESI-LRMS. After completion, the solvent was evaporated under reduced pressure and the residue was purified by preparative RP-HPLC. After lyophilization, 185 mg (69%) of **17** as white solid was obtained. m.p. 207-224 °C.

^{1}H NMR (D$_2$O, 250 MHz), δ (ppm): 1.99-1.85 (m, 2H); 3.17 (br.s, 12H); 3.33-3.23 (m, 6H); 3.54 (br.s, 4H); 3.65 (s, 2H). **^{13}C{^{1}H} NMR** (D$_2$O, 62.9 MHz), δ (ppm): 20.2 ($^1J_{PC}$ = 128.7 Hz); 46.6; 47.1; 47.2; 47.4; 48.3; 53.2; 169.3; 172.1. **^{31}P{^{1}H} NMR** (D$_2$O, 100 MHz), δ (ppm): 24.6 (s).

ESI-LRMS (±): for C$_{16}$H$_{31}$N$_4$O$_9$P: calcd 455.5 (M+H)$^+$, found 455.4 (M+H)$^+$.

Preparation of Ln^{3+} complexes of ligand 16 and 17. Ln^{3+} complexes **16** and **17** were prepared from the respective solution of the ligand (1 eq) and the solution of LnCl$_3$.6H$_2$O (0.9-1 eq). The reaction mixture was stirred at 60-70° C for 18 h. pH of the solution was periodically checked and adjusted to 7.0-8.0 using a solution of NaOH (1 M) or HCl (1 N). Finally, the reaction mixture was passed through chelex-100 to trap free Ln^{3+}, and the Ln-loaded complex was eluted. The fractions were lyophilized and white solids were obtained. The absence of free Ln^{3+} ion was checked with xylenol orange indicator.
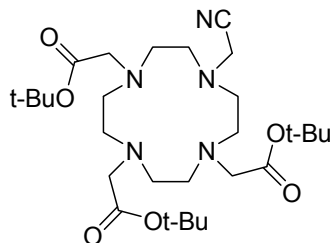
Gd-16. **ESI-MS** (±): calcd $C_{20}H_{36}GdN_4O_9P$: m/z 665.1; found 664.3 (M-H)⁻.

Eu-16. **ESI-MS** (±): calcd $C_{20}H_{36}EuN_4O_9P$: m/z 660.1; found 659.1 (M-H)⁻.

Gd-17. **ESI-MS** (±): calcd $C_{16}H_{26}GdN_4O_9P^{2-}$: m/z 607.1; found 606.2 (M-H)⁻.

Eu-17. **ESI-MS** (±): calcd $C_{16}H_{26}GdN_4O_9P^{2-}$: m/z 602.1; found 601.5(M-H)⁻.

**[4,7-Bis-butoxycarbonylmethyl-10-(cyanomethyl)-1,4,7,10-tetraaza-cyclododec-1-yl]-acetic acid *tert*-butyl ester (18).**

A solution of **3** (4.0 g, 7.8 mmol) and K_2CO_3 (4.3 g, 31.2 mmol) in 40 mL MeCN was stirred at room temperature for 1 h. Bromoacetonitrile (0.65 mL, 9.3 mmol) was added in one aliquot to the above solution and the reaction mixture was refluxed for 8 h**.** The reaction was monitored by TLC. After completion, the reaction mixture was filtered through a G-4 sintered funnel, filtrate was evaporated under reduced pressure and the residue was purified by column chromatography (silica gel, 5% MeOH in CH_2Cl_2, R_f = 0.55) to give 3.36 g (78%) of **18** as brownish gum**.**

¹H NMR (CDCl₃, 250 MHz), δ (ppm): 1.23 (s, 9H); 1.27 (s, 18H); 2.06-2.21 (m, 6H); 2.39-2.78 (m, 10H); 2.89 (s, 4H); 3.01 (s, 2H); 3.63 (s, 2H). **¹³C NMR** (CDCl₃, 62.9 MHz), δ (ppm): 27.7; 27.8; 42.7; 50.1; 50.4; 50.6; 50.7; 55.8; 56.2; 56.7; 82.4; 82.8; 115.2; 172.9; 173.4.

ESI-MS (±): calcd $C_{28}H_{51}N_5O_6$: m/z 554.3 (M+H)⁺; found 554.8 (M+H)⁺.

[4,7-Bis-butoxycarbonylmethyl-10-(2-aminoethyl)-1,4,7,10-tetraaza-cyclododec-1-yl]-acetic acid *tert*-butyl ester (19).

122
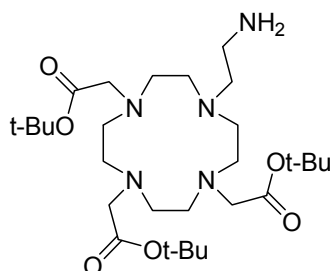
A solution of **18** (3.0 g, 5.4 mmol), Ra-Ni (1.5 g) and H_2 (50 psi) in 7N NH_3/MeOH (30 mL) was stirred at room temperature in Parr-apparatus for 6 h. The reaction was monitored by TLC. After completion, the reaction mixture was filtered through a G-4 sintered funnel, filtrate was evaporated under reduced pressure and the residue was purified by column chromatography (silica gel, 10% MeOH in CH_2Cl_2, R_f = 0.45) to give 2.17 g (72%) of **19** as off white solid.

^{1}H NMR ($CDCl_3$, 250 MHz), δ (ppm): 1.38 (s, 9H); 1.40 (s, 18H); 2.17-2.75 (m, 18H); 2.84 (br s, 4H); 3.03 (s, 4H); 3.10 (s, 2H). **^{13}C NMR** ($CDCl_3$, 62.9 MHz), δ (ppm): 27.2; 27.3; 38.0; 48.5; 48.8; 49.1; 49.6; 52.9; 54.9; 55.1; 81.3; 81.5; 171.5; 171.9.

ESI-MS (±): calcd $C_{28}H_{55}N_5O_6$: m/z 558.4 $(M+H)^+$; found 558.5 $(M+H)^+$.

General method for the synthesis of compounds 22-24.

The solutions of **19** (for compound **22-23**) and **21** (for compound **24**) (2.5 equivalent) in dry DMF were added dropwise to the solution of DTPA-bisanhydride/EDTA-bisanhydride (1 equivalent) in dry DMF (5 mL) at 0-5°C for 30 min under continuous nitrogen flow. The reaction mixtures were stirred overnight at 50°C. The progresses of reaction were monitored by ESI-MS. After completion, the solvent was evaporated under reduced pressure. The crude products were purified by preparative RP-HPLC.

5,8-bis(carboxymethyl)-10-oxo-2-(2-oxo-2-(2-(4,7,10-tris(2-*tert*-butoxy-2-oxoethyl)-1,4,7,10-tetraazacyclododecan-1-yl)ethylamino)ethyl)-13-(4,7,10-tris(2-*tert*-butoxy-2-oxoethyl)-1,4,7,10-tetraazacyclododecan-1-yl)-2,5,8,11-tetraazatridecane-1-carboxylic acid (22).

RP-HPLC: method A, λ = 214 nm, RT = 21 min. Yield: 1.03 g (39%) of **22** as yellowish gum.
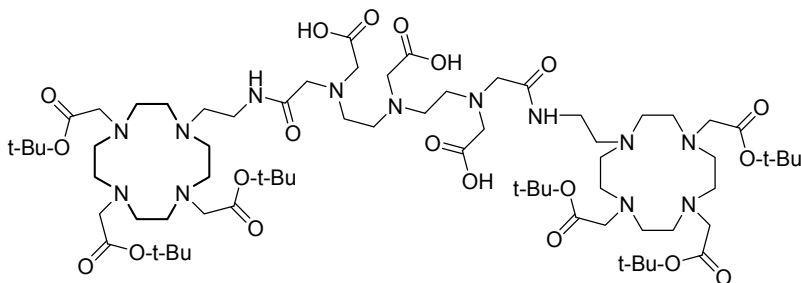
¹H NMR (CDCl₃, 250 MHz), δ (ppm): 1.52 (s, 36H); 1.54 (s, 18H); 2.76-3.17 (m, 20H); 3.18-3.47 (m, 16H); 3.49-3.68 (m, 16H); 3.70-3.89 (m, 13H); 3.96 (br s, 6H); 4.14 (br s, 4H). **¹³C NMR** (CDCl₃, 62.9 MHz), δ (ppm): 29.4; 29.5; 33.2; 47.9; 49.3; 50.0; 51.3; 51.7; 52.2; 52.9; 54.9; 56.6; 57.7; 60.1; 60.8; 81.4; 81.6; 168.8; 170.2; 170.3; 172.3; 176.2.

ESI-MS (±): calcd $C_{70}H_{129}N_{13}O_{20}$: m/z 1470.9 (M-H)⁻; found 1471.3 (M-H)⁻.

2,2'-(4,11-dioxo-1,14-bis(4,7,10-tris(2-*tert*-butoxy-2-oxoethyl)-1,4,7,10-tetraazacyclododecan-1-yl)-3,6,9,12-tetraazatetradecane-6,9-diyl)diacetic acid (23).

RP-HPLC: method A, λ = 214 nm, RT = 24 min. Yield: 1.13 g (52%) of **23** as colorless gum.
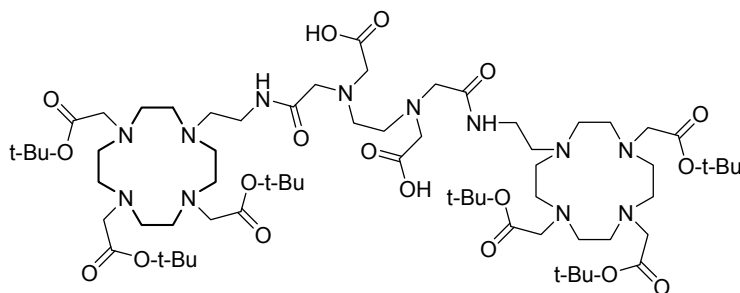
¹H NMR (CDCl₃, 250 MHz), δ (ppm): 1.46 (s, 36H); 1.48 (s, 18H); 2.60 (br s, 4H); 2.73-2.79 (m, 18H); 3.02-3.08 (m, 7H); 3.12 (s, 4H); 3.19 (br s, 3H); 3.27-3.31 (m, 2H); 3.35 (s, 8H); 3.40 (s, 4H), 3.42 (s, 6H); 3.47 (br s, 6H); 3.54-3.61 (m, 2H); 3.66 (d, *J=5.33*, 2H); 3.70 (d, *J=2.66*, 2H). **¹³C NMR** (CDCl₃, 62.9 MHz), δ (ppm): 27.6; 27.7; 33.5; 47.8; 49.3; 49.9; 50.6; 52.8; 53.7; 55.0; 55.9; 59.7; 59.9; 80.9; 81.0; 169.7; 169.9; 172.6; 175.1.

ESI-MS (±): calcd $C_{66}H_{122}N_{12}O_{18}$: m/z 1371.9 (M+H)⁺; found 1371.9 (M+H)⁺.

2,2'-2,2'-(carboxymethylazanediyl)bis(ethane-2,1-diyl)bis((2-oxo-2-(4-((4,7,10-tris(2-tert-butoxy-2-oxoethyl)-1,4,7,10-tetraazacyclododecan-1-yl)methyl)phenylamino)ethyl)azanediyl)diacetic acid (24).

RP-HPLC: method A, λ = 254 nm, RT = 22 min. Yield: 1.32 g (46%) of **24** as yellowish gum.
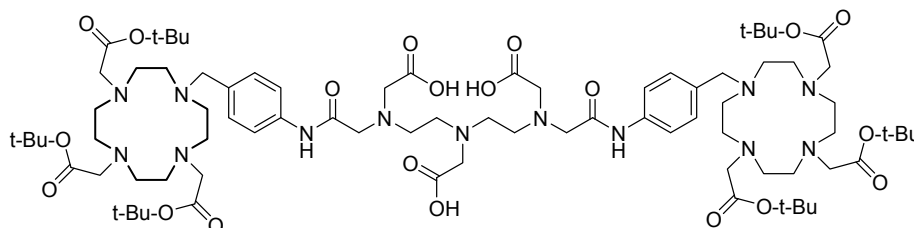
¹H NMR (CDCl₃, 250 MHz), δ (ppm): 1.44 (s, 36H); 1.46 (s, 18H); 2.71-2.89 (m, 20H); 2.92-3.04 (m, 9H); 3.10 (br s, 5H); 3.20 (s, 4H); 3.28 (br s, 10H); 3.31-3.36 (m, 4H); 3.38 (s, 2H); 3.44 (s, 8H); 3.48 (s, 4H); 3.81 (br s, 2H); 4.14 (br s, 3H); 6.88-7.25 (m, 4H); 7.80-8.11 (m, 4H). **¹³C NMR** (CDCl₃, 62.9 MHz), δ (ppm): 27.9; 28.0; 48.8; 48.9; 49.8; 50.7; 50.9; 51.7; 52.1; 52.7; 55.8; 56.2; 56.3; 61.4; 81.3; 81.4; 120.2; 122.7; 124.9; 128.9; 139.4; 169.8; 169.9; 170.3; 170.6; 175.6.

ESI-MS (±): calcd $C_{80}H_{133}N_{13}O_{20}$: m/z 1594.9 (M-H)⁻; found 1595.1 (M-H)⁻.

General method for the synthesis of 25, 26 and 27.

Neat TFA (20ml) was added to the previously obtained compounds **22-24** and the reactions were kept at rt for 18 h. TFA was then evaporated, dissolved in a minimum volume of MeOH (1 mL) followed by dropwise addition of diethyl ether at 0-5˚C and stir gently for 1 h at room temperature. The compounds were precipitated and precipitates were filtered through a G-4 sintered funnel under continuous nitrogen flow. The precipitates were dissolved in water, neutralized by adding 1M NaOH and the crude products were purified by preparative RP-HPLC.

N,N-bis{1-[{[({1-[1,4,7-tris(carboxymethyl)-1,4,7,10-tetraazacyclododecane-10-yl]eth-2-yl}amino)carbonyl]methyl}-(carboxymethyl)amino]eth-2-yl}aminoacetic acid (25).

RP-HPLC: method B, λ = 214 nm, RT = 2.8 min. Yield: 0.22 g (57%) of **25** as white solid.

Materials and Methods
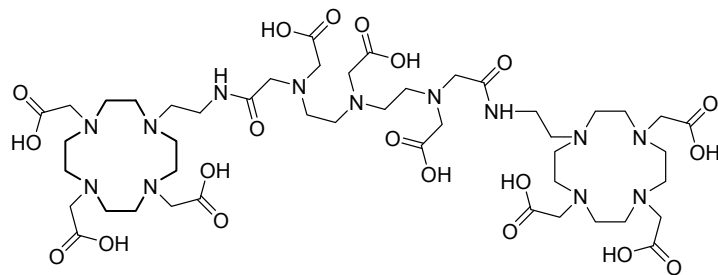
**¹H NMR** (D₂O, 250 MHz), δ (ppm): 3.01 (br s, 8H); 3.04 -3.17 (m, 16H); 3.23-3.41 (m, 18H); 3.46 (br s, 6H); 3.56 (br s, 8H); 3.62 (s, 4H); 4.08 (s, 10H). **¹³C NMR** (D₂O, 62.9 MHz), δ (ppm): 32.2; 46.8; 47.7; 47.8; 49.0; 49.1; 50.2; 50.8; 51.2; 51.8; 52.2; 53.5; 54.1; 164.7; 167.2; 170.7; 171.2; 171.3.

ESI-MS (±): calcd $C_{46}H_{81}N_{13}O_{20}$: m/z 1134.5 (M-H)⁻; found 1134.8 (M-H)⁻.

***N,N*-bis[1-({[({alpha-[1,4,7-tris(carboxymethyl)-1,4,7,10-tetraazacyclododecane-10-yl]-*p*-tolylamino}carbonyl)methyl]-(carboxymethyl)}amino)eth-2-yl] aminoacetic acid (26).**

   RP-HPLC: method B, λ = 254 nm, RT = 2.4 min. Yield: 0.22 g (58%) of **26** as white solid.
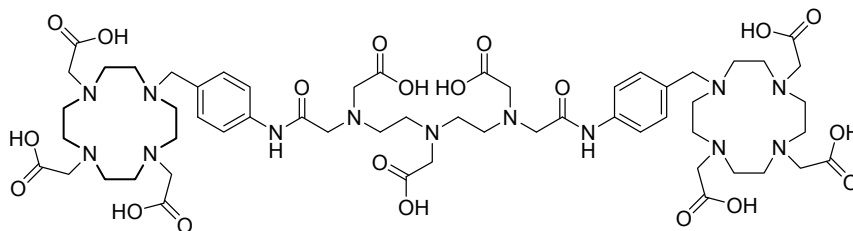
**¹H NMR** (D₂O, 250 MHz), δ (ppm): 2.87-2.99 (m, 8H); 3.12-3.22 (m, 12H); 3.24-3.34 (m, 20H); 3.41 (t, *J=5.97*, 5H); 3.54 (br s, 8H); 3.58 (s, 2H); 3.60 (s, 2H); 3.81 (br s, 4H); 7.30-7.37 (m, 4H); 7.38-7.43 (m, 2H); 7.44-7.52 (m, 2H). **¹³C NMR** (D₂O, 62.9 MHz), δ (ppm): 45.9; 46.8; 48.1; 48.2; 48.6; 50.6; 53.5; 54.2; 54.8; 56.2; 56.3; 56.9; 119.4; 121.5; 124.9; 128.1; 134.6; 168.6; 169.5; 169.8; 173.0; 175.9.

ESI-MS (±): calcd $C_{56}H_{86}N_{13}O_{20}$: m/z 1258.6 (M-H)⁻; found 1259.0 (M-H)⁻.

1,2-bis[{[({1-[1,4,7-tris(carboxymethyl)-1,4,7,10-tetraazacyclododecane-10-yl]eth-2-yl}amino)carbonyl]methyl}-(carboxymethyl)amino]ethane (27).

   RP-HPLC: method B, λ = 214 nm, RT = 3.4 min. Yield: 0.26 g (68%) of **27** as off white solid.
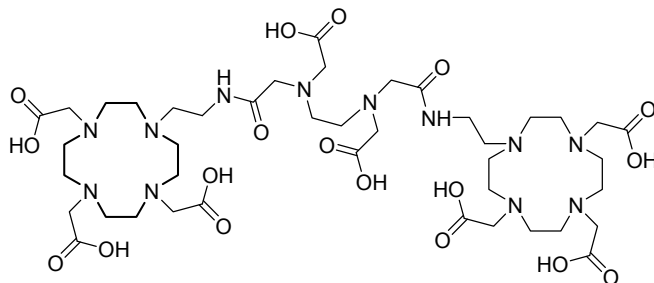
¹H NMR (D₂O, 250 MHz), δ (ppm): 2.88 -2.97 (m, 4H); 2.98-3.17 (16, H); 3.21 (s, 4H); 3.24 (br s, 2H); 3.26-3.47 (m, 23H); 3.52 (s, 4H); 3.70 (br s, 8H); 3.78 (br s, 4H).

¹³C NMR (D₂O, 62.9 MHz), δ (ppm): 37.9; 50.8; 51.5; 53.0; 53.4; 53.7; 53.9; 54.2; 57.9; 59.2; 59.8; 172.3; 174.1; 176.6; 178.4.

ESI-MS (±): calcd $C_{42}H_{75}N_{12}O_{18}$: m/z 1033.5 (M-H)⁻; found 1033.6 (M-H)⁻.

Preparation of the Ln³⁺ Complexes of 25-27.

The Ln³⁺ complexes of **26**, **27** and **28** were prepared by mixing the ligand and the LnCl₃. 6H₂O solutions in 1:2 molar ratios. The reaction mixture was stirred at 50-60° C for 18 h. The pH was periodically adjusted to 7.0-7.5 using a solution of NaOH (1 M). After 18 h, the reaction mixture was cooled down and passed through chelex-100 at room temperature to trap eventual free Ln³⁺, and the Ln³⁺-loaded complex was recovered. The absence of free Ln³⁺ was checked with xylenol orange indicator. The fractions were lyophilized and white solids were obtained.

Gd-25 ESI-MS (-): calcd $C_{46}H_{75}Gd_2N_{13}O_{20}$: m/z 1443.6; found 1443.9 (M-H)⁻.

Eu-25 ESI-MS (-): calcd $C_{46}H_{75}Eu_2N_{13}O_{20}$: m/z 1433.1; found 1433.7 (M-H)⁻.

Gd-26 ESI-MS (-): calcd $C_{56}H_{79}Gd_2N_{13}O_{20}$: m/z 1567.8; found1566.8 (M-H)⁻.

Eu-26 ESI-MS (-): calcd $C_{56}H_{79}Eu_2N_{13}O_{20}$: m/z 1557.2; found 1556.6 (M-H)⁻.

Gd-27 ESI-MS (-): calcd $C_{42}H_{68}Gd_2N_{12}O_{18}$: m/z 1342.5; found 1341.9 (M-H)⁻.

Eu-27 ESI-MS (-): calcd $C_{42}H_{68}Eu_2N_{12}O_{18}$: m/z 1331.9; found 1332.2 (M-H)⁻.

[4,7-Bis-butoxycarbonylmethyl-10-(2-cyanoethyl)-1,4,7,10-tetraaza-cyclododec-1-yl]-acetic acid *tert*-butyl ester (28).


127
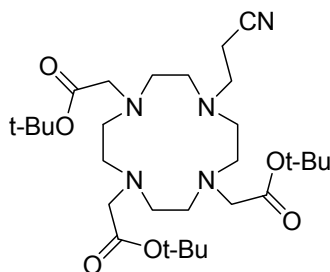
A solution of **3** (4.0 g, 7.8 mmol), TEA (1.57 g, 15.6 mmol) and acrylonitrile (0.83 g, 15.6 mmol) in 50 mL MeOH was stirred at room temperature for 24 h. The reaction was monitored by TLC. After completion, the solvent was evaporated under reduced pressure and the crude product was purified by flash column chromatography (silica gel, 5% MeOH in CH_2Cl_2, R_f = 0.55) to give 3.5 g (79%) of **28** as transparent gum**.**

^{1}H NMR (CDCl$_3$, 250 MHz), δ (ppm): 1.24 (s, 18H); 1.26 (s, 9H); 2.03-2.30 (m, 3H); 2.40-2.74 (m, 7H); 2.76-3.12 (s, 12H); 3.42 (s, 2H); 3.51 (s, 2H). **^{13}C NMR** (CDCl$_3$, 62.9 MHz), δ (ppm) 14.5; 27.7; 27.8; 49.1; 50.2; 50.8; 50.9; 51.3; 55.6; 56.4; 82.22; 82.6; 118.8; 172.5; 173.1.

ESI-HRMS (+): calcd $C_{29}H_{53}N_5O_6$: m/z 568.40686 (M+H)$^+$; found 568.40714 (M+H)$^+$.

[4,7-Bis-butoxycarbonylmethyl-10-(3-aminopropyl)-1,4,7,10-tetraaza-cyclododec-1-yl]-acetic acid *tert*-butyl ester (29).
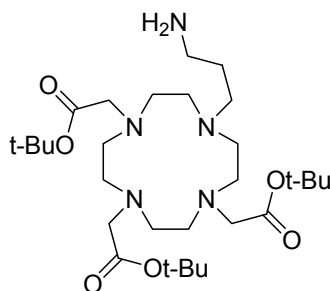

A solution of **28** (3.0 g, 5.3 mmol), Ra-Ni (1.5 g) and H$_2$ (50 psi) in 7N NH$_3$/MeOH (30 mL) was stirred at room temperature in Parr-apparatus for 6 h. The reaction was monitored by TLC. After completion, the reaction mixture was filtered through a G-4 sintered funnel, filtrate was evaporated under reduced pressure and the residue was purified by column chromatography (silica gel, 10% MeOH in CH_2Cl_2, R_f = 0.5) to give 2.41 g (80%) of **29** as off white solid.

^{1}H NMR (CDCl$_3$, 400 MHz), δ (ppm): 1.41 (s, 27H); 1.61 (br s, 2H); 2.85–2.20 (m, 16H); 3.42–2.99 (m, 8H); 8.19 (br s, 2H). **^{13}C NMR** (CDCl$_3$, 100 MHz), δ (ppm): 22.9; 27.1; 27.2; 38.5; 41.8; 48.9; 49.4; 50.1; 52.2; 55.9; 57.2; 81.1; 81.8; 169.8; 172.0.

ESI-HRMS (+): calcd $C_{29}H_{57}N_5O_6$: m/z 572.43816 (M+H)$^+$; found 572.43826 (M+H)$^+$.

6,9-bis(carboxymethyl)-11-oxo-3-(2-oxo-2-(3-(4,7,10-tris(2-tert-butoxy-2-oxoethyl)-1,4,7,10-tetraazacyclododecan-1-yl)propylamino)ethyl)-15-(4,7,10-tris(2-tert-butoxy-2-oxoethyl)-1,4,7,10-tetraazacyclododecan-1-yl)-3,6,9,12-tetraazapentadecan-1-oic acid (30).
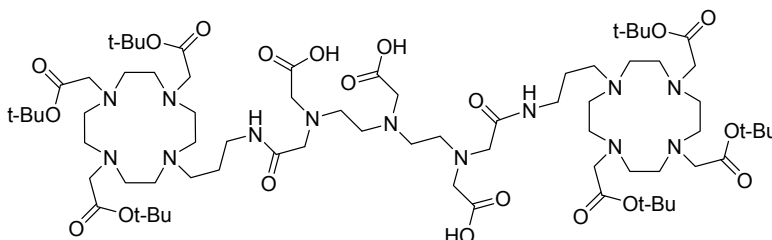

The solutions of **29** (2.5 equivalent) in dry DMF were added dropwise to the solution of DTPA- bisanhydride (1 equivalent) in dry DMF (5 mL) at 0-5˚C for 30 min under continuous nitrogen flow. The reaction mixtures were stirred overnight at 50˚C. The progresses of reaction were monitored by ESI-MS. After completion, the solvent was evaporated under reduced pressure. The crude products were purified by preparative RP-HPLC. RP-HPLC: method A, λ = 214 nm, RT = 24 min. Yield: 0.8 g (32%) of **30** as yellowish gum.

^{1}H NMR (MeOD, 250 MHz), δ (ppm): 1.29 (s, 36H); 1.30 (s, 18H); 1.50-1.63 (m, 2H); 1.83 (br s, 2H); 2.46-2.70 (m, 15H); 3.07-3.34 (m, 14H); 3.44 (s, 3H); 3.52 (s, 2H); 3.62-3.70 (m, 4H). **^{13}C NMR** (MeOD, 62.9 MHz), δ (ppm) 24.2; 28.6; 28.9; 37.4; 51.0; 51.1; 51.6; 52.6; 53.5; 54.4; 55.6; 56.4; 57.4; 58.4; 82.7; 83.1; 171.6; 172.3; 174.4; 176.5; 177.7.

ESI-MS (±): calcd $C_{72}H_{133}N_{13}O_{20}$: m/z 1499.9 (M-H)$^-$; found 1499.3 (M-H)$^-$.

N,N-**bis{1-[{[({1-[1,4,7-tris(carboxymethyl)-1,4,7,10-tetraazacyclododecane-10-yl]prop-2-yl}amino)carbonyl]methyl}-(carboxymethyl)amino]prop-2-yl}aminoacetic acid (31)**.
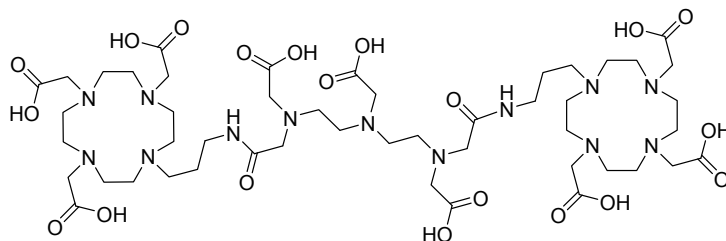
Neat TFA (15ml) was added to the previously obtained compounds **30** and the reaction was kept at rt for 18 h. TFA was then evaporated, dissolved in a minimum volume of MeOH (1 mL) followed by dropwise addition of diethyl ether at 0-5°C and stir gently for 1 h at room temperature. The compounds were precipitated and precipitates were filtered through a G-4 sintered funnel under continuous nitrogen flow. The precipitates were dissolved in water, neutralized by adding 1M NaOH and the crude products were purified by preparative RP-HPLC. RP-HPLC: method B, λ = 214 nm, RT = 2.9 min. Yield: 0.14 g (57%) of **31** as white solid.

^{1}H NMR (D$_2$O, 250 MHz), δ (ppm): 1.82 (br s, 3H); 2.97 (br s, 2H); 3.03 -3.17 (m, 21H); 3.18-3.38 (m, 21H); 3.62 (br s, 4H); 3.66 (br s, 4H); 3.77 (s, 2H); 3.80 (s, 2H). **^{13}C NMR** (D$_2$O, 62.9 MHz), δ (ppm): 23.3; 36.5; 48.8; 49.3; 49.6; 49.9; 51.2; 52.1; 54.8; 55.4; 57.3; 57.5; 170.4; 172.0; 173.4; 174.2; 174.4.

ESI-MS (±): calcd C$_{48}$H$_{85}$N$_{13}$O$_{20}$: m/z 1163.3 (M-H)$^-$; found 1163.8 (M-H)$^-$.

di-*tert*-butyl 2,2'-(ethane-1,2-diylbis(benzylazanediyl))diacetate (32).
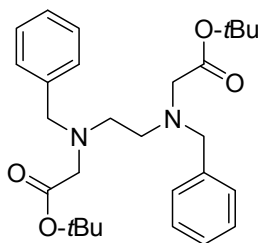
A solution of dibenzylethylenediamine (5 g, 20.8 mmol) and K$_2$CO$_3$ (7.19 g, 52.1 mmol) in 5 mL MeCN was stirred at room temperature for 1 h. *tert*-butylbromoacetate (8.94 g, 45.8 mmol) was added in one aliquot to the above solution and the reaction mixture was refluxed for 3 h**.** The reaction was monitored by TLC, using CH$_2$Cl$_2$:MeOH, 9:1 as mobile phase. TLC plates were developed in an iodine chamber and R_f of (**32**) was 0.7. After completion, the reaction mixture was poured

into 50 mL water and extracted with CH_2Cl_2 (3x50 ml). The organic layer was evaporated under reduced pressure and purified by column chromatography (silica gel, 5% MeOH in CH_2Cl_2) to give 5.1 g (76%) of **32** as off white solid**.**

^{1}H NMR (CDCl$_3$, 250 MHz), δ (ppm): 1.45 (s, 18H); 2.71-2.92 (m, 4H); 3.4 (s, 4H); 3.8 (s, 4H); 7.2-7.4 (m, 10H). **^{13}C NMR** (CDCl$_3$, 62.9 MHz), δ (ppm): 28.2; 51.6; 54.9; 58.5; 81.0; 127.3; 128.3; 129.2; 138.4; 170.6.

ESI-MS (±): calcd $C_{20}H_{22}N_2O_2$: m/z 323.4 (M+H)$^+$ and found 323.6 (M+H)$^+$.

**di-*tert*-butyl 2,2'-(ethane-1,2-diylbis(azanediyl))diacetate (33).**
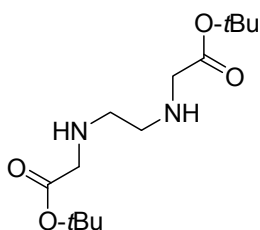
A solution of **32** (4.0 g, 12.4 mmol), (10%) Pd-C (1 g w/w) and H_2 (50 psi) in MeOH (40 mL) was stirred at room temperature in Parr-apparatus for 8 h. The reaction was monitored by TLC. After completion, the reaction mixture was filtered through a G-4 sintered funnel, filtrate was evaporated under reduced pressure and the residue was purified by column chromatography (silica gel, 10% MeOH in CH_2Cl_2, R_f = 0.25) to give 1.41 g (80%) of **33** as transparent oil.

^{1}H NMR (CDCl$_3$, 250 MHz), δ (ppm): 1.47 (s, 18H); 2.8-3.2 (m, 4H); 3.6 (s, 4H). **^{13}C NMR** (CDCl$_3$, 62.9 MHz), δ (ppm): 28.1; 48.7; 50.1; 82.4; 169.8.

ESI-MS (±): calcd $C_6H_{10}N_2O_2$: m/z 143.1 (M+H)$^+$; found 143.3 (M+H)$^+$.

***tert*-butyl 2-(2-bromo-N-(2-(2-bromo-N-(2-tert-butoxy-2-oxoethyl)acetamido)ethyl)acetamido)acetate (34).**
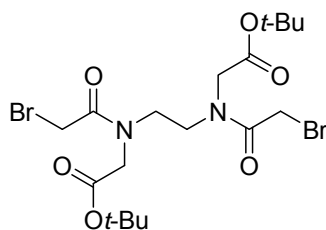
A solution of **33** (1.2 g, 8.5 mmol) in 50 mL CH_2Cl_2 and 50 mL water was stirred at room temperature and dropwise addition of bromo-acetylbromide (4.27 g, 21.1 mmol) for 1 h. During addition of bromo-acetylbromide, 1M K_2CO_3 solution was also added to maintain the pH between 8-8.5. Reaction mixture was stirred for another 3 h at room temperature and the reaction was monitored by TLC, using CH_2Cl_2:MeOH, 9:1 as mobile phase. TLC plates were developed in an iodine chamber and R_f of **(34)** was 0.65. After completion, the organic layer was separated The solvent was evaporated under reduced pressure and purified by column chromatography (silica gel, 5% MeOH in CH_2Cl_2) to give 2.32 g (52%) of **34** as transparent oil**.**

^{1}H NMR (CDCl$_3$, 250 MHz), δ (ppm): 1.43 (s, 18H); 3.50 (s, 4H); 3.61-3.91 (m, 4H); 4.06 (s, 4H). **^{13}C NMR** (CDCl$_3$, 62.9 MHz), δ (ppm): 25.9; 26.2; 28.0; 45.2; 51.7; 83.0; 167.6; 167.9.

ESI-MS (±): calcd $C_{18}H_{30}Br_2N_2O_6$: m/z 531.1 (M+H)$^+$ and found 531.6 (M+H)$^+$.

**(tris-*tert*-butyl-DO3A-methylamide)$_2$-EDTA (35).**
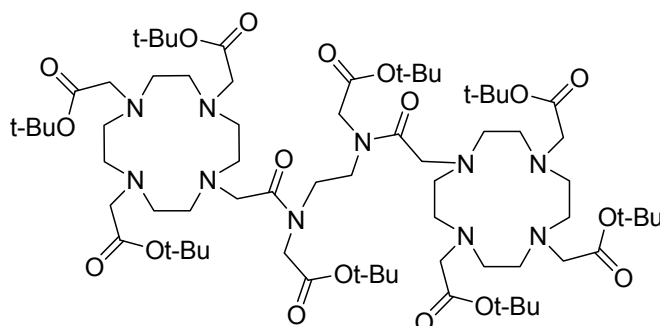
A solution of **3** (5.15 g, 10.0 mmol) and K_2CO_3 (2.08 g, 15.1 mmol) in 5 mL DMF was stirred at room temperature for 1 h. **34** (2 g, 3.8 mmol) was added in one aliquot to the above solution and the reaction mixture was heated at 70-80°C for overnight**.** The reaction progress was checked by TLC, using CH_2Cl_2:MeOH, 9:1 as mobile phase. TLC plates were developed in an iodine chamber and R_f of **(35)** was 0.3. After completion, the reaction mixture was poured into 100 mL water and extracted with CH_2Cl_2 (3x50 ml). The organic layer was evaporated under reduced pressure and purified by column chromatography (silica gel, 10% MeOH in CH_2Cl_2) to give 2.53 g (48%) of **35** as off white solid**.**

¹H NMR (CDCl₃, 250 MHz), δ (ppm): 1.27 (s, 18H); 1.29 (s, 18H); 1.32 (s, 36H); 1.85-3.59 (m, 52H); 4.01 (s, 4H). **¹³C NMR** (CDCl₃, 62.9 MHz), δ (ppm): 27.8; 28.2; 44.7; 47.0; 47.1; 49.4; 50.2; 51.7; 53.5; 54.9; 55.7; 81.4; 81.6; 81.7; 82.3; 168.3; 168.5; 169.1; 172.1; 172.6.

ESI-MS (±): calcd $C_{70}H_{128}N_{10}O_{18}$: m/z 1398.8 $(M+H)^+$ and found 1399.2 $(M+H)^+$.

(DO3A-methylamide)₂-EDTA (36).
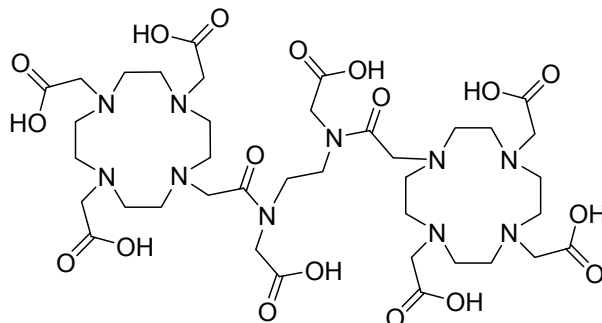
A solution of **35** (2.0 g, 1.4 mmol) in TFA (20 mL) was stirred at room temperature for 18-20 h. The reaction was monitored by ESI-MS. The solvent was evaporated under reduced pressure and dissolved in a minimum volume of MeOH (1 mL) followed by addition of diethyl ether dropwise at 0-5°C and stir for 1 h at room temperature. The compound was precipitated and filtered through a G-4 sintered funnel under nitrogen. The precipitate was dissolved in water and neutralized by adding 1 M Na₂CO₃ and the crude products were purified by preparative RP-HPLC. RP-HPLC: method B, λ = 214 nm, RT = 2.9 min. Yield: 0.43 g (31%) of **36** as white solid.

¹H NMR (D₂O, 250 MHz), δ (ppm): 2.90-3.36 (m, 16H); 3.27-3.52 (m, 24H); 3.55-3.63 (d, J=7.13 Hz, 3H); 3.67-3.82 (m, 9H); 3.83-3.92 (m, 4H). **¹³C NMR** (D₂O, 62.9 MHz), δ (ppm): 45.2; 48.2; 51.4; 51.6; 52.6; 53.2; 55.4; 55.5; 55.9; 56.6; 170.7; ; 175.4; 175.6; 176.2; 177.1.

ESI-MS (±): calcd $C_{38}H_{64}N_{10}O_{18}$: m/z 947.9 $(M-H)^-$; found 948.3 $(M-H)^-$.

(S)-methyl   2-(benzyloxycarbonylamino)-6-(5-((3aS,4S,6aR)-2-oxo-hexahydro-1H-thieno[3,4-d]imidazol-4-yl)pentanamido)hexanoate (37).
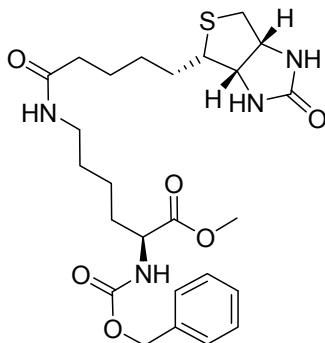
A solution of α-N-carbobenzyloxy-L-lysine methyl ester (2 g, 6.8 mmol), biotin (1.7 g, 6.9 mmol), NMM (1.5 mL, 14.9 mmol) and HOBt (1.44 g, 7.5 mmol) in DMF (5 mL) was stirred at 0-5°C for 15 min and then EDC (1.01 g, 7.5 mmol) was added. The reaction mixture was stirred overnight at room temperature. The progress of reaction was monitored by TLC using CH_2Cl_2:MeOH, 9:1 and Rf of **(37)** was 0.45. After completion, the reaction mixture was poured in water, extracted with EtOAc (3x100 mL), organic layer was dried over Na_2SO_4, filtered, filtrate was evaporated under reduced pressure and purified by column chromatography (silica gel, 10% MeOH in CH_2Cl_2) to give 2.19 g (62%) of **37** as off white solid.

^{1}H NMR (CDCl₃, 400 MHz), δ (ppm): 1.25-1.36 (m, 4H); 1.37-1.47 (m, 2H); 1.50-1.67 (m, 5H), 1.68-1.79 (m, 1H); 2.09 (t, *J*=7.43 Hz, 2H); 2.54-2.62 (m, 1H); 2.70-2.80 (m, 1H); 2.97-3.04 (m, 1H); 3.05-3.18 (m, 2H); 3.65 (s, 3H); 4.11-4.18 (m, 1H); 4.19-4.27 (m, 1H); 4.31-4.37 (m, 1H); 5.02 (s, 2H); 5.98 (s, 2H); 6.56 (t, *J*=6.83 Hz, 1H); 6.73 (s, 1H); 7.19-7.32 (m, 5H). **^{13}C NMR** (CDCl₃, 100 MHz), δ (ppm): 22.5; 25.6; 27.9; 28.2; 28.8; 31.7; 35.8; 38.7; 40.4; 52.3; 53.7; 55.7; 60.1; 61.7; 66.8; 127.9; 128.1; 128.4; 136.2; 156.2; 164.3; 173.2; 173.4.

ESI-HRMS (+): calcd $C_{25}H_{36}N_4O_6S$: m/z 521.2428 (M+H)$^{+}$; found 521.2429 (M+H)$^{+}$.

(S)-2-(benzyloxycarbonylamino)-6-(5-((3aS,4S,6aR)-2-oxo-hexahydro-1H-thieno[3,4-d]imidazol-4-yl)pentanamido)hexanoic acid (38).

Materials and Methods

A solution of **37** (2 g, 3.8 mmol) in 50 mL of THF:MeOH:water (3:2:2) was stirred at 0-5˚C for 15 min and then LiOH (0.18 g, 7.7 mmol) was added. The reaction mixture was stirred for 2 h at room temperature. The progress of the reaction was
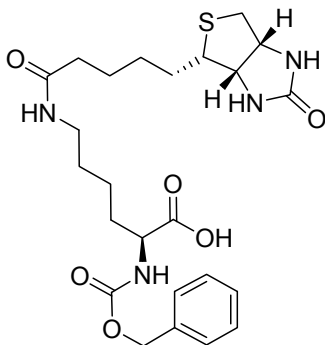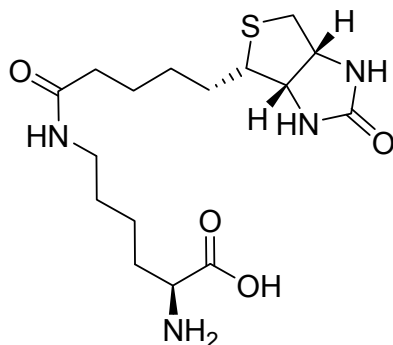

checked by ESI-MS. After completion, the reaction mixture was concentrated under reduced pressure. The compound was purified by preparative RP-HPLC (method C, λ = 214 nm, RT = 14 min). After lyophilization, 1.3 g (67%) of **38** as white powder was obtained.

¹H NMR (CDCl₃, 250 MHz), δ (ppm): 1.22-1.34 (m, 4H); 1.35-1.45 (m, 2H); 1.50-1.67 (m, 5H), 1.66-1.75 (m, 1H); 2.01 (t, J=7.43 Hz, 2H); 2.50-2.60 (m, 1H); 2.68-2.78 (m, 2H); 2.94-3.00 (m, 1H); 3.01-3.12 (m, 2H); 4.06-4.12 (m, 1H); 4.14-4.22 (m, 1H); 429-4.35 (m, 1H); 5.09 (s, 2H); 5.82 (s, 2H); 6.42-6.47 (m, 1H); 6.69 (s, 1H); 7.16-7.32 (m, 5H). **¹³C NMR** (CDCl₃, 62.9 MHz), δ (ppm): 22.5; 25.6; 27.9; 28.2; 28.8; 31.7; 35.8; 38.7; 40.4; 53.7; 55.7; 60.1; 61.7; 66.8; 127.9; 128.1; 128.4; 136.2; 156.2; 164.3; 173.2; 173.4.

ESI-HRMS (±): calcd C₂₄H₃₄N₄O₆S: m/z 507.2278 (M+H)⁺; found 507.2279 (M+H)⁺.

**(S)-2-amino-6-(5-((3aS,4S,6aR)-2-oxo-hexahydro-1H-thieno[3,4-d]imidazol-4-yl)pentanamido)hexanoic acid (39).**

A solution of **38** (0.2 g, 0.39 mmol), (10%) Pd-C (0.05 g) and H_2 (50 psi) in MeOH (10 mL) was stirred at room temperature in Parr-apparatus for 6 h. The reaction was monitored by ESI-MS. After completion, the reaction mixture was filtered through a G-4 sintered funnel; filtrate was evaporated under reduced pressure. The compound was purified by preparative RP-HPLC (method C, λ = 214 nm, RT = 9.5 min). After lyophilization, 0.09 g (66%) of **39** as white powder was obtained.

^{1}H NMR (D$_2$O, 250 MHz), δ (ppm): 1.14-1.21 (m, 2H); 1.37-1.47 (m, 2H); 1.50-1.67 (m, 5H), 1.68-1.79 (m, 1H); 2.09 (m, 2H); 2.54-2.62 (m, 1H); 2.70-2.80 (m, 2H); 2.97-3.04 (m, 1H); 3.05-3.18 (m, 3H); 4.11-4.18 (m, 1H); 4.19-4.27 (m, 1H); 4.30-4.36 (m, 1H). **^{13}C NMR** (D$_2$O, 62.9 MHz), δ (ppm): 22.3; 25.4; 28.4; 29.2; 29.5; 34.0; 35.6; 40.9; 41.5; 55.4; 55.8; 60.8; 62.3; 164.0; 174.2; 174.9.

ESI-HRMS (+): calcd $C_{16}H_{28}N_4O_4S$: m/z 373.1904 (M+H)$^+$; found 373.1903 (M+H)$^+$.

tri-*tert*-butyl 2,2',2''-(10-(2-((S)-2-(benzyloxycarbonylamino)-6-(5-((3aS,4S,6aR)-2-oxo-hexahydro-1H-thieno[3,4-d]imidazol-4-yl)pentanamido)hexanamido)ethyl)-1,4,7,10-tetraazacyclododecane-1,4,7-triyl)triacetate (40).
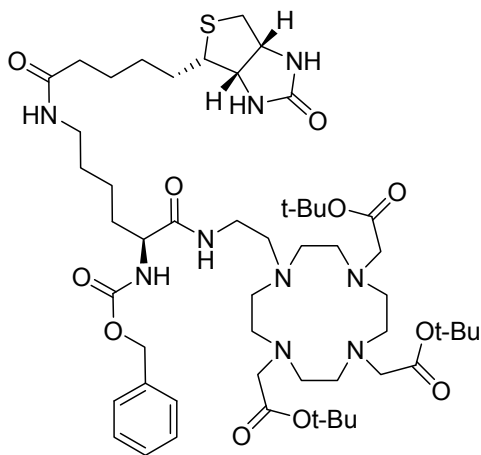
A solution of **19** (0.88 g, 1.58 mmol), **38** (0.8 g, 1.58 mmol), NMM (0.35 mL, 3.4 mmol) and HOBt (0.33 g, 1.74 mmol) in DMF (5 mL) was stirred at 0-5°C for 15 min and then EDC (0.23 g, 1.74 mmol) was added. The reaction mixture was stirred overnight at room temperature. The progress of reaction was monitored by ESI-MS. After completion of reaction DMF was evaporated under reduced pressure and

purified by preparative RP-HPLC (method C, λ = 214 nm, RT = 24.8 min). After lyophilization, 0.76 g (48%) of **40** as white powder was obtained.

^{1}H NMR (CDCl$_3$, 250 MHz), δ (ppm): 1.13-1.27 (m, 4H); 1.22 (s, 18H); 1.42 (s, 9H); 1.51-1.89 (m, 8H); 1.98 (t, J=7.33 Hz, 2H); 2.10-2.38 (m, 1H); 2.42-3.18 (m, 19H); 3.22-3.37 (m, 2H); 3.39-3.44 (m, 1H); 3.48-3.97 (m, 8H); 4.02-4.10 (m, 1H); 4.11-4.20 (m, 1H); 427-4.31 (m, 1H); 5.04 (s, 2H); 5.27 (s, 2H); 5.57-5.67 (m, 1H); 6.30-6.52 (m, 2H); 7.20-7.50 (m, 5H). **^{13}C NMR** (CDCl$_3$, 62.9 MHz), δ (ppm): 17.9; 18.5; 22.7; 23.3; 28.2; 29.4; 29.7; 31.9; 33.4; 33.5; 39.8; 41.1; 48.4; 50.2; 51.8; 52.3; 53.6; 56.2; 56.3; 56.6; 56.7; 56.9; 60.1; 62.0; 66.6; 81.9; 82.1; 127.8; 128.1; 128.5; 135.6; 155.6; 161.9; 169.7; 169.9; 170.4; 173.7.

ESI-HRMS (±): calcd C$_{52}$H$_{87}$N$_9$O$_{11}$S: m/z 1046.6318 (M+H)$^+$; found 1046.6320 (M+H)$^+$.

2,2',2''-(10-(2-((S)-2-amino-6-(5-((3aS,4S,6aR)-2-oxo-hexahydro-1H-thieno[3,4-d]imidazol-4-yl)pentanamido)hexanamido)ethyl)-1,4,7,10-tetraazacyclododecane-1,4,7-triyl)triacetic acid (41).
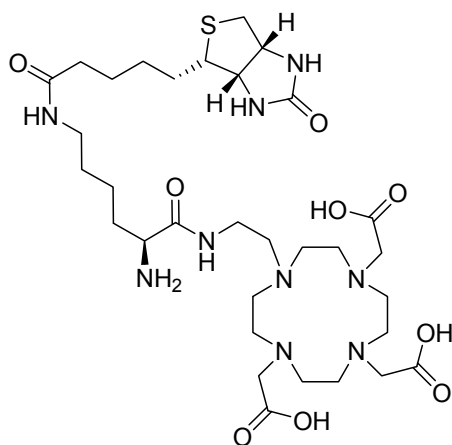
A solution of **40** (0.7 g, 0.67 mmol), (10%) Pd-C (0.18 g) and H$_2$ (50 psi) in MeOH (20 mL) was stirred at room temperature in Parr-apparatus for 8 h. The reaction was monitored by ESI-MS. After completion, the reaction mixture was filtered through a G-4 sintered funnel; filtrate was evaporated under reduced pressure. This crude product was further dissolve in TFA (20 mL) and stirred at room temperature for 18-20 h. ESI-MS was confirmed the completion of reaction. The solvent was evaporated under reduced pressure and dissolved in a minimum volume

of MeOH (1 mL) followed by addition of diethyl ether dropwise at 0-5˚C and stir for 1 h at room temperature. The compound was precipitated and filtered through a G-4 sintered funnel under nitrogen. The precipitate was dissolved in water and neutralized by adding 1 M Na_2CO_3 and the crude product were purified by preparative RP-HPLC (method B, $\lambda = 214$ nm, RT = 2.9 min. Yield: 0.26 g (54%) of **41** as white solid).

¹H NMR (D₂O, 250 MHz), δ (ppm): 1.31-2.08 (m, 12H); 2.24 (t, *J*=7.23 Hz, 2H); 2.60-4.30 (m, 31H); 4.33-4.48 (m, 1H); 4.50-4.53 (m, 1H); 4.54-4.58 (m, 1H). **¹³C NMR** (D₂O, 62.9 MHz), δ (ppm): 19.4; 20.4; 22.9; 25.4; 25.6; 27.9; 33.3; 33.8; 34.2; 34.5; 36.5; 37.4; 45.4; 46.7; 48.9; 50.9; 53.0; 54.2; 56.5; 58.0; 59.8; 162.7; 172.8; 173.1; 173.5; 179.4.

ESI-MS (±): calcd $C_{32}H_{57}N_9O_9S$: m/z 744.9 (M+H)⁺; found 744.6 (M+H)⁺.

(S)-tri-*tert*-butyl 2,2',2''-(10-(2-(5-(benzyloxycarbonylamino)-6-methoxy-6-oxohexylamino)-2-oxoethyl)-1,4,7,10-tetraazacyclododecane-1,4,7-triyl)triacetate (44).
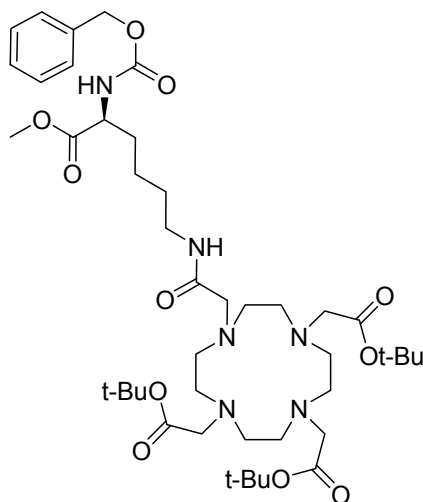
A solution of **43** (1 g, 1.75 mmol), α-N-carbobenzyloxy-L-lysine methyl ester (0.565 g, 1.92 mmol), NMM (0.38 mL, 3.8 mmol) and HOBt (0.37 g, 1.92 mmol) in DMF (5 mL) was stirred at 0-5˚C for 15 min and then EDC (0.26 g, 1.92 mmol) was added. The reaction mixture was stirred overnight at room temperature. The progress of reaction was monitored by TLC using CH_2Cl_2:MeOH, 9:1 and R_f of **(44)** was 0.4. After completion, the reaction mixture was poured in excess of water and extracted

with EtOAc (3x100 mL). Combined organic layers were dried over Na_2SO_4, filtered, filtrate was evaporated under reduced pressure and the residue was purified by column chromatography (silica gel, 10% MeOH in CH_2Cl_2) to give 0.77 g (52%) of **44** as off white solid.

¹³C NMR (CDCl₃, 62.9 MHz), δ (ppm): 21.9; 26.9; 27.0; 30.6; 37.6; 47.6; 49.2; 51.2; 52.5; 53.3; 54.7; 55.1; 65.6; 80.7; 80.8; 126.8; 126.9; 127.4; 135.5; 155.4; 170.6; 171.4; 172.2; 173.4.

ESI-HRMS (+): calcd $C_{43}H_{72}N_6O_{11}$: m/z 871.5151 $(M+Na)^+$; found 871.5160 $(M+Na)^+$.

(S)-2,2',2''-(10-(2-(5-amino-5-carboxypentylamino)-2-oxoethyl)-1,4,7,10-tetraazacyclododecane-1,4,7-triyl)triacetic acid (45).
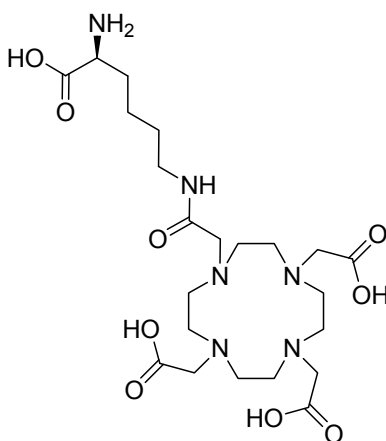
A solution of **44** (0.5 g, 0.59 mmol), (10%) Pd-C (0.13 g) and H_2 (50 psi) in MeOH (20 mL) was stirred at room temperature in Parr-apparatus for 8 h. The reaction was monitored by ESI-MS. After completion, the reaction mixture was filtered through a G-4 sintered funnel; filtrate was evaporated under reduced pressure. This crude product was further dissolve in TFA (20 mL) and stirred at room temperature for overnight. TFA was evaporated under reduced pressure. A solution of crude product in 20 mL of THF:MeOH:water (3:2:2) was stirred at 0-5°C for 15 min and then LiOH (0.11 g, 4.7 mmol) was added. The reaction mixture was stirred for 2 h at room temperature. The progress of the reaction was monitored by ESI-MS. After

completion, the solvent was evaporated under reduced pressure and the residue was purified by preparative HPLC (method B, λ = 214 nm, RT = 3.6 min). After lyophilization, 0.18 g (58%) of **45** as off-white solid was obtained.

^{1}H NMR (D$_2$O, 250 MHz), δ (ppm): 1.34-1.51 (m, 2H); 1.53-1.63 (m, 2H); 2.92-3.36 (m, 12H); 123.39-3.59 (m, 11H); 3.75-3.92 (m, 4H). **^{13}C NMR** (D$_2$O, 62.9 MHz), δ (ppm): 21.2; 27.4; 29.0; 38.5; 48.4; 50.6; 51.7; 52.7; 53.5; 54.7; 56.5; 169.9; 170.9; 172.0; 176.5.

ESI-MS (±): calcd C$_{22}$H$_{40}$N$_6$O$_9$: m/z 533.6 (M+H)$^+$; found 533.5 (M+H)$^+$.

(S)-methyl 2-(benzyloxycarbonylamino)-6-(2-cyanoethylamino)hexanoate (46).
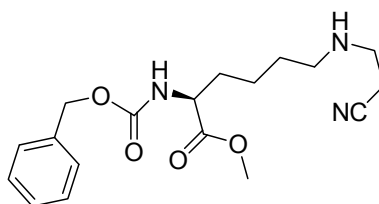
A solution of α-N-carbobenzyloxy-L-lysine methyl ester (2 g, 6.8 mmol), TEA (1.9 mL, 13.6 mmol) and acrylonitrile (0.9 mL, 13.6 mmol) in 20 mL MeOH was stirred at room temperature for 18 h. The reaction was monitored by TLC using CH$_2$Cl$_2$:MeOH, 9.5:0.5 as mobile phase. TLC plate was developed in an iodine chamber and R_f of **(46)** was 0.6. After completion, the solvent was evaporated under reduced pressure and purified by column chromatography (silica gel, 5% MeOH in CH$_2$Cl$_2$) to give 1.77 g (75%) of **46** as yellowish gum.

^{1}H NMR (CDCl$_3$, 250 MHz), δ (ppm): 1.25-1.34 (m, 2H); 1.36-1.46 (m, 2H); 1.54-1.64 (m, 2H); 1.70-1.82 (m, 1H); 2.40 (t, J=6.66 Hz, 2H); 2.53 (t, J=6.87 Hz, 2H); 2.80 (t, J=6.62 Hz, 2H); 3.66 (s, 3H); 4.26-4.31 (m, 1H); 5.03 (s, 2H); 5.43-5.52 (m, 1H); 7.21-7.3 (m, 5H). **^{13}C NMR** (CDCl$_3$, 62.9 MHz), δ (ppm) 18.2; 22.4; 28.9; 31.9; 44.6; 48.3; 52.0; 53.4; 66.6; 118.4; 127.7; 127.9; 128.2; 135.9; 155.6; 172.6.

ESI-HRMS (+): calcd C$_{18}$H$_{25}$N$_3$O$_4$: m/z 348.1917 (M+H)$^+$; found 348.1917 (M+H)$^+$.

(S)-methyl 2-(benzyloxycarbonylamino)-6-(N-(2-cyanoethyl)-5-((3aR,4R,6aS)-2-oxo-hexahydro-1H-thieno[3,4-d]imidazol-4-yl)pentanamido)hexanoate (47).

Materials and Methods

A solution of **46** (1.5 g, 4.3 mmol), biotin (1.16 g, 4.8 mmol), N,N-diisopropylethylamine (0.18 mL, 1.7 mmol) and PyBroP (4.03 g, 8.6 mmol) in CH_2Cl_2 (50 mL) was stirred overnight at room temperature. The progress of reaction was monitored by TLC using CH_2Cl_2:MeOH, 9:1 and R_f of **(47)** was 0.45. After completion, the reaction mixture was poured in water, extracted with CH_2Cl_2 (3x100 mL), organic layer was dried over Na_2SO_4, filtered, filtrate was evaporated under reduced pressure and purified by column chromatography (silica gel, 10% MeOH in CH_2Cl_2) to give 1.54 g (62%) of **47** as off-white solid.
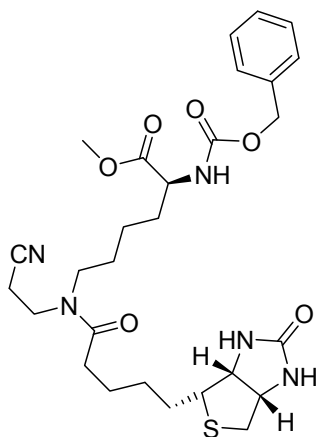

¹H NMR (CDCl₃, 250 MHz), δ (ppm): 1.16-1.42 (m, 6H); 1.43-1.70 (m, 7H); 1.72-1.85 (m, 1H); 2.25 (t, *J*=6.64 Hz, 2H); 2.46-2.69 (m, 4H); 2.73-2.84 (m, 1H); 3.00-3.11 (m, 1H); 3.20-3.30 (m, 2H); 3.37-3.53 (m, 2H); 3.67 (s, 3H); 4.14-4.22 (m, 1H); 4.25-4.32 (m, 1H); 4.34-4.41 (m, 1H); 5.04 (s, 2H); 5.67 (br s, 1H); 5.77-5.93 (m, 1H); 6.15 (br s, 1H); 7.21-7.31 (m, 5H). **¹³C NMR** (CDCl₃, 62.9 MHz), δ (ppm) 16.2; 22.5; 24.9; 28.1; 28.3; 28.5; 32.0; 32.4; 40.4; 42.6; 48.9; 52.4; 53.5; 55.4; 60.1; 61.8; 66.9; 118.4; 127.9; 128.1; 128.4; 136.2; 156.0; 163.9; 172.9; 173.4.

ESI-HRMS (+): calcd $C_{28}H_{39}N_5O_6S$: m/z 574.2693 (M+H)⁺; found 574.2700 (M+H)⁺.

(S)-methyl 6-(N-(3-aminopropyl)-5-((3aR,4R,6aS)-2-oxo-hexahydro-1H-thieno[3,4-d]imidazol-4-yl)pentanamido)-2-(benzyloxycarbonylamino)hexanoate (48).
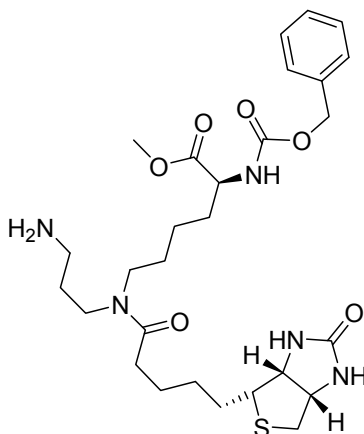
A solution of **47** (0.8 g, 1.4 mmol), Ra-Ni (0.2 g) and H_2 (50 psi) in 7N NH_3/MeOH (20 mL) was stirred at room temperature in Parr-apparatus for 6 h. The progress of the reaction was monitored by ESI-MS. After completion, the solvent was evaporated under reduced pressure and the residue was purified by preparative HPLC (method C, λ = 214 nm, RT = 11.2 min). After lyophilization, 0.56 g (70%) of **48** as off-white solid was obtained.

^{1}H NMR (CDCl$_3$, 250 MHz), δ (ppm): 1.08-1.98 (m, 15H); 2.24 (br s, 2H); 2.47-3.44 (m, 8H); 3.65 (s, 3H); 3.88-4.59 (m, 3H); 5.01 (s, 2H); 5.66-6.37 (m, 1H); 6.39-7.00 (m, 1H); 7.16-7.33 (m, 5H); 8.02 (br s, 3H). **^{13}C NMR** (CDCl$_3$, 62.9 MHz), δ (ppm) 22.2; 24.9; 25.6; 27.8; 28.4; 31.0; 32.2; 36.8; 39.7; 42.2; 45.0; 47.7; 49.4; 52.7; 55.3; 60.2; 62.1; 66.6; 127.5; 128.1; 128.5; 136.3; 157.2; 165.1; 174.2; 175.7.

ESI-HRMS (+): calcd $C_{28}H_{43}N_5O_6S$: m/z 578.3006 $(M+H)^+$; found 578.3010 $(M+H)^+$.

tri-*tert*-butyl 2,2',2''-(10-((S)-5-(methoxycarbonyl)-3,15-dioxo-10-(5-((3aR,4R,6aS)-2-oxo-hexahydro-1H-thieno[3,4-d]imidazol-4-yl)pentanoyl)-1-phenyl-2-oxa-4,10,14-triazahexadecan-16-yl)-1,4,7,10-tetraazacyclododecane-1,4,7-triyl)triacetate (49).

A solution of **48** (0.3 g, 0.52 mmol), **43** (0.3 g, 0.52 mmol), NMM (0.12 mL, 1.0 mmol) and HOBt (0.11 g, 0.57 mmol) in DMF (15 mL) was stirred at 0-5°C for 15 min and then EDC (0.08 g, 0.57 mmol) was added. The reaction mixture was stirred overnight at room temperature. The progress of the reaction was monitored by ESI-MS. After completion, the solvent was evaporated under reduced pressure and the

residue was purified by preparative HPLC (method C, λ = 214 nm, RT = 25.4 min). After lyophilization, 0.28 g (48%) of **49** as off-white solid was obtained.
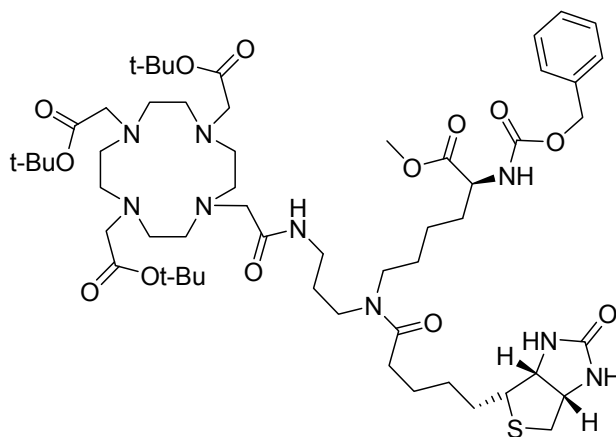
¹H NMR (CDCl₃, 250 MHz), δ (ppm): 1.10-1.30 (m, 2H); 1.42 (s, 18H); 1.52 (s, 10H); 1.60-1.95 (m, 12H); 2.03 (br s, 2H); 2.34 (br s, 3H); 2.62-2.99 (m, 6H); 3.32-3.94 (m, 20H); 3.76 (br s, 6H); 3.94-3.98 (m, 2H); 4.23-4.43 (m, 2H); 4.47-4.63 (m, 1H); 5.12 (s, 2H); 5.48-5.77 (m, 1H); 7.29-7.43 (m, 5H).

ESI-MS (±): calcd C₅₆H₉₃N₉O₁₃S: m/z 1133.5 (M+H)⁺; found 1133.2 (M+H)⁺.

2,2',2''-(10-(2-(3-(N-((S)-5-amino-5-carboxypentyl)-5-((3aR,4R,6aS)-2-oxo-hexahydro-1H-thieno[3,4-d]imidazol-4-yl)pentanamido)propylamino)-2-oxoethyl)-1,4,7,10-tetraazacyclododecane-1,4,7-triyl)triacetic acid (50).
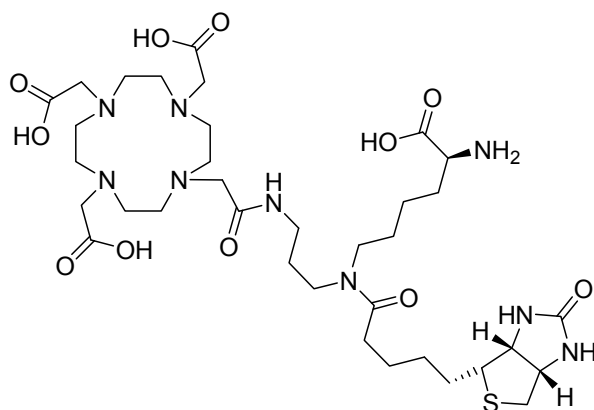
A solution of **49** (0.25 g, 0.22 mmol), (10%) Pd-C (0.07 g) and H₂ (50 psi) in MeOH (20 mL) was stirred at room temperature in Parr-apparatus for 8 h. The

reaction was monitored by ESI-MS. After completion, the reaction mixture was filtered through a G-4 sintered funnel; filtrate was evaporated under reduced pressure. This crude product was further dissolve in TFA (20 mL) and stirred at room temperature for overnight. TFA was evaporated under reduced pressure. A solution of crude product in 20 mL of THF:MeOH:water (3:2:2) was stirred at 0-5°C for 15 min and then LiOH (0.11 g, 4.7 mmol) was added. The reaction mixture was stirred for 2 h at room temperature. The progress of the reaction was monitored by ESI-MS. After completion, the solvent was evaporated under reduced pressure and the residue was purified by preparative HPLC (method B, λ = 214 nm, RT = 3.8 min). After lyophilization, 0.1 g (56%) of **50** as off-white solid was obtained.

^{1}H NMR (D$_2$O, 250 MHz), δ (ppm): 1.20-2.16 (m, 16H); 2.47 (t, *J*=7.32 Hz, 2H); 2.70-3.90 (m, 32H); 4.40-4.53 (m, 1H); 4.24-4.28 (m, 1H). **^{13}C NMR** (D$_2$O, 62.9 MHz), δ (ppm): 24.9; 27.8; 28.2; 30.9; 32.8; 35.0; 39.7; 42.4; 46.2; 47.9; 48.4; 50.7; 50.9; 51.2; 53.2; 53.8; 57.1; 58.1; 58.6; 63.0; 64.8; 164.2; 165.3; 167.2; 177.1; 178.0; 178.8.

ESI-MS (±): calcd C$_{35}$H$_{61}$N$_9$O$_{11}$S: m/z 816.9 (M+H)$^+$; found 817.1 (M+H)$^+$.

(S)-6-(N-(3-aminopropyl)-5-((3aR,4R,6aS)-2-oxo-hexahydro-1H-thieno[3,4-d]imidazol-4-yl)pentanamido)-2-(benzyloxycarbonylamino)hexanoic acid (51).

A solution of **48** (0.25 g, 0.43 mmol) in 20 mL of THF:MeOH:water (3:2:2) was stirred at 0-5°C for 15 min and then LiOH (0.02 g, 0.86 mmol) was added. The reaction mixture was stirred for 2 h at room temperature. The progress of the reaction was monitored by ESI-MS. After completion, the solvent was evaporated under
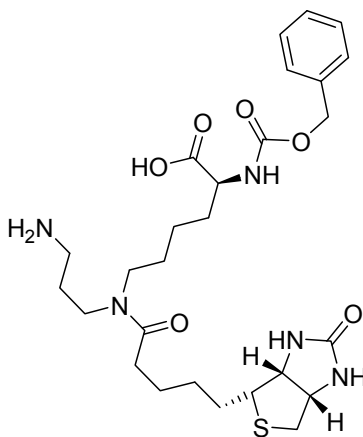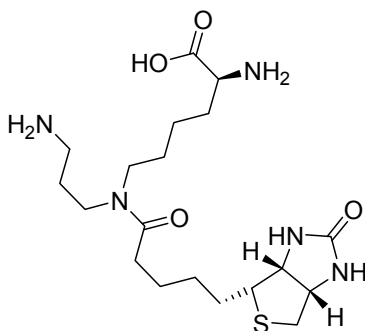
reduced pressure and the residue was purified by preparative HPLC (method C, λ = 214 nm, RT = 9.4 min). After lyophilization, 0.2 g (82%) of **51** as off-white solid was obtained.

^{1}H NMR (D$_2$O, 250 MHz), δ (ppm): 1.12-1.88 (m, 15H); 2.18-2.28 (m, 2H); 2.47-3.44 (m, 8H); 3.88-4.59 (m, 3H); 5.01 (s, 2H); 7.16-7.33 (m, 5H). **^{13}C NMR** (D$_2$O, 62.9 MHz), δ (ppm) 25.1; 27.6; 29.3; 30.5; 34.4; 35.0; 39.9; 42.4; 45.5; 51.6; 56.9; 58.0; 58.8; 59.9; 63.3; 64.7; 69.3; 72.5; 130.3; 130.9; 131.4; 139.3; 160.2; 167.8; 173.7; 178.7.

ESI-MS ($\pm$): calcd C$_{27}$H$_{41}$N$_5$O$_6$S: m/z 564.7 (M+H)$^+$; found 564.5 (M+H)$^+$.

(S)-2-amino-6-(N-(3-aminopropyl)-5-((3aR,4R,6aS)-2-oxo-hexahydro-1H-thieno[3,4-d]imidazol-4-yl)pentanamido)hexanoic acid (52).

Reaction 1: A solution of **51** (0.09 g, 0.16 mmol), (10%) Pd-C (0.03 g) and H$_2$ (50 psi) in MeOH (10 mL) was stirred at room temperature in Parr-apparatus for 6 h. The reaction was monitored by ESI-MS. After completion, the reaction mixture was filtered through a G-4 sintered funnel; filtrate was evaporated under reduced pressure.

Reaction 2: Compound **57** (0.1 g, 0.02 mmol) was dissolved in neat formic acid (5 ml) with stirring at room temperature for 2 h. The reaction was monitored by ESI-MS. After completion, the pH was adjusted to 7 using 1M Na$_2$CO$_3$.

The residue was purified by preparative HPLC (method C, λ = 214 nm, RT = 8.2 min). After lyophilization, 78% of **52** as off-white solid compound was obtained.

^{1}H NMR (D$_2$O, 250 MHz), δ (ppm): 1.40-1.86 (m, 10H); 1.93-2.15 (m, 4H); 2.53 (t, J=7.02 Hz, 2H); 2.81-2.90 (m, 1H); 2.98-3.16 (m, 3H); 3.38-3.60 (m, 5H); 4.15-4.25 (m, 1H); 4.46-4.54 (m, 1H); 4.66-4.72 (m, 1H). **^{13}C NMR** (D$_2$O, 62.9 MHz), δ (ppm)

22.5; 24.0; 27.2; 27.3; 38.0; 41.0; 43.1; 48.5; 48.8; 49.1; 49.6; 52.9; 54.9; 55.1; 61.3; 61.5; 161.2; 171.5; 171.9.

ESI-MS (±): calcd $C_{19}H_{35}N_5O_4S$: m/z 430.2482 (M+H)$^+$; found 430.2480 (M+H)$^+$.

(S)-6-(N-(3-fluoresceinthioureapropyl)-5-((3aR,4R,6aS)-2-oxo-hexahydro-1H-thieno[3,4-d]imidazol-4-yl)pentanamido)-2-(benzyloxycarbonylamino)hexanoic acid (53).
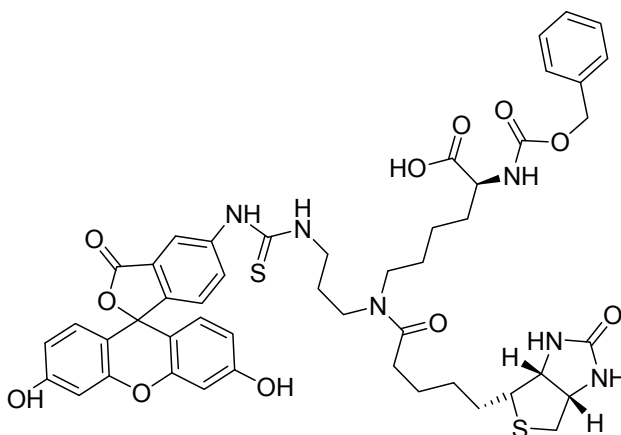

A solution of **51** (0.1 g, 0.18 mmol) in 10 mL of water was stirred at room temperature and FITC (0.08 g, 0.21 mmol) was added at pH 8.5. During stirring, pH was maintained at 8.0-8.5 by addition of 1M Na_2CO_3. The reaction mixture was stirred for 18-20 h at room temperature in dark. The reaction was monitored by ESI-MS. The reaction mixture was evaporated under reduced pressure and the residue was purified by preparative HPLC (method C, λ = 254 nm, RT = 20.6 min). After lyophilization, 0.09 g (55%) of **53** as dark orange solid compound was obtained.

^{1}H NMR (D$_2$O, 250 MHz), δ (ppm): 1.14-1.31 (m, 4H); 1.36-1.59 (m, 6H); 1.60-1.74 (m, 2H); 2.13-2.29 (m, 2H); 2.40-2.73 (m, 1H); 2.82-3.02 (m, 1H); 3.11-3.14 (m, 4H); 3.16 (s, 4H); 3.88-4.13 (m, 4H); 4.20-4.29 (m, 2H); 4.90 (m, 2H); 6.49-6.57 (m, 2H); 6.61-6.79 (m, 4H); 6.96-7.18 (m, 7H); 7.57-8.14 (m, 1H). **^{13}C NMR** (D$_2$O, 62.9 MHz), δ (ppm) 24.2; 26.7; 28.3; 29.5; 29.7; 29.9; 32.6; 33.8; 41.2; 43.1; 44.3; 46.8; 55.1; 57.1; 61.8; 63.5; 67.8; 85.7; 102.7; 103.4; 113.7; 115.7; 124.6; 126.9; 128.9; 129.1; 129.6; 131.3; 131.5; 136.4; 138.4; 142.8; 156.0; 158.8; 164.3; 170.3; 175.5; 175.8; 176.1; 179.9.

ESI-MS (±): calcd $C_{48}H_{52}N_6O_{11}S_2$: m/z 954.0 (M+H)$^+$; found 954.2 (M+H)$^+$.

Materials and Methods

(S)-2-amino-6-(N-(3-fluoresceinthioureapropyl)-5-((3aR,4R,6aS)-2-oxo-hexahydro-1H-thieno[3,4-d]imidazol-4-yl)pentanamido)hexanoic acid (54).
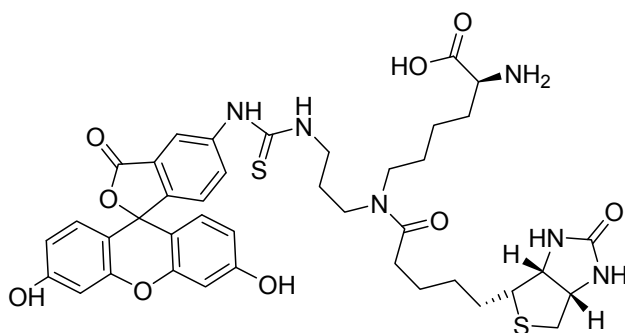
Reaction 1: A solution of **53** (0.08 g, 0.10 mmol), (10%) Pd-C (0.02 g) and H_2 (50 psi) in MeOH (10 mL) was stirred at room temperature in Parr-apparatus for 2-6 h. The reaction was monitored by ESI-MS and observed that under this condition compound was degrading.

Reaction 2: Compound **58** (0.15 g, 0.16 mmol) was dissolved in neat formic acid (5 ml) with stirring at room temperature for 2 h. The reaction was monitored by ESI-MS. After completion, the pH was adjusted to 8 using 1M NaOH.

The residue was purified by preparative HPLC (method C, λ = 214 nm, RT = 18.4 min). After lyophilization, 0.11 g (88%) of **54** as dark orange solid compound was obtained.

^{1}H NMR (D$_2$O, 250 MHz), δ (ppm): 1.23-1.36 (m, 1H); 1.53-1.75 (m, 4H); 1.79-2.01 (m, 4H); 2.06-2.23 (m, 3H); 2.57-2.73 (m, 2H); 2.85-3.02 (m, 3H); 3.26-3.45 (m, 2H); 3.71 (s, 4H); 3.80-3.94 (m, 2H); 4.02-4.10 (m, 1H); 4.48-4.86 (m, 3H); 6.89-7.04 (m, 3H); 7.40-7.60 (m, 3H); 7.85-8.15 (m, 3H). **^{13}C NMR** (D$_2$O, 62.9 MHz), δ (ppm) 19.8; 22.9; 24.4; 25.7; 26.3; 28.0; 30.4; 37.5; 40.8; 43.6; 45.7; 46.7; 52.5; 53.2; 57.9; 59.8; 101.5; 107.1; 110.2; 111.8; 116.4; 120.7; 127.0; 128.5; 129.1; 136.5; 138.6; 156.3; 160.4; 162.9; 171.1; 173.1; 173.6; 177.9.

ESI-MS (±): calcd $C_{40}H_{46}N_6O_9S_2$: m/z 819.9 (M+H)$^+$; found 820.4 (M+H)$^+$.

(S)-methyl 2-amino-6-(N-(2-cyanoethyl)-5-((3aR,4R,6aS)-2-oxo-hexahydro-1H-thieno[3,4-d]imidazol-4-yl)pentanamido)hexanoate (55).

A solution of **47** (0.7 g, 1.2 mmol), (10%) Pd-C (0.18 g) and H_2 (50 psi) in 10 mL MeOH was stirred at room temperature in Parr-apparatus for 6 h. The reaction was monitored by ESI-MS. After completion, the reaction mixture was filtered through a G-4 si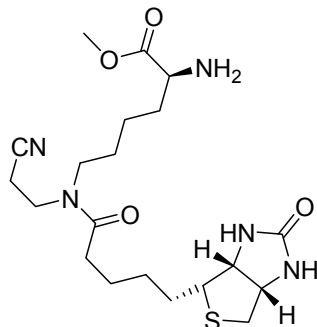ntered funnel; filtrate was evaporated under reduced pressure and the residue was purified by preparative RP-HPLC (method C, λ = 214 nm, RT = 12.5 min). After lyophilization, 0.45 g (84%) of **55** as off-white solid was obtained.

^{13}C NMR (CDCl$_3$, 62.9 MHz), δ (ppm) 16.3; 22.5; 23.6; 27.7; 28.5; 32.4; 34.5; 34.6; 41.4; 45.5; 45.9; 51.4; 53.4; 54.9; 60.3; 62.0; 119.3; 163.3; 175.8; 176.1.

ESI-HRMS (+): calcd $C_{20}H_{33}N_5O_4S$: m/z 440.2326 $(M+H)^+$; found 440.2325 $(M+H)^+$.

(S)-methyl 2-(*tert*-butoxycarbonylamino)-6-(N-(2-cyanoethyl)-5-((3aR,4R,6aS)-2-oxo-hexahydro-1H-thieno[3,4-d]imidazol-4-yl)pentanamido)hexanoate (56).
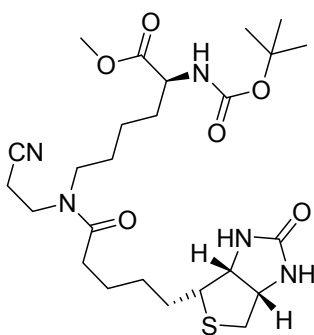
A solution of **55** (0.4 g, 0.91 mmol) and TEA (0.51 mL, 3.6 mmol) in 20 mL CH$_2$Cl$_2$ was stirred at 0-5°C for 15 min. Di-tert-butyl dicarbonate (0.51 mL, 3.6 mmol) was dissolved in 5 mL CH$_2$Cl$_2$ and added dropwise in reaction mixture at 0-5°C. After addition reaction mixture was stirred for 3 h at room temperature. The

progress of reaction was monitored by TLC using CH_2Cl_2:MeOH, 9:1 and R_f of (**56**) was 0.3. After completion, the reaction mixture was poured in water, extracted with CH_2Cl_2 (3x100 mL), organic layer was dried over Na_2SO_4, filtered, filtrate was evaporated under reduced pressure and purified by column chromatography (silica gel, 10% MeOH in CH_2Cl_2) to give 0.43 g (88%) of **56** as light yellowish gum.

13C NMR (CDCl₃, 62.9 MHz), δ (ppm) 16.4; 22.5; 23.6; 27.7; 28.5; 28.7; 32.4; 34.5; 34.6; 41.4; 45.5; 45.9; 51.4; 53.4; 54.9; 60.3; 62.0; 81.1; 119.3; 155.8; 163.3; 175.8; 176.1.

ESI-MS (±): calcd $C_{25}H_{41}N_5O_6S$: m/z 540.7 $(M+H)^+$; found 540.5 $(M+H)^+$.

(S)-6-(N-(3-aminopropyl)-5-((3aR,4R,6aS)-2-oxo-hexahydro-1H-thieno[3,4-d]imidazol-4-yl)pentanamido)-2-(*tert*-butoxycarbonylamino)hexanoic acid (57).

A solution of **56** (0.4 g, 0.74 mmol), Ra-Ni (0.1 g) and H_2 (50 psi) in 7N NH_3/MeOH:water (10:1 mL) was stirred at room temperature in Parr-apparatus for 6 h. The reaction was monitored by ESI-MS. After completion, the reaction mixture was filtered through a G-4 sintered funnel, filtrate was evaporated under reduced pressure and the residue was purified by preparative RP-HPLC (method C, λ = 214 nm, RT = 10.2 min). After lyophilization, 0.23 g (58%) of **57** as off-white solid was obtained.
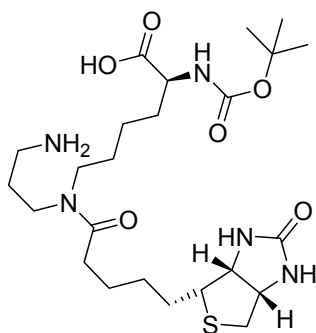
1H NMR (MeOD, 250 MHz), δ (ppm): 1.24 (s, 9H); 1.28-1.36 (m, 2H); 1.39-1.61 (m, 6H); 1.63-1.85 (m, 3H); 2.26 (t, *J*=7.32 Hz, 2H); 2.47-2.57 (m, 2H); 2.65-2.85 (m, 3H); 2.99-3.08 (m, 1H); 3.11-3.16 (m, 2H); 3.17 (s, 3H); 3.28 (t, *J*=6.41 Hz, 1H); 3.73-3.93 (m, 1H); 4.10-4.19 (m, 1H); 4.28-4.37 (m, 1H). **13C NMR** (MeOD, 62.9 MHz), δ (ppm). 22.4; 23.2; 25.5; 26.0; 27.2; 27.9; 28.7; 29.0; 30.4; 31.6; 32.6; 37.3; 40.1; 42.5; 56.1; 60.8; 62.5; 79.7; 157.3; 165.3; 174.3; 175.5.

Materials and Methods

ESI-MS (±): calcd $C_{24}H_{43}N_5O_6S$: m/z 530.6 (M+H)$^+$; found 530.7 (M+H)$^+$.

(S)-6-(N-(3-fluoresceinthioureapropyl)-5-((3aR,4R,6aS)-2-oxo-hexahydro-1H-thieno[3,4-d]imidazol-4-yl)pentanamido)-2-(*tert*-butoxycarbonylamino)hexanoic acid (58).
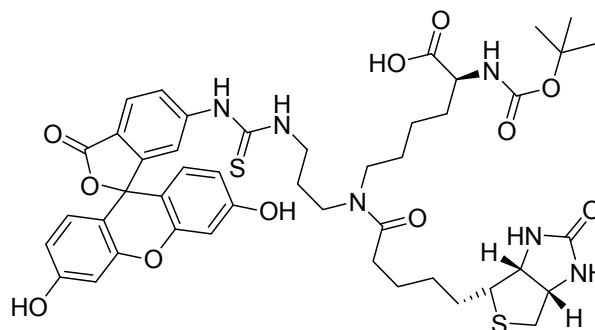
A solution of **57** (0.2 g, 0.38 mmol) in 10 mL of water was stirred at room temperature and FITC (0.18 g, 0.45 mmol) was added at pH 8.5. During stirring, pH was maintained at 8.0-8.5 by addition of 1M Na_2CO_3. The reaction mixture was stirred for 18-20 h at room temperature in dark. The reaction was monitored by ESI-MS. The reaction mixture was evaporated under reduced pressure and the residue was purified by preparative HPLC (method C, λ = 254 nm, RT = 21.5 min). After lyophilization, 0.19 g (50%) of **58** as dark orange solid compound was obtained.

¹H NMR (D₂O, 250 MHz), δ (ppm): 1.01-1.06 (m, 1H); 1.21 (s, 9H) 1.23-1.29 (m, 2H); 1.34-1.54 (m, 5H); 1.58-1.85 (m, 2H); 2.13-2.25 (m, 1H); 2.38-2.74 (m, 1H); 2.87-3.00 (m, 1H); 3.03-3.28 (m, 10H); 3.32-3.50 (m, 2H); 3.81-3.93 (m, 2H); 4.00-4.29 (m, 1H); 6.48-6.60 (m, 2H); 6.63-6.83 (m, 5H); 6.96-7.05 (m, 1H); 7.57-8.14 (m, 1H). **¹³C NMR** (D₂O, 62.9 MHz), δ (ppm) 24.2; 26.7; 28.3; 29.5; 29.7; 29.9; 32.6; 33.8; 41.2; 43.1; 44.3; 46.8; 55.1; 57.1; 61.8; 63.5; 67.8; 80.4; 85.8; 103.4; 105.6; 113.7; 115.7; 123.4; 128.9; 129.1; 129.6; 131.3; 131.5; 138.4; 142.8; 156.0; 158.8; 164.3; 170.3; 175.5; 175.8.

ESI-MS (±): calcd $C_{45}H_{54}N_6O_{11}S_2$: m/z 920.0 (M+H)$^+$; found 919.9 (M+H)$^+$.

Materials and Methods

methyl 2-(benzyloxycarbonylamino)-3-bromopropanoate (59).
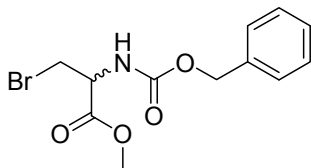
N-bromosuccinimide (1.41 g, 7.9 mmol) was slowly added to a solution of N-carbobenzyloxy-L-serine methyl ester (1.0 g, 3.95 mmol) and PPh_3 (2.1 g, 7.9 mmol) in DMF (50 mL). The mixture was stirred at 50 °C for 30 min; MeOH (2 mL) was added to destroy the excess reagent. After 5 min, ether (200 mL) was added, the organic layer was washed with water (100 mL), saturated $NaHCO_3$ (150 mL), brine (200 mL), and dried over Na_2SO_4. The progress of reaction was monitored by TLC using n-hexane:EtOAc, 7:3 and R_f of (**59**) was 0.45. The crude product was purified by flash column chromatography (silica gel, 30% EtOAc in n-hexane) to give 0.68 g (54%) of **59** as light yellowish gum.

^{1}H NMR (CDCl$_3$, 400 MHz), δ (ppm): 3.4-3.7 (m, 5H); 4.57-4.62 (m, 1H); 4.91 (s, 2H); 5.49-5.58 (m, 1H); 7.07-7.28 (m, 5H). **^{13}C NMR** (CDCl$_3$, 100 MHz), δ (ppm) 33.6; 53.0; 54.2; 67.2; 128.0; 128.2; 128.4; 139.5; 159.5; 169.2.

ESI-MS (+): calcd $C_{12}H_{14}BrNO_4$: m/z 317.1 (M+H)$^+$; found 317.3 (M+H)$^+$.

methyl   2-(benzyloxycarbonylamino)-3-(1,4,7,10-tetraazacyclododecan-1-yl)propanoate (60).
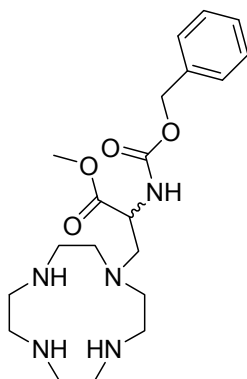
59 (0.6 g, 1.9 mmol) was added dropwise in a solution of cyclen (2.00 g, 11.6 mmol) in toluene (100 mL) at room temperature. The reaction mixture was refluxed for 18 h. The reaction mixture was filtered through a G-4 sintered funnel; filtrate was

151

evaporated under reduced pressure, dissolved in 200 mL CH_2Cl_2, extracted from the water (4x100 ml). The organic layers were combined, dried over sodium sulfate and then concentrated in vacuum to yield 0.34 g (44%) of **60** as colorless oil.

^{1}H NMR (CDCl$_3$, 250 MHz), δ (ppm): 2.20-3.02 (m, 18H); 3.69 (s, 3H); 4.36 (br s, 1H); 5.02 (s, 2H); 5.07-5.25 (m, 4H); 7.25-7.40 (m, 5H). **^{13}C NMR** (CDCl$_3$, 62.9 MHz), δ (ppm) 43.5; 52.5; 53.2; 53.7; 53.9; 55.0; 59.9; 66.3; 127.7; 128.9; 132.1; 134.2; 161.4; 176.8.

ESI-HRMS (±): calcd $C_{20}H_{33}N_5O_4$: m/z 408.2605 $(M+H)^+$; found 408.2607 $(M+H)^+$.

[4,7-Bis-butoxycarbonylmethyl-10-{2-(benzyloxycarbonylamino)-3-methoxy-3-oxopropyl}-1,4,7,10-tetraaza-cyclododec-1-yl]-acetic acid *tert*-butyl ester (61).
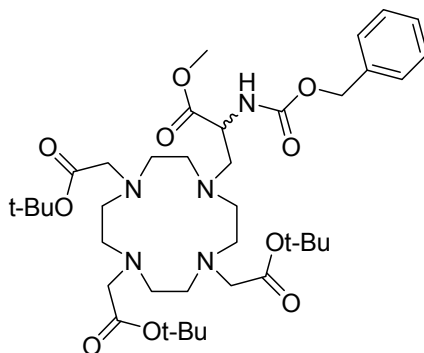
A solution of **60** (0.3 g, 0.74 mmol), sodium carbonate (0.49 g, 5.9 mmol) and *tert*–butylbromoacetate (0.35 mL, 2.4 mmol) in MeCN (100 ml) was stirred at 70°C for overnight. The reaction was monitored by TLC. After completion, the reaction mixture was filtered and washed with CH_2Cl_2 (3x50 ml). The organic solvent was evaporated under reduced pressure and the residue was purified by column chromatography (silica gel, 5% MeOH in CH_2Cl_2, R_f = 0.55) to give 0.45 g (82%) of **61** as a yellow gum.

^{1}H NMR (CDCl$_3$, 250 MHz), δ (ppm): 1.32 (s, 9H); 1.39 (s, 18H); 1.83-2.56 (m, 8H); 2.60-3.50 (m, 16H); 3.66 (s, 3H); 4.47 (br s, 1H); 4.71 (br s, 1H); 5.24 (s, 2H); 7.16-7.42 (m, 5H). **^{13}C NMR** (CDCl$_3$, 62.9 MHz), δ (ppm): 27.8; 28.0; 50.3; 50.5; 51.3; 52.3; 52.6; 53.3; 55.5; 56.1; 56.5; 66.9; 82.1; 82.4; 127.7; 127.9; 128.3; 135.9; 157.0; 171.8; 172.7; 173.1.

ESI-HRMS (±): calcd $C_{38}H_{63}N_5O_{10}$: m/z 750.4647 $(M+H)^+$; found 750.4641 $(M+H)^+$.

2-(benzyloxycarbonylamino)-3-(4,7,10-tris(2-tert-butoxy-2-oxoethyl)-1,4,7,10-tetraazacyclododecan-1-yl)propanoic acid (62).
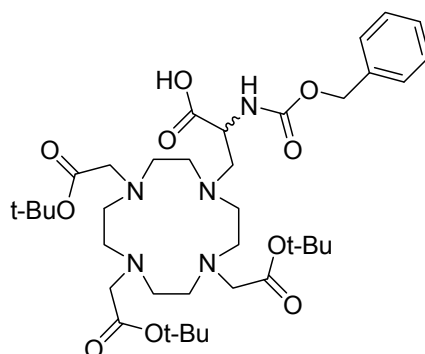
A solution of **6** (0.1 g, 0.13 mmol) in 7 mL of THF:MeOH:water (3:2:2) was stirred at 0-5˚C for 15 min and then LiOH (6.5 mg, 0.27 mmol) was added. The reaction mixture was stirred for 2 h at room temperature. The progress of the reaction was checked by ESI-MS. After completion, the reaction mixture was concentrated under reduced pressure, 0.76 g (64%) of **62** as white powder was obtained.

^{1}H NMR (CDCl$_3$, 250 MHz), δ (ppm): 1.35 (s, 9H); 1.41 (s, 18H); 1.90-2.72 (m, 8H); 2.80-3.62 (m, 16H); 4.65 (br s, 1H); 4.89 (br s, 1H); 5.41 (s, 2H); 7.11-7.32 (m, 5H). **^{13}C NMR** (CDCl$_3$, 62.9 MHz), δ (ppm): 27.2; 27.3; 51.3; 51.5; 53.3; 53.6; 54.3; 56.5; 567.1; 57.5; 66.6; 82.6; 82.8; 127.9; 130.1; 130.3; 136.9; 158.0; 171.3; 172.4; 173.5.

ESI-MS (±): calcd C$_{37}$H$_{61}$N$_5$O$_{10}$: m/z 736.9 (M+H)$^+$; found 737.1 (M+H)$^+$.

[4,7-Bis-butoxycarbonylmethyl-10-(2-amino-3-methoxy-3-oxopropyl)-1,4,7,10-tetraaza-cyclododec-1-yl]-acetic acid *tert*-butyl ester (63).
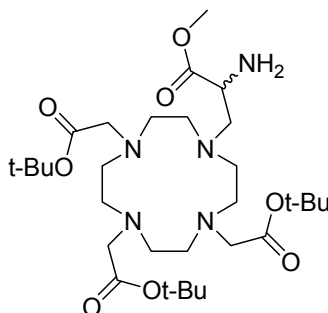

A solution of **61** (0.3 g, 0.4 mmol), (10%) Pd-C (0.1 g) and H$_2$ (50 psi) in MeOH (10 mL) was stirred at room temperature in Parr-apparatus for 6 h. The

reaction was monitored by ESI-MS. After completion, the reaction mixture was filtered through a G-4 sintered funnel; filtrate was evaporated under reduced pressure. The residue was purified by column chromatography (silica gel, 10% MeOH in CH$_2$Cl$_2$, R_f = 0.45) to give 0.2 g (80%) of **63** as an off white solid.

^{1}H NMR (CDCl$_3$, 250 MHz), δ (ppm): 1.38 (s, 9H); 1.39 (s, 18H); 1.91-2.51 (m, 8H); 2.52-2.96 (m, 10H); 3.02 (s, 2H); 3.10-3.42 (m, 7H); 3.49-3.37 (m, 3H). **^{13}C NMR** (CDCl$_3$, 62.9 MHz), δ (ppm): 27.1; 27.7; 48.9; 50.5; 51.8; 52.3; 55.3; 55.7; 55.9; 56.2; 60.3; 81.9; 82.3; 172.2; 172.8; 175.5.
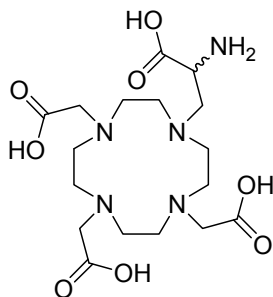
ESI-HRMS (±): calcd C$_{30}$H$_{57}$N$_5$O$_8$: m/z 616.4279 (M+H)$^+$; found 616.4278 (M+H)$^+$.

[4,7-Bis-carboxymethyl-10-(2-amino-2-carboxyethyl)-1,4,7,10-tetraaza-cyclododec-1-yl]-acetic acid (64).

A solution of **63** (0.15 g, 0.24 mmol) in TFA (10 mL) was stirred at room temperature for 18-20 h. The reaction was monitored by ESI-MS. The solvent was evaporated under reduced pressure and dissolved in a minimum volume of MeOH (1 mL) followed by addition of diethyl ether dropwise at 0-5°C and stir for 1 h at room temperature. The compound was precipitated and filtered through a G-4 sintered funnel under nitrogen. The precipitate was dissolved in water and neutralized by adding 1 M Na$_2$CO$_3$ and the crude products were purified by preparative RP-HPLC. RP-HPLC: method B, λ = 214 nm, RT = 2.4 min. Yield: 55 mg (52%) of **64** as white solid.

^{1}H NMR (D$_2$O, 250 MHz), δ (ppm): 1.93-2.64 (m, 8H); 2.58-3.02 (m, 12H); 3.18-3.52 (m, 3H); 3.59-3.47 (m, 2H). **^{13}C NMR** (D$_2$O, 62.9 MHz), δ (ppm): 50.1; 56.1; 56.4; 57.0; 57.2; 57.4; 57.6; 59.8; 174.2; 174.8; 177.5.

ESI-HRMS (±): calcd C$_{17}$H$_{31}$N$_5$O$_8$: m/z 434.2245 (M+H)$^+$; found 434.2281 (M+H)$^+$.

9. REFERENCES

(1) Sanders, E. J.; Wridw, M. A. *International review in cytology* **1978**, *163*, 105-173.

(2) Beckmann, N.; Mueggler, T.; Allegrini, P. R.; Laurent, D.; Rudin, M. *Anat Rec* **2001**, *265*, 85-100.

(3) Boesch, C. *Mol Aspects Med* **1999**, *20*, 185-318.

(4) Hogemann, N.; Basilion, R.; Weissleder, R. *Radiologe* **2001**, *41*, 116-120.

(5) Rudin, M.; Beckmann, N.; Porszasz, R.; Reese, T.; Bochelen, D.; Sauter, A. *NMR Biomed* **1999**, *12*, 69-97.

(6) Sen, D. S.; Pellecchia, M. *Curr Opin Drug Discov Devel* **2001**, *4*, 479-492.

(7) Weissleder, R. *Nat Rev Cancer* **2002**, *2*, 11-8.

(8) Belliveau, J. W.; Kennedy, D. N., Jr.; McKinstry, R. C.; Buchbinder, B. R.; Weisskoff, R. M.; Cohen, M. S.; Vevea, J. M.; Brady, T. J.; Rosen, B. R. *Science* **1991**, *254*, 716-9.

(9) Logothetis, N. K.; Pauls, J.; Augath, M.; Trinath, T.; Oeltermann, A. *Nature* **2001**, *412*, 150-7.

(10) Ogawa, S.; Lee, T. M.; Kay, A. R.; Tank, D. W. *Proc Natl Acad Sci U S A* **1990**, *87*, 9868-72.

(11) Logothetis, N. K.; Merkle, H.; Augath, M.; Trinath, T.; Ugurbil, K. *Neuron* **2002**, *35*, 227-242.

(12) Bogdanov, A., Jr.; Weissleder, R. *Trends Biotechnol* **1998**, *16*, 5-10.

(13) Lok, C. *Nature* **2001**, *412*, 372-4.

(14) Meade, T. *Acad Radiol* **2001**, *8*, 1-3.

(15) Merbach, A. E.; Toth, E. *The chemistry of contrast agents in medical resonance imaging, John wiley & sons, ltd.*

(16) Meade, T. J.; Taylor, A. K.; Bull, S. R. *Curr Opin Neurobiol* **2003**, *13*, 597-602.

(17) Caravan, P.; Ellison, J. J.; McMurry, T. J.; Lauffer, R. B. *Chem Rev* **1999**, *99*, 2293-352.

(18) Solomon, I. *J Chem Phys* **1957**, *101*, 572.

(19) Bloembergen, N. *J Chem Phys* **1957**, *101*, 572.

(20) Oudkerk, M.; Sijens, P. E.; Van Beek, E. J.; Kuijpers, T. J. *Invest Radiol* **1995**, *30*, 75-8.

(21) Roy, C. S.; Sherrington, C. S. *J Physiol* **1890**, *11*, 85-158 17.

(22) Wunderbaldinger, P.; Josephson, L.; Weissleder, R. *Acad Radiol* **2002**, *9 Suppl 2*, S304-6.

(23) Ogawa, S.; Menon, R. S.; Tank, D. W.; Kim, S. G.; Merkle, H.; Ellermann, J. M.; Ugurbil, K. *Biophys J* **1993**, *64*, 803-12.

(24) Paty, D. W.; Li, D. K. *Ann Neurol* **1996**, *40*, 951-3.

(25) Aime, S.; Botta, M.; Fasano, M.; Terreno, E. *Chem Soc Rev* **1998**, *27*, 19-29.

(26) Aime, S.; Cabella, C.; Colombatto, S.; Crich, S. G.; Gianolio, E.; Maggioni, F. *J Megn Reson Imag* **2001**, *14*, 636-648.

(27) Lauffer, R. B. *Magn Reson Med* **1991**, *22*, 339-42; discussion 343-6.

(28)   Rocklage, S. M.; Watson, A. D. *J Magn Reson Imaging* **1993**, *3*, 167-78.

(29)   Toth, E.; Helm, L.; Merbach, A. E. *Topics in Curr Chem* **2002**, *221*, 61-101.

(30)   Tweedle, M. F.; Eaton, S. M.; Eckelman, W. C.; Gaughan, G. T.; Hagan, J. J.; Wedeking, P. W.; Yost, F. J. *Invest Radiol* **1988**, *23 Suppl 1*, S236-9.

(31)   Wickline, S. A.; Lanza, G. M. *Proc Intl Soc Mag Reson Med* **2001**, *9*, 2.

(32)   Yuh, W. T. *J Magn Reson Imaging* **1999**, *10*, 221-2.

(33)   Aime, S.; Barge, A.; Delli Castelli, D.; Fedeli, F.; Mortillaro, A.; Nielsen, F. U.; Terreno, E. *Magn Reson Med* **2002**, *47*, 639-48.

(34)   Aime, S.; Delli Castelli, D.; Fedeli, F.; Terreno, E. *J Am Chem Soc* **2002**, *124*, 9364-5.

(35)   Zhang, S.; Wu, K.; Sherry, A. D. *Angew Chem Int Ed Engl* **1999**, *38*, 3192-3194.

(36)   Moats, R.; Fraser, S.; Meade, T. *Angew Chem Int Ed Engl* **1997**, *36*, 725-728.

(37)   Jacobs, R. E.; Ahrens, E. T.; Meade, T. J.; Fraser, S. E. *Trends Cell Biol* **1999**, *9*, 73-6.

(38)   Louie, A. Y.; Huber, M. M.; Ahrens, E. T.; Rothbacher, U.; Moats, R.; Jacobs, R. E.; Fraser, S. E.; Meade, T. J. *Nat Biotechnol* **2000**, *18*, 321-5.

(39)   Li, W.-H.; Fraser, S.; Meade, T. *J Am Chem Soc* **1999**, *121*, 1413-1414.

(40)   Li, W.-H.; Parigi, G.; Fragai, M.; Luchinat, C.; Meade, T. J. *Inorg Chem* **2002**, *41*, 4018-4024.

(41)   Gerweck, L. E.; Seetharaman, K. *Cancer Res* **1996**, *56*, 1194-8.

(42)   Mikawa, M.; Miwa, N.; Akaike, T.; Maruyama, A. *Proceedings of the International Symposium on controlled Release of Bioactive Materials* **1999**, 1158-1159.

(43)   Aime, S.; Crich, S. G.; Botta, M.; Giovenzana, G.; Palmisano, G.; Sisti, M. *Chem Commun* **1999**, *38*, 1577-1578.

(44)   Aime, S.; Barge, A.; Botta, M.; Howard, J. A. K.; Kataky, R.; Lowe, M. P.; Moloney, J. M.; Parker, D.; de sousa, A. S. *Chem Commun (Cambridge)* **1999**, 1047.

(45)   Lowe, M. P.; Parker, D.; Reany, O.; Aime, S.; Botta, M.; Castellano, G.; Gianolio, E.; Pagliarin, R. *J Am Chem Soc* **2001**, *123*, 7601-9.

(46)   Woods, M.; Kiefer, G. E.; Bott, S.; Castillo-Muzquiz, A.; Eshelbrenner, C.; Michaudet, L.; McMillan, K.; Mudigunda, S. D.; Ogrin, D.; Tircso, G.; Zhang, S.; Zhao, P.; Sherry, A. D. *J Am Chem Soc* **2004**, *126*, 9248-56.

(47)   Lowe, M. P. *Curr Pharm Biotechnol* **2004**, *5*, 519-28.

(48)   Hanaoka, k.; Kikuchi, Y.; Urano, Y.; Nagano, T. *J. Chem. Soc. Perkin Trans. 2* **2001**, 1840.

(49)   Trokowski, R.; Ren, J.; Kalman, F. K.; Sherry, A. D. *Angew Chem Int Ed Engl* **2005**, *44*, 6920-3.

(50)   Comblin, V.; Gilsoul, D.; Hermann, M.; Humbelt, V.; Jacques, V.; Mesbahi, M.; Sauvage, C.; Desreux, J. F. *Coord. Chem. Rev.* **1999**, *185-186*, 451.

(51)   Que, E. L.; Chang, C. J. *J Am Chem Soc* **2006**, *128*, 15942-3.

(52)   Rudin, M. *Nat Biotechnol* **2000**, *18*, 383.

(53) Anelli, P. L.; Bertini, I.; Fragai, M.; Lattuada, L.; Luchinat, C.; Parigi, G. *Eur J Inorg Chem* **2000**, 625-630.

(54) Perez, J. M.; O'Loughin, T.; Simeone, F. J.; Weissleder, R.; Josephson, L. *J Am Chem Soc* **2002**, *124*, 2856-7.

(55) Aime, S.; Botta, M.; Dastru, W.; Fasano, M.; Panero, M.; Arnelli, A. *Inorg Chem* **1993**, *32*, 2068-2071.

(56) Artemov, D. *J Cell Biochem* **2003**, *90*, 518-24.

(57) Raemer, P.; Bader, A.; Weissleder, R. *J Magn Reson Imaging* **1998**, *8*, 687-689.

(58) Leveille-Webster, C. R.; Rogers, J.; Arias, I. M. *Hepatology* **1996**, *23*, 1631-41.

(59) Ni, Y.; Marchal, G.; Herijgers, P.; Flameng, W.; Petre, C.; Ebert, W.; Hilger, C. S.; Pfefferer, D.; Semmler, W.; Baert, A. L. *Acad Radiol* **1996**, *3 Suppl 2*, S395-7.

(60) Frullano, L.; Rohovec, J.; Aime, S.; Maschmeyer, T.; Prata, M. I.; de Lima, J. J.; Geraldes, C. F.; Peters, J. A. *Chemistry* **2004**, *10*, 5205-17.

(61) Artemov, D.; Mori, N.; Ravi, R.; Bhujwalla, Z. M. *Cancer Res* **2003**, *63*, 2723-7.

(62) Boerman, O. C.; van Schaijk, F. G.; Oyen, W. J.; Corstens, F. H. *J Nucl Med* **2003**, *44*, 400-11.

(63) Sharkey, R. M.; Karacay, H.; Griffiths, G. L.; Behr, T. M.; Blumenthal, R. D.; Mattes, M. J.; Hansen, H. J.; Goldenberg, D. M. *Bioconjug Chem* **1997**, *8*, 595-604.

(64) Goodwin, D. A.; Meares, C. F.; Osen, M. *J Nucl Med* **1998**, *39*, 1813-8.

(65) Axworthy, D. B.; Reno, J. M.; Hylarides, M. D.; Mallett, R. W.; Theodore, L. J.; Gustavson, L. M.; Su, F.; Hobson, L. J.; Beaumier, P. L.; Fritzberg, A. R. *Proc Natl Acad Sci U S A* **2000**, *97*, 1802-7.

(66) Hainsworth, J.; Harrison, P.; Mather, S. J. *Bioconjug Chem* **2005**, *16*, 1468-74.

(67) Sakahara, H.; Saga, T. *Adv Drug Deliv Rev* **1999**, *37*, 89-101.

(68) Goodwin, D. A.; Meares, C. F. *Cancer Suppl* **1997**, *80*, 2675-2680.

(69) Zitvogel, L.; Tursz, T. *Nat Biotechnol* **2005**, *23*, 1372-4.

(70) de Vries, J. M.; Lesterhuis, W. J.; Barentsz, J. O.; Verdijk, P.; van Krieken, J. H.; Boerman, O. C.; Oyen, W. J. G.; Bonenkamp, J. J.; Boezeman, J. B.; Adema, G. J.; Bulte, J. W. M.; Scheenen, T. W. J.; Punt, C. J. A.; Heerschap, A.; Figdor, C. G. *Nat Biotechnol* **2005**, *23*, 1407-1413.

(71) Tacken, P. J.; de Vries, I. J.; Gijzen, K.; Joosten, B.; Wu, D.; Rother, R. P.; Faas, S. J.; Punt, C. J.; Torensma, R.; Adema, G. J.; Figdor, C. G. *Blood* **2005**, *106*, 1278-85.

(72) Dirksen, A.; Langereis, S.; de Waal, B. F. M.; van Genderen, M. H. P.; Meijer, E. W.; de Lussanet, Q. G.; Hackeng, T. M. *Org Lett* **2004**, *6*, 4857-4860.

(73) Modo, M.; Cash, D.; Mellodew, K.; Williams, S. C.; Fraser, S. E.; Meade, T. J.; Price, J.; Hodges, H. *Neuroimage* **2002**, *17*, 803-11.

(74) Modo, M.; Mellodew, K.; Cash, D.; Fraser, S. E.; Meade, T. J.; Price, J.; Williams, S. C. *Neuroimage* **2004**, *21*, 311-7.

(75) Crich, S. G.; Biancone, L.; Cantaluppi, V.; Duo, D.; Esposito, G.; Russo, S.; Camussi, G.; Aime, S. *Magn Reson Med* **2004**, *51*, 938-44.

(76)   Li, M.; Meares, C. F.; Zhong, G. R.; Miers, L.; Xiong, C. Y.; DeNardo, S. J. *Bioconjug Chem* **1994**, *5*, 101-4.

(77)   McCall, M. J.; Diril, H.; Meares, C. F. *Bioconjug Chem* **1990**, *1*, 222-6.

(78)   Rana, T. M.; Meares, C. F. *Bioconjug Chem* **1990**, *1*, 357-62.

(79)   Li, M.; Meares, C. F. *Bioconjug Chem* **1993**, *4*, 275-83.

(80)   Sieving, P. F.; Watson, A. D.; Rocklage, S. M. *Bioconjug Chem* **1990**, *1*, 65-71.

(81)   Herrmann, A.; Mihov, G.; Vandermeulen, G. W. M.; Klok, H.-A.; Mullen, K. *Tetrahedron* **2003**, *59*, 3925-3935.

(82)   Dirksen, A.; Langereis, S.; De Waal, B. F. M.; Van Genderen, M. H. P.; Hackeng, T. M.; Meijer, E. W. *Chem Commun* **2005**, 2811-2813.

(83)   Pfeuffer, J.; Merkle, H.; Beyerlien, M.; Steudel, T.; Logothetis, N. K. *Magn Reson Imag* **2004**, *22*, 1343-1359.

(84)   Mishra, A. K.; Chatal, J. F. *New J. Chem.* **2001**, *25*, 336-339.

(85)   Gries, H.; Raduechel, B.; Speck, U.; Weinmann, H. J. **1988**.

(86)   Duimstra, J. A.; Femia, F. J.; Meade, T. J. *J Am Chem Soc* **2005**, *127*, 12847-55.

(87)   Pope, S. J. A.; Kenwright, A. M.; Heath, S. L.; Faulkner, S. *Chem Commun* **2003**, *13*, 1550-1551.

(88)   Beylin, V. G.; Goel, O. P. *Org Prep and Proc Int* **1987**, *19*, 78-80.

(89)   Weizmann, Y.; Patolsky, F.; Katz, E.; Willner, I. *J Am Chem Soc* **2003**, *125*, 3452-4.

(90)   Rivera, V. R.; Merrill, G. A.; White, J. A.; Poli, M. A. *Anal Biochem* **2003**, *321*, 125-30.

(91)   Cao, R.; Gu, Z.; Hsu, L.; Patterson, G. D.; Armitage, B. A. *J Am Chem Soc* **2003**, *125*, 10250-6.

(92)   Caswell, K. K.; Wilson, J. N.; Bunz, U. H.; Murphy, C. J. *J Am Chem Soc* **2003**, *125*, 13914-5.

(93)   Bickel, U.; Yoshikawa, T.; Pardridge, W. M. *Adv Drug Deliv Rev* **2001**, *46*, 247-79.

(94)   Wilchek, M.; Bayer, E. A. *Methods Enzymol* **1990**, *184*, 123-38.

(95)   Hnatowich, D. J.; Virzi, F.; Rusckowski, M. *J Nucl Med* **1987**, *28*, 1294-302.

(96)   Wilbur, D. S.; Hamlin, D. K.; Chyan, M. K.; Kegley, B. B.; Pathare, P. M. *Bioconjug Chem* **2001**, *12*, 616-23.

(97)   Rusckowski, M.; Fogarasi, M.; Fritz, B.; Hnatowich, D. J. *Nucl Med Biol* **1997**, *24*, 263-8.

(98)   Gruaz-Guyon, A.; Raguin, O.; Barbet, J. *Curr Med Chem* **2005**, *12*, 319-38.

(99)   Forster, G. J.; Santos, E. B.; Smith-Jones, P. M.; Zanzonico, P.; Larson, S. M. *J Nucl Med* **2006**, *47*, 140-9.

(100)   Huber, M. M.; Staubli, A. B.; Kustedjo, K.; Gray, M. H.; Shih, J.; Fraser, S. E.; Jacobs, R. E.; Meade, T. J. *Bioconjug Chem* **1998**, *9*, 242-9.

(101)   Weissleder, R.; Mahmood, U. *Radiology* **2001**, *219*, 316-33.

(102)   Bottrill, M.; Kwok, L.; Long, N. J. *Chem Soc Rev* **2006**, *35*, 557-71.

(103)   Fulton, D. A.; O'Halloran, M.; Parker, D.; Senanayake, P. K.; Botta, M.; Aime, S. *Chem Commun* **2005**, 474.

(104) Fulton, D. A.; Elemento, E. M.; Aime, S.; Chaabane, J. A.; Botta, M.; Parker, D. *Chem Commun* **2006**, 1064.

(105) Lothar, H. *Prog Nuc Mag Res Spec* **2006**, *49*, 45.

(106) Jacques, V.; Desreux, J. F. *Topics in Curr Chem* **2001**, *221*, 123.

(107) Lebduskova, P.; Hermann, P.; Helm, L.; Toth, E.; Kotek, J.; Binnemans, K.; Rudovsky, J.; Lukes, I.; Merbach, A. E. *Dalton Trans* **2007**, 493.

(108) Lukes, I.; Kotek, J.; Vojtisek, P.; Hermann, P. *Coord. Chem. Rev.* **2001**, *216-217*, 287.

(109) Popov, K.; Ronkkomaki, H.; Laujunen, L. H. J. *Pure Appl Chem* **2001**, *73*, 1641.

(110) Aime, S.; Botta, M.; Garino, E.; Crich, S. G.; Giovenzana, G.; Pagliarin, R.; Palmisano, G.; Sisti, M. *Chem Eur J* **2000**, *6*, 2609.

(111) Baranyai, Z.; Gianolio, E.; Ramalingam, K.; Swenson, R.; Ranganathan, R.; Bruecher, E.; Aime, S. *Contrast Med Mol Imaging* **2007**, *2*, 94.

(112) Aime, S.; Gianolio, E.; Corpillo, D.; Cavallotti, C.; Palmisano, G.; Sisti, M. *Helv Chim Acta* **2003**, *86*, 615.

(113) Aime, S.; Botta, M.; Frullano, L.; Geninatti Crich, S.; Giovenzana, G.; Pagliarin, R.; Palmisano, G.; Sirtori, F. R.; Sisti, M. *J Med Chem* **2000**, *43*, 4017-24.

(114) Garcia-Martin, M. L.; Martinez, G. V.; Raghunand, N.; Sherry, A. D.; Zhang, S.; Gillies, R. J. *Magn Reson Med* **2006**, *55*, 309-15.

(115) Rudovsky, J.; Cigler, P.; Kotek, J.; Hermann, P.; Vojtisek, P.; Lukes, I.; Peters, J. A.; Vander Elst, L.; Muller, R. N. *Eur J Chem* **2005**, *11*, 2373.

(116) Vojtisek, P.; Cigler, P.; Kotek, J.; Rudovsky, J.; Hermann, P.; Lukes, I. *Inorg Chem* **2005**, *44*, 5591.

(117) Taborsky, P.; Lubal, P.; Havel, J.; Kotek, J.; Hermann, P.; Lukes, I. *Collect Czech Chem Commun* **2005**, *70*, 1909.

(118) Bruce, J. I.; Dickins, R. S.; Govenlock, L. J.; Gunnlaugsson, T.; Lopinski, S.; Lowe, M. P.; Parker, D.; Peacock, R. D.; Perry, J. J. B.; Aime, S.; Botta, M. *J Am Chem Soc* **2000**, *122*, 9674.

(119) Dickins, R. S.; Aime, S.; Batsanov, A. S.; Beeby, A.; Botta, M.; Bruce, J. I.; Howard, J. A.; Love, C. S.; Parker, D.; Peacock, R. D.; Puschmann, H. *J Am Chem Soc* **2002**, *124*, 12697-705.

(120) Aime, S.; Gianolio, E.; Giovenzana, G.; Pagliarin, R.; Sisti, M.; Palmisano, G.; Lowe, M. P.; Parker, D. *JBIC* **2000**, *5*, 488.

(121) Nivorozhkin, A. L.; Kolodziej, A. F.; Caravan, P.; Greenfield, M. T.; Lauffer, R. B.; McMurry, T. J. *Angew Chem Int Ed Engl* **2001**, *40*, 2903-2906.

(122) Caravan, P.; Greenfield, M. T.; Li, X.; Sherry, A. D. *Inorg Chem* **2001**, *40*, 6580.

(123) Zech, S. G.; Eldredge, H. B.; Lowe, M. P.; Caravan, P. *Inorg Chem* **2007**, *46*, 3576.

(124) Livramento, J. B.; Weidensteiner, C.; Prata, M. I.; Allegrini, P. R.; Geraldes, C. F.; Helm, L.; Kneuer, R.; Merbach, A. E.; Santos, A. C.; Schmidt, P.; Toth, E. *Contrast Media Mol Imaging* **2006**, *1*, 30-9.

(125) Mishra, A.; Pfeuffer, J.; Mishra, R.; Engelmann, J.; Mishra, A. K.; Ugurbil, K.; Logothetis, N. K. *Bioconjug Chem* **2006**, *17*, 773-80.

(126) Takahashi, M.; Uematsu, H.; Hatabu, H. *Eur J Radiol* **2003**, *46*, 45.

(127) Parker, D.; Dickins, R. S.; Puschmann, H.; Crossland, C.; Howard, J. A. *Chem Rev* **2002**, *102*, 1977-2010.

(128) Parker, D. *Chem Soc Rev* **2004**, *33*, 156-65.

(129)   Bretonniere, Y.; Cann, M. J.; Parker, D.; Slater, R. *Org Biomol Chem* **2003**, *2*, 1624.

(130)   Massimini, M.; Amzica, F. *J Neurophysiol* **2001**, *85*, 1346-50.

(131)   Silver, I. A.; Erecinska, M. *J Gen Physiol* **1990**, *95*, 837-66.

(132)   Charles, A. *Glia* **1998**, *24*, 39-49.

(133)   Atanasijevic, T.; Shusteff, M.; Fam, P.; Jasanoff, A. *Proc Natl Acad Sci U S A* **2006**, *103*, 14707-12.

(134)   Tsien, R. Y. *Biochemistry* **1980**, *19*, 2396-404.

(135)   Graeppi, N.; Powell, D. H.; Laurenczy, G.; Zekany, L.; Merbach, A. E. *Inorg Chim Acta* **1994**, *235*, 311.

(136)   Amman, C.; Meyer, P.; Merbach, A. E. *J Magn Reson* **1982**, *46*, 319.

(137)   Raiford, D. S.; Fisk, C. L.; Becker, E. D. *Anal Chem* **1979**, *51*, 2050.

(138)   Zitha-Bovens, E.; Vander Elst, L.; Muller, R. N.; van Bekkum, H.; Peters, J. A. *Eur J Inorg Chem* **2001**, 3101.

(139)   Yerly, F. *VISUALISEUR* **1999**, *2.3.4*, Lausanne, Switzerland.

(140)   Yerly, F. *OPTIMISEUR* **1999**, *2.3.4.*, Lausanne Switzerland.

(141)   Aime, S.; Cravotto, G.; Crich, S. G.; Giovenzana, G. B.; Ferrari, G. B.; Palmisano, G.; Sisti, M. *Tetrahedron Lett* **2002**, *43*, 783.

(142)   Wong, W.; Li, C. *PCT Int Appl* **2005**, 23 pp. CODEN: PIXXD2 WO 2005003105 A I 20050113.

(143)   Faulkner, S.; Pope, S. J. *J Am Chem Soc* **2003**, *125*, 10526-7.

(144)   Dhingra, K.; Fouskova, P.; Angelovski, G.; Maier, M. E.; Logothetis, N. K.; Toth, E. *J Biol Inorg Chem* **2007**.

(145)   The IUPAC Stability Constants Database, S.-D. A. S. a. K. J. P. **1999**, http//www.acadsoft.co.uk.

(146)   De, W.; Horrocks, J. W.; Sudnick, D. R. *J Am Chem Soc* **1979**, *101*, 334.

(147)   Supkowski, R. M.; De, W.; Horrocks, J. W. *Inorg Chim Acta* **2002**, *340*, 44.

(148)   Beeby, A.; Clarkson, I. M.; Dickins, R. S.; Faulkner, S.; Parker, D.; L., R.; de Sousa, A. S.; Williams, J. A. G.; Woods, M. *J chem Soc., Parkin Trans* **1999**, *2*, 493.

(149)   Albin, M.; Farber, G. K.; Horrocks, J. W. *Inorg Chem* **1984**, *23*, 1648.

(150)   Geier, G.; Jorgensen, C. K. *Chem Phys Lett* **1971**, 263.

(151)   Toth, E.; Ni Dhubhghaill, O. M.; Besson, G.; Helm, L.; Merbach, A. E. *Magn Res Chem* **1999**, *37*, 701.

(152)   Yerly, F.; Dunand, F. A.; Toth, E.; Figueirinha, A.; Kovacs, Z.; Sherry, A. D.; Geraldes, C. F. G. C.; Merbach, A. E. *J Inorg Chem* **2000**, 1001.

(153)   Helm, L.; Merbach, A. E. *Chem Rev* **2005**, *105*, 1923-59.

(154)   Lebduskova, P.; Sour, A.; Helm, L.; Toth, E.; Kotek, J.; Binnemans, K.; Rudovsky, J.; Lukes, I.; Merbach, A. E. *Dalton Trans* **2006**, 3399.

(155)   Botta, M. *Eur J Inorg Chem* **2000**, 399.

(156)   Rudovsky, J.; Botta, M.; Hermann, P.; Koridze, A.; Aime, S. *Dalton Trans* **2006**, 2323.

(157)   Rudovsky, J.; Kotek, J.; Hermann, P.; Lukes, I.; Mainero, V.; Aime, S. *Org Biomol Chem* **2005**, *3*, 112.

(158)   Kotek, J.; Lebduskova, P.; Hermann, P.; Vander Elst, L.; Muller, R. N.; Maschmeyer, T.; Lukes, I.; Peters, J. A. *Chem Eur J* **2003**, *9*, 5899.

(159)   Lebduskova, P.; Kotek, J.; Hermann, P.; Vander Elst, L.; Muller, R. N.; Lukes, I.; Peters, J. A. *Bioconjug Chem* **2004**, *15*, 881-9.

(160)   Powell, D. H.; Dhubghaill, O. M. N.; Pubanz, D.; Helm, L.; Lebedev, Y. S.; Schlaepfer, W.; Merbach, A. E. *J Am Chem Soc* **1996**, *118*, 9333.

(161)   Rudovsky, J.; Hermann, P.; Botta, M.; Aime, S.; Lukes, I. *Chem Commun (Camb)* **2005**, 2390-2.

(162)   Rudovsky, J.; Botta, M.; Hermann, P.; Hardcastle, K. I.; Lukes, I.; Aime, S. *Bioconjug Chem* **2006**, *17*, 975-87.

(163)   Congreve, A.; Parker, D.; Gianolio, E.; Botta, M. *Dalton Trans* **2004**, 1441-5.

(164)   Weiss, P.; Hiscoe, H. N. *J Exp Zool* **1948**, *107*, 315-395.

(165)   Kobbert, C.; Apps, R.; Bechmann, I.; Lanciego, J. L.; Mey, J.; Thanos, S. *Prog Neurobiol* **2000**, *62*, 327-51.

(166)   Baizer, J. S.; Ungerleider, L. G.; Desimone, R. *J Neurosci* **1991**, *11*, 168-90.

(167)   Cowan, W. M.; Gottlieb, D. I.; Hendrickson, A. E.; Price, J. L.; Woolsey, T. A. *Brain Res* **1972**, *37*, 21-51.

(168)   Felleman, D. J.; Van Essen, D. C. *Cereb Cortex* **1991**, *1*, 1-47.

(169)   Jones, E. G.; Powell, T. P. *Brain* **1970**, *93*, 793-820.

(170)   Lanciego, J. L.; Wouterlood, F. G. *J Neurosci Methods* **2000**, *103*, 1-2.

(171)   Saint-Cyr, J. A.; Ungerleider, L. G.; Desimone, R. *J Comp Neurol* **1990**, *298*, 129-56.

(172)   Seltzer, B.; Pandya, D. N. *Brain Res* **1978**, *149*, 1-24.

(173)   Koretsky, A. P.; Silva, A. C. *NMR Biomed* **2004**, *17*, 527-31.

(174)   Lee, J. H.; Koretsky, A. P. *Curr Pharm Biotechnol* **2004**, *5*, 529-37.

(175)   Pautler, R. G.; Silva, A. C.; Koretsky, A. P. *Magn Reson Med* **1998**, *40*, 740-8.

(176)   Drapeau, P.; Nachshen, D. A. *J Physiol* **1984**, *348*, 493-510.

(177)   Leergaard, T. B.; Bjaalie, J. G.; Devor, A.; Wald, L. L.; Dale, A. M. *Neuroimage* **2003**, *20*, 1591-600.

(178)   Saleem, K. S.; Pauls, J. M.; Augath, M.; Trinath, T.; Prause, B. A.; Hashikawa, T.; Logothetis, N. K. *Neuron* **2002**, *34*, 685-700.

(179)   Sloot, W. N.; Gramsbergen, J. B. *Brain Res* **1994**, *657*, 124-32.

(180)   Tjalve, H.; Mejare, C.; Borg-Neczak, K. *Pharmacol Toxicol* **1995**, *77*, 23-31.

(181)   Tjalve, H.; Henriksson, J.; Tallkvist, J.; Larsson, B. S.; Lindquist, N. G. *Pharmacol Toxicol* **1996**, *79*, 347-56.

(182)   Van der Linden, A.; Verhoye, M.; Van Meir, V.; Tindemans, I.; Eens, M.; Absil, P.; Balthazart, J. *Neuroscience* **2002**, *112*, 467-74.

(183)   Watanabe, T.; Frahm, J.; Michaelis, T. *NMR Biomed* **2004**, *17*, 554-68.

(184)   Hazell, A. S. *Neurochem Int* **2002**, *41*, 271-7.

(185)   Takeda, A. *Brain Res Brain Res Rev* **2003**, *41*, 79-87.

(186)   Zwingmann, C.; Leibfritz, D.; Hazell, A. S. *J Cereb Blood Flow Metab* **2003**, *23*, 756-71.

(187)   Zwingmann, C.; Leibfritz, D.; Hazell, A. S. *Neurotoxicology* **2004**, *25*, 573-87.

(188)   Somjen, G. G. *Ions in the brain, Oxford University, in press* **2004**.

(189)   Wolf, D. E.; Vallant, J.; Peck, R. L.; Folkers, K. *J Am Chem Soc* **1952**, 2002.

(190)   Horikawa, K.; Armstrong, W. E. *J Neurosci Methods* **1988**, *25*, 1-11.

(191)   Kita, H.; Armstrong, W. *J Neurosci Methods* **1991**, *37*, 141-50.

(192)   Lapper, S. R.; Bolam, J. P. *J Neurosci Methods* **1991**, *39*, 163-74.

(193)   Wirsig-Wiechmann, C. R. *J Neurosci Methods* **1994**, *51*, 213-6.

(194)   Baumgartner, E. R.; Suormala, T.; Wick, H.; Bausch, J.; Bonjour, J. P. *J Inherit Metab Dis* **1985**, *8 Suppl 1*, 59-64.

(195)   Baumgartner, E. R.; Suormala, T. M.; Wick, H.; Probst, A.; Blauenstein, U.; Bachmann, C.; Vest, M. *Pediatr Res* **1989**, *26*, 260-6.

(196)   Hymes, J.; Wolf, B. *Clin Chim Acta* **1996**, *255*, 1-11.

(197)   Axworthy, D. B.; Theodore, L. J.; Gustavson, L. M.; Reno, J. M. *United State Patent* **1997**, *5*, 608-660.

(198)   Sabatino, G.; Chinol, M.; Paganelli, G.; Papi, S.; Chelli, M.; Leone, G.; Papini, A. M.; De Luca, A.; Ginanneschi, M. *J Med Chem* **2003**, *46*, 3170-3.

(199)   Subramanian, R.; Meares, C. F. *(D. M. Goldenberg, Ed.) Academic Pubs., Boston* **1991**, 183-199.

(200)   Moi, M. K.; Meares, C. F.; McCall, M. J.; Cole, W. C.; DeNardo, S. J. *Anal Biochem* **1985**, *148*, 249-53.

(201)   Moi, M. K.; Meares, C. F.; DeNardo, S. J. *J Am Chem Soc* **1988**, *110*, 6266.

(202)   Gansow, O. A. *Int J Rad Appl Instrum B* **1991**, *18*, 369-81.

(203)   Meares, C. F.; Moi, M. K.; Diril, H.; Kukis, D. L.; McCall, M. J.; Deshapnde, S. V.; DeNardo, S. J.; Snook, D.; Epenetos, A. A. *Br J Cancer Suppl* **1990**, *10*, 21-6.

(204)   Parker, D. *Chem. Soc. Rev.* **1990**, *19*, 271.

(205)   Deshpande, S. V.; DeNardo, S. J.; Kukis, D. L.; Moi, M. K.; McCall, M. J.; DeNardo, G. L.; Meares, C. F. *J Nucl Med* **1990**, *31*, 473-9.

(206)   McMurry, T. J.; Brechbiel, M.; Kumar, K.; Gansow, O. A. *Bioconjug Chem* **1992**, *3*, 108-17.

(207)   Anelli, P. L.; Lattuada, L.; Gabellini, M.; Recanati, P. *Bioconjug Chem* **2001**, *12*, 1081-4.

(208)   Renn, O.; Meares, C. F. *Bioconjug Chem* **1992**, *3*, 563-9.

(209)   Allen, M. J.; Meade, T. J. *J Biol Inorg Chem* **2003**, *8*, 746-50.

(210)   Berthezene, Y.; Vexler, V.; Price, D. C.; Wisner-Dupon, J.; Moseley, M. E.; Aicher, K. P.; Brasch, R. C. *Invest Radiol* **1992**, *27*, 346-51.

(211)   Prantner, A. M.; Sharma, V.; Garbow, J. R.; Piwnica-Worms, D. *Mol Imaging* **2003**, *2*, 333-41.

(212)   Thiers, R. C. *Methods Biochem Anal* **1957**, *5*, 273-335.

My academic teachers were:

Anurag Mishra

BIOGRAPHICAL DATA:

Date and place of birth: 27.02.1976. Unnao, India

Citizenship: Republic of India

Family Status: Married

Languages: Hindi (native), English (fluent), German (working knowledge).

EDUCATION:

- *Ph.D. (Dr.rer.Nat.)***,** December 2003 till now.

Faculty of Chemistry and Pharmacy, University of Tuebingen, Tuebingen, Germany.

- *Masters in Science (MSc. Pharmaceutical Chemistry)*, July 1997 to October 1999.

Institute of Chemical Sciences (*ICS*), Devi Ahilyabai Vishwavidhyalay (*DAVV*) Indore, India.

Score of the exam. 86% (9.34 CGPA out of 10) aggregate.

- *Bachelor in Science (BSc.)*: July 1994 to June 1997.

Bipin Bihari Degree College, Bundelkhand University, Jhansi, India

Score of the exam. 78% aggregate.

PROFESSIONAL EXPERIENCE:

1. Ph.D. (Dr. rer. Nat.), pursuing since December 2003, Max Planck Institute for biological cybernetics, Tuebingen, Germany and Faculty of Chemistry and Pharmacy, University of Tuebingen, Tuebingen, Germany.

http://www.kyb.mpg.de/lo/index.html

2. Diploma thesis entitled "Design, synthesis and characterization of smart MR contrast agents' sensitive to pH / calcium changes during neural activity" from December 2003 to May 2004 under the supervision of Prof. Dr. Klaus Albert at University of Tuebingen.

3. Research Chemist in Medicinal Chemistry Division, New Drug Discovery Research, Ranbaxy Research Laboratories, Gurgaon, India from August 2001 to November 2003.

164

4. Development Chemist in New Drug Research (NDR), Oncology and Biotechnology Division, Dabur Research Foundation, Sahibabad, India from October 1999 to July 2001.

5. Project trainee (Partial fulfilment of Master's Degree) in Division of Pharmaceutics, Central Drug Research Institute (CDRI), Lucknow, India from April 1999 to June 1999.

Project entitled: "Studies on isoniazid and rifampicin in a microsphere formulation" under the supervision of Dr. A. K. Dwivedi and Dr. Amit Mishra.

6. Summer trainee (Partial fulfilment of Master's Degree) at Medicinal Chemistry Division, Central Drug Research Institute (CDRI), Lucknow, India from June 1998 to July 1998. Project entitled: "Synthesis of organic compounds and awareness for good laboratory practice" under the supervision of Dr. A. P. Bhaduri and Dr. Preeti Gupta.

PUBLICATIONS:

Patents:

- Anand N., S. Mohammad, S. Sharma, G. S. Kapkoti, P. Gupta, **A. Mishra**, A. Chugh and A. Tiwari: 1-Alkylpiperazinyl-pyrrolidin-2,5-dione derivatives as adrenergic receptor antagonists. (PCT Int. Appl. (2005), 102 pp. CODEN: PIXXD2 WO 2005/037282) (2005).

- Mohammad S., S. Sharma, G. C. Yadav, G. S. Kapkoti, **A. Mishra**, P. Gupta, N. Anand, A. Chugh and K. Nanda: Preparation of piperazine derivatives, particularly piperazinyl-pyrrolidine-2,5-dione, piperazinyl-tetrahydroisoindole-1,3-dione, and piperazinyl-piperidine-2,6-dione derivatives, as adrenergic receptor antagonists for treating benign prostatic hyperplasi. (PCT Int. Appl. (2005), 150 pp. CODEN: PIXXD2 WO 2005/118537) (2005).

Journal Articles:

- **Mishra A.**, J. Pfeuffer, R. Mishra, J. Engelmann, A. Mishra, K. Ugurbil and N. K. Logothetis: A New Class of Gd-based DO3A-ethylamine-derived Targeted Contrast Agents for MR and Optical Imaging. *Bioconjugate Chemistry 17* (2006), 773-780.

- **Mamedov I.**, **Mishra A.**, G. Angelovski, H. A. Mayer, L.-O. Pålsson, D. Parker and N. K. Logothetis. Synthesis and Characterization of Lanthanide Complexes of DO3A-Alkylphosphonates. *Dalton Transactions*, in press, 2007 (first two authors contributed equally).

- **Mishra A.**, P. Fouskova, G. Angelovski, E. Balogh, Anil K. Mishra, N. K. Logothetis, E. Toth: Facile Synthesis and Relaxation Properties of Novel Bis-polyazamacrocyclic Gd^{3+} Complexes: an Attempt towards Calcium Sensitive MRI Contrast Agents. *Inorg. Chem.,* in press (2007).

Conference Papers:

- Mishra A. K., J. Pfeuffer, **A. Mishra** and N.K. Logothetis: Design, synthesis and characterization of new smart MR contrast agents sensitive to pH. Proc ISMRM, Miami, 2582 (2005).

- **Mishra A.**, J. Pfeuffer, R. Mishra, N.K. Logothetis and A. K. Mishra: Multifunctional gadolinium-based ligand DO3A-EA as novel precursor for conjugation with bioorganic molecules to develop smart contrast agents for MR imaging. Proc ISMRM, Miami, 2592 (2005).

- **Mishra A.**, J. Pfeuffer, K Albert, A. K. Mishra and N. K. Logothetis: Facile Synthesis of Gd-DO3A-EA Conjugated with DTPA: A Novel Calcium Dependent MR Contrast Agent. Proc SMI, Cologne (2005).

- **Mishra A.**, J. Pfeuffer, N.K. Logothetis and A. K. Mishra: Multipurpose gadolinium-based ligand DO3A-EA as precursor for conjugation with organic molecules to develop smart and targeted contrast agents for MR and optical imaging. Proc ISMC, Dresden (2005).

- **Mishra A.**, P. Fouskova, E. Balogh, G. Angelovski, N. K. Logothetis, E. Jakab Toth: Facile Synthesis and Relaxation Properties of Three Novel Bis-macrocycles: Attempt towards Calcium Sensitive MRI Contrast Agents. SMI, Providence, *accepted* (2007).

Talks:

- **A. Mishra**, Mamedov I., Pfeuffer J., Angelovski G., Laurent S., Elst L. V., Muller R. N., Mayer H. A., Albert K., and Logothetis N. K.: DO3A Based Mono(alkylphosphonate) Complexes as Potential pH-sensitive Contrast Agents for MR Imaging, EMRF, Vilnius, Lithuania (2006).
- **A. Mishra**, Mamedov I., Pfeuffer J., Angelovski G., Laurent S., Elst L. V., Muller R. N., Mayer H. A., Albert K., and Logothetis N. K.: DO3A Based Mono(alkylphosphonate) Complexes as Potential pH-sensitive Contrast Agents for MR Imaging. GRC Metals in Medicine, Oxford (2006).